ROBUST OPTIMAL BOUNDARY AND SPATIAL FIELD CONTROL OF DISTRIBUTED PARAMETER SYSTEMS

BY

MASAKO KISHIDA

DISSERTATION

Submitted in partial fulfillment of the requirements
for the degree of Doctor of Philosophy in Mechanical Engineering
in the Graduate College of the
University of Illinois at Urbana-Champaign, 2010

Urbana, Illinois

Doctoral Committee:

Professor Geir E. Dullerud, Chair
Professor Richard D. Braatz, Director of Research
Assistant Professor Srinivasa M. Salapaka
Assistant Professor Prashant Mehta

ABSTRACT

The control of distributed parameter systems (DPS) is an interesting and challenging research field studied since the 1960s. An increasing number of DPS control problems in aerospace, materials, chemistry, biology, and other disciplines have attracted many mathematicians and engineers to this field in recent years. Many of these applications have been driven by new technologies for manufacturing, actuation, and sensing. Especially interesting are spatial field control problems that are challenging due to having a very large number of degrees of freedom, which is in contrast to the boundary control problems commonly investigated in the literature.

Computationally efficient methods for the robust and optimal control of DPS are derived that incorporate such techniques as basis function expansions, method of moments, model predictive control, and analytical function theory. These control methods are demonstrated by application to linear and nonlinear DPS described by reaction-diffusion-convection equations, including for some boundary and spatial field control problems that have not been investigated in the literature. Initially open-loop optimal control solutions are derived for a linear PDE, followed by generalizations to nonlinear reaction kinetics, coupled reactions, and feedback. The results also include an extension of internal model control that is applicable to linear infinite-dimensional systems.

While DPS control problems can be highly sensitive to uncertainties, robust control theory for DPS is not as well developed as for lumped parameter systems. Nonconservative approaches are derived for the analysis and control for DPS with worst-case uncertainties that are fairly general in terms of both the uncertainty description and the dynamics of the DPS. These methods provide the same level of assurance for model uncertainties in DPS as what was previously available only for lumped parameter systems.

ACKNOWLEDGMENTS

It has been a privilege to work with my advisor, Richard D. Braatz, who has supported and guided me with his extraordinary patience and full of knowledge. This thesis would not have been possible without him, and all thanks to him, I enjoyed stress-free life while learning many things during my Ph.D.

I am grateful to the members of my thesis committee – Geir E. Dullerud, Srinivasa M. Salapaka, and Prashant Mehta. I would like to acknowledge my dearest fellows, Kwang Ki Kim (김광기) and Takashi Tanaka (田中宗資) at the University of Illinois at Urbana-Champaign, and Tomotake Sasaki (佐々木智丈) at the University of Tokyo, for sharing valuable discussions and pleasant time. Outside the research, I would like to thank to Yu-Chi Tai (戴玉琪) for giving me wonderful piano lessons, which have been a great comfort and joy.

Finally, my special thanks go to everybody who was important to complete this thesis work.

Masako Kishida (岸田昌子)

"Chambana", IL

June 2010

Financial support is acknowledged from

- the National Institute of Biomedical Imaging and Bioengineering (NIBIB 5RO1EB005181)
- the National Science Foundation (Grant Numbers 0426328 and 0828123)
- the Institute for Advanced Computing Applications and Technologies

TABLE OF CONTENTS

LIST OF TABLES

LIST OF FIGURES

CHAPTER 1

INTRODUCTION

1.1 Background

Control of distributed parameter systems (DPS) is an interesting and challenging research area studied since the 1960s. As DPS control problems are pervasive in diverse industrial applications in aerospace, materials, chemistry, and biology, the field has attracted many theorists and engineers in recent years. One research objective is to successfully bridge theory and application, by developing controller design methods that are both theoretically rigorous and computationally feasible and general enough to be implemented in a wide range of applications. Another objective is to develop techniques that are able to explicitly address the effects of model uncertainties, with the same level of assurance in which model uncertainties are addressed for linear lumped parameter systems (LPS) [60, 190].

DPS encompasses a variety of engineering applications from flexible aerospace vehicles to micro-electro-mechanical systems (MEMS) and chemical reactors (Figure 1.1). The states and responses of these systems are functions of spatial and temporal variables and are usually described by one or more partial differential equations (PDEs), in contrast to LPS that are modeled by ordinary differential equations (ODEs) or differential-algebraic equations (DAEs). PDEs more accurately describe many physical systems but are more challenging to handle theoretically and computationally, such that many dynamics and control problems that are considered largely solved for LPS have remained challenging for DPS.

For the purposes of systems analysis or controller design, PDEs are usually approximated by a system of ODEs via the finite difference method [149], proper orthogonal decomposition [2], or other methods. The advantage of such approximations is that many control design methods (e.g., linear quadratic gaussian control, H_∞-optimal control, model predictive control, differential geometric methods, and μ-optimal control) are directly applicable to the approximated finite-dimensional systems. However, depending on the PDEs,

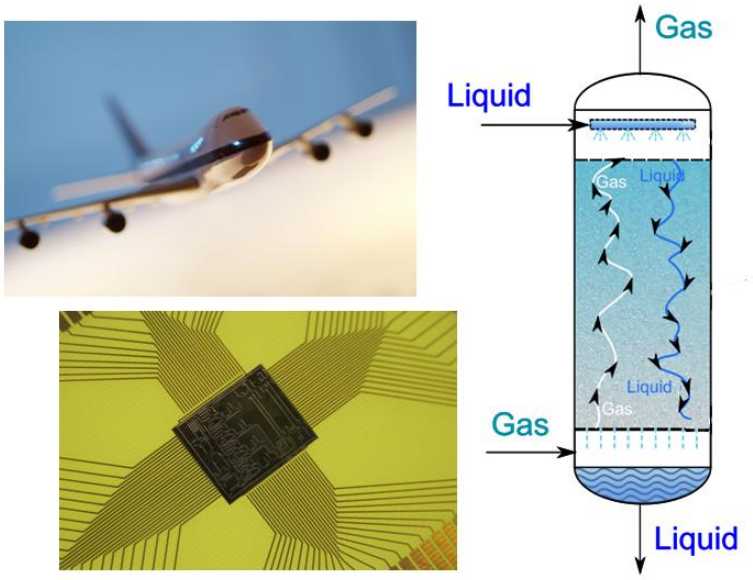

Figure 1.1: Applications of DPS include aircraft, MEMS, and packed bed reactor. Courtesy of Microsoft Clip Art, Maggie Bartlett (Wikipedia), and Aushulz (Wikimedia), respectively.

such procedures can result in a very high dimension for the ODEs that can disguise important spatiotemporal dynamic behavior with a loss in understanding, elegance, and efficiency that could be obtained by direct solution of the DPS (e.g., see discussion by [31, 123] and citations therein). Sometimes the discretization procedure masks the underlying structure and dynamics of the DPS so much that the designed control system performs well for the discretized model but is not even stable when applied to the PDE [31, 153]. On the other hand, the analysis or controller design of a DPS by directly dealing with the PDE often requires mathematics that are not known by most control engineers, such as infinite-dimensional operator theory [49], non-harmonic Fourier series [6, 175], and Carleman estimates [77].

In this thesis, computationally efficient methods are proposed for the robust and optimal controls of DPS, in which robustness is ensured regardless of whether (i) the PDEs are approximated by ODEs before the design of a finite-dimensional controller, or (ii) an infinite-dimensional controller designed directly from the PDEs is approximated by a finite-dimensional controller. A suite of control techniques are demonstrated by application to linear and nonlinear DPS described by reaction-diffusion(-convection) equations, which are also used to define some boundary and spatial field control problems that have heretofore not been investigated in the literature. Initial optimal control solutions are provided for a linear PDE, with approaches proposed to generalize the results to (i) nonlinear processes, (ii) coupled reaction, and (iii) feedback.

1.2 Some History

Theory on the optimal control of DPS was pioneered in the early 1960s [32, 131, 135]. Many computational algorithms and application papers were published in the 1970s [42, 169]. A standard approach for solving optimal control problems for DPS writes the control and/or state vector in terms of a set of basis functions and then analytically or numerically optimizes over the coefficients in the expansion [82]. Basis function expansions that have been used to solve optimal control problems include piecewise constant [82], piecewise linear [39, 144], Fourier series [95], Chebyshev series [200, 201], and Lagrange polynomials [65, 83].

The control variables for DPS can be lumped or distributed. *Boundary control* is a class of control problems for DPS that has been commonly studied (e.g., [191]), in which manipulation only occurs at the boundaries. *Spatial field control* is another class of control problems for DPS in which manipulation occurs as a spatial field. These latter control problems are motivated by applications in noise cancellation, vibration reduction, epidemiology, chemothapeutic drug delivery, and tissue engineering [88, 109, 146, 154, 192]. The interior of a spatial domain provides much more controllability than the boundary, which can be quite limited depending on the shape of the desired spatial field and the spatiodynamics of the DPS. At the same time, spatial field control problems have much more degrees of freedom than the corresponding boundary control problems. While the brute-force application of control vector parameterization [170] may be applied to boundary control and most other optimal control problems, field control problems need to be formulated with care to arrive at a computationally feasible solution. For example, a finite-difference discretization of the control vector in a 3D spatial field control problem can have 10^8 or more degrees of freedom [109], which is beyond the capability of existing optimization software executed on today's fastest computers.

The spatial field control literature includes many theoretical results on controllability and the structure of the optimal control for certain classes of PDEs when the spatial field is continuous or consists of a finite number of point sources (e.g., see [15, 124, 125] and citations therein) but has relatively few contributions that compute the optimal control for specific applications. An exception is [146] that computes H_2- and H_∞-optimal vibration controllers for the case in which the manipulation is restricted to discrete positions in the spatial domain. The spatial formulation results in better performance than applying H_2- and H_∞-control to a lumped-parameter representation.

The robustness of control for DPS has been analyzed by (i) application of the Monte Carlo method to the full simulation code [157], (ii) running the full simulation code for all parameters obtained by gridding the parameter space [157], and (iii) Lyapunov functions [164]. The first two classes of numerical algorithms can produce robustness margins with a low level of conservatism but are computationally expensive for problems with multiple spatial dimensions and parameters. The last approach is not always computationally expensive but tends to apply to specific control structures or is conservative. Worst-case and probabilistic robustness of finite-time DPS can be analyzed by first approximating the original PDE by a power series or polynomial chaos expansion and then applying methods developed for analyzing robustness for such

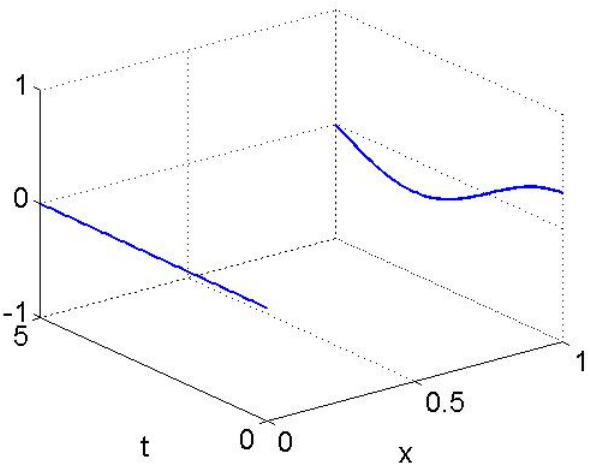

Figure 1.2: An example of a control input for a boundary control problem, where the time domain is $t \in [0, 5]$, the spatial domain is $x \in (0, 1)$, and the manipulated boundary is at $x = 1$.

expansions [137, 152]. For worst-case analysis, linear matrix inequalities (LMIs) and power iteration methods can be applied to compute tight upper and lower bounds, respectively, on the worst-case deviations of the states and control objectives (e.g., see [7, 60] and citations therein). Randomized algorithms [35, 132, 199] have been developed that can be applied to analyze probabilistic robustness for general series expansions; analytical expressions are available for low-order expansions [152].

1.3 Overview of the Thesis

This thesis considers two types of control architecture to achieve the reference field—*boundary control* and *spatial field control* (see Figures 1.2 and 1.3).

Definition 1.3.1. *The **optimal boundary control problem** is the minimization of the quadratic cost*

$$\min_{u_i(x,y,z,t)\in\mathcal{U}_i(x,y,z,t)} \sum_i \int_0^{t_f}\int_{V_i} (R_i(x,y,z,t) - C_i(x,y,z,t))^2 dV_i dt, \tag{1.1}$$

*where, for species i, V_i is the spatial domain of interest, R_i is the reference (desired) field, C_i is the controlled field that is related to the control input u_i by known PDEs, and $\mathcal{U}_i$ is the set of allowable manipulated **boundaries**, which can be continuous or discrete in space and time.*

Although boundary control has been studied extensively, many questions remain open such as (i) how to nonconservatively analyze the effects on model uncertainties in a computationally feasible manner, (ii) which control strategies are the best for a particular system, or (iii) whether these strategies can be combined to create better strategies.

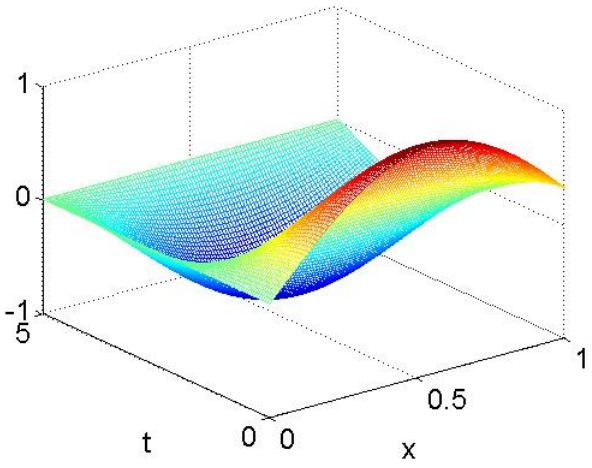

Figure 1.3: An example of a control input for a spatial field control problem, where the time domain is $t \in [0, 5]$ and the manipulated field covers the spatial domain $x \in (0, 1)$.

Definition 1.3.2. *The **optimal spatial field control problem** is the minimization of the quadratic cost*

$$\min_{u_i(x,y,z,t)\in\mathcal{U}_i(x,y,z,t)} \sum_i \int_0^{t_f}\int_{V_i} (R_i(x,y,z,t) - C_i(x,y,z,t))^2 dV_i dt, \tag{1.2}$$

*where for species i, V_i is the spatial domain of interest, R_i is the reference (desired) field, C_i is the controlled field that is related to the manipulated **fields** u_i by known PDEs, and $\mathcal{U}_i$ is the set of allowable manipulated fields, which can be continuous or discrete in space and time.*

Spatial field control can achieve control performance that cannot be obtained by boundary control. Optimal control algorithms must be designed with care, however, to avoid having excessive computational costs.

This thesis is organized as shown in Figure 1.4. Chapter 2, 3, and 7 consider boundary control problems and Chapter 4, 5, 6, and 8 consider spatial field control problems. Below is a summary of each chapter.

Chapter 2 addresses the 1D boundary control of the reaction-diffusion-convection equation, which is primarily motivated by tissue engineering (Figure 1.5). This chapter provides the most detailed description of tissue engineering in the thesis. Four approaches are compared for determining optimal boundary control trajectories for a distributed parameter system with reaction, diffusion, and convection: (i) basis function expansion, (ii) method of moments, (iii) internal model control, and (iv) model predictive control. A preliminary version of this chapter, which was the first formulation of stem cell tissue engineering as an optimal control problem, was presented at the 2008 American Control Conference [112].

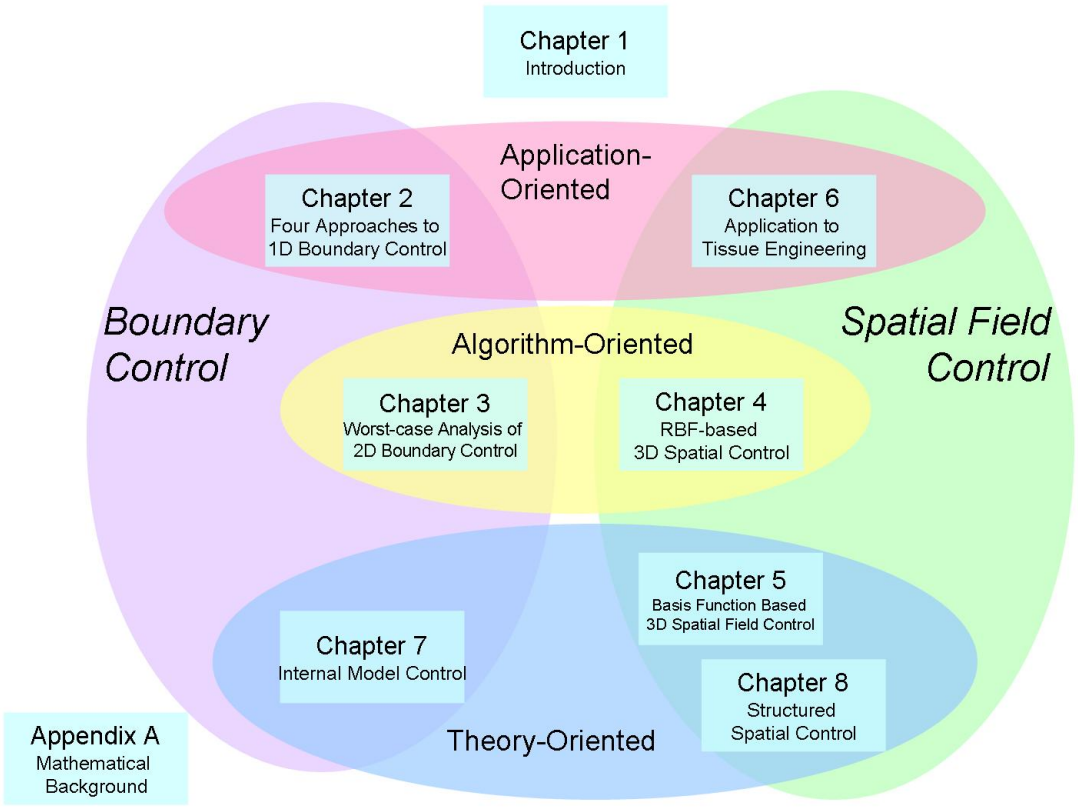

Figure 1.4: Structure of the thesis

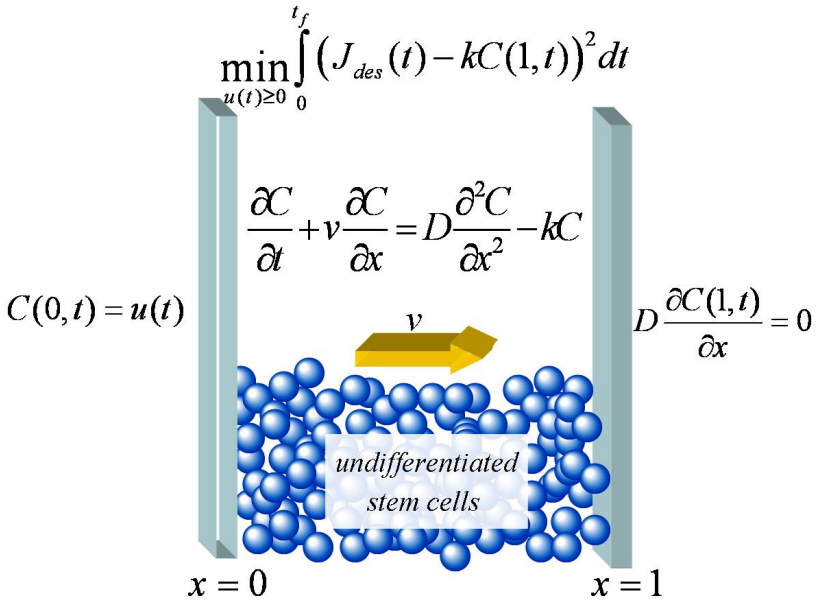

Figure 1.5: Boundary control at $x = 0$ with a Neumann boundary condition at $x = 1$ for a stem cell tissue engineering application (Chapter 2).

Chapter 3 treats the worst-case analysis of the effects of parametric uncertainties on boundary control problems for finite-time DPS by using series expansions (Figure 1.6). For example, with a vector of uncertain variables λ,

$$\lambda = \hat{\lambda} + \delta\lambda, \tag{1.3}$$

where $\hat{\lambda}$ is the vector of nominal values and $\delta\lambda$ is a vector of uncertainties, the second-order power series expansion for an output y is

$$\delta y_2 := M\delta\lambda + \delta\lambda^T H \delta\lambda \approx y(\lambda) - y(\hat{\lambda}), \tag{1.4}$$

where

$$M_i := \frac{\partial y}{\partial \lambda_i}\Big|_{\lambda=\hat{\lambda}}, \tag{1.5}$$

$$H_{ij} := \frac{1}{2}\frac{\partial^2 y}{\partial \lambda_i \partial \lambda_j}\Big|_{\lambda=\hat{\lambda}}. \tag{1.6}$$

The robustness analysis approach is demonstrated for a two-dimensional Dirichlet boundary control with reaction and diffusion. A preliminary version of this chapter, which was the first application of polynomial-time worst-case robustness analysis to a boundary control problem, was presented at the Eighteenth International Symposium on Mathematical Theory of Networks and Systems [108].

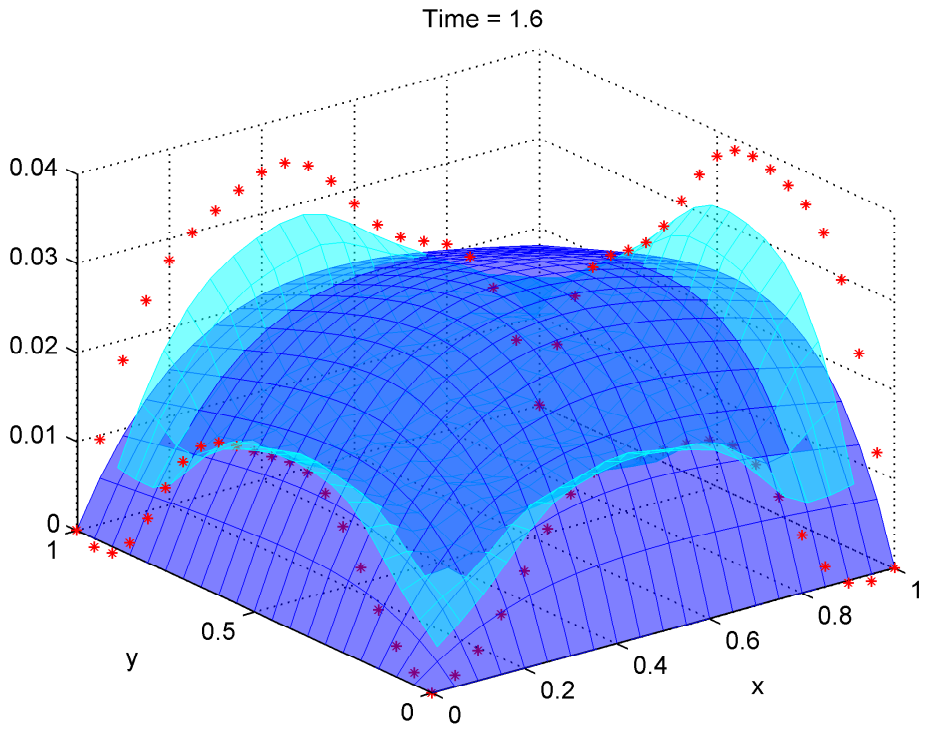

Figure 1.6: Reference field $R(x, y, t)$ (blue), boundary control variables (red asterisks), and optimal concentration field $C_{opt}(x, y, t)$ (cyan) field at a particular time instance (Chapter 3).

Chapter 4 considers the optimal control of the 3D reaction-diffusion-convection equation by application of radial basis functions (RBFs). The approach has three steps (Figure 1.7):

1. Express the target field by a sum of Gaussians,
2. Determine the Gaussian control input that produces each Gaussian output, and
3. Construct the overall control input as a sum of the Gaussian control inputs obtained in Step 2.

The approach is applicable to optimal control problems for linear spatially-distributed systems, for which the process output is expressed as a convolution of the system's kernel and its inputs. A novel feature is the insensitivity of its computational cost to the sharpness of spatial variations in the state or optimal control fields. A preliminary version of this chapter was presented at the 2009 European Control Conference [110].

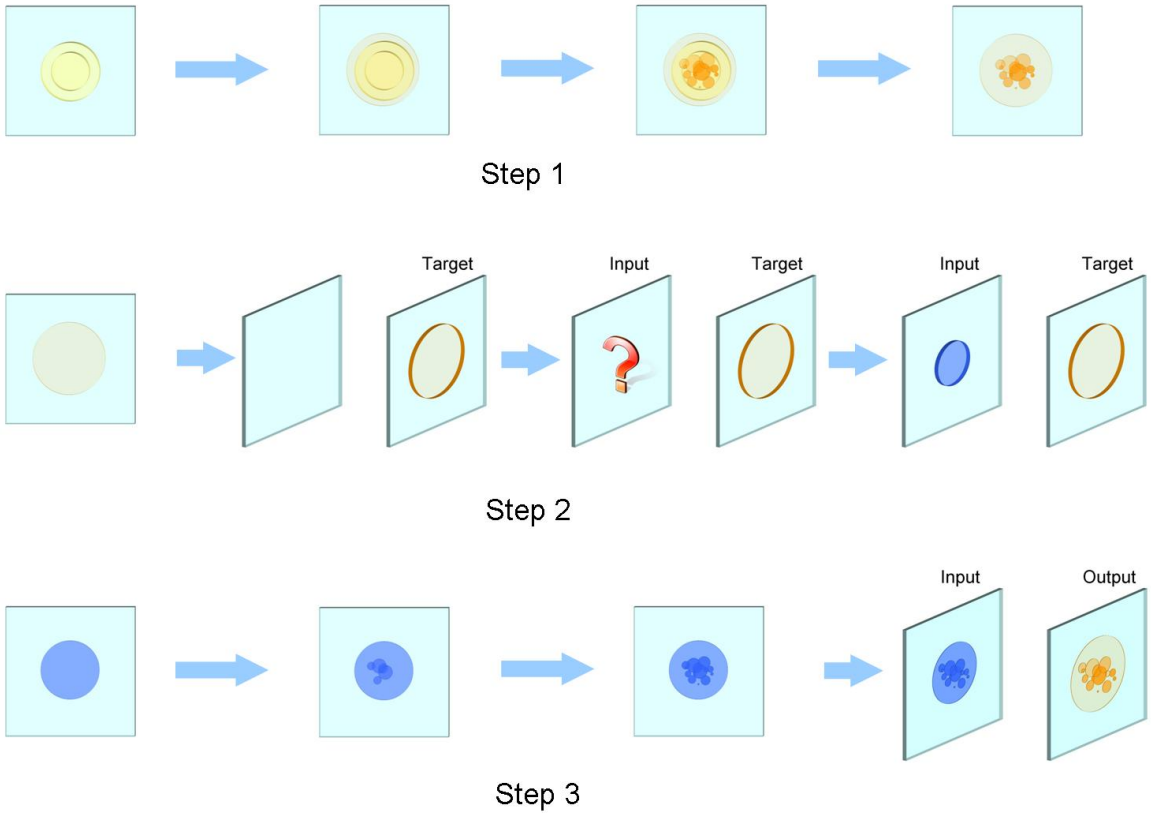

Figure 1.7: Schematics of each step of the proposed RBF-based boundary control approach (Chapter 4).

Chapter 5 formulates and solves optimal control problems in which the manipulation is distributed over a 3D spatial field with constraints on the spatial variation (Figure 1.8). The spatial variation constraints on the manipulated field $u(x, y, z, t)$ are specified by the integers M, N, and L in a 3D Fourier series

$$u(x,y,z,t) = \frac{1}{8} \sum_{m=-M}^{M} \sum_{n=-N}^{N} \sum_{l=-L}^{L} u_{mnl}(t) e^{(m\pi x + n\pi y + l\pi z)j} \tag{1.7}$$

with the optimal control problem being the determination of the $u_{mnl}(t)$ for $-M \leq m \leq M$, $-N \leq n \leq N$, and $-L \leq l \leq L$. The approach is demonstrated for the 3D reaction-diffusion-convection equation (some sample results are in Figure 1.9). The chapter includes a discussion of the extension of the approach to coupled PDEs. A preliminary version of this chapter, which was the first to consider this spatially-constrained 3D spatial field control problem, was presented at the 2009 American Control Conference [109].

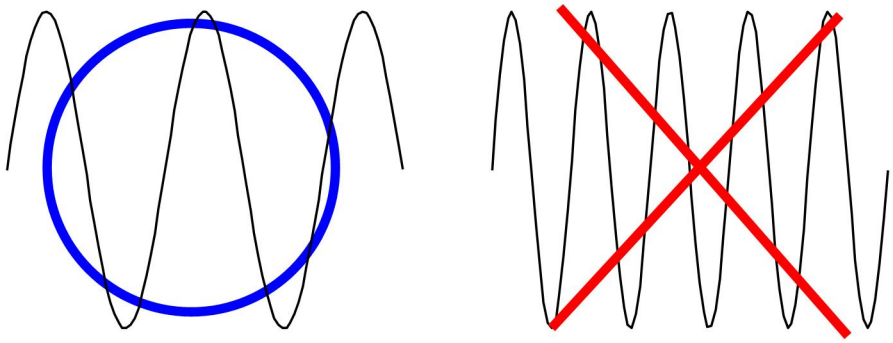

Figure 1.8: Spatial variational constraint allows only low spatial frequencies in the manipulated field (Chapter 5).

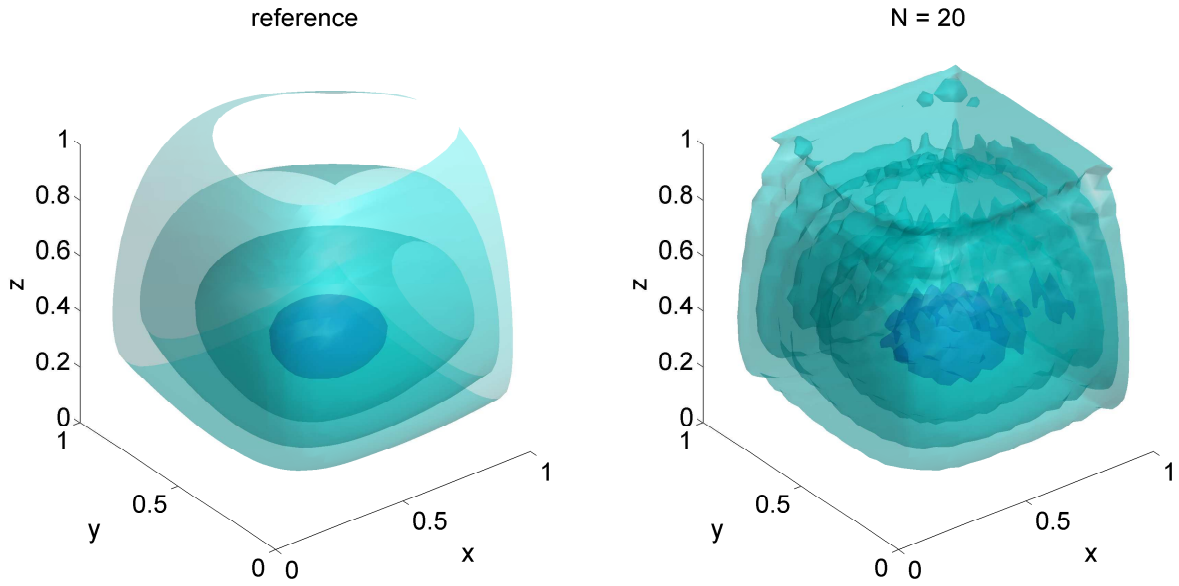

Figure 1.9: Isosurfaces for the reference and optimal concentration fields (Chapter 5).

As in Chapter 4, the main focus of Chapter 6 is the tissue engineering application. A state-constrained spatial field control problem motivated is solved in which the manipulation occurs over a spatial field and the state field is constrained *both* in spatial frequency and by a PDE that effects the manipulation (Figure 1.10). An optimization algorithm combines 3D Fourier series, which are truncated to satisfy the spatial frequency constraints, with exploitation of structural characteristics of the PDEs. A preliminary version of this chapter, which was the first to consider this control problem, was presented at the 2010 American Control Conference [113].

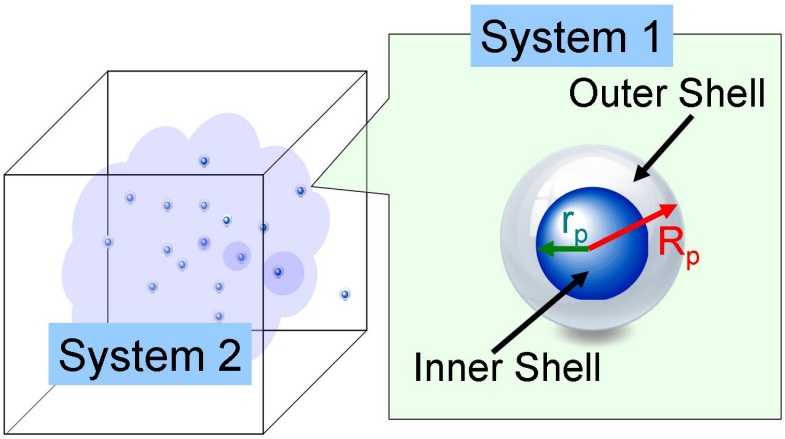

Figure 1.10: Overview of the distributed parameter systems in Chapter 6. System 1 is described by a PDE that is parameterized by spatial positions x, y, and z, with matches boundary conditions to a reaction-diffusion-convection equation describing System 2.

Chapter 7 extends the internal model control (IMC) design method to linear infinite-dimensional systems. An infinite-dimensional filter is coupled with the inverse of the infinite-dimensional transfer function between the process input and output, to produce a physically realizable controller with a tuning parameter for trading off nominal performance with robustness (Figure 1.11). A preliminary version of this chapter, which was the first to propose infinite-dimensional filters for IMC design, was presented at the 2008 Conference on Decision and Control [107].

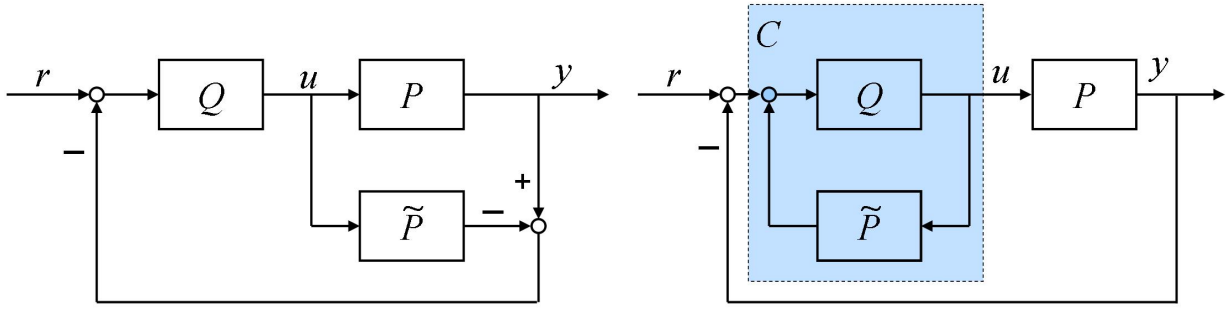

(a) IMC (b) Classical

Figure 1.11: Classical (left) and internal model (right) control structures (Chapter 7).

Chapter 8 exploits the algebraic structure of the system of ordinary differential equations that arise from spatial discretization of the PDE to analyze and design feedback controllers that are robust to bounded perturbations in the parameters of the original PDE. As a prototypical problem, the approach is illustrated for the spatial field control of a reaction-diffusion system whose spatial discretization has a state matrix that is circulant symmetric (Figure 1.12). This is the first consideration of simultaneuous robustness to both real parametric uncertainties and unmodeled dynamics uncertainties in circulant symmetric systems. A preliminary version of this chapter will be presented at the 2010 Multi-Conference on Systems and Control [111].

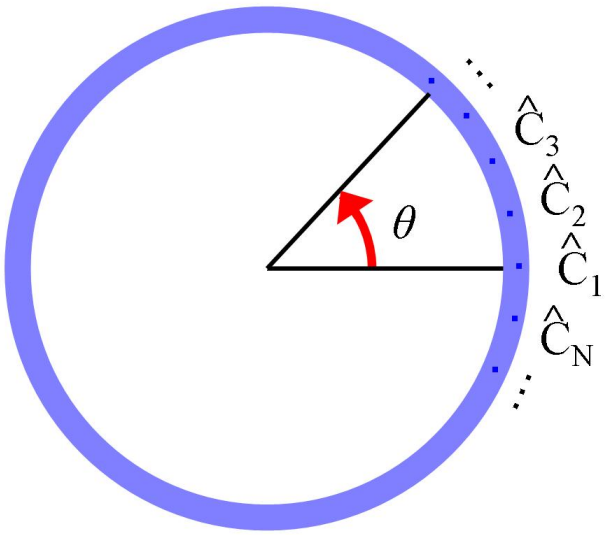

Figure 1.12: A distributed parameter system with reaction, diffusion, and circular symmetry (Chapter 8).

Appendix A reviews some mathematical tools repeatedly used in this thesis.

CHAPTER 2

FOUR APPROACHES TO 1D BOUNDARY CONTROL

A control problem motivated by tissue engineering is formulated and solved in which control of the uptake of growth factors (signaling molecules) is necessary to spatially and temporally regulate cellular processes for the desired growth or regeneration of a tissue. Four approaches are compared for determining optimal boundary control trajectories for a distributed parameter model with reaction, diffusion, and convection: (i) basis function expansion, (ii) method of moments, (iii) internal model control (IMC), and (iv) model predictive control (MPC). The method-of-moments approach is very computationally efficient while enforcing a nonnegativity constraint on the control input. While more computationally expensive than methods (i)-(iii), the MPC formulation significantly reduced the computational cost compared to simultaneous optimization of the entire control trajectory. A comparison of the pros and cons of each of the four approaches suggests that an algorithm that combines multiple approaches is most promising for solving the optimal control problem for multiple spatial dimensions.

2.1 Introduction

"Tissue engineering is an interdisciplinary field that applies the principles of engineering and the life sciences toward the development of biological substitutes that restore, maintain, or improve tissue function" [122].

The primary goal of tissue engineering is the production of biological tissues for clinical use. One of the main manufacturing strategies utilizes the attachment or encapsulation of cells within a tissue matrix that is typically made of collagen or synthetic polymers (see Figure 2.1) [22, 122, 127, 106]. Beyond receiving nutrients and releasing waste products, the development of a healthy functioning tissue requires that the cells uptake hormones, drugs, or signaling molecules in a controlled way [13, 121, 145, 38, 187, 58]. For example, in the development of tissues from stem cells, the stem cells must uptake growth factors, which are proteins

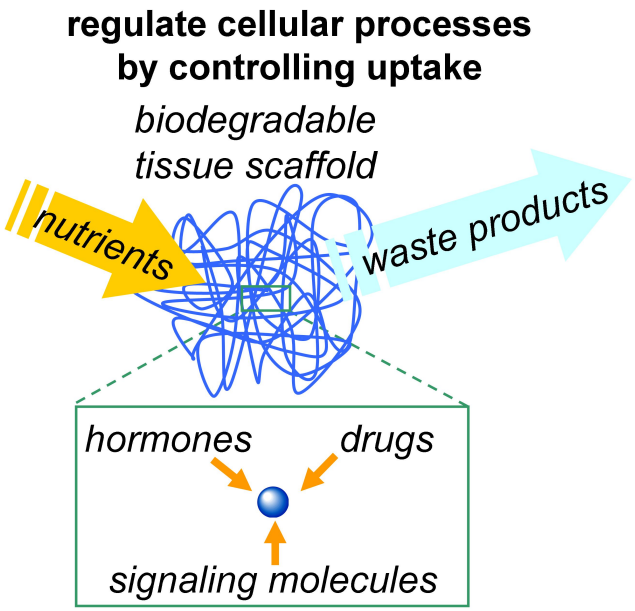

Figure 2.1: Overview of tissue engineering protocols for creating a functioning tissue or organ.

that regulate cellular processes such as stimulating cellular proliferation and cell differentiation. The spatial and temporal control of the cellular uptake can be achieved through localized release (e.g., [183, 41, 193]).

Many materials and devices have been created for releasing molecules in a controlled way [178]. Biodegradable polymeric nano- or microparticles have been developed that can be placed within a tissue matrix to provide localized timed release [120]. These particles include spheres, core-shell particles, and capsules that encapsulate small molecules, proteins, or DNA including growth factors or other signalling molecules or, in the case of microcapsules, can contain cells that excrete hormones or other macromolecules (see Figure 2.2) [122]. Techniques have been established to make highly uniform particles that produce a wide variety of highly reproducible release profiles by manipulating physical dimensions or by combining different types of particles [16, 198]. These particles can be accurately positioned and attached to a tissue matrix using such technologies as solid free-form fabrication [47] and layer-by-layer stereolithography [141], so as not to move until the particles have released their payloads to the cells.

The tissue engineering application motivates the formulation of an optimal control problem for the release of molecules from biodegradable polymeric nano- or microparticles to achieve a desired temporal and spatial uptake rate for cells within a tissue matrix. A potential application is to control the development of a tissue from stem cells within a matrix, so that the timed release of different growth factors in various locations form the multiple types of cells needed for the functioning components of a tissue. The shape and dimensions of these components are a function of both the spatial and temporal release of growth factors (e.g., [183]).

This chapter compares four approaches to solving the optimal control problem for one spatial dimension

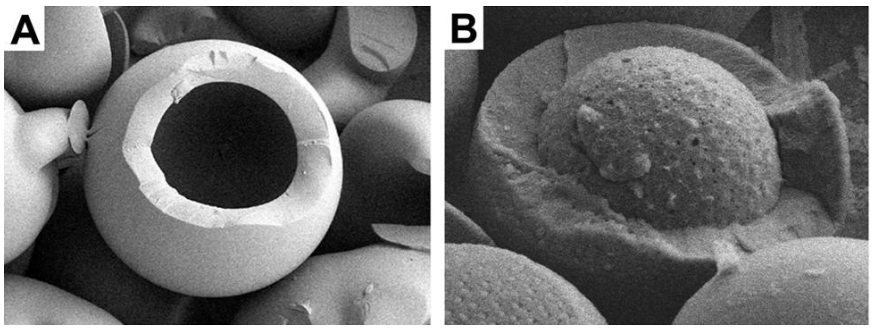

Figure 2.2: Examples of biodegradable polymer microparticles: (A) microcapsules, which in application have a core of liquid with dissolved molecules to be released, (B) a core-shell particle, in which both the core and shell consist of porous polymers in which molecules for release can be incorporated. Courtesy of Daniel W. Pack .

to provide insights into how to best address the much more complicated case of multiple spatial dimensions addressed later in this thesis. Section 2.2 formulates molecular release within a biological tissue as a distributed parameter optimal control problem. Sections 2.3-2.6 solve the control problem using four methods: basis function expansion, method of moments, internal model control, and model predictive control. Finally, Section 2.7 provides a summary and recommendations on how to solve the optimal control problem with higher spatial dimensions.

2.2 Problem Setup

To keep the nomenclature consistent, the term *growth factor* will refer to the molecule being released, although the theory and algorithms also directly apply to other molecules such as drugs, hormones, and DNA for gene therapy. Spatial and temporal control of the cellular uptake rate in a biological tissue under the influence of reaction, diffusion, and convection can be formulated as a distributed parameter optimal control problem:

$$\min_{u_j \in \mathcal{U}_j} \sum_j \int_0^{t_f} \int_V (J_{des,j}(x,y,z,t) - R_j(x,y,z,t))^2 dV dt, \tag{2.1}$$

where $J_{des,j}$ is the desired cellular uptake rate for species j, R_j is its cellular uptake rate, and its concentration C_j is the solution to the reaction-diffusion-convection equation [194]

$$\frac{\partial C_j}{\partial t} + v \cdot \nabla C_j = \nabla \cdot (D_j \nabla C_j) - R_j, \tag{2.2}$$

where (x, y, z) are the spatial coordinates defined over domain V, t_f is the final time of interest, v is a known velocity field as a function of the spatial coordinates, and D_j is the effective diffusion coefficient for species j. Depending on the specific tissue engineering application, the optimal control variables u_j can be either distributed throughout the spatial domain such as in the case that controlled release particles are integrated

into the tissue matrix, or can be a subset $\mathcal{U}_j$ of the boundary conditions on the surface of the domain V. This model (2.2) considers applications in which the minimum length scales of interest in the domain V are larger than the maximum dimensions of the molecules, cells, and polymer particles that release growth factors. The cellular uptake kinetics and desired rate $J_{des,j}$ are determined in small-scale biological experiments so as to produce a desired response, such as differentiation to form a desired type of cell [13, 122, 194]. The rates of growth factor binding or unbinding with the scaffold or extracellular matrix, and the rates of degradation due to enzymes can be incorporated into R_j. The model (2.2) is appropriate in the early stages of tissue development, before substantial cell migration and proliferation occur. The situation in which signaling molecules are produced by cells which are then taken up by other cells (cell-cell communication) requires only minor modification of (2.2).

A standard approach to solving the above optimal control problem is the finite difference method, in which the control variable $u_j(x,y,z,t)$ and state $C_j(x,y,z,t)$ are discretized with respect to the spatial and time variables, inserted into (2.1)-(2.2), and solved numerically as an algebraic optimization problem. The difficulty in applying this approach using the standard discretization of the control and state (e.g., $C_j(x_k,y_l,z_m,t_n)$) is the large number of degrees of freedom. For example, for a single three-dimensional (3D) state, 100 discretization points in each spatial dimension and in time results in $100^4 = 10^8$ degrees of freedom in the algebraic optimization. The large dimensionality of such distributed parameter control problems is well recognized in the optimal control literature (e.g., [116, 171]). While many approaches have been proposed, no single algorithm dominates the literature or applications and it is generally accepted that the best approach depends on the details of the optimal control problem being solved.

To gain insight into how to best solve the 3D optimal control problem (2.1)-(2.2), this chapter solves the 1D optimal control problem for a single species with manipulatable boundary condition and linear cellular uptake kinetics:

$$\min_{u(t)\geq 0} \int_0^{t_f} (J_{des}(t) - kC(1,t))^2 dt \tag{2.3}$$

subject to the partial differential equation (PDE)

$$\frac{\partial C}{\partial t} + v\frac{\partial C}{\partial x} = D\frac{\partial^2 C}{\partial x^2} - kC, \ \forall x \in (0,1), \ \forall t > 0, \tag{2.4}$$

with initial and boundary conditions

$$C(x,0) = 0, \tag{2.5}$$

$$C(0,t) = u(t), \tag{2.6}$$

$$D\frac{\partial C}{\partial x}\Big|_{x=1} = 0. \tag{2.7}$$

The reference trajectory $J_{des}(t) \geq 0, \forall t > 0$ is a desired cellular uptake rate at one boundary (at $x = 1$)

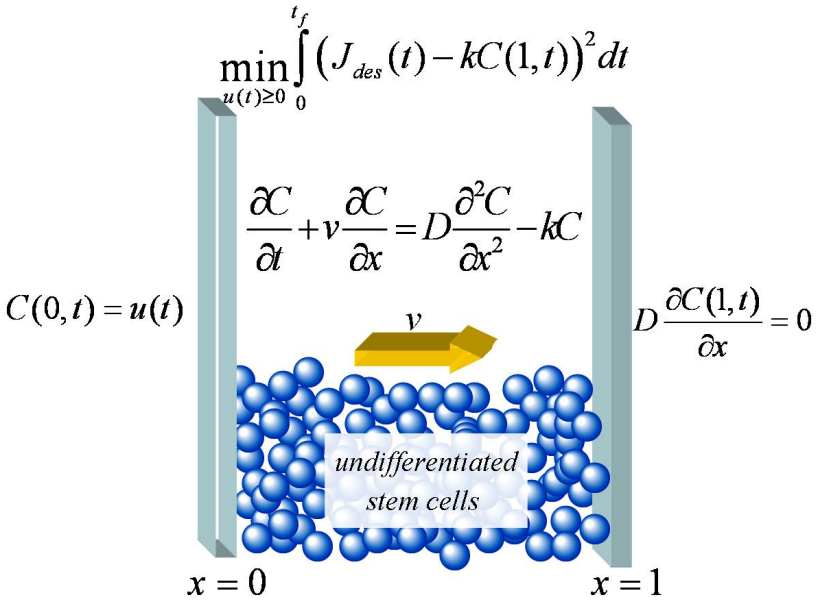

Figure 2.3: Boundary control at $x = 0$ with a Neumann boundary condition at $x = 1$.

and the control trajectory is the concentration $u(t)$ at the other boundary ($x = 0$) (see Figure 2.3). The control input $u(t)$ is the concentration of growth factor, which is nonnegative. This problem arises when the objective is to ensure that a desired time-varying uptake of a growth factor occurs at a specified distance (of 1 dimensionless unit) from a position where the growth factor is released through micro- or nanoparticles or is carried with fluid entering the tissue at $x = 0$ (this fluid also brings nutrients such as glucose to the cells). The cells within the domain would uptake at least as much growth factor as cells at $x = 1$, ensuring that all of the cells within the domain respond to the growth factor.

2.3 Basis Function Expansion

This method generalizes an approach studied in the mid-1980s to solve optimal control problems for systems described by ordinary differential equations [171] to PDEs, in a similar manner as has been done for sheet and film processes (e.g., see [62, 69, 71], and citations therein) as well as nonlinear PDEs such as Burgers equation [116]. To apply this method, start with the analytical solution to the PDE (2.4):

$$C(1,t) = e^{\frac{v}{2D}} D \sum_{n=1}^{\infty} \mu_n B_n \sin(\sqrt{\mu_n}) \int_0^t u(\tau) e^{-(\frac{v^2}{4D} + k + \mu_n D)(t-\tau)} d\tau, \tag{2.8}$$

where

$$B_n = 4\frac{\frac{v}{v+2D}\left(\frac{\sin\sqrt{\mu_n}}{\sqrt{\mu_n}} - \cos\sqrt{\mu_n}\right) - 1 + \cos\sqrt{\mu_n}}{2\sqrt{\mu_n} - \sin(2\sqrt{\mu_n})} \tag{2.9}$$

and μ_n is the nth root of

$$\tan\sqrt{\mu_n} = -2\sqrt{\mu_n}D/v. \tag{2.10}$$

Parameterize the control trajectory

$$u(t) \approx \sum_{i=1}^{n} a_i\phi_i(t) = a^T\phi(t), \tag{2.11}$$

in terms of any set of linearly independent basis functions $\{\phi_i(t)\}$, where

$$a = \begin{bmatrix} a_1 \\ a_2 \\ \vdots \\ a_n \end{bmatrix}, \quad \phi(t) = \begin{bmatrix} \phi_1(t) \\ \phi_2(t) \\ \vdots \\ \phi_n(t) \end{bmatrix}. \tag{2.12}$$

With $f_i(t)$ defined as the solution to the PDE (2.3) for the input $\phi_i(t)$,

$$f_i(t) = e^{\frac{v}{2D}} D \sum_{n=1}^{\infty} \mu_n B_n \sin(\sqrt{\mu_n}) \int_0^t \phi_i(\tau) e^{-(\frac{v^2}{4D} + k + \mu_n D)(t-\tau)} d\tau, \tag{2.13}$$

and

$$f(t) = \begin{bmatrix} f_1(t) \\ f_2(t) \\ \vdots \\ f_n(t) \end{bmatrix}, \tag{2.14}$$

the optimal control problem with $u(t)$ parameterized by (2.11) can be written as

$$\min_{a^T\phi(t)\geq 0} \int_0^{t_f} (J_{des}(t) - ka^T f(t))^2 dt \tag{2.15}$$

as the function (2.8) is a linear operator on $u(t)$. While this approach does reduce the optimization over a function $u(t)$ to the optimization of a finite number of parameters a, the inequality constraint (2.15) remains defined over a continuum. The simplification occurs by dropping the nonnegativity constraint on $u(t)$ to enable an approximate analytical solution to the optimal control problem to be obtained:

$$\frac{d}{da}\int_0^{t_f} \left(J_{des}^2(t) - 2kJ_{des}(t)a^T f(t) + (ka^T f(t))^2\right) dt \tag{2.16}$$

$$= \int_0^{t_f} \left(-2kJ_{des}(t)f(t) + 2k^2 f(t)f^T(t)a\right) dt = 0, \tag{2.17}$$

$$\implies a = \frac{1}{k}\left(\int_0^{t_f} f(t)f^T(t)dt\right)^{-1} \int_0^{t_f} J_{des}(t)f(t)dt \tag{2.18}$$

$$\implies u(t) = \phi^T(t)a = \frac{\phi^T(t)}{k}\left(\int_0^{t_f} f(t)f^T(t)dt\right)^{-1} \int_0^{t_f} J_{des}(t)f(t)dt. \tag{2.19}$$

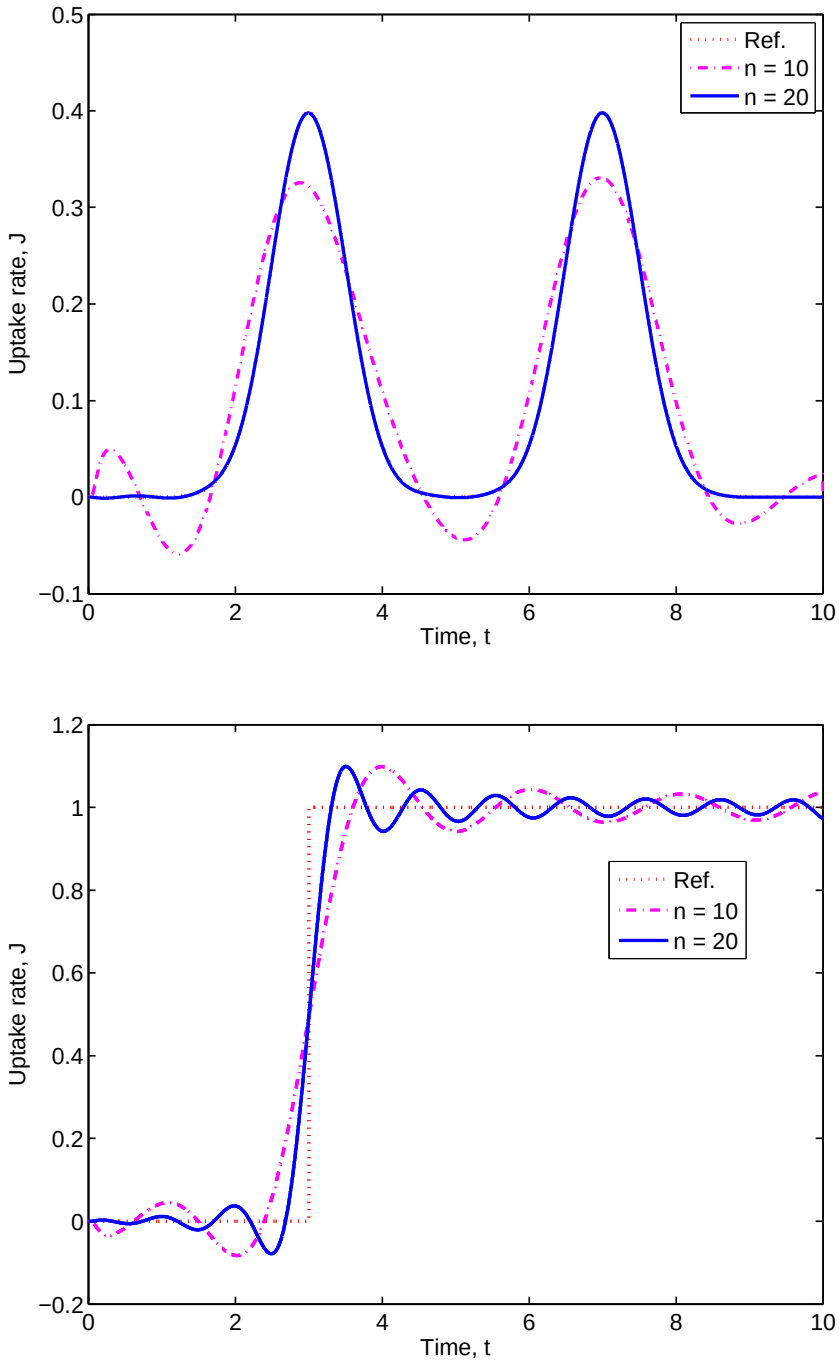

Figure 2.4: Outputs using the basis function expansion approach for reference trajectories that are Gaussian and step functions (for $D = v = 1$ and $k = 7.6$, which are the nondimensionalized parameters used for the entire chapter). The number of basis functions is n and the number of eigenfunctions for the spatial variable was 10. The negative uptake rate is the result of a negative growth factor release, which is not physically realizable. Gaussian reference trajectories are reported in the literature as being desirable for some tissue engineering applications, e.g., [73].

There are many choices of basis functions [62, 71] for which the temporal accuracy to the solution of the unconstrained optimal control problem is specified directly by the number of basis functions. A set of basis functions that provides excellent performance for one reference trajectory can give poor performance for another. For example, excellent tracking performance is obtained for a Gaussian reference trajectory [54], using 20 terms in a truncated Fourier cosine series [75] as the basis functions $\phi_i(t)$ (see Figure 2.4(a)). On the other hand, this same set of basis functions (i) can have oscillations near discontinuities along the time axis due to the Gibbs phenomenon [80, 204], and (ii) does not take into account the nonnegativity constraint on the control variable, which can result in constraint violations. Figure 2.4(b) shows both deficiencies for a step reference trajectory.

2.4 Method of Moments

While the method of moments has been widely applied for the solution of optimal control problems involving population balance models [27, 168], the approach has had little application to other control problems. An exception is its application to determine the control needed to bring a distributed parameter system with nonzero initial condition to quiescent conditions in the least time [33]. Here we present a new and very different approach to applying method of moments to optimal control problems, that utilizes analytical expressions derived for the moments of the output variables in a partial differential equation in terms of the moments of the input variables.

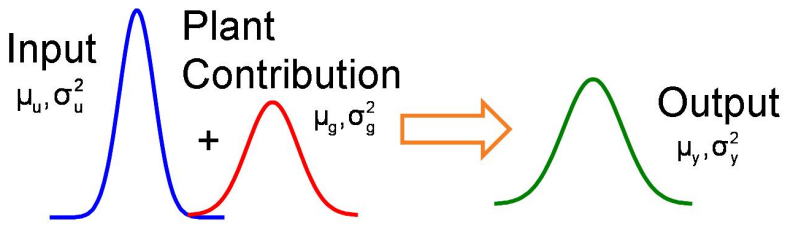

Figure 2.5: A schematic of the approach of applying the Method of Moments to the optimal control problem.

For a linear system g with a bounded input $u(t)$ that approaches zero sufficiently fast as $t \to \infty$ and a bounded output $y(t)$, the input and output are related by [5]

$$\mu_y = \mu_g + \mu_u, \tag{2.20}$$

$$\sigma_y^2 = \sigma_g^2 + \sigma_u^2, \tag{2.21}$$

where μ_f is the mean residence time defined by

$$\mu_f = \frac{\int_0^\infty t f(t)dt}{\int_0^\infty f(t)dt}, \tag{2.22}$$

and σ_f^2 is the variance

$$\sigma_f^2 = \frac{\left(\int_0^\infty t^2 f(t)dt\right)\left(\int_0^\infty f(t)dt\right) - \left(\int_0^\infty t f(t)dt\right)^2}{\left(\int_0^\infty f(t)dt\right)^2}, \tag{2.23}$$

which is a measure of the spread of the function $f(t)$ about its mean (Figure 2.5). The subscript y refers to output, u refers to input, and g refers to the linear system relating u and y. Equations (2.20) and (2.21) can be proved using the Laplace transforms of the input ($U(s)$), output ($Y(s)$), and process ($Y(s) = G(s)U(s)$). First note that

$$(-1)^n U^{(n)}(0) = \int_0^\infty t^n u(t)dt \tag{2.24}$$

provided the integral exists [5],[1] where $U^{(n)}$ is the nth derivative of $U(s)$ with respect to s. Equations (2.20) and (2.21) follow from (2.24) and application of the chain rule:

$$\begin{aligned}
\mu_y &= \frac{\int_0^\infty t y(t)dt}{\int_0^\infty y(t)dt} \\
&= \frac{-Y^{(1)}(0)}{Y(0)} \\
&= \frac{-G^{(1)}(0)U(0) - G(0)U^{(1)}(0)}{G(0)U(0)} \\
&= -\frac{G^{(1)}(0)}{G(0)} - \frac{U^{(1)}(0)}{U(0)} \\
&= \mu_g + \mu_u,
\end{aligned} \tag{2.25}$$

$$\begin{aligned}
\sigma_y^2 + \mu_y^2 &= \frac{\int_0^\infty t^2 y(t)dt}{\int_0^\infty y(t)dt} \\
&= \frac{Y^{(2)}(0)}{Y(0)} \\
&= \frac{G^{(2)}(0)U(0) + 2G^{(1)}(0)U^{(1)}(0) + U^{(2)}(0)G(0)}{G(0)U(0)} \\
&= \frac{G^{(2)}(0)}{G(0)} + 2\frac{G^{(1)}(0)}{G(0)}\frac{U^{(1)}(0)}{U(0)} + \frac{U^{(2)}(0)}{U(0)} \\
&= \sigma_g^2 + \mu_g^2 + 2\mu_g\mu_u + \sigma_u^2 + \mu_u^2,
\end{aligned} \tag{2.26}$$

which implies (2.21), after application of (2.25).

When used together, equations (2.20), (2.21), and (2.24) enable the determination of the mean residence

[1] Existence is implied, for example, if the Laplace transform of the function $u(t)$ is analytic in the closed right-half plane.

time and spread of the output of a linear system without analytical or numerical determination of $g(t)$ or $y(t)$. This property is especially useful for distributed parameter systems for which these functions are unknown, or are known but described by complicated infinite series. Analytical expressions can be derived for μ_g and σ_g directly from the Laplace transform of the PDE with respect to time, and μ_y and σ_y computed easily from (2.20) and (2.21).

To illustrate these ideas, consider the transfer function obtained by taking the Laplace transform of (2.3) with respect to time. By taking Laplace transform, the PDE (2.3) becomes

$$DC'' - vC' - (k+s)C = 0. \tag{2.27}$$

By solving the characteristic equation, the eigenvalues are found to be

$$\xi_{1,2} = \frac{v \pm \sqrt{v^2 + 4D(k+s)}}{2D}. \tag{2.28}$$

The solution is of the form

$$C(x,s) = Ae^{\xi_1 x} + Be^{\xi_2 x}, \tag{2.29}$$

where A and B are to be determined from the boundary conditions (2.6) and (2.7):

$$C(0,s) = A + B = 0, \tag{2.30}$$

$$C'(1,s) = A\xi_1 e^{\xi_1} + B\xi_2 e^{\xi_2} = 0. \tag{2.31}$$

By solving (2.30) and (2.31),

$$A = -\frac{\xi_2 e^{\xi_2}}{\xi_1 e^{\xi_1} - \xi_2 e^{\xi_2}} U(s), \tag{2.32}$$

$$B = \frac{\xi_1 e^{\xi_1}}{\xi_1 e^{\xi_1} - \xi_2 e^{\xi_2}} U(s), \tag{2.33}$$

which results in the solution

$$C(x,s) = \frac{\xi_1 e^{\xi_1} e^{\xi_2 x} - \xi_2 e^{\xi_2} e^{\xi_1 x}}{\xi_1 e^{\xi_1} - \xi_2 e^{\xi_2}} U(s). \tag{2.34}$$

At the location of the interest $x = 1$,

$$\begin{aligned} C(1,s) &= \frac{\xi_1 e^{\xi_1+\xi_2} - \xi_2 e^{\xi_2+\xi_1}}{\xi_1 e^{\xi_1} - \xi_2 e^{\xi_2}} U(s) \\ &= e^{v/D} \frac{\xi_1 - \xi_2}{\xi_1 e^{\xi_1} - \xi_2 e^{\xi_2}} U(s). \end{aligned} \tag{2.35}$$

This implies that the transfer function is

$$G(s) = \frac{kC(1,s)}{U(s)} = ke^{v/D}\frac{\xi_1 - \xi_2}{\xi_1 e^{\xi_1} - \xi_2 e^{\xi_2}}. \tag{2.36}$$

From (2.24), exact analytical expressions for

$$\mu_g = -\frac{G^{(1)}(0)}{G(0)}, \tag{2.37}$$

$$\sigma_g = \sqrt{\frac{G^{(2)}(0)}{G(0)} - \left(\frac{G^{(1)}(0)}{G(0)}\right)^2}, \tag{2.38}$$

are obtained from $G(s)$ using Mathematica or Maple. The expressions for μ_g and σ_g derived in the time domain are more complicated. Insertion of $u(t) = \delta(t)$ into the analytical solution (2.8) results in

$$\mu_g = \frac{\int_0^\infty tC(1,t)dt}{\int_0^\infty C(1,t)dt} = \frac{\sum_{n=1}^{\infty} \frac{\mu_n B_n \sin\sqrt{\mu_n}}{(v^2/4D + k + \mu_n D)^2}}{\sum_{n=1}^{\infty} \frac{\mu_n B_n \sin\sqrt{\mu_n}}{v^2/4D + k + \mu_n D}} \tag{2.39}$$

$$\sigma_g^2 + \mu_g^2 = \frac{\int_0^\infty t^2 C(1,t)dt}{\int_0^\infty C(1,t)dt} = \frac{2\sum_{n=1}^{\infty} \frac{\mu_n B_n \sin\sqrt{\mu_n}}{(v^2/4D + k + \mu_n D)^3}}{\sum_{n=1}^{\infty} \frac{\mu_n B_n \sin\sqrt{\mu_n}}{v^2/4D + k + \mu_n D}}, \tag{2.40}$$

where each μ_n in (2.10) has to be solved iteratively. Depending on the values for the model parameters v, D, and k, a large number of terms in the summations may be needed for the convergence.

While moments have been applied to the analysis of PDEs for decades [4], here we apply these expressions to obtain a highly computationally efficient algorithm for solving an optimal boundary control problem. The reference trajectory J_{des} is decomposed into a linear combination of nonnegative basis functions, each of which is parameterized by mean time $\mu_{y,i}$ and variance $\sigma_{y,i}^2$. The form of the basis function is selected such that the shape of the optimal control trajectory ϕ_i is known and parameterized by mean time and variance that are computed from the known μ_g, σ_g, (2.20), and (2.21):

$$\mu_{\phi,i} = \mu_{y,i} - \mu_g, \tag{2.41}$$

$$\sigma_{\phi,i}^2 = \sigma_{y,i}^2 - \sigma_g^2. \tag{2.42}$$

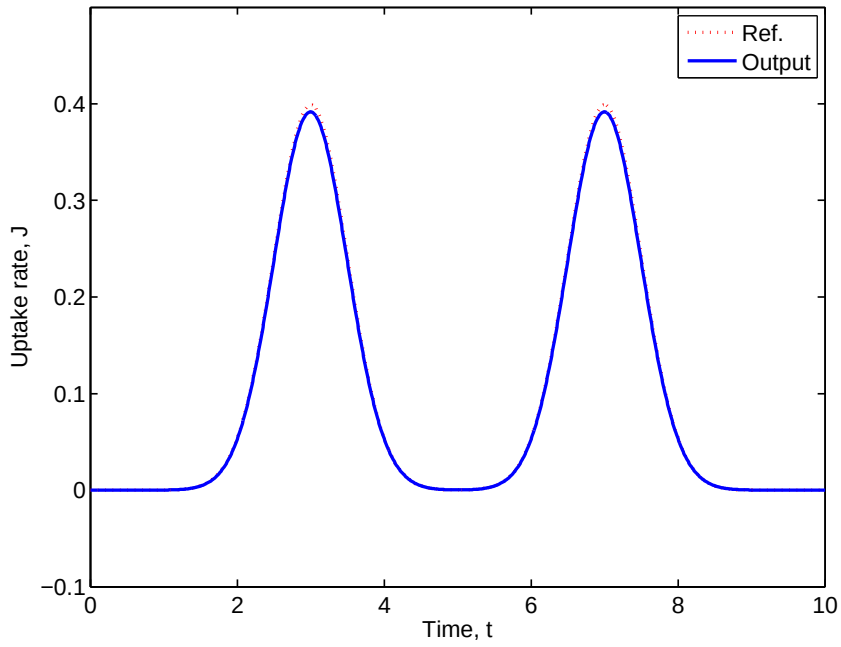

Figure 2.6: Optimal uptake rate computed using the method-of-moments approach. With $v = D = 1$ and $k = 7.6$, and the transfer function (2.36), Maple gives $G(0) = \lim_{s\to 0} G(s) = 1.289$, $G^{(1)}(0) = \lim_{s\to 0} \frac{\partial G(s)}{\partial s} = -0.2163$, and $G^{(2)}(0) = \lim_{s\to 0} \dfrac{\partial^2 G(s)}{\partial s^2} = 0.04828$. These values imply that $\mu_g = \frac{0.2163}{1.289} = 0.1678$, $\sigma_g^2 + \mu_g^2 = \frac{0.04828}{1.289} = 0.03746$, $\sigma_y^2 = \sigma_u^2 + 0.00930$, and $\mu_y = \mu_u + 0.168$, which agree with values obtained by the time-domain expressions (2.39)-(2.40).

The overall optimal control trajectory is computed by summing the optimal control trajectories corresponding to each of the basis functions, as in (2.11). This approach provides nearly perfect tracking for a Gaussian reference trajectory using Gaussian basis functions [54], for which the optimal control trajectories are Gaussian-like functions (see Figure 2.6). This approach is very computationally efficient for computing a nonnegative optimal control trajectory.

2.5 Internal Model Control

The analytical expressions derived for internal model control [148] apply to real-rational functions with time delay rather than to the irrational transfer function (2.36). One approach to deriving a real-rational transfer function for the PDE (2.3) starts by taking the Laplace transform of (2.8) to obtain

$$G(s) = e^{\frac{v}{2D}D} \sum_{n=1}^{\infty} \frac{\mu_n B_n \sin\sqrt{\mu_n}}{s + v^2/4D + k + \mu_n D}. \tag{2.43}$$

Even with a large number of terms in the summation, this transfer function can have very different high frequency behavior than the PDE (see Figure 2.7). This observation is consistent with the more general observation that analytical solutions for PDEs can have very slow convergence, in which case the solution obtained from a finite number of terms can have poor accuracy [56].

A more promising approach to deriving a real-rational transfer function is to apply the second-order finite-difference method to discretize the spatial variable in (2.3):

$$\frac{dC_i}{dt} = D\frac{C_{i+1} - 2C_i + C_{i-1}}{(\Delta x)^2} - v\frac{C_{i+1} - C_{i-1}}{2\Delta x} - kC_i, \tag{2.44}$$

where each C_i is a concentration, which is a function of time, that corresponds to an equally spaced spatial location with grid spacing Δx, $C_1 = C(0,t)$, $C_n = C(1,t)$, and $C_{n+1} = C_{n-1}$. The state-space equations for the discretized system are

$$\begin{aligned}\frac{d}{dt}\begin{bmatrix} C_1 \\ C_2 \\ \vdots \\ C_n \end{bmatrix} = \Bigg(&\frac{D}{(\Delta x)^2}\begin{bmatrix} -2 & 1 & 0 & \cdots & 0 \\ 1 & -2 & 1 & \ddots & \vdots \\ 0 & \ddots & \ddots & \ddots & 0 \\ \vdots & \ddots & 1 & -2 & 1 \\ 0 & \cdots & 0 & 2 & -2 \end{bmatrix} - \frac{v}{2\Delta x}\begin{bmatrix} 0 & 1 & 0 & \cdots & 0 \\ -1 & 0 & 1 & \ddots & \vdots \\ 0 & \ddots & \ddots & \ddots & 0 \\ \vdots & \ddots & -1 & 0 & 1 \\ 0 & \cdots & 0 & 0 & 0 \end{bmatrix} \\ &-k\begin{bmatrix} 1 & 0 & \cdots & 0 \\ 0 & \ddots & \ddots & \vdots \\ \vdots & \ddots & \ddots & 0 \\ 0 & \cdots & 0 & 1 \end{bmatrix}\Bigg)\begin{bmatrix} C_1 \\ C_2 \\ \vdots \\ C_n \end{bmatrix} + \left(\frac{D}{(\Delta x)^2} + \frac{v}{2\Delta x}\right)\begin{bmatrix} 1 \\ 0 \\ \vdots \\ 0 \end{bmatrix} u(t),\end{aligned} \tag{2.45}$$

$$y = kC(1,t) = \begin{bmatrix} 0 & \cdots & 0 & k \end{bmatrix}\begin{bmatrix} C_1 \\ C_2 \\ \vdots \\ C_n \end{bmatrix}. \tag{2.46}$$

The transfer function from $u(t)$ to $y(t) = kC(1,t)$ is

$$G_r(s) = C(sI - A)^{-1}B, \tag{2.47}$$

where

$$A = \begin{bmatrix} -\frac{2D}{(\Delta x)^2} - k & \frac{D}{(\Delta x)^2} - \frac{v}{2\Delta x} & 0 & \cdots & 0 \\ \frac{D}{(\Delta x)^2} + \frac{v}{2\Delta x} & -\frac{2D}{(\Delta x)^2} - k & \frac{D}{(\Delta x)^2} - \frac{v}{2\Delta x} & \ddots & \vdots \\ 0 & \ddots & \ddots & \ddots & 0 \\ \vdots & \ddots & \frac{D}{(\Delta x)^2} + \frac{v}{2\Delta x} & -\frac{2D}{(\Delta x)^2} - k & \frac{D}{(\Delta x)^2} - \frac{v}{2\Delta x} \\ 0 & \cdots & 0 & \frac{2D}{(\Delta x)^2} & -\frac{2D}{(\Delta x)^2} - k \end{bmatrix}, \tag{2.48}$$

$$B = \begin{bmatrix} \frac{D}{(\Delta x)^2} + \frac{v}{2\Delta x} \\ 0 \\ \vdots \\ 0 \end{bmatrix}, \quad C = \begin{bmatrix} 0 & \cdots & 0 & k \end{bmatrix}. \tag{2.49}$$

This approximate transfer function for the PDE is very accurate over the frequency range of the interest, even with a coarse spatial discretization (see Bode plots in Figure 2.7).

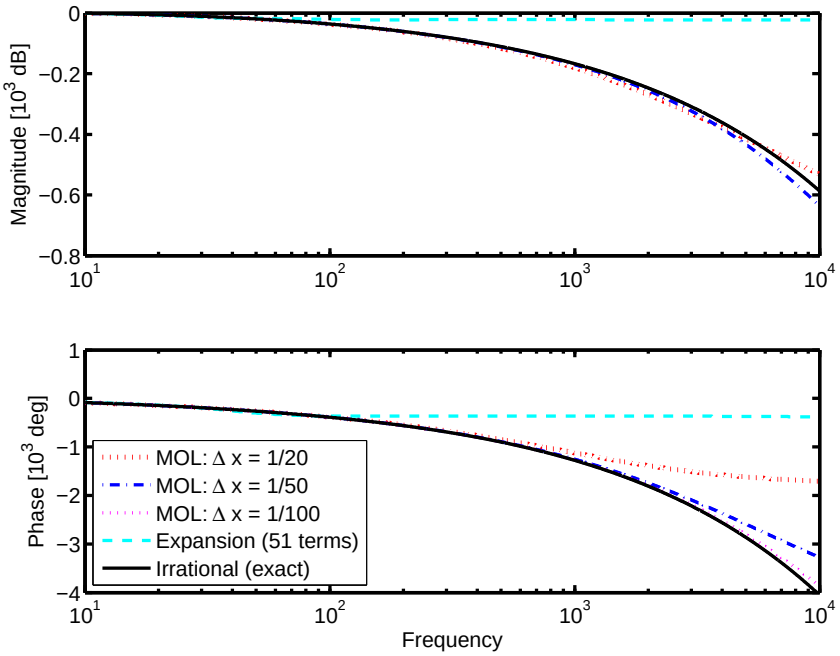

Figure 2.7: Bode plots of various transfer functions.

The real-rational transfer function (2.47) is minimum phase, for which the IMC controller is [148]

$$Q(s) = \frac{F(s)}{G_r(s)}, \tag{2.50}$$

where

$$F(s) = \frac{1}{(\lambda s + 1)^n} \tag{2.51}$$

and λ is the IMC tuning parameter. Applications of IMC for Gaussian and step reference trajectories are shown in Figure 2.8, with λ tuned large enough that the control variable is nonnegative. This approach can give insight into the form of the optimal control trajectory, but is sub-optimal and does not handle general constraints; extensions of IMC to handle constraints [207] are not optimal with respect to the optimization objective (2.3).

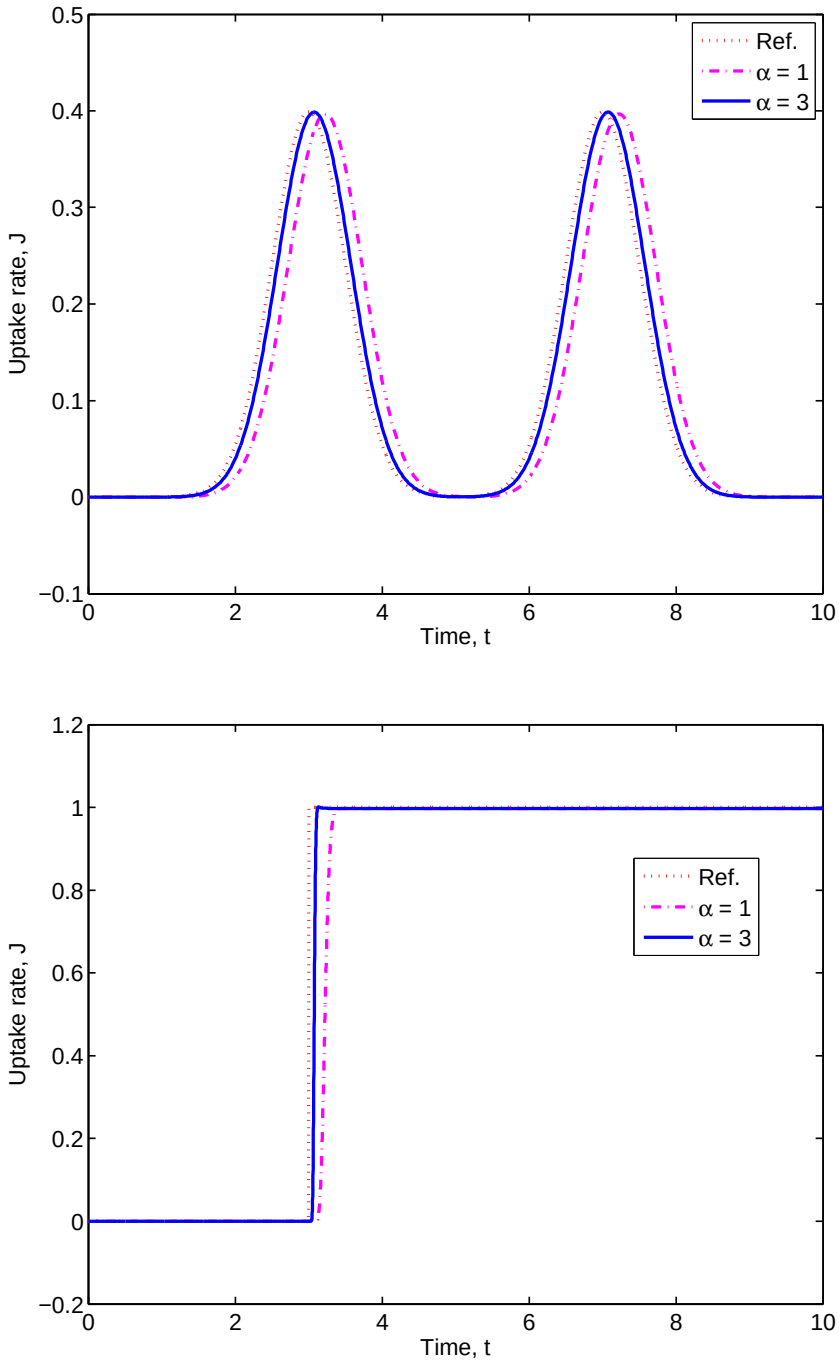

Figure 2.8: Outputs obtained using the IMC approach with $\Delta x = 1/20$ and $\lambda = 0.0112174/\alpha$.

2.6 Model Predictive Control

Model predictive control (MPC) is a well-known method for solving optimal control problems with constraints [128] that has been applied to distributed parameter systems in industry since the late 1970s [165]. Since the early 1990s, many researchers have proposed the application of MPC to lumped parameter models for distributed parameter systems in which the actuation is distributed along a physical boundary (e.g., see [71] and citations therein). Very few papers have considered MPC implementations based on more sophisticated models of distributed parameter systems (see [184, 185] and citations therein). Most closely related to this application, Shang et al. [184, 185] developed an unconstrained MPC formulation that exploits the special characteristics of convection-dominated processes, whereas Patwardhana et al. [162] applied a rather modern state-space MPC formulation to a model similar to (2.3).

In contrast to the usual application of MPC to closed-loop control problems, here MPC is used to solve an open-loop optimal control problem. Also, most MPC formulations assume a staircase control trajectory. To achieve a continuous control trajectory, here the input-output process model was augmented by an integrator and the actual control variable was computed from the integral of the MPC control variable. This MPC formulation is a modification of a standard state-space formulation [14].

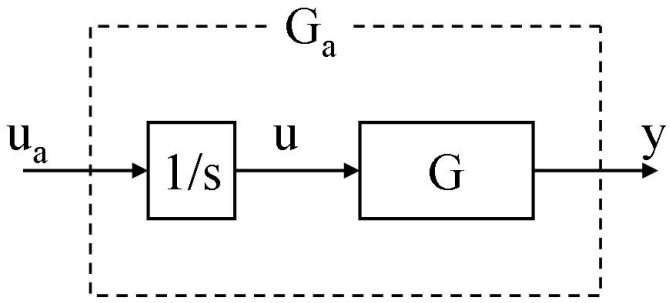

Figure 2.9: Relation between original and augmented continuous-time process models.

2.6.1 MPC Setup

The control trajectory in the tissue engineering application is better modeled as being continuous, which is much more accurately represented by a piecewise-linear rather than the staircase trajectory usually used in MPC formulations. A piecewise-linear trajectory can be implemented by augmenting the process input with an integrator (see Figure 2.9), where u_a is a staircase trajectory. The resulting PDE can be spatially and temporally discretized using the finite-difference method, which is equivalent to converting the continuous-

time model of $G_r(s)/s$ into discrete time, to obtain the state-space model

$$x_a(k+1) = A_a x_a(k) + B_a u_a(k), \tag{2.52}$$

$$y(k) = C_a x_a(k), \tag{2.53}$$

where x_a is the state vector with an integrator and u_a is the control variable for the augmented system (its derivative is u). The value for u_a at time instant k is obtained by solving the optimization:

$$\min_{\Delta u_a(k|k),\ldots,\Delta u_a(k+m-1|k)} \sum_{i=1}^{p} |y(k+i|k) - r(k+i)|^2 \tag{2.54}$$

subject to

$$\Delta u_a(k+i|k) = 0, \quad i = m, \ldots, p-1, \tag{2.55}$$

$$\int_0^t u_a(\tau)d\tau = u(t) \geq 0, \tag{2.56}$$

where

$$\Delta u_a(k) := u_a(k) - u_a(k-1), \tag{2.57}$$

p is the prediction horizon, m is the control horizon, $\Delta u_a(k)$ is the control increment, and "$(k+i|k)$" is the value predicted for time instant $k+i$ based on the information available at time instant k, and $r(k)$ is the reference variable J_{des} at time instant k. At time instant k, the piecewise-linear control trajectory

$$u(t) = \int_0^t u_a(\tau)d\tau \tag{2.58}$$

is implemented on the process, where $u_a(k) = u_a(k-1) + \Delta u_a(k|k)^*$ and $\Delta u_a(k|k)^*$ is the first element of the optimal sequence. The above process is repeated at each sampling instant based on the updated variables.

Prediction

From (2.52) and (2.53), the prediction at time instance k of the future output trajectory is

$$\begin{bmatrix} y(k+1) \\ \vdots \\ y(k+p) \end{bmatrix} = S_x x(k) + S_{u1} u(k-1) + S_u \begin{bmatrix} \Delta u_a(k) \\ \vdots \\ \Delta u_a(k+p-1) \end{bmatrix}, \tag{2.59}$$

where

$$S_x = \begin{bmatrix} C_a A_a \\ C_a A_a^2 \\ \vdots \\ C_a A_a^p \end{bmatrix}, \tag{2.60}$$

$$S_{u1} = \begin{bmatrix} C_a B_a \\ C_a B_a + C_a A_a B_a \\ \vdots \\ \sum_{j=1}^{p} C_a A_a^{j-1} B_a \end{bmatrix}, \tag{2.61}$$

$$S_u = \begin{bmatrix} C_a B_a & 0 & \cdots & 0 \\ C_a B_a + C_a A_a B_a & C_a B_a & \ddots & \vdots \\ \vdots & \vdots & \ddots & 0 \\ \sum_{j=1}^{p} C_a A_a^{j-1} B_a & \sum_{j=1}^{p-1} C_a A_a^{j-1} B_a & \cdots & C_a B_a \end{bmatrix}. \tag{2.62}$$

Optimization Variables

Equation (2.59) relates p outputs $y(k+1|k), \ldots, y(k+p|k)$ and p inputs $\Delta u_a(k|k), \ldots, \Delta u_a(k+p-1|k)$, while only m free optimization variables $\Delta u_a(k), \ldots, \Delta u_a(k+m-1)$ are available. With the optimization variables defined as $z(k+i) := \Delta u_a(k+i)$ for $i = 0, \cdots, m-1$ the last vector of (2.59) is related to the vector z by

$$\begin{bmatrix} \Delta u_a(k) \\ \vdots \\ \Delta u_a(k+p-1) \end{bmatrix} = J_m \begin{bmatrix} z(k) \\ \vdots \\ z(k+m-1) \end{bmatrix}, \tag{2.63}$$

where

$$J_m = \begin{bmatrix} I_m \\ 0_{(p-m)\times m} \end{bmatrix}. \tag{2.64}$$

Objective Function

The MPC objective (2.54) can be written in terms of z as

$$\begin{aligned} J(z) &= \left\| \begin{bmatrix} y(k+1) \\ \vdots \\ y(k+p) \end{bmatrix} - \begin{bmatrix} r(k+1) \\ \vdots \\ r(k+p) \end{bmatrix} \right\|_2^2 \\ &= z^T K_{\Delta u} z + 2 \left(\begin{bmatrix} r(k+1) \\ \vdots \\ r(k+p) \end{bmatrix}^T K_r + u(-1)^T K_u + x(0)^T K_x \right) z + \text{constant} \end{aligned} \tag{2.65}$$

where

$$K_{\Delta u} = J_m^T S_u^T S_u J_m, \tag{2.66}$$

$$K_r = -S_u J_m, \tag{2.67}$$

$$K_u = S_{u1}^T S_u J_m, \tag{2.68}$$

$$K_x = S_x^T S_u J_m. \tag{2.69}$$

Constraints

Satisfying (2.56) requires that $u(i) \geq 0$ for all $i = k+1, \cdots, k+p$, which can be written as

$$\Delta t \begin{bmatrix} 1 & 0 & \cdots & 0 \\ 2 & \ddots & \ddots & \vdots \\ \vdots & \ddots & \ddots & 0 \\ p & \cdots & 2 & 1 \end{bmatrix} \begin{bmatrix} \Delta u_a(k) \\ \vdots \\ \Delta u_a(k+p-1) \end{bmatrix} \geq - \begin{bmatrix} 1 \\ \vdots \\ 1 \end{bmatrix} u(k) - \Delta t \begin{bmatrix} 1 \\ \vdots \\ p \end{bmatrix} u_a(k-1), \tag{2.70}$$

where Δt is the sampling time. Insertion of (2.63) results in the expression in terms of z.

MPC Simulation Results

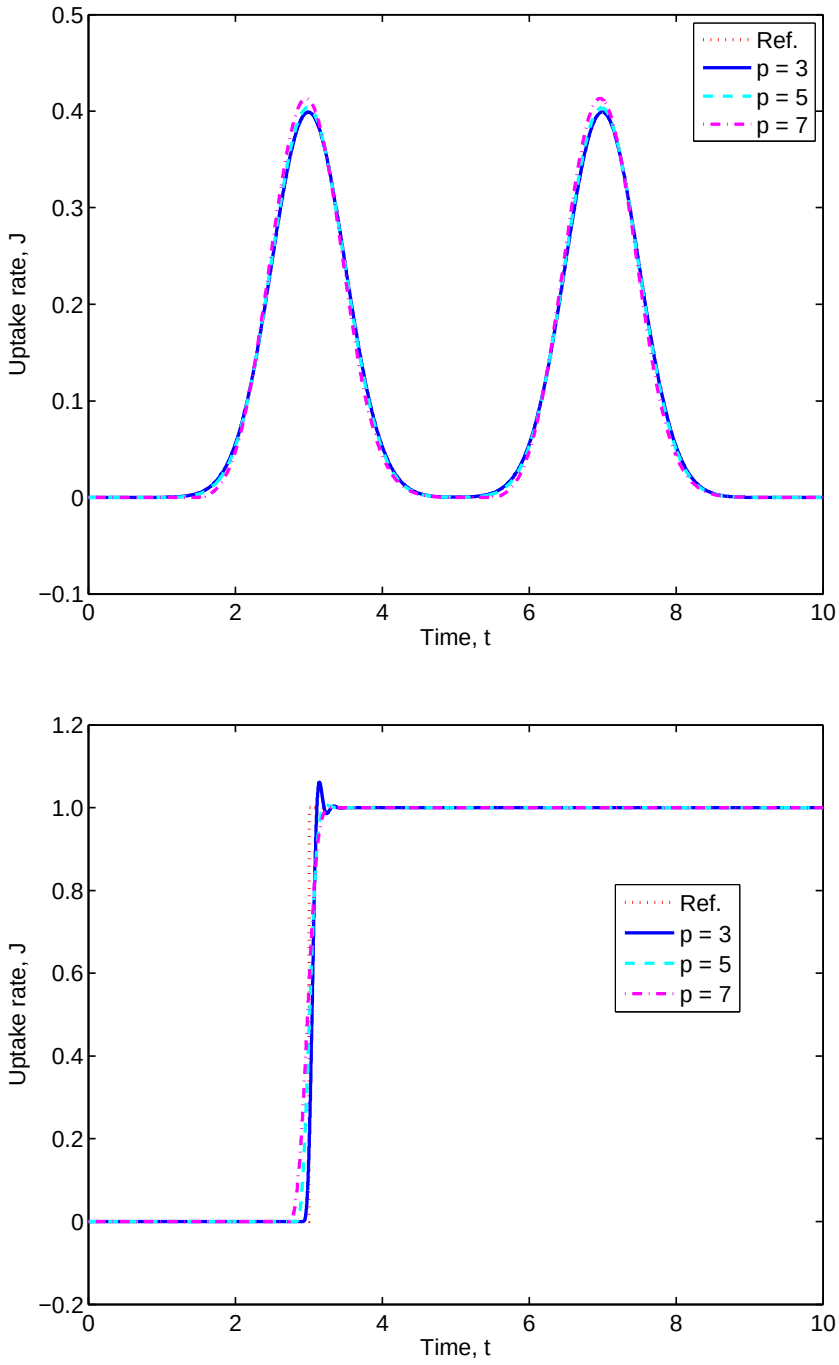

Figure 2.10: MPC outputs for a control horizon of $m = 2$ and a sampling time $\Delta t = 1/10$ obtained for a state-space model obtained by the finite-difference method with $\Delta x = 1/20$.

The convex quadratic program (2.65)-(2.70) was solved at each time instant k by using the *qpdantz* implementation of the Dantzig-Wolfe algorithm in the Matlab Model Predictive Control toolbox [14]. The

MPC formulation gave good reference tracking with short control and prediction horizons as long as the sampling time was small enough (see Figure 2.10).

2.6.2 Computational Requirements

The computational cost of MPC is an important consideration when extending this approach to a larger number of spatial dimensions (2.1)-(2.2). The computational cost for solving (2.65)-(2.70) is a linear or cubic function of the horizons, depending on the details of the numerical implementation [10, 37, 167, 197]. For implementations with a cubic cost dependency, the number of flops required for the MPC computation is orders of magnitude lower than for simultaneous optimization of (2.3) over of the entire time period. For implementations with a linear cost dependency, the MPC approach is similar to simultaneous optimization. More importantly, the MPC implementation with small horizons requires orders-of-magnitude less memory, which is a major consideration for a PDE model with three spatial dimensions.

The 1D optimal control problem is simple enough that simultaneous optimization could be implemented, by choosing m and p to span the entire length of the reference trajectory and dropping the use of the receding horizon. A regularization term of $10^{-4}I$ was added to $K_{\Delta u}$ in the optimization objective (2.54) to remove numerical ill-conditioning that arose due to the large number of degrees of freedom. The time-domain plots were very similar to those obtained from the best MPC tuning (in Figure 2.10), with the total computational cost for both approaches being about 0.1 second as measured by averaging the computation time on an Intel Core Duo computer over 10 trials measured using the Matlab program *tic-toc*.[2] Applying MPC to the optimal control problem resulted in nearly globally optimal results, with many orders-of-magnitude reduction in memory requirements. This suggests that MPC is promising for solving the optimal control problem (2.1) for a larger number of spatial dimensions.

2.7 Conclusions

The strengths and weaknesses of four approaches were investigated for the solution of an optimal control problem motivated by tissue engineering. A basis function expansion approach was computationally efficient but could violate the nonnegativity constraint on the control input and could lead to oscillations at discontinuities (see Figure 2.4(b)), depending on the selection of basis functions and the reference trajectory. Basis functions that have been applied to other distributed parameter systems with convection and diffusion [62, 71] may have promise in this particular application. The internal model control method does not take constraints explicitly into account when optimizing the control objective, and detuning the IMC tuning parameter to satisfy the nonnegativity constraint led to sluggish performance compared to the method-of-moments approach (compare Figures 2.6 and 2.8(a)).

[2]The total computational cost for MPC could be reduced by using warm starting [10, 37].

The new optimal control method based on the method of moments was very highly computationally efficient while enforcing the nonnegativity constraint on the control trajectory (see Figure 2.6). While providing higher performance than IMC for a smooth reference trajectory, it is unclear how to best generalize the approach to deal with state constraints or reference trajectories with discontinuities. The MPC approach was the most powerful method, with the ability to handle control and state constraints, but was also the most computationally expensive. Some results were presented that are of broader interest to the optimal control field:

1. the proposed method-of-moments approach to solving optimal control problems is different from and goes beyond its applications to population balance models [27, 138, 168],

2. MPC is shown to be a useful approach for solving some *non*-receding horizon optimal control problems (in particular, problems in which nearly optimal performance is obtained for a small control horizon).

The chapter considered many approaches to solving the optimal control problem for one spatial dimension, to provide insights into how to best address the much more complicated case of three spatial dimensions. Recall that the 3D control problem (2.1)-(2.2) has too many degrees of freedom to be solved by direct temporal and spatial discretization. The results in Sections 2.3-2.6 suggest that the 3D optimal control problem may be solvable by a combination of multiple design methods. The generality and near optimality of MPC observed in Section 2.3 suggests that MPC is very promising for solving the 3D control problem (2.1)-(2.2). The near optimality of the basis function expansion approach in Section 2.3 suggests that parameterization of the control input in terms of basis functions within such a 3D MPC algorithm would lead to minimal loss in performance for some reference trajectories while further reducing the computational time. The good suboptimal solution obtained by the method-of-moments approach motivates the development of 3D extensions to provide warm starts for a 3D MPC optimization, to speed convergence (such as extension would involve cross-moments, e.g., [138]). Nonlinear uptake kinetics could be addressed by successive solution of linearized problems, just as nonlinear MPC problems are typically solved as a series of linearized MPC problems [129].

CHAPTER 3

WORST-CASE ANALYSIS OF 2D BOUNDARY CONTROL

It is well-known that optimal control trajectories can be highly sensitive to perturbations in the model parameters. Numerical algorithms are presented for the worst-case analysis of the effects of parametric uncertainties on boundary control problems for finite-time distributed parameter systems. The approach is based on replacing the full-order model of the system with a power series or polynomial chaos expansion that is analyzed by linear matrix inequalities or power iterations, which are polynomial-time algorithms. Application to the Dirichlet boundary control of the reaction-diffusion equation to track a desired two-dimensional concentration field illustrates the promise of the approach.

3.1 Introduction

The boundary control of distributed parameter systems (DPS) has received increased interest in recent years for a wide range of applications in mechanical, chemical, and biomedical engineering [25], [133], including microchemical systems [24], tissue engineering [113], and glass cooling [119]. While the analysis of the effects of parametric uncertainties is well established for lumped parameter systems (e.g., see [26],[60],[208]), the field is much less mature for DPS. The three most popular classes of uncertainty analysis approaches for DPS discussed in the control literature are based on (1) application of the Monte Carlo method to the full simulation code (e.g., [157]), (2) running the full simulation code for all parameters obtained by gridding the parameter space (e.g., [157]), and (3) Lyapunov functions (e.g., [164]). The first two classes of numerical algorithms can produce robustness margins with a low level of conservatism but are computationally expensive for problems with multiple spatial dimensions and parameters. For example, using a relatively coarse grid of ten points per parameter requires $10^{\dim(p)}$ runs of the full simulation code, where p is the vector of uncertain parameters. This is computationally feasible only for systems with a small number of parameters. The third class of robustness analysis methods for DPS is not always computationally expensive but apply

only to specific control structures and/or are conservative.

This chapter describes the use of series expansions for worst-case analysis of the effects of uncertainties on boundary control problems for finite-time DPS. The approach is based on the same philosophy as polynomial chaos and power series expansions applied in the environmental field [159], which is to first compute an approximation to the full simulation model, followed by application of robustness analysis to the approximate model. The very low computational cost of the approximate model enables the application of the Monte Carlo method or gridding the parameter space, as in methods (1) and (2) above, as well as the application of polynomial-time norm-based analytical methods as applied here, which include the application of linear matrix inequalities to compute tight upper bounds and power iterations to compute lower bounds on the worst-case deviations of the states and control objectives. The proposed approach is illustrated by application to a boundary control problem for a reaction-diffusion equation with two spatial dimensions.

3.2 Worst-case Analysis

The proposed approach for worst-case robustness analysis of finite-time DPS is to first approximate the original partial differential equation (PDE) by a power series or polynomial chaos expansion and then apply polynomial-time analysis tools developed for providing tight bounds on the worst-case deviations for such expansions [137], [152]. To simplify the presentation, model parameter uncertainties and implementation biases in the boundary control inputs will be collectively referred to as "uncertainties" and collected into a single vector $\delta\lambda$ which is related to the vector of uncertain variables λ and the vector of nominal values λ_{nom} by

$$\lambda := \lambda_{nom} + \delta\lambda. \tag{3.1}$$

The uncertainty set is described by

$$E_\lambda = \{\lambda : \lambda = \lambda_{nom} + \delta\lambda, \|W\delta\lambda\|_r \leq 1\}, \tag{3.2}$$

where W is a specified positive-definite weighting matrix and $\|\cdot\|_r$ is any well-defined norm. For the case where the set of λ contains time-invariant vectors, examples of such norms are the Hölder 1-, 2-, and ∞-norms. For the 2-norm, the uncertainty set is described by a hyperellipsoid. An uncertainty set described by independent upper and lower bounds on each parameter

$$E_\lambda = \{\lambda : \lambda = \hat{\lambda}_{nom} + \delta\hat{\lambda}, \delta\underline{\lambda} \leq \delta\hat{\lambda} \leq \delta\bar{\lambda}\}, \tag{3.3}$$

where the vectors $\delta\underline{\lambda}$ and $\delta\bar{\lambda}$ are the lower and upper bounds on the vector of uncertainties, can be rewritten in terms of (3.2) for $r = \infty$ by specifying[1]

$$W_{ii} = \frac{2}{\delta\bar{\lambda}_i - \delta\underline{\lambda}_i}, \quad W_{ij} = 0, \ \forall i \neq j, \tag{3.4}$$

$$\lambda_{nom} = \hat{\lambda}_{nom} + \frac{1}{2}(\delta\bar{\lambda} + \delta\underline{\lambda}). \tag{3.5}$$

While only a single norm is treated here to simplify the notation, the results can be generalized to the case in which different norms are specified for different sets of elements of λ. This would be useful, for example, if the uncertainties associated with some variables lie within a hyperellipsoidal uncertainty set while the uncertainties of other variables lie within lower and upper bounds on each variable.

The worst-case positive and negative deviations due to uncertainties are defined by

$$\delta\bar{y}_{w.c.} := \max_{\lambda \in E_\lambda} \{y(\lambda) - y(\hat{\lambda})\}, \tag{3.6}$$

and

$$\delta\underline{y}_{w.c.} := \min_{\lambda \in E_\lambda} \{y(\lambda) - y(\hat{\lambda})\} \tag{3.7}$$

where y is a state or output at a particular time t of interest. In general, solving these optimizations is NP-hard [29, 28] and is especially computationally expensive for DPS. This optimization can be greatly simplified, however, by inserting a power series or polynomial chaos expansion of finite order for y into (3.6) and (3.7), for which tight bounds on the worst-case deviation in y and an estimate for a worst-case uncertainty vector can be computed using dual norms, linear matrix inequalities, or power iterations. This approach also applies to any sufficiently smooth function of the states or control objectives.

The power series or polynomial chaos expansion only needs to be an accurate representation for y within the trajectory bundle defined by the uncertainty description, and does not need to be an accurate representation for the entire state space. This enables the use of fairly low order expansions to obtain accurate estimate of worst-case deviation, with low computational cost. The remainder of this section presents specific expressions for robust analysis for first- and second-order expansions, and the procedure for higher order expansions.

3.2.1 First-Order Series Expansion

Define the first-order expansion written in terms of deviation variables as

$$\delta y_1 := M\delta\lambda \approx y(\lambda) - y(\lambda_{nom}), \tag{3.8}$$

[1] $\delta\bar{\lambda}_i \neq \delta\underline{\lambda}_i$ for all i because λ is an uncertain vector.

where

$$M_i := \left.\frac{\partial y}{\partial \lambda_i}\right|_{\lambda=\lambda_{nom}}, \tag{3.9}$$

provided that y is differentiable in λ. The optimization (3.6) with this first-order expansion used in the objective can be solved analytically for a wide variety of norms including all of the Hölder norms. For example, for the ∞-norm the solution is

$$\max_{\|W\delta\lambda\|_\infty \leq 1} \delta y_1 = \max_{\|W\delta\lambda\|_\infty \leq 1} M\delta\lambda = \max_{\|W\delta\lambda\|_\infty \leq 1} |M\delta\lambda| = \|MW^{-1}\|_1, \tag{3.10}$$

which a standard result for dual norms. A worst-case uncertainty vector is[2]

$$\delta\lambda_{w.c.} = W^{-1}e, \tag{3.11}$$

where

$$e_i = \frac{(MW^{-1})_i}{|(MW^{-1})_i|}. \tag{3.12}$$

With this worst-case uncertainty vector, the first-order estimate of the maximum worst-case deviation in y is

$$\delta\bar{y}_{1,w.c.} = M\delta\lambda_{w.c.} = \sum_i \left|(MW^{-1})_i\right|. \tag{3.13}$$

The first-order estimate of the minimum worst-case deviation in y is

$$\delta\underline{y}_{1,w.c.} = -M\delta\lambda_{w.c.} = -\sum_i \left|(MW^{-1})_i\right|, \tag{3.14}$$

which is obtained by using $-\delta\lambda_{w.c.}$ for the worst-case uncertainty vector.

3.2.2 Second- and Higher Order Expansions

Similarly, define the second-order expansion as

$$\delta y_2 := M\delta\hat{\lambda} + \delta\hat{\lambda}^T H\delta\hat{\lambda} \approx y(\hat{\lambda}) - y(\hat{\lambda}_{nom}), \tag{3.15}$$

where

$$M_i := \left.\frac{\partial y}{\partial \hat{\lambda}_i}\right|_{\hat{\lambda}=\hat{\lambda}_{nom}}, \tag{3.16}$$

and

$$H_{ij} := \frac{1}{2}\left.\frac{\partial^2 y}{\partial\hat{\lambda}_i\partial\hat{\lambda}_j}\right|_{\hat{\lambda}=\hat{\lambda}_{nom}}, \tag{3.17}$$

[2]This vector is not necessarily unique.

for any doubly differentiable function. The second-order estimates of the maximum and minimum worst-case deviations in y are

$$\delta\bar{y}_{2,w.c.} := \max_{\delta\hat{\lambda}} \delta y_2, \tag{3.18}$$

$$\delta\underline{y}_{2,w.c.} := \min_{\delta\hat{\lambda}} \delta y_2, \tag{3.19}$$

subject to the constraint (3.3).

The estimates can be written in terms of the mixed structured singular value μ [29]. For any real k,

$$\max_{\delta\underline{\lambda}\le\delta\hat{\lambda}\le\delta\bar{\lambda}} |\delta y_2| = \max_{\delta\underline{\lambda}\le\delta\hat{\lambda}\le\delta\bar{\lambda}} |M\delta\hat{\lambda} + \delta\hat{\lambda}^T H\delta\hat{\lambda}| \ge k \quad \Longleftrightarrow \quad \mu_\Delta(N) \ge k, \tag{3.20}$$

where

$$N := \begin{bmatrix} 0 & 0 & kw \\ kH & 0 & kHz \\ z^T H + M & w^T & z^T Hz + Mz \end{bmatrix}, \tag{3.21}$$

$$w := \frac{1}{2}(\delta\bar{\lambda} - \delta\underline{\lambda}), \tag{3.22}$$

$$z := \frac{1}{2}(\delta\bar{\lambda} + \delta\underline{\lambda}), \tag{3.23}$$

the perturbation block $\Delta = \mathrm{diag}(\Delta_r, \Delta_r, \delta_c)$, Δ_r consists of independent real scalars, and δ_c is a complex scalar. This implies that

$$\max_{\delta\underline{\lambda}\le\delta\hat{\lambda}\le\delta\bar{\lambda}} |\delta y_2| = \max_{\mu_\Delta(N)\ge k} k := k_\Delta \tag{3.24}$$

where the right-hand side can be computed from a single skewed mixed structured singular value calculation [72]. The worst-case perturbation vector determines whether the perturbation $\delta\lambda$ that achieves the maximum in

$$\max_{\delta\underline{\lambda}\le\delta\hat{\lambda}\le\delta\bar{\lambda}} |\delta y_2| \tag{3.25}$$

produces a positive or negative δy_2, which corresponds to $\delta\bar{y}_{2,w.c.}$ or $\delta\underline{y}_{2,w.c.}$, respectively. If the δy_2 computed by insertion of this worst-case perturbation into the quadratic equation is positive,

$$\delta\bar{y}_{2,w.c.} = k_\Delta, \tag{3.26}$$

define

$$\delta\tilde{y}_2 := \delta y_2 - k_\Delta, \tag{3.27}$$

then

$$\max_{\delta\underline{\lambda}\le\delta\hat{\lambda}\le\delta\bar{\lambda}} |\delta\tilde{y}_2| = \max_{\mu_\Delta(\tilde{N})\ge\tilde{k}} \tilde{k} := \tilde{k}_\Delta, \tag{3.28}$$

where

$$\tilde{N} := \begin{bmatrix} 0 & 0 & \tilde{k}w \\ \tilde{k}H & 0 & \tilde{k}Hz \\ z^TH + M & w^T & z^THz + Mz - k_\Delta \end{bmatrix}. \tag{3.29}$$

That $\delta\tilde{y}_2$ can take any value in the interval

$$[\delta\underline{y}_{2,w.c.} - k_\Delta, 0] \tag{3.30}$$

implies that

$$\tilde{k}_\Delta = -\delta\underline{y}_{2,w.c.} + k_\Delta \tag{3.31}$$

and

$$\delta\underline{y}_{2,w.c.} = k_\Delta - \tilde{k}_\Delta \tag{3.32}$$

so that both the minimum and maximum perturbation in y_2 are determined.

If the δy_2 computed by insertion of the worst-case perturbation from (3.24) into the quadratic equation is negative,

$$\delta\underline{y}_{2,w.c.} = -k_\Delta, \tag{3.33}$$

define

$$\delta\hat{y}_2 := \delta y_2 + k_\Delta, \tag{3.34}$$

then

$$\max_{\delta\underline{\lambda}\le\delta\hat{\lambda}\le\delta\bar{\lambda}} |\delta\hat{y}_2| = \max_{\mu_\Delta(\hat{N})\ge\hat{k}} \hat{k} := \hat{k}_\Delta, \tag{3.35}$$

where

$$\hat{N} := \begin{bmatrix} 0 & 0 & \hat{k}w \\ \hat{k}H & 0 & \hat{k}Hz \\ z^TH + M & w^T & z^THz + Mz + k_\Delta \end{bmatrix}. \tag{3.36}$$

That $\hat{y}_2$ can take any value in the interval

$$[0, \delta\bar{y}_{2,w.c.} + k_\Delta] \tag{3.37}$$

implies that

$$\hat{k}_\Delta = \delta\bar{y}_{2,w.c.} + k_\Delta \tag{3.38}$$

and

$$\delta\bar{y}_{2,w.c.} = \hat{k}_\Delta - k_\Delta, \tag{3.39}$$

indicating again that the minimum and maximum values for y_2 can be computed from two skewed mixed structured singular value calculations.

An alternative approach can be derived based on an *a priori* upper bound c on $|\delta y_2|$ over (3.3). Such an upper bound can be determined using the relation

$$\delta\hat{\lambda} = \lambda_{nom} - \hat{\lambda}_{nom} + \delta\lambda \tag{3.40}$$

and applying some standard results from linear algebra:

$$\begin{aligned}
&\max_{\delta\underline{\lambda}\le\delta\hat{\lambda}\le\delta\bar{\lambda}} |M\delta\hat{\lambda} + \delta\hat{\lambda}^T H\delta\hat{\lambda}| \\
&= \max_{\|W\delta\lambda\|_\infty\le 1} |M(\lambda_{nom} - \hat{\lambda}_{nom} + \delta\lambda) + (\lambda_{nom} - \hat{\lambda}_{nom} + \delta\lambda)^T H(\lambda_{nom} - \hat{\lambda}_{nom} + \delta\lambda)| \\
&= \max_{\|W\delta\lambda\|_\infty\le 1} |M(\lambda_{nom} - \hat{\lambda}_{nom}) + (\lambda_{nom} - \hat{\lambda}_{nom})^T H(\lambda_{nom} - \hat{\lambda}_{nom}) \\
&\qquad\qquad + (M + 2(\lambda_{nom} - \hat{\lambda}_{nom})^T H + \delta\lambda^T H)\delta\lambda| \\
&\le |M(\lambda_{nom} - \hat{\lambda}_{nom}) + (\lambda_{nom} - \hat{\lambda}_{nom})^T H(\lambda_{nom} - \hat{\lambda}_{nom})| \\
&\qquad\qquad + \max_{\|W\delta\lambda\|_\infty\le 1} |(M + 2(\lambda_{nom} - \hat{\lambda}_{nom})^T H + \delta\lambda^T H)\delta\lambda| \\
&\le |M(\lambda_{nom} - \hat{\lambda}_{nom}) + (\lambda_{nom} - \hat{\lambda}_{nom})^T H(\lambda_{nom} - \hat{\lambda}_{nom})| \\
&\qquad\qquad + \max_{\|W\delta\lambda\|_\infty\le 1} \|(M + 2(\lambda_{nom} - \hat{\lambda}_{nom})^T H + \delta\lambda^T H)W^{-1}\|_1 := c
\end{aligned} \tag{3.41}$$

where the latter optimization can be solved in polynomial-time by linear programming. For such an upper bound c,

$$\delta\bar{y}_{2,w.c.} + c = \max_{\delta\underline{\lambda}\le\delta\hat{\lambda}\le\delta\bar{\lambda}} \delta y_2 + c \ge k_c \quad\Longleftrightarrow\quad \mu_\Delta(N_c) \ge k_c, \tag{3.42}$$

where

$$N_c := \begin{bmatrix} 0 & 0 & k_c w \\ k_c H & 0 & k_c H z \\ z^T H + M & w^T & z^T H z + M z + c \end{bmatrix}, \tag{3.43}$$

and the maximum positive value for δy_2 can be computed from

$$\delta\bar{y}_{2,w.c.} = \max_{\mu_\Delta(N_c)\ge k_c} k_c - c. \tag{3.44}$$

Similarly, selecting a negative c with high enough magnitude to ensure that $\delta y_2 + c < 0$[3] results in

$$\delta \underline{y}_{2,w.c.} = - \max_{\mu_\Delta(N_c) \geq k_c} k_c - c. \tag{3.45}$$

A polynomial-time upper bound for the calculation of the skewed mixed structured singular value and a corresponding worst-case perturbation can be computed using linear matrix inequalities [155]. This upper bound is often tight for practical problems, and can be complemented with a polynomial-time lower bound computed by a power iteration [206] to assess conservatism. The advantage of the above k_Δ procedure for computing $\delta \underline{y}_{2,w.c.}$ and $\delta \bar{y}_{2,w.c.}$ is that the approach does not introduce a potentially large number c into the matrix in the skewed mixed structured singular value calculation. The advantage of the c procedure is that lower and upper bounds in the skewed mixed structured singular value calculation directly translate into lower and upper bounds on $\underline{y}_{2,w.c.}$ and $\bar{y}_{2,w.c.}$ via (3.44) and (3.45). This translation is messier for the k_Δ procedure (details not shown for brevity).

Higher order approximations and other norms on the uncertainty set (3.2) can be computed by using multidimensional realization algorithms (e.g., [176]) and the generalized-norm structured singular value (e.g., [43]), respectively.[4]

3.3 Boundary Control Problem

The remainder of this chapter illustrates this robustness analysis approach for the boundary control of the DPS:

$$\frac{\partial C}{\partial t} = D \left(\frac{\partial^2 C}{\partial x^2} + \frac{\partial^2 C}{\partial y^2} \right) - kC, \tag{3.46}$$

with boundary conditions

$$C(0, y, t) = u_{x0}(y, t), \tag{3.47}$$

$$C(1, y, t) = u_{x1}(y, t), \tag{3.48}$$

$$C(x, 0, t) = u_{y0}(x, t), \tag{3.49}$$

$$C(x, 1, t) = u_{y1}(x, t), \tag{3.50}$$

and zero initial condition

$$C(x, y, 0) = 0. \tag{3.51}$$

This parabolic PDE describes the concentration or temperature field C for a reacting solid with mass or heat transfer occurring via molecular motion (diffusion or thermal conduction, respectively), where D is the

[3] For example, selecting c equal to negative the value in (3.41) will work.
[4] These approaches also enable the use of rational approximations.

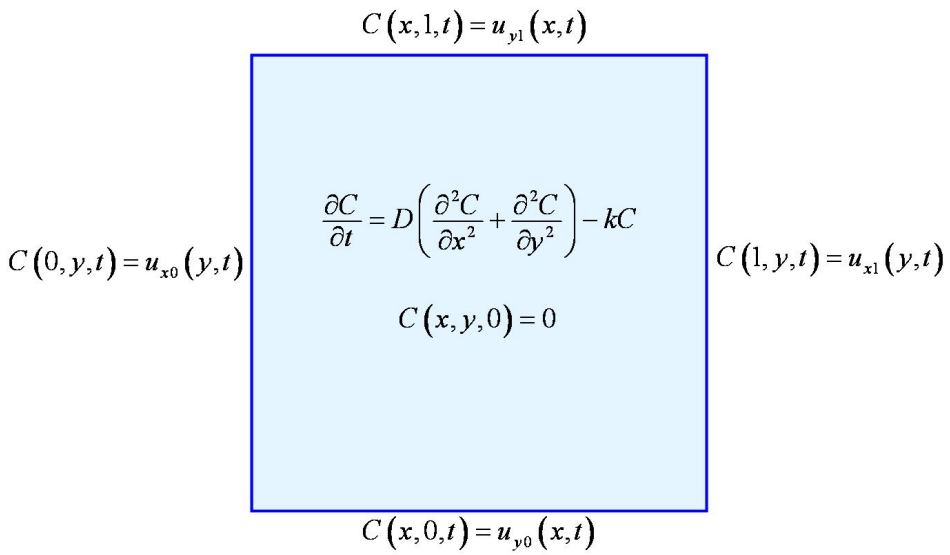

Figure 3.1: Two-dimensional boundary control problem.

diffusion coefficient and k is the reaction rate constant. The control objective is to find feasible boundary control inputs

$$u(x,y,t) = \begin{bmatrix} u_{x0}(y,t) & u_{x1}(y,t) & u_{y0}(x,t) & u_{y1}(x,t) \end{bmatrix}^T \tag{3.52}$$

that produce a field $C(x,y,t)$ that is as close as possible to a reference field $R(x,y,t)$,

$$\min_{u \in \mathcal{U}} \int_0^{t_f} \int_0^1 \int_0^1 \left(R(x,y,t) - C(x,y,t)\right)^2 dxdydt, \tag{3.53}$$

where $\mathcal{U}$ is the domain of the optimization variable $u(x,y,t)$ (sometimes this constraint is necessary to ensure that the boundary control inputs are physically implementable).

3.4 Optimal Control Design

With the boundary control trajectories parameterized in terms of the eigenfunctions of the PDE (3.46) in space and Heaviside step functions S in time,

$$u_{x0}(y,t) = \sum_{i=1}^{I}\sum_{j=1}^{J} a_{x0ij} \sin i\pi y \; S(t-\tau_j), \tag{3.54}$$

$$u_{x1}(y,t) = \sum_{i=1}^{I}\sum_{j=1}^{J} a_{x1ij} \sin i\pi y \; S(t-\tau_j), \tag{3.55}$$

$$u_{y0}(x,t) = \sum_{i=1}^{I}\sum_{j=1}^{J} a_{y0ij} \sin i\pi x \; S(t-\tau_j), \tag{3.56}$$

$$u_{y1}(x,t) = \sum_{i=1}^{I}\sum_{j=1}^{J} a_{y1ij} \sin i\pi x \; S(t-\tau_j), \tag{3.57}$$

the solution to the PDE is

$$C(x,y,t) = \mathbf{a}^T\mathbf{C}, \tag{3.58}$$

where

$$\mathbf{a} = \begin{bmatrix} a_{x011} \\ \vdots \\ a_{x01J} \\ a_{x021} \\ \vdots \\ a_{x0IJ} \\ a_{x111} \\ \vdots \\ a_{x1IJ} \\ a_{y011} \\ \vdots \\ a_{y0IJ} \\ a_{y111} \\ \vdots \\ a_{y1IJ} \end{bmatrix}, \qquad \mathbf{C} = \begin{bmatrix} C_{x011}(x,y,t) \\ \vdots \\ C_{x01J}(x,y,t) \\ C_{x021}(x,y,t) \\ \vdots \\ C_{x0IJ}(x,y,t) \\ C_{x111}(x,y,t) \\ \vdots \\ C_{x1IJ}(x,y,t) \\ C_{y011}(x,y,t) \\ \vdots \\ C_{y0IJ}(x,y,t) \\ C_{y111}(x,y,t) \\ \vdots \\ C_{y1IJ}(x,y,t) \end{bmatrix}, \tag{3.59}$$

and each element of $\mathbf{C}$ corresponds to the solution to the PDE with its corresponding element of $\mathbf{a}$ equal to 1 with all other entries equal to zeros. With $\mathcal{U}$ defined as the constraint that the control input is nonnegative,

substituting (3.58) into the objective function (3.53) gives

$$\min_{\mathbf{a}} \quad \int_0^{t_f}\int_0^1\int_0^1 \left(R(x,y,t) - \mathbf{a}^T\mathbf{C}\right)^2 dxdydt \tag{3.60}$$
$$u(x,y,t) \geq 0$$

which has the same solution as the nonlinear program

$$\begin{aligned} \min \quad & \frac{1}{2}\mathbf{a}^T\mathbf{G}\mathbf{a} + \mathbf{f}^T\mathbf{a}, \\ -Q(x,y)\mathbf{a} \leq 0 \\ 0 \leq x \leq 1 \\ 0 \leq y \leq 1 \end{aligned} \tag{3.61}$$

where

$$\mathbf{G} = \int_0^{t_f}\int_0^1\int_0^1 \mathbf{C}\mathbf{C}^T dxdydt, \tag{3.62}$$
$$\mathbf{f} = -\int_0^{t_f}\int_0^1\int_0^1 R(x,y,t)\mathbf{C}^T dxdydt, \tag{3.63}$$
$$Q(x,y) = \text{diag}(v_x, v_x, v_y, v_y), \tag{3.64}$$

v_x is a row vector collecting $\sin i\pi y\ S(t-\tau_j)$, and v_y is a row vector collecting $\sin i\pi x\ S(t-\tau_j)$ for $i = 1, \cdots, I$ and $j = 1, \cdots, J$. This nonlinear program can be approximately solved to any degree of accuracy as a quadratic program with linear constraints by replacing the constraints by the finite set of linear inequalities that results from evaluating the nonlinear inequality constraint for a fine mesh of (x, y) points over the spatial domain. The significant increase in the number of inequality constraints is offset by the ready availability of very efficient software for solving quadratic programs with large numbers of linear inequality constants. For the case of no constraints, the optimal control inputs are parameterized by

$$\mathbf{a} = -\mathbf{G}^{-1}\mathbf{f}, \tag{3.65}$$

with the optimal field being

$$C_{opt}(x,y,t) = -(\mathbf{G}^{-1}\mathbf{f})^T\mathbf{C}. \tag{3.66}$$

For analysis of the worst-case deviations in the optimal C, the perturbations in the uncertain variables are

$$\delta\lambda = \begin{bmatrix} \delta D & \delta k & \delta u_{x0} & \delta u_{x1} & \delta u_{y0} & \delta u_{y1} \end{bmatrix}^T, \tag{3.67}$$

where the last four elements are time-invariant additive errors on the four boundary control trajectories.

3.5 Numerical Example

3.5.1 Optimal Control Design

Let the reference field

$$R(x,y,t) = \left(e^{-x} - e^{-3x}\right)\left(e^{-y} - e^{-4y}\right)\left(e^{-t} - e^{-2t}\right) \tag{3.68}$$

with the dimensionless constants $D = 1$ and $k = 7.6$, and the boundary control of the form

$$u_{x0}(y,t) = \sum_{i=1}^{5}\sum_{j=1}^{5} a_{x0ij} \sin i\pi y \; S(t-\tau_j), \tag{3.69}$$

$$u_{x1}(y,t) = \sum_{i=1}^{5}\sum_{j=1}^{5} a_{x1ij} \sin i\pi y \; S(t-\tau_j), \tag{3.70}$$

$$u_{y0}(x,t) = \sum_{i=1}^{5}\sum_{j=1}^{5} a_{y0ij} \sin i\pi x \; S(t-\tau_j), \tag{3.71}$$

$$u_{y1}(x,t) = \sum_{i=1}^{5}\sum_{j=1}^{5} a_{y1ij} \sin i\pi x \; S(t-\tau_j), \tag{3.72}$$

where $\{\tau_1, \cdots, \tau_5\} = \{0.5, 1.0, 1.5, 2.0, 2.5\}$ and no constraints on u for simplicity.[5] The boundary control problem is to determine the optimal values of $a_{x0ij}, a_{x1ij}, a_{y0ij}$, and a_{y1ij} for $i, j = 1, \ldots, 5$. The reference field and output field obtained by optimal boundary controls are shown in Figure 3.2. At this particular time instance, the optimal concentration field is mostly higher than than the reference field near the boundaries and lower in the interior.

3.5.2 Robustness Analysis

Consider upper and lower bounds on the uncertain variables (3.67) as

$$\delta\bar{\lambda} = \begin{bmatrix} 0.1 & 1 & 0.001 & 0.001 & 0.001 & 0.001 \end{bmatrix}^T, \tag{3.73}$$

$$\delta\underline{\lambda} = -\delta\bar{\lambda}. \tag{3.74}$$

This uncertainty set is equivalent to (3.2) with the weight matrix

$$W = \mathrm{diag}(10, 1, 1000, 1000, 1000, 1000), \tag{3.75}$$

[5] An example of a boundary control problem in which the constraints could probably be dropped is for a first-order reversible reaction occurring in a solid with high equilibrium value for the concentration, in which case (3.46) would be written in terms of deviations from the equilibrium concentration.

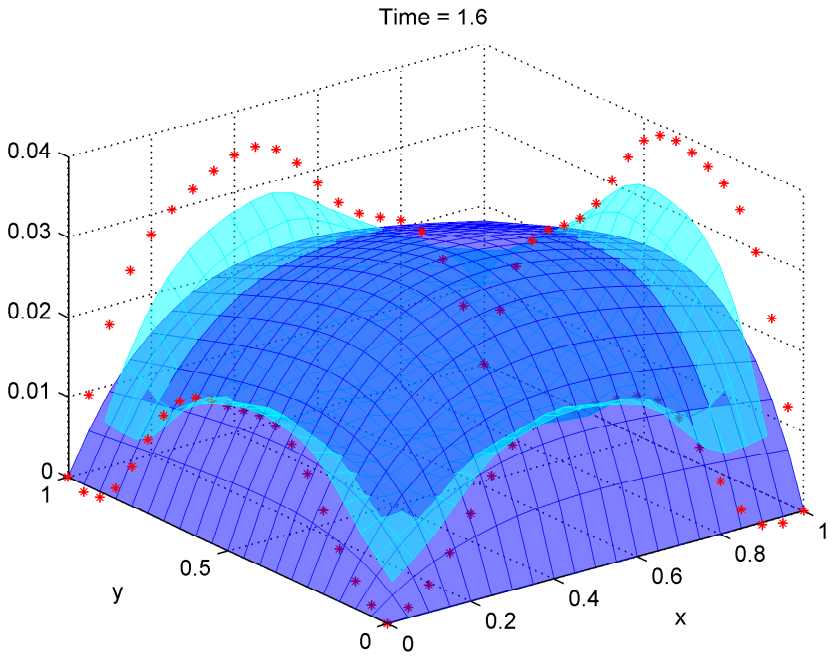

Figure 3.2: Reference $R(x, y, t)$ (blue) and optimal $C_{opt}(x, y, t)$ (cyan) fields at $t = 1.6$. The red asterisks are the boundary control input at $t = 1.6$ (the values for C_{opt} on the boundary are the same as the asterisks).

and $r = \infty$. For this example, M and H can be obtained analytically from the solution of the PDE obtained by separation of variables or the Fourier series method.

To assess the accuracy of the series expansions, and hence their suitability for use in robustness analysis, the worst-case deviations over the extreme points of the uncertainty set for each fixed (x, y, t) in the field were computed for the PDE (3.46) and the first-order (3.8) and second-order (3.15) expansions:

$$\delta C_{ep} = \max_{\delta\hat{\lambda}_i \in \{\delta\underline{\lambda}_i, \delta\bar{\lambda}_i\}} |C(\lambda_{nom} + \delta\hat{\lambda}) - C(\lambda_{nom})|, \tag{3.76}$$

$$\delta C_{1,ep} = \max_{\delta\hat{\lambda}_i \in \{\delta\underline{\lambda}_i, \delta\bar{\lambda}_i\}} |M\delta\hat{\lambda}|, \tag{3.77}$$

$$\delta C_{2,ep} = \max_{\delta\hat{\lambda}_i \in \{\delta\underline{\lambda}_i, \delta\bar{\lambda}_i\}} |M\delta\hat{\lambda} + \delta\hat{\lambda}^T H \delta\hat{\lambda}|, \tag{3.78}$$

$$\delta\bar{C}_{2,w.c.} = \max_{\delta\underline{\lambda} \le \delta\hat{\lambda} \le \delta\bar{\lambda}} M\delta\hat{\lambda} + \delta\hat{\lambda}^T H \delta\hat{\lambda}, \tag{3.79}$$

$$\delta\underline{C}_{2,w.c.} = \min_{\delta\underline{\lambda} \le \delta\hat{\lambda} \le \delta\bar{\lambda}} M\delta\hat{\lambda} + \delta\hat{\lambda}^T H \delta\hat{\lambda} \tag{3.80}$$

where the subscript "ep" denotes that this optimization is over the extreme points, and tight upper and lower bounds on (3.79) and (3.80) were obtained using the linear matrix inequality (LMI) and power iteration options, respectively, in the "mussv" command in the Matlab Robust Control Toolbox [8]. The worst-case maximum deviations in the field due to uncertainties are not spatially uniform across the surface (see Figure 3.3). The effects of the uncertainties are significant, with the worst-case deviation being >10% of the nominal value of the field for some times and spatial positions. The uncertainties in the dimensionless diffusivity and reaction rate constant do not affect the worst-case deviations on the boundaries of the spatial domain, since the values of the field on the boundaries are specified by the boundary control inputs marked by asterisks in Figure 3.3. The worst-case deviations of the concentration field at the boundaries are equal to the worst-case perturbations of the boundary control inputs, and those perturbations are felt uniformly throughout the spatial domain, as would be expected based on physical considerations.

The worst-case maximum deviations in the concentration fields computed for the second-order polynomial expansion are shown in Figure 3.4. The closeness of the concentration field computed from the LMI upper bound with that evaluated at the extreme points, which provides a lower bound on the worst-case perturbation, indicates that the LMI upper bound is a very accurate quantification of the worst-case perturbation based on the second-order expansion. Since the true worst-case concentration field based on the second-order expansion must be between the two concentration fields in Figure 3.4, the small differences between the concentration fields in Figure 3.4 provide an upper bound on the conservatism introduced by using linear matrix inequalities for the robustness analysis.

The maximum and minimum perturbations in the concentration fields based on the second-order expansion, $\delta\bar{C}_{2,w.c.}$ and $\delta\underline{C}_{2,w.c.}$, computed using linear matrix inequalities are shown in Figure 3.5. Based on the tight upper bounds on the worst-case perturbations in the concentration fields, the maximum and

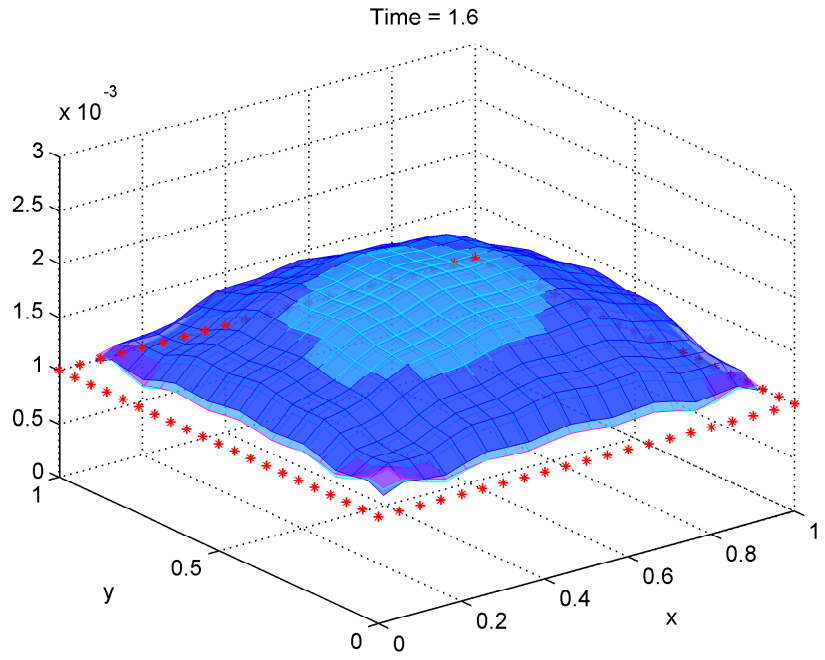

Figure 3.3: Maximum positive deviations in the controls δu (asterisks) and the concentration fields (surface meshes) due to uncertainties estimated by δC_{ep} (magenta), $\delta C_{1,ep}$ (blue), and $\delta C_{2,ep}$ (cyan), at time $t = 1.6$.

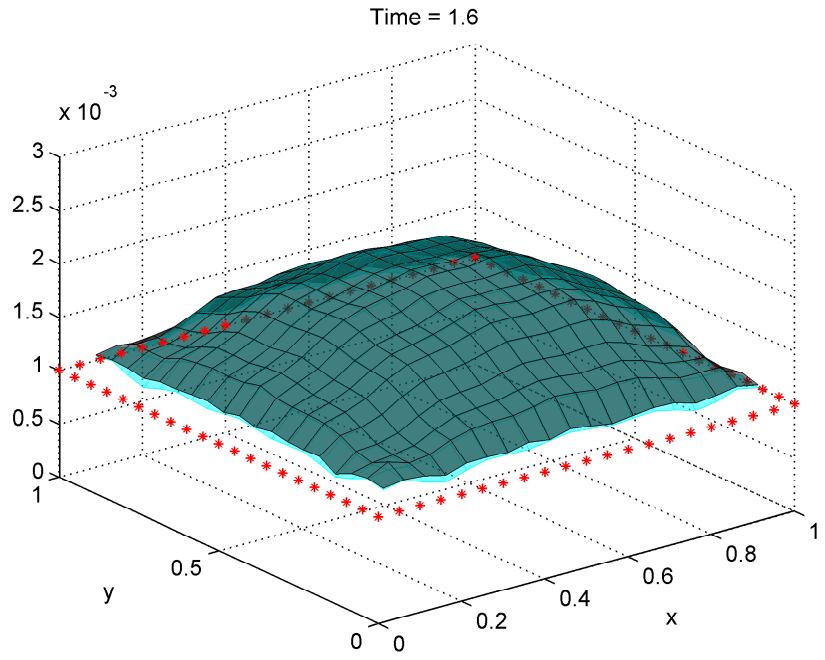

Figure 3.4: Maximum positive deviations in the controls δu (asterisks) and concentration fields (surface meshes) estimated by $\delta C_{2,ep}$ (cyan) and $\delta \bar{C}_{2,w.c.}$ computed by linear matrix inequalities (dark gray), which provides a tight upper bound, at time $t = 1.6$.

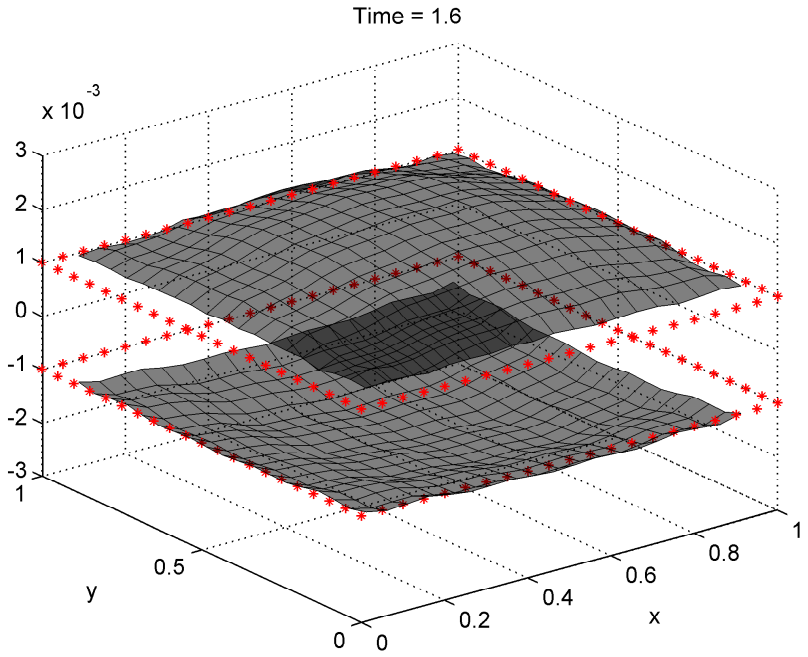

Figure 3.5: Maximum positive and negative deviations in the controls δu (asterisks) and concentration fields ($\delta\bar{C}_{2,w.c.}$ and $\delta\underline{C}_{2,w.c.}$) estimated by linear matrix inequalities (dark gray meshes), at time $t = 1.6$. The average difference of the absolute values (i.e., $\delta\bar{C}_{2,w.c.} + \delta\underline{C}_{2,w.c.}$) at each location is -5.1310×10^{-5}, indicating asymmetry of the uncertainty region about the $\delta C = 0$ plane. The maximum absolute difference is 1.6024×10^{-4}, which is about 16% of the space between consecutive horizontal dashed lines.

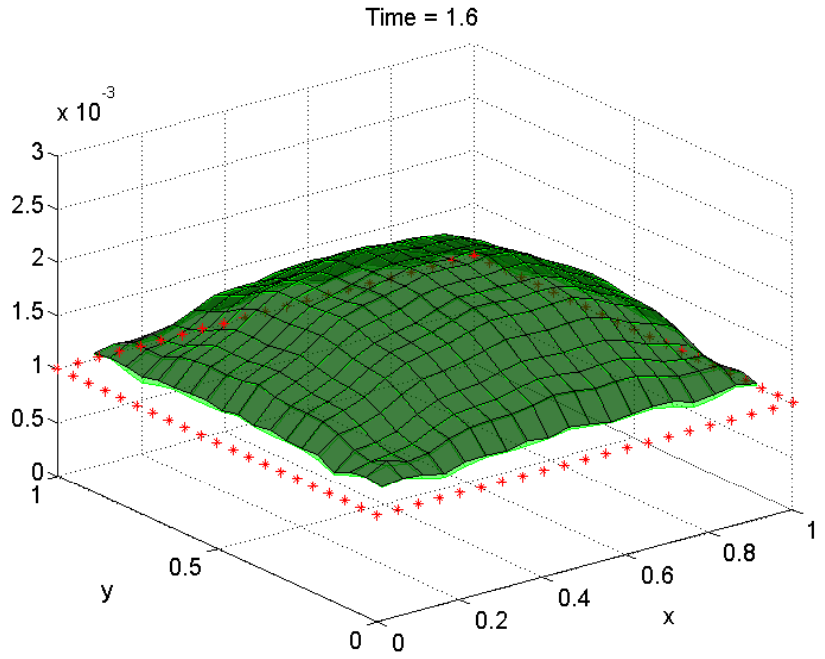

Figure 3.6: Maximum positive deviations in the controls δu (asterisks), and upper bound (dark green mesh) and lower bound (light green mesh) for the maximum positive deviations for the second-order expansion of the concentration field ($\delta\bar{C}_{2,w.c.}$). The average difference between the upper and lower bounds at each location is 9.4803×10^{-6} and the maximum absolute difference is 5.8634×10^{-5}.

minimum deviations in the concentration fields are very similar in magnitude, but are not quite the same. There is some asymmetry of the uncertainty region for the concentration fields, which is not surprising as the concentration field depends nonlinearly on the dimensionless diffusion coefficient and reaction rate constant.

The polynomial-time upper and lower bounds for the most positive and most negative deviations of the second-order expansion computed by linear matrix inequalities and power iteration are plotted in Figures 3.6 and 3.7. The average difference between the upper and lower bounds is $<10^{-5}$, which is less than three orders-of-magnitude lower than the magnitude of the perturbations, which is $>10^{-3}$. The average relative difference in the upper and lower bounds is less than 1% of the deviation in the concentration fields. The maximum relative difference between the upper and lower bounds is about 6%, which can be observed along the edges of the surfaces shown in Figure 3.6. The polynomial-time upper and lower bounds are 2 to 3 times tighter for computation of the most negative deviations than for the most positive deviations.

The effects of uncertainties significantly vary over time, as the reference field values change, with the first- and second-order expansions closely tracking the perturbed concentration fields (see Figures 3.8 and 3.9). The second-order expansion is much more accurate than the first-order expansion for the spatial average and at $(x, y) = (1/4, 1/4)$, but not significantly more accurate for $(x, y) = (1/2, 1/2)$. The expansions have an error of $\sim 10^{-4}$ for much of the spatial domain. For the entire time period, the polynomial-time LMI

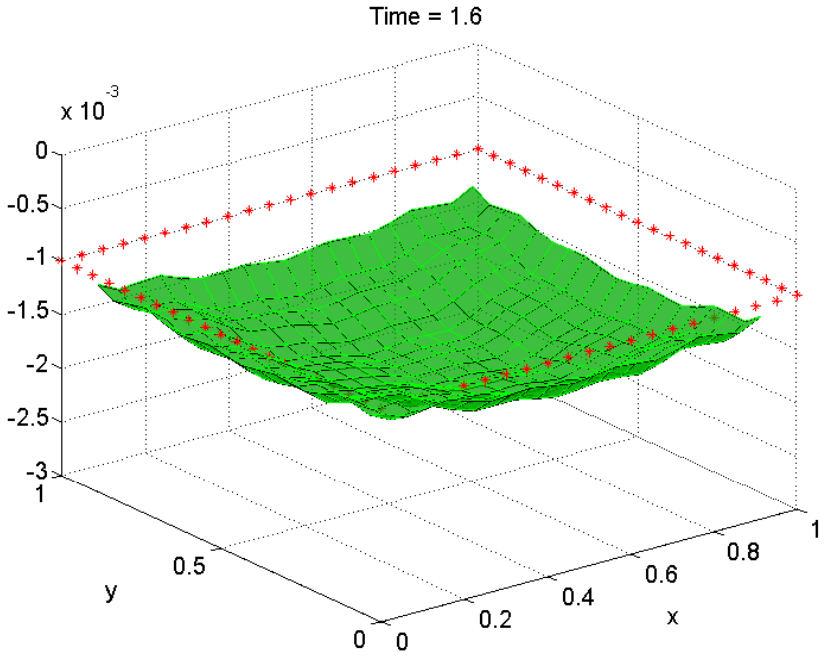

Figure 3.7: Most negative deviations in the controls δu (asterisks) and upper bound (dark green mesh) and lower bound (light green mesh) for the most negative deviations for the second-order expansion of the concentration field ($\delta \underline{C}_{2,w.c.}$). The average difference between the upper and lower bounds at each location is 4.8051×10^{-6} and the maximum absolute difference is 1.6487×10^{-5}.

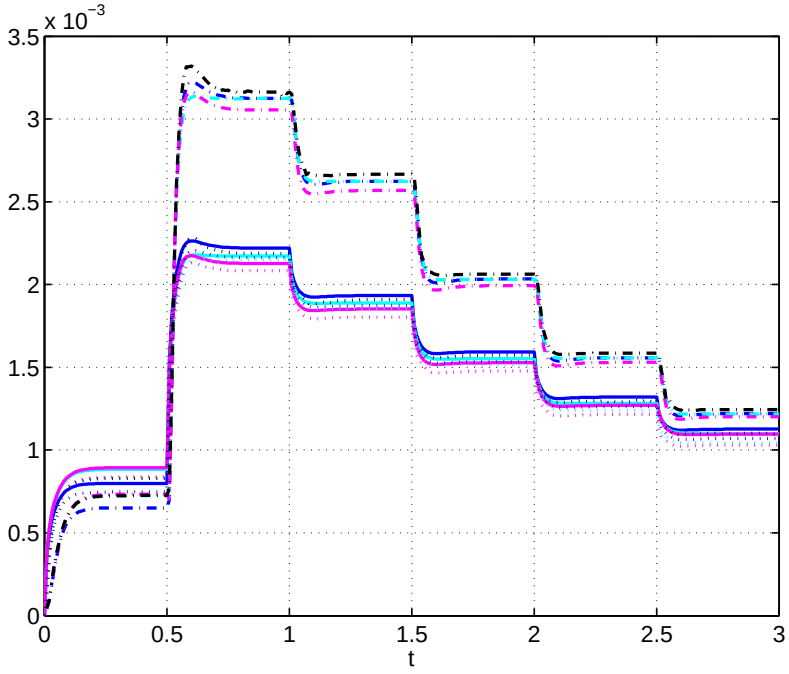

Figure 3.8: Maximum deviations in the field values due to uncertainties estimated by δC_{ep} (magenta), $\delta C_{1,ep}$ (blue), and $\delta C_{2,ep}$ (cyan), averaged over the spatial domain (-), and δC_{ep} (magenta), $\delta C_{1,ep}$ (blue), $\delta C_{2,ep}$ (cyan), and $\max\{\delta \bar{C}_{2,w.c}, -\delta \underline{C}_{2,w.c}\}$ (black, as computed from the LMI upper bound using "mussv") at $(x, y) = (1/2, 1/2)$ (-·) and $(x, y) = (1/4, 1/4)$ $(\cdots)$

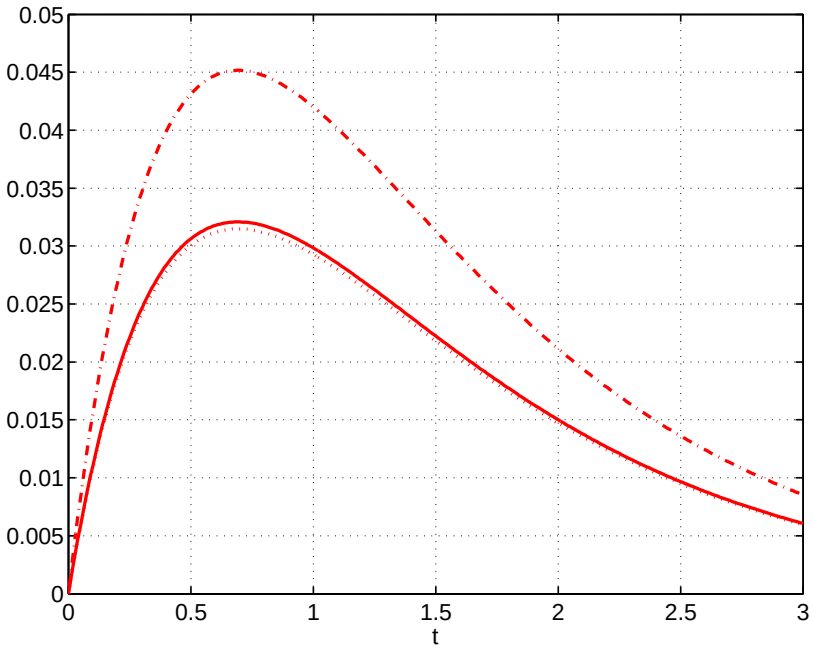

Figure 3.9: Reference field values, averaged over the spatial domain (-), at $(x, y) = (1/2, 1/2)$, (-·) and $(x, y) = (1/4, 1/4)$ $(\cdots)$

upper bound for the second-order expansion is very close to the lower bound obtained by evaluating the concentration field at the vertices of the uncertainty set (see Figure 3.8).

3.6 Conclusions

Methods are presented for the worst-case analysis of the effects of uncertainties on boundary control problems for finite-time distributed parameter systems that utilize low-order approximation of the mapping from uncertainties to output. Upper and lower bounds on the worst-case perturbations for each level of approximation are computed in polynomial-time by power iteration or linear matrix inequalities. For a two-dimensional problem involving simultaneous reaction and diffusion, the worst-case estimates obtained by first- and second-order expansions were very close to the worst-case estimates computed by using the original system. On average the polynomial-time upper and lower bounds were within 1% of each other, with a maximum difference of about 6%. The relatively low computational cost of these polynomial-time analysis tools indicates the feasibility of their incorporation into numerical algorithms for the design of optimal boundary controls for finite-time distributed parameter systems to be robust to uncertainties in model parameters and control implementation.

CHAPTER 4

RBF-BASED 3D SPATIAL CONTROL

Solving optimal control problems for spatially-distributed systems with multiple spatial dimensions can be computationally expensive. A numerical algorithm is proposed that combines a radial basis function expansion for the target trajectory with moment analysis. The approach is applicable to optimal control problems for linear spatially-distributed systems, for which the solution is expressed as a convolution of the system's kernel and its inputs. A novel feature is the insensitivity of its computational cost to the sharpness of spatial variations in the state or optimal control fields. This approach is applied to the optimal control of the three-dimensional reaction-diffusion-convection equation in which the control input and target are defined over two-dimensional spatial fields.

4.1 Introduction

While some numerical methods for solving optimal control problems are based on Pontryagin's maximum principle and the Hamilton-Jacobi-Bellman equation [12, 20], a more popular approach for solving finite-time optimal control problems is to expand the optimization and/or state vector in terms of a basis function expansion and then analytically or numerically optimize over the coefficients in the expansion [82]. Basis function expansions that have been used to solve optimal control problems include piecewise constant [82], piecewise linear [39, 144], Fourier series [95], Chebyshev series [200, 201], and Legendre polynomials [65, 83]. When this control parameterization approach is applied to optimal control problems in which the control variable is defined over multiple spatial dimensions, the number of basis functions and the corresponding computational cost increase dramatically. There has been growing interest in solving the optimal control problem at each sampling instance within a receding or shrinking horizon (so-called "model predictive control") [63, 150], in which case the computational cost of most approaches can be orders-of-magnitude too high even when the partial differential equation(s) describing the system is linear.

This chapter proposes an approach for solving optimal control problems that has several key differences from past algorithms. First, the target variable is expanded in terms of radial basis functions (RBFs), which is especially useful for control problems in which the target variable is defined over a two- or three-dimensional (2D or 3D) field. While RBFs have been applied to various control systems problems including the identification of nonlinear black-box models [188] and adaptive control [180], to our knowledge RBFs have not been applied to solve optimal control problems based on first-principles models for spatially-distributed systems. The second advance is the use of moment analysis to derive analytical expressions for the optimal and suboptimal solution of optimal control problems.

The specific implementations explored in this chapter use Gaussian functions in the RBFs. The target variable is expressed as a sum of Gaussian functions with variable center and radius, with the means and variances of input, output, and system related by analytical formulae that can be derived from moment analysis [4]. The representation of the target variable in terms of these RBFs can be computed by standard software [81, 158]. The proposed method exploits the fact that the mean and variance are additive for functions related by the convolution operation. This method can be applied to systems in which the output is the convolution of the system's integral kernel and the input to the system. This includes any linear system that has a transfer function, as a transfer function in the Laplace domain corresponds to the convolution kernel in the time domain. This approach is most useful for the optimal control of spatially-distributed systems that have a very large number of control degrees of freedom, especially when the control and target variables are 2D or 3D spatial fields.

For concreteness, the proposed approach is presented within the context of the 2D spatial control of the reaction-diffusion-convection equation (RDCE) in an unbounded 3D domain, for three different target fields. This is followed by a discussion on the application of the approach to other linear systems.

4.2 Optimal Control Problem

The RDCE describes a very large range of chemical and biological processes, including packed bed reactors [52], release of pharmaceuticals from biodegradable polymeric drug delivery devices [186], and transport of growth factors through biological tissue [112]. Consider the 3D RDCE with uniform fluid flow:

$$\frac{\partial C}{\partial t} = D\left(\frac{\partial^2 C}{\partial x^2} + \frac{\partial^2 C}{\partial y^2} + \frac{\partial^2 C}{\partial z^2}\right) - v\frac{\partial C}{\partial z} - kC + \Psi(x, y, z, t), \tag{4.1}$$

where

$$\Psi(x, y, z, t) = \delta(z)u(x, y, t) \quad \text{in} \quad \Omega = \{(x, y, z) | -\infty < x, y, z < \infty\}, \tag{4.2}$$

$$C(x, y, z, 0) = 0, \tag{4.3}$$

C is the solute concentration, $D > 0$ is the diffusion coefficient, $v > 0$ is the fluid velocity, $k > 0$ is the reaction rate constant, and δ is the Dirac delta function. The diffusion is assumed to be isotropic, which simplifies the presentation and is true in most applications; the generalization to non-isotropic diffusion is straightforward by introduction of a diffusion tensor [181], with an increase in notational complexity. The spatial coordinates have been rotated so that the uniform fluid flow is in the z-direction, to reduce notational complexity. The generalization to multiple species in solution, in which case (4.1) is written for each species, is also straightforward.

The form of $\Psi(x, y, z, t) = \delta(z)u(x, y, t)$ describes a source of mass which can be introduced non-uniformly anywhere in the $z = 0$ plane. This form describes, for example, the release of pharmaceuticals or other molecules from biodegradable polymeric nano- or microspheres of fixed position that can be manufactured to produce a target mass release profile [198, 17, 18]. The control input is the 2D field $u(x, y, t)$ and the control objective is to produce a target 2D concentration field at the $z = 1$ plane. This objective is also equivalent to tracking the rate of consumption of mass by reaction in this plane, as the reaction rate for this process is proportional to the solute concentration. The target 2D field can be represented as an analytical expression $C(x, y, 1, t)$ or as a set of discrete points in the $z = 1$ plane.

The above optimal control problem is related to a channel flow control problem considered by Krstic [115], as both control problems define manipulations over a 2D spatial field defined in 3D spatial domain. The control objective of Krstic's problem is closed-loop stabilization, whereas our control objective is to track a 2D target field. His control problems also consider different PDEs.

4.3 Optimal Control Procedure

Within the context of this particular optimal control problem, the proposed procedure consists of the following three steps.

Step 1: Fit a RBF expansion to a given target 2D concentration field $C_{target}(x, y, 1, t)$ as a weighted sum of Guassian functions $\bar{C}_{target,i}(x, y, 1, t)$, by minimizing the error norm

$$\left\| C_{target}(x, y, 1, t) - \sum_{i=1}^{n} \bar{C}_{target,i}(x, y, 1, t) \right\|, \tag{4.4}$$

with the optimization variables being the means and variances for each $\bar{C}_{target,i}(x, y, 1, t)$. This chapter uses the 2-norm, but any other well-defined norm could be used.

Step 2: Determine the control input field $u_i(y, z, t)$ that produces a 2D concentration field at $z = 1$ that matches each Gaussian function $\bar{C}_{target,i}(x, y, 1, t)$, either exactly or nearly exactly by using moment analysis.

Step 3: Perform a weighted sum of the individual control input fields to determine the overall control input field $u(x, y, t)$.

Step 1 exploits the ready availability of software for fitting RBF expansions [81, 158]. This solution of the optimization in Step 1 is the main cost of the proposed procedure. Still, its numerical solution is orders of magnitude less expensive than a spatially-distributed optimal control problem, as Step 1 is an algebraic optimization that does not involve the solution of any partial differential equations.

Step 2 of the procedure exploits the existence of exact or approximate analytical solutions to the optimal control problem when the target 2D concentration field is a Gaussian function. For this particular application, the analysis will utilize the analytical solution to the RDCE:

$$C_\delta(x, y, z, t) = \frac{1}{(4\pi Dt)^{3/2}} \exp\left(-\frac{x^2 + y^2 + (z - vt)^2}{4Dt} - kt\right) \tag{4.5}$$

$$= \psi_{0,2Dt}(x)\psi_{0,2Dt}(y)\psi_{vt,2Dt}(z)\exp(-kt) \tag{4.6}$$

where

$$\psi_{\mu,\sigma^2}(x) := \frac{1}{\sqrt{2\pi\sigma^2}} \exp\left\{-\frac{(x-\mu)^2}{2\sigma^2}\right\} \tag{4.7}$$

and similarly for y and z, for a control input represented by Dirac delta functions, $\Psi(x, y, z, t) = \delta(x)\delta(y)\delta(z)\delta(t)$.

This expression can be used to write the analytical solution to the RDCE at $z = 1$ for an arbitrary control input field $u(x, y, t)$ as

$$C(x, y, 1, t) = C_\delta(x, y, 1, t) \otimes u(x, y, t). \tag{4.8}$$

where $\otimes$ is the time and spatial convolutions of the two functions. Both Steps 2 and 3 of the procedure exploit the linearity of the operator between the control input field $u(x, y, t)$ and the target field $\bar{C}_{target}(x, y, 1, t)$.

The next sections apply the proposed control procedure to three optimal control problems, which correspond to three types of target fields:

Example 1: a 2D field at a particular time instance,

Example 2: a time-invariant 2D field, and

Example 3: a time-varying 2D field.

The first example is used to motivate the proposed optimal control procedure. The subsequent examples are more realistic optimal control problems. This chapter illustrates the approach using uncorrelated Gaussians as RBF; the overall approach applies to general correlated Gaussians.

4.4 Example 1: A 2D Spatial Field at a Particular Time Instance

Consider the optimal control problem with the objective to achieve a target 2D concentration field at the $z = 1$ plane at a particular time instance, in which solute can be released at $z = 0$ at any previous time t. This problem is over-specified (that is, has multiple solutions for $u(x, y, t)$), so an additional requirement is introduced that minimal total solute mass should be released at $z = 0$. The motivation for this additional objective is that in practical problems the solute molecules released at $z = 0$ is usually expensive.

4.4.1 Step 1

Without loss in generality, while simplifying the subsequent notation, define the time axis so that

$$t^* = \frac{-3D + \sqrt{9D^2 + (4kD + v^2)}}{4kD + v^2} \tag{4.9}$$

is the time in which it is desired for the 2D concentration field that spans the $z = 1$ plane to reach its target. With this specification of the time axis, it can be shown[1] that the concentration is maximum with respect to z at $z = 1$ at $t = t^*$ for a Dirac delta control input $u(x, y, t) = \tilde{u}(x, y)\delta(t)$ at $z = 0$ introduced at $t = 0$.

From (4.6), for control input $u(x, y, t) = \delta(x)\delta(y)\delta(t)$ at $z = 0$, the analytical expression for the concentration at the $z = 1$ plane at time $t = t^*$ is

$$C_\delta(x, y, 1, t^*) = m_{t^*}\psi_{0,2Dt^*}(x)\psi_{0,2Dt^*}(y), \tag{4.10}$$

where

$$m_{t^*} = \frac{\exp\left(-\dfrac{(1 - vt^*)^2}{4Dt^*} - kt^*\right)}{\sqrt{4\pi Dt^*}}. \tag{4.11}$$

This implies that the minimum possible variance that can be achieved by this system is $2Dt^*$. The objective is to minimize the error between the sum-of-Gaussians target field

$$\bar{C}_{target}(x, y, 1, t^*) = \sum_{i=1}^{n} \bar{C}_{target,i}(x, y, 1, t^*) \tag{4.12}$$

$$= \sum_{i=1}^{n} w_i \psi_{\bar{\mu}_{xi},\bar{\sigma}^2_{xi}}(x)\psi_{\bar{\mu}_{yi},\bar{\sigma}^2_{yi}}(y) \tag{4.13}$$

with the constraints

$$\bar{\sigma}^2_{xi} > 2Dt^*, \tag{4.14}$$

$$\bar{\sigma}^2_{yi} > 2Dt^*, \tag{4.15}$$

[1] Solve $\frac{\partial C_\delta}{\partial t} = 0$ for t with $z = 1$ and $x = y = 0$. The function $\frac{\partial C_\delta}{\partial t}$ is concave and the obtained t achieves the maximum.

for all i, and the true target 2D field $C_{target}(x, y, 1, t^*)$ at time $t = t^*$. The optimization variables in (4.13), which are weights, means, and variances (i.e., w_i, $\bar{\mu}_{xi}$, and $\bar{\sigma}^2_{xi}$) can be determined by using any of the available numerical algorithms and software for fitting RBF networks to 2D data.

4.4.2 Step 2

The analytical solution to the RDCE (4.1) with the control input

$$u(x, y, t) = \psi_{\mu_{xu},\sigma^2_{xu}}(x)\psi_{\mu_{yu},\sigma^2_{yu}}(y)\delta(t), \tag{4.16}$$

is

$$C(x, y, 1, t^*) = C_\delta(x, y, 1, t^*) \otimes u(x, y, t) \tag{4.17}$$

$$= m_{t^*}\psi_{\mu_{xu},\sigma^2_{xu}+2Dt^*}(x)\psi_{\mu_{yu},\sigma^2_{yu}+2Dt^*}(y), \tag{4.18}$$

which can be shown by direct substitution into the RDCE (4.1).

Therefore, the control input field $u_i(x, y, t)$ that produces

$$\bar{C}_{target,i}(x, y, 1, t^*) = w_i\psi_{\bar{\mu}_{xi},\bar{\sigma}^2_{xi}}(x)\psi_{\bar{\mu}_{yi},\bar{\sigma}^2_{yi}}(y), \tag{4.19}$$

is

$$u_i(x, y, t) = m_i\psi_{\mu_{xi},\sigma^2_{xi}}(x)\psi_{\mu_{yi},\sigma^2_{yi}}(y)\delta(t), \tag{4.20}$$

where

$$m_i = \frac{w_i}{m_{t^*}}, \tag{4.21}$$

$$\mu_{xi} = \bar{\mu}_{xi}, \qquad \sigma^2_{xi} = \bar{\sigma}^2_{xi} - 2Dt^*, \tag{4.22}$$

$$\mu_{yi} = \bar{\mu}_{yi}, \qquad \sigma^2_{yi} = \bar{\sigma}^2_{yi} - 2Dt^*. \tag{4.23}$$

Since optimization problem in the Step 1 is solved to satisfy $\bar{\sigma}^2_{xi} > 2Dt^*$ and $\bar{\sigma}^2_{yi} > 2Dt^*$, σ^2_{xi} and σ^2_{yi} are well-defined.

4.4.3 Step 3

Simply sum up

$$u(x, y, t) = \sum_{i=1}^{n} m_i\psi_{\mu_{xi},\sigma^2_{xi}}(x)\psi_{\mu_{yi},\sigma^2_{yi}}(y)\delta(t). \tag{4.24}$$

4.4.4 Discussion

For this example Steps 2 and 3 introduce no error, such that the only error introduced in the procedure is the fitting of the RBF expansion in Step 1.

The target field is assumed to be bounded, that is,

$$\|C_{target}(x,y,1,t)\|_2^2 \equiv \int_{-\infty}^{\infty}\int_{-\infty}^{\infty} C_{target}^2(x,y,1,t)dxdy < M \tag{4.25}$$

for some finite positive M for any fixed time t. The universal approximation property of RBF expansions [160, 161], which is a variation on the well-known result by Cybenko [51] for sigmoidal functions, implies that, for any $\epsilon > 0$, there exists n such that

$$\|C_{target}(x,y,1,t^*) - \bar{C}_{target}(x,y,1,t^*)\|_2 < \epsilon \tag{4.26}$$

for some $\bar{\mu}_{xi}$, $\bar{\mu}_{yi}$, $\bar{\sigma}_{xi}^2$, and $\bar{\sigma}_{yi}^2$, for $i = 1, \cdots, n$. Not all of these target fields are feasible, as the diffusion process forces a certain amount of smoothness in the target field. In particular, the target field is always smoother than the sharpest past control input field, with (4.18) implying that the sharpest target field has standard deviations of $2Dt^*$ in the x and y directions, which is obtained for a control input described by Dirac delta functions in y and z. This suggests a parameterization of feasible target fields as those C_{target} for which, for any ϵ, there exists an n that satisfies (4.26) for some $\bar{\mu}_{xi}$, $\bar{\mu}_{yi}$, $\bar{\sigma}_{xi}^2 > 2Dt^*$, and $\bar{\sigma}_{yi}^2 > 2Dt^*$, for $i = 1, ..., n$.

4.5 Example 2: A Time-invariant 2D Spatial Field

Consider the control objective of achieving a target of time-invariant 2D concentration field.

4.5.1 Step 1

Step 1 is similar to Example 1, but this time the minimization is performed at the steady-state instead of a particular time instance. For a time-invariant control input $u(x,y,t) = \delta(x)\delta(y)$ at $z = 0$, the analytical expression for the concentration at the $z = 1$ plane is

$$\lim_{t\to\infty} \int_0^t C_\delta(x,y,1,\tau)\delta(x)\delta(y)d\tau \tag{4.27}$$

which is equivalent to

$$C_s(x,y,1) = \int_0^\infty C_\delta(x,y,1,t)dt \tag{4.28}$$

$$= \frac{\exp\left(\frac{v - \sqrt{4Dk+v^2}\sqrt{x^2+y^2+1}}{2D}\right)}{4\pi D\sqrt{x^2+y^2+1}}. \tag{4.29}$$

By symmetry, (4.29) has means

$$\mu_x = \mu_y = 0, \tag{4.30}$$

and the variances are obtained by numerically calculating

$$\sigma_x^2 = \sigma_y^2 = \frac{\int_{-\infty}^{\infty}\int_{-\infty}^{\infty} x^2 C_s(x,y,1)dxdy}{\int_{-\infty}^{\infty}\int_{-\infty}^{\infty} C_s(x,y,1)dxdy}, \tag{4.31}$$

or by application of two-dimensional moment analysis [85, 96].

The objective is to minimize the error between the sum of Gaussians target field

$$\bar{C}_{target}(x,y,1) = \sum_{i=1}^{n} \bar{C}_{target,i}(x,y,1) \tag{4.32}$$

$$= \sum_{i=1}^{n} w_i \psi_{\bar{\mu}_{xi},\bar{\sigma}_{xi}^2}(x)\psi_{\bar{\mu}_{yi},\bar{\sigma}_{yi}^2}(y) \tag{4.33}$$

with the constraints

$$\bar{\sigma}_{xi}^2 > \sigma_x^2, \tag{4.34}$$

$$\bar{\sigma}_{yi}^2 > \sigma_y^2, \tag{4.35}$$

for all i, and the true target 2D field $C_{target}(x,y,1)$. As before, the optimization variables in (4.33), which are weights, means, and variances (i.e., w_i, $\bar{\mu}_{xi}$, and $\bar{\sigma}_{xi}^2$), can be determined by using any of the available numerical algorithms and software for fitting RBF networks to 2D data.

4.5.2 Step 2

Step 2 selects the control input field for each Gaussian to produce an output concentration field at $z = 1$ that exactly matches the means and variances of the target field.

For a time-invariant control input field,

$$u(x,y) = \psi_{\mu_{xu},\sigma_{xu}^2}(x)\psi_{\mu_{yu},\sigma_{yu}^2}(y), \tag{4.36}$$

the output field at steady-state is

$$C(x,y,1) = C_s(x,y,1) \otimes u(x,y), \tag{4.37}$$

which has means and variances

$$\mu_{xu}, \quad \mu_{yu}, \quad \sigma_x^2 + \sigma_{xu}^2, \quad \sigma_y^2 + \sigma_{yu}^2. \tag{4.38}$$

The Gaussian control input field $u_i(x,y,t)$ that produces an output field with the same means and variances as (4.33) is

$$u_i(x,y) = m_i \psi_{\mu_{xi},\sigma_{xi}^2}(x) \psi_{\mu_{yi},\sigma_{yi}^2}(y), \tag{4.39}$$

where

$$m_i = \frac{w_i}{\int_{-\infty}^{\infty}\int_{-\infty}^{\infty} C_s(x,y,1)dxdy}, \tag{4.40}$$

$$\mu_{xi} = \bar{\mu}_{xi} - \mu_x, \qquad \sigma_{xi}^2 = \bar{\sigma}_{xi}^2 - \sigma_x^2, \tag{4.41}$$

$$\mu_{yi} = \bar{\mu}_{yi} - \mu_y, \qquad \sigma_{yi}^2 = \bar{\sigma}_{yi}^2 - \sigma_y^2, \tag{4.42}$$

and m_i was introduced for normalization purposes (i.e., matching the zeroth moment). This input field gives

$$C_i(x,y,1) = C_s(x,y,1) \otimes u_i(x,y) \tag{4.43}$$

as the solution to the RDCE (4.1).

The optimization problem in Step 1 is solved to satisfy $\bar{\sigma}_{xi}^2 > \sigma_x^2$ and $\bar{\sigma}_{yi}^2 > \sigma_y^2$, which implies that the σ_{xi}^2 and σ_{yi}^2 are well-defined.

4.5.3 Step 3

Select the overall control input field as

$$u(x,y) = \sum_{i=1}^{n} m_i \psi_{\mu_{xi},\sigma_{xi}^2}(x) \psi_{\mu_{yi},\sigma_{yi}^2}(y). \tag{4.44}$$

4.5.4 Discussion

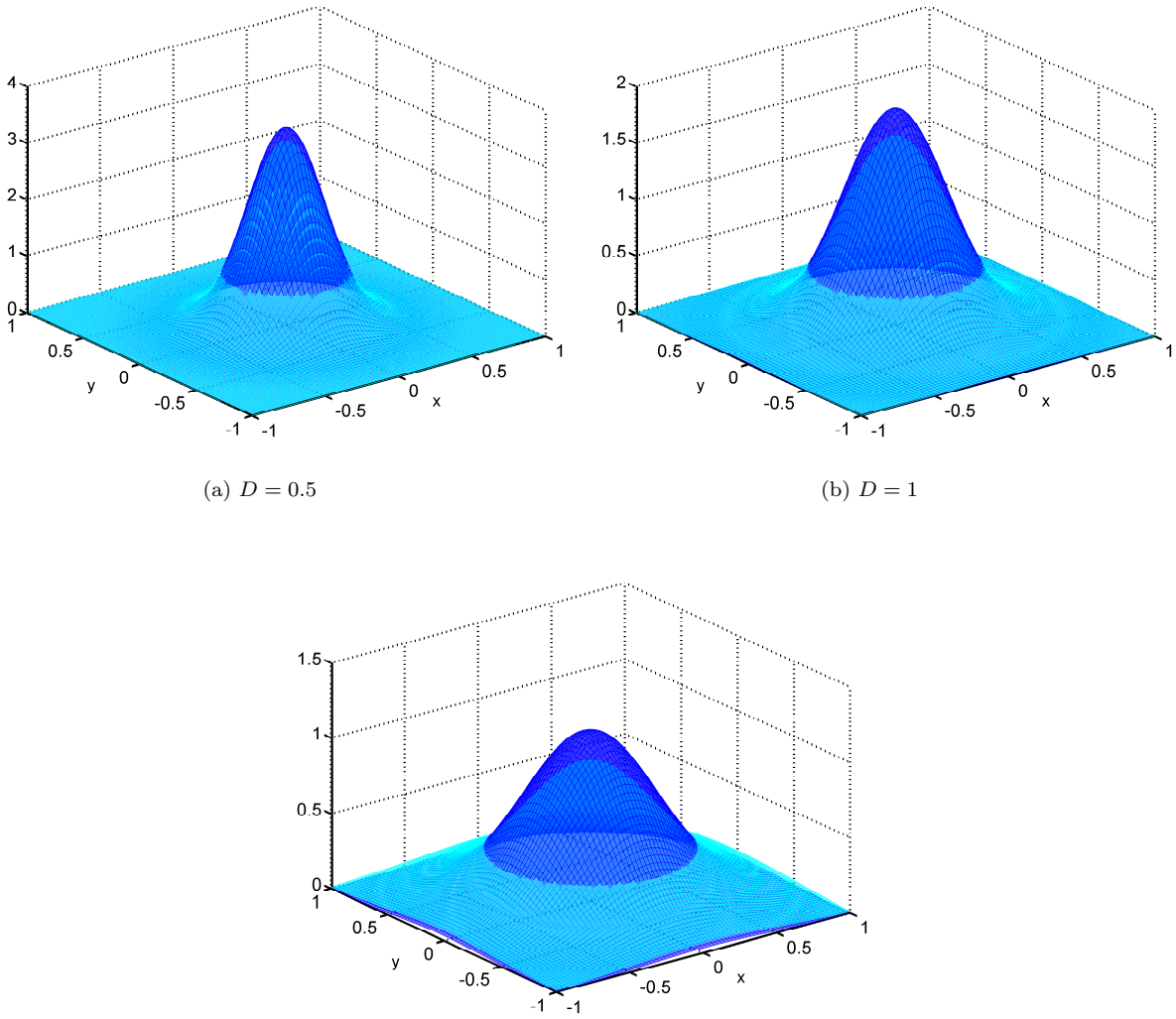

(a) $D = 0.5$

(b) $D = 1$

(c) $D = 2$

Figure 4.1: System kernels $C_\delta(x, y, 1, t^*)$ (blue) and $C_s(x, y, 1)$ (cyan), with $k = 7.6$ and $v = 20$.

Figure 4.1 compares the system's kernel of Examples 1 and 2 with different diffusion coefficients D. As $C_\delta(x, y, 1, t^*)$ and $C_s(x, y, 1)$ are nonlinear functions of D, v, and k, the shape of the kernels changes in a nonlinear fashion. For fixed v and k, increased diffusion coefficient corresponds to concentration fields $C_\delta(x, y, 1, t^*)$ and $C_s(x, y, 1)$ that are more spread out, as expected. The field $C_s(x, y, 1)$ is flatter than the Gaussian function $C_\delta(x, y, 1, t^*)$ with $C_\delta(x, y, 1, t^*)$ having a larger value around the center and $C_s(x, y, 1)$ having larger values away from the center.

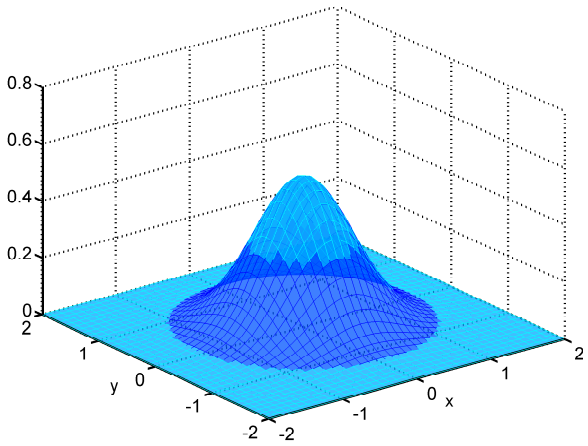

(a) $D = 0.5$

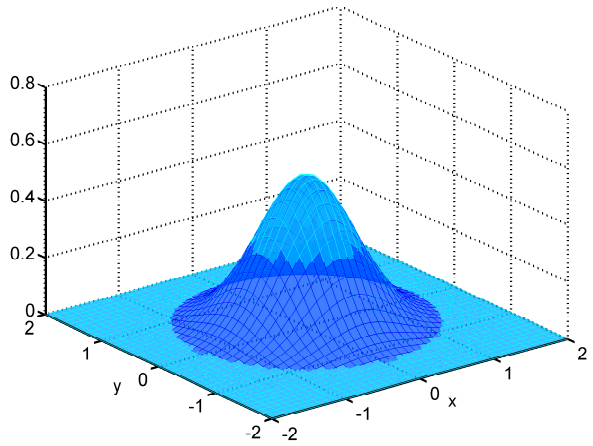

(b) $D = 1$

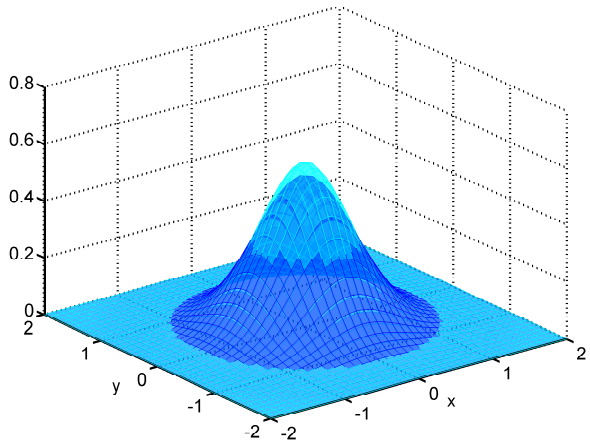

(c) $D = 2$

Figure 4.2: Gaussian reference and output field for Example 1 (which are exactly the same, blue) and output field for Example 2 (cyan), with $k = 7.6$ and $v = 20$.

Figure 4.2 shows the matching of a single Gaussian reference field. The Gaussian reference was chosen to have large enough variances so that there is no constraints in limiting the input fields, and the figures show purely the effect of the convolutions. The reference field is exactly achieved in Example 1, while the Example 2 deforms the Gaussian slightly. As it could have been guessed from Figure 4.2, the larger the diffusion coefficient is, the larger the difference between the output field and reference field.

When multiple Gaussians are used, smoother reference fields can be more closely matched than spiky reference fields. The complexity of the reference field affects Step 1. A reference field with spikes would require some small variances in some terms in the RBF expansion, but each variance needs to satisfy a

constraint that is function of the parameters of the PDE. If the spatial derivatives of the spikes are too high then the output field will be smoother than the reference; this result cannot be avoided by any other control approaches because it is a restriction comes from the system's inherent spatiotemporal dynamics.

4.6 Example 3: A Time-varying 2D Spatial Field

Consider the optimal control problem in which that objective is to achieve a target time-varying 2D concentration field.

4.6.1 Step 1

Equation (4.6) has means

$$\mu_x = \mu_y = 0, \tag{4.45}$$

$$\mu_t = \frac{\int_0^\infty \int_\infty^\infty \int_\infty^\infty t C_\delta(x,y,1,t) dxdydt}{\int_0^\infty \int_\infty^\infty \int_\infty^\infty C_\delta(x,y,1,t) dxdydt} \tag{4.46}$$

$$= \frac{2D + \sqrt{4kD + v^2}}{4kD + v^2}, \tag{4.47}$$

and variances

$$\sigma_x^2 = \sigma_y^2 \tag{4.48}$$

$$= \frac{\int_0^\infty \int_\infty^\infty \int_\infty^\infty x^2 C_\delta(x,y,1,t) dxdydt}{\int_0^\infty \int_\infty^\infty \int_\infty^\infty C_\delta(x,y,1,t) dxdydt} \tag{4.49}$$

$$= \frac{2D\left(2D + \sqrt{4kD + v^2}\right)}{4kD + v^2}, \tag{4.50}$$

$$\sigma_t^2 = \frac{\int_0^\infty \int_\infty^\infty \int_\infty^\infty t^2 C_\delta(x,y,1,t) dxdydt}{\int_0^\infty \int_\infty^\infty \int_\infty^\infty C_\delta(x,y,1,t) dxdydt} - \mu_t^2 \tag{4.51}$$

$$= \frac{2D\left(4D + \sqrt{4kD + v^2}\right)}{(4kD + v^2)^2}. \tag{4.52}$$

The objective is to minimize the error between the sum-of-Gaussians target field

$$\bar{C}_{target}(x,y,1,t^*) = \sum_{i=1}^{n} \bar{C}_{target,i}(x,y,1,t) \tag{4.53}$$

$$= \sum_{i=1}^{n} w_i \psi_{\bar{\mu}_{xi},\bar{\sigma}_{xi}^2}(x) \psi_{\bar{\mu}_{yi},\bar{\sigma}_{yi}^2}(y) \psi_{\bar{\mu}_{ti},\bar{\sigma}_{ti}^2}(t), \tag{4.54}$$

with the constraints

$$\bar{\sigma}_{xi}^2 > \sigma_x^2, \tag{4.55}$$

$$\bar{\sigma}_{yi}^2 > \sigma_y^2, \tag{4.56}$$

$$\bar{\sigma}_{ti}^2 > \sigma_t^2, \tag{4.57}$$

for all i, and the true target 2D field $C_{target}(x, y, 1, t)$. The optimization variables in (4.13), which are weights, means, and variances (i.e., w_i, $\bar{\mu}_{xi}$, and $\bar{\sigma}_{xi}^2$) can be determined by using any of the available numerical algorithms and software for fitting RBF networks to 2D data.

4.6.2 Step 2

For the control input $u(x, y, t) = \delta(x)\delta(y)\delta(t)$ at $z = 0$, the analytical expression for the concentration at the $z = 1$ plane is (4.6), so that the analytical solution to the RDCE (4.1) with the control input

$$u(x, y, t) = \psi_{\mu_{xu},\sigma_{xu}^2}(x)\psi_{\mu_{yu},\sigma_{yu}^2}(y)\psi_{\mu_{tu},\sigma_{tu}^2}(t), \tag{4.58}$$

is

$$C(x, y, 1, t) = C_\delta(x, y, 1, t) \otimes u(x, y, t), \tag{4.59}$$

which has means

$$\mu_{xu}, \quad \mu_{yu}, \quad \mu_t + \mu_{tu}, \tag{4.60}$$

and variances

$$\sigma_x^2 + \sigma_{xu}^2, \quad \sigma_y^2 + \sigma_{yu}^2, \quad \sigma_t^2 + \sigma_{tu}^2. \tag{4.61}$$

The Gaussian control input field $u_i(x, y, t)$ that produces an output field with the desired means and variances is

$$u_i(x, y, t) = m_i\psi_{\mu_{xi},\sigma_{xi}^2}(x)\psi_{\mu_{yi},\sigma_{yi}^2}(y)\psi_{\mu_{ti},\sigma_{ti}^2}(t), \tag{4.62}$$

where

$$m_i = \frac{w_i}{\int_0^t \int_{-\infty}^{\infty} \int_{-\infty}^{\infty} C_\delta(x, y, 1, t)dxdydt}, \tag{4.63}$$

$$\mu_{xi} = \bar{\mu}_{xi} - \mu_x, \quad \sigma_{xi}^2 = \bar{\sigma}_{xi}^2 - \sigma_x^2, \tag{4.64}$$

$$\mu_{yi} = \bar{\mu}_{yi} - \mu_y, \quad \sigma_{yi}^2 = \bar{\sigma}_{yi}^2 - \sigma_y^2, \tag{4.65}$$

$$\mu_{ti} = \bar{\mu}_{ti} - \mu_t, \quad \sigma_{ti}^2 = \bar{\sigma}_{ti}^2 - \sigma_t^2. \tag{4.66}$$

where m_i was introduced for normalization purposes (i.e., matching the zeroth moment). This input field gives

$$C_i(x, y, 1, t) = C_\delta(x, y, 1, t) \otimes u_i(x, y, t) \tag{4.67}$$

as the solution to the RDCE (4.1).

Since the optimization problem in the Step 1 is constrained to satisfy $\bar{\sigma}_{xi}^2 > \sigma_x^2$, $\bar{\sigma}_{yi}^2 > \sigma_y^2$, and $\bar{\sigma}_{ti}^2 > \sigma_t^2$, the σ_{xi}^2, σ_{yi}^2 and σ_{ti}^2 are well-defined.

4.6.3 Step 3

The control input field from the application of Step 3 is

$$u(x, y, t) = \sum_{i=1}^{n} m_i \psi_{\mu_{xi}, \sigma_{xi}^2}(x) \psi_{\mu_{yi}, \sigma_{yi}^2}(y) \psi_{\mu_{ti}, \sigma_{ti}^2}(t). \tag{4.68}$$

4.6.4 Discussion

The system's kernel in Example 3 at $t = t^*$ with different diffusion coefficients D are the same as $C_\delta(x, y, 1, t^*)$ in Figure 4.1. Figure 4.3 show the matching of a single Gaussian reference field. As in the last section, the reference Gaussian was chosen to have large enough variances that there exists a Guassian input that nearly produces the reference Gaussian (which is the same Gaussian function with another factor that is a function of time), and the figures show purely the effect of time convolutions. Similar to Example 2, Example 3 deforms the Gaussian reference field slightly. As guessed from Example 2, the larger the diffusion coefficient, the larger the difference between the output field and reference field.

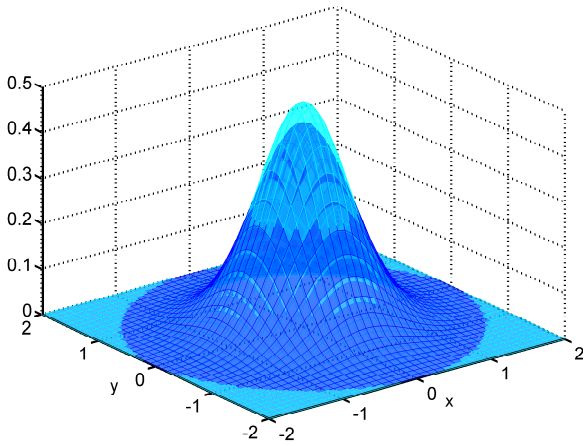

(a) $D = 0.5$

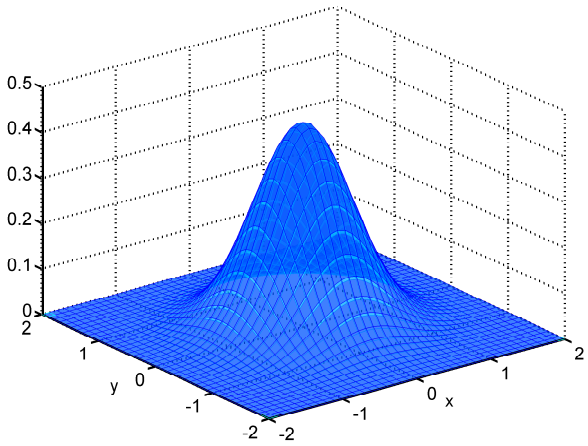

(b) $D = 1$

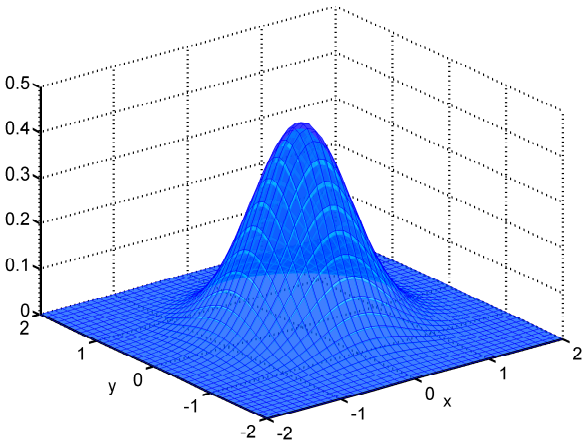

(c) $D = 2$

Figure 4.3: Gaussian reference (mean time $t = 0.1$, blue) and output field for Example 3 (cyan) at time $t = 0.25$ for $k = 7.6$ and $v = 20$.

4.7 Simulations

In this section, optimal control problems are solved by using the Fortran simulated annealing code SIMANN [81], with the system having constant values $D = 1$, $k = 7.6$, and $v = 20$. The reference field for Examples 1 and 2 (Figure 4.4) is Matlab's MEMBRANE function, which is an L-shaped membrane, with parameter values

$$l = 1, \quad m = 10, \quad n = 9, \quad np = 9, \tag{4.69}$$

where

- $l =$ index of eigenfunction
- $m =$ number of points on 1/3 of boundary (the size of the output is $(2m + 1) \times (2m + 1)$)
- $n =$ number of terms in the summation
- $np =$ number of terms in the partial summation

and stretched spatially by a factor of five. For Example 3, the same function is multiplied by $\sin \frac{\pi t}{1.8}$ to obtain a time-varying reference field. See [147] for the details of this function.

In Step 1, the data points were taken uniformly in space (and uniformly in time for Example 3). The numbers of data points, RBF terms, and optimization variables are summarized in Table 4.1.

Table 4.1: Step 1

	Ex. 1	Ex. 2	Ex. 3
# of data points in Step 1	441	441	15,876
# of terms in RBF expansion	5	5	5
# of optimization variables	25	25	35

In all three examples, the differences between the 2D concentration field at $z = 1$ and the target can be reduced by using more terms in the RBF expansion.

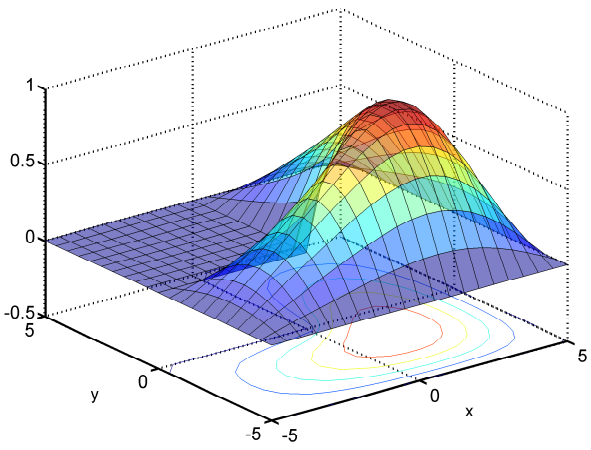

(a) Ex. 1 and 2

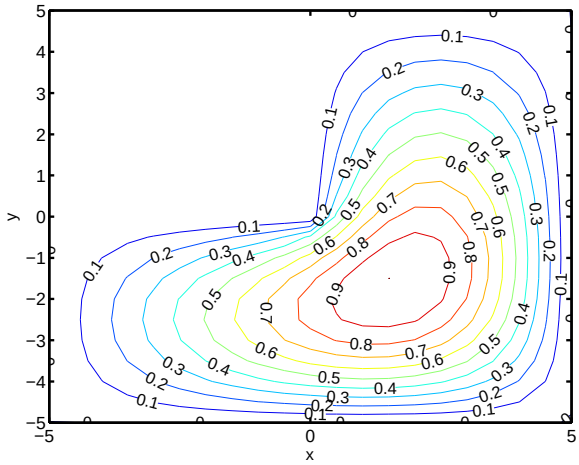

(b) Ex. 1 and 2

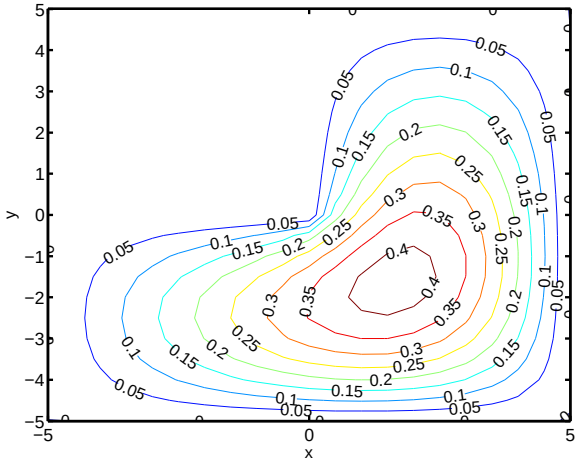

(c) Ex. 3

Figure 4.4: (a,b) Reference field with topographical maps for Examples 1 and 2 and (c) topographical map for Example 3 at $t = 0.25$.

4.7.1 Example 1

The results of applying the optimal control input field (Figure 4.5a) obtained by applying the procedure is shown in Figure 4.5c. The 2D concentration field at $z = 1$ is indistinguishable from the RBF expansion of the target field (compare with Figure 4.5b), and in fact, theoretically they are exactly the same.

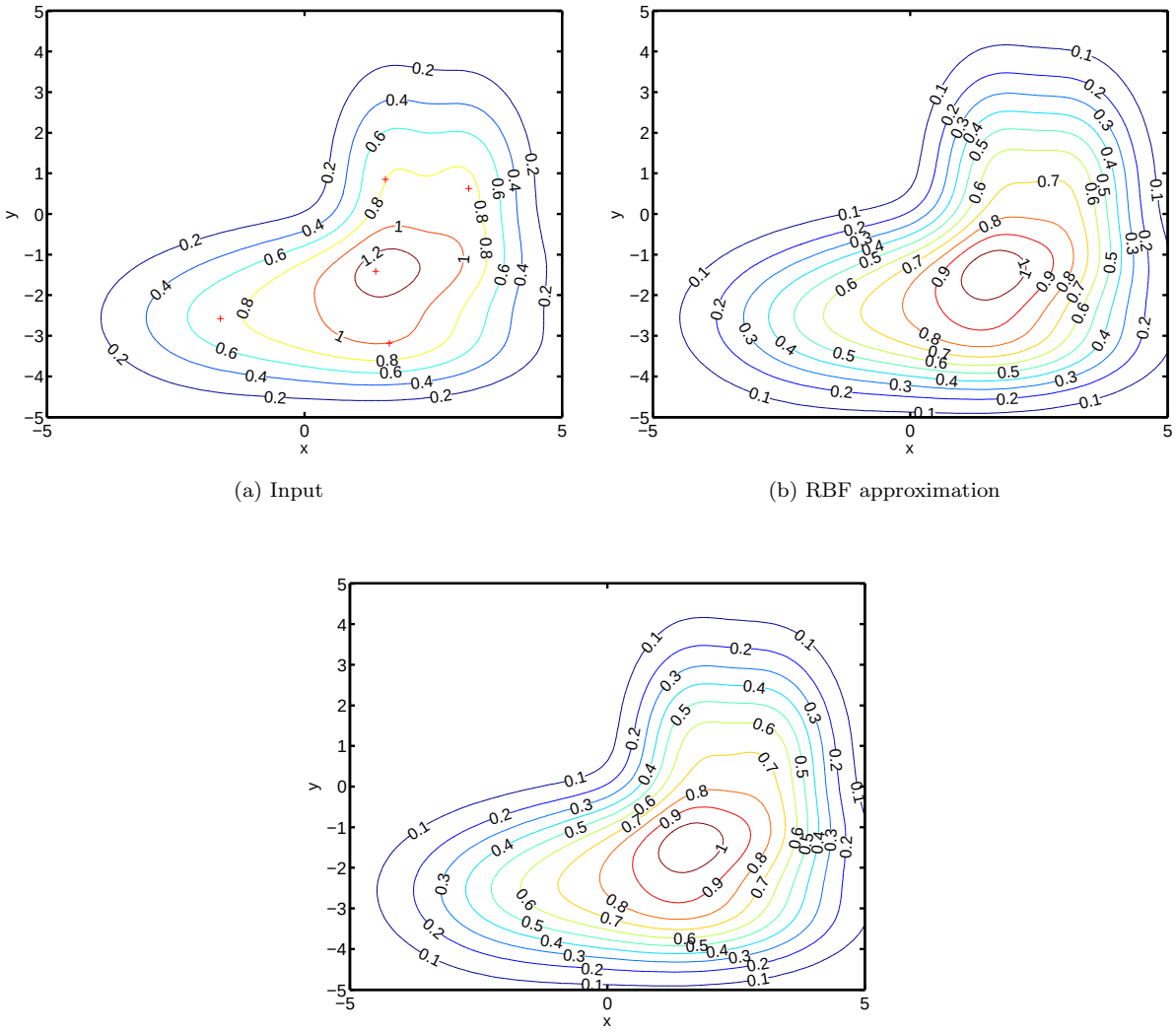

(a) Input

(b) RBF approximation

(c) output

Figure 4.5: Topographical maps for Example 1. Red + indicates the center of the Gaussians for the input field.

4.7.2 Example 2

The results of applying the optimal control input field (Figure 4.6a) is in Figure 4.6c. Although the optimal control procedure is not globally optimal, the resulting 2D concentration field at $z = 1$ is indistinguishable by eye from the RBF expansion of the target field (Figure 4.6b) for those particular parameter values (i.e., $D = 1$, $k = 7.6$, and $v = 20$) and the reference field.

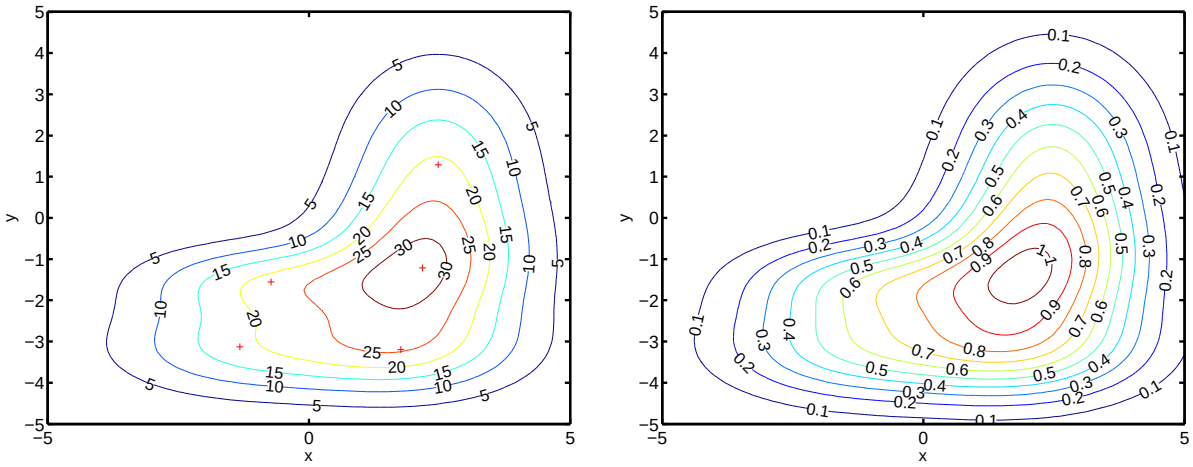

(a) Input

(b) RBF approximation

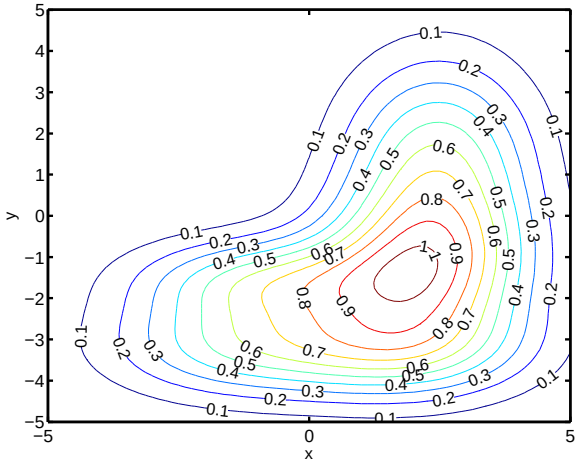

(c) output

Figure 4.6: Topographical maps for Example 2. Red + indicates the center of the Gaussians for the input field.

4.7.3 Example 3

A snapshot of the topographical map for the reference concentration field is in Figure 4.4c. The results of applying the optimal control input field (Figure 4.7a) is in Figure 4.7c. As in the Example 2, although the optimal control procedure is not globally optimal, as the resulting convolution is not Gaussian, the resulting 2D concentration field at $z = 1$ is indistinguishable by eye from the RBF expansion of the target field (Figure 4.7b).

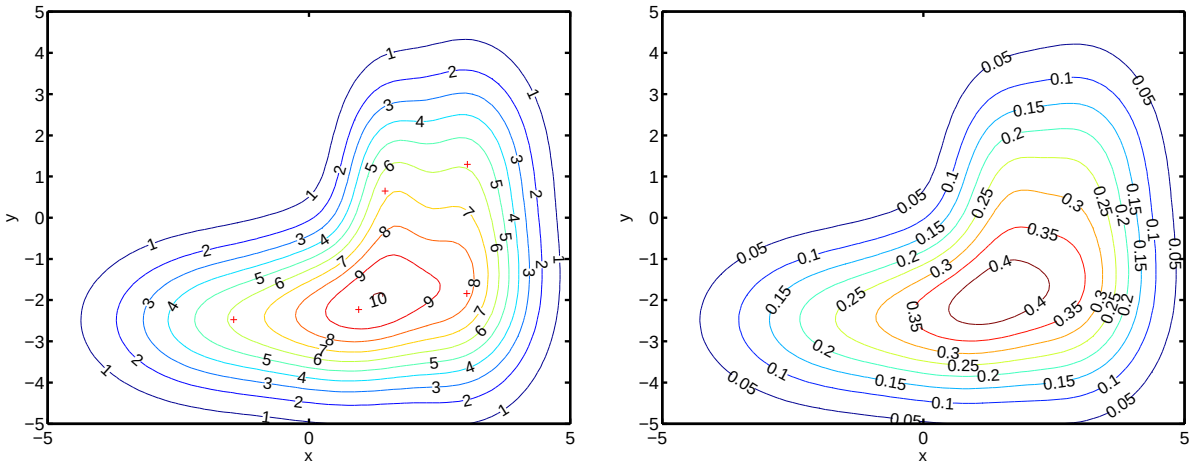

(a) Input

(b) RBF approximation

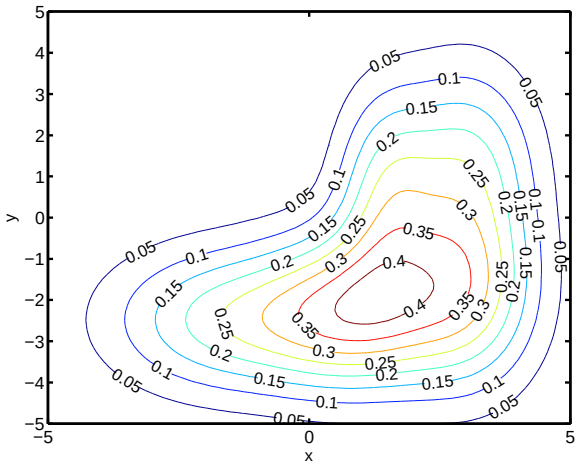

(c) output

Figure 4.7: Topographical maps for Example 3 at $t = 0.25$. Red + indicates the center of the Gaussians for the input field.

4.8 Generalizations

A procedure that combines RBF expansions with moment analysis was proposed for the solution of optimal control problems for linear spatially-distributed systems with multiple spatial dimensions. While this approach was motivated by a particular 2D spatial control problem, a simplification of the approach can be applied to PDEs with one spatial dimension or even to systems of ordinary differential equations (in which case the RBF expansion is only with respect to the time variable). The computational requirements of the optimal control procedure is low enough that it can be applied at each time instance in a shrinking- or receding-horizon control algorithm. The most expensive computational tasks are the determination of the RBF expansion of the target field and, in some cases, the system moments, which can be computed off-line. The on-line computation is simple analytical expressions to compute the moments of the individual terms in the summation for the control input field in terms of the system and target moments.

As the computational efficiency of the approach is directly related to the number of terms in the RBF expansion, the efficiency increases as the reference field becomes more smooth. On the other hand, the computational cost is not a function of the smoothness of the state or control input fields. *This is a major advantage over other control parameterization approaches*, which focus on expansions of the state and/or optimal control instead of the reference.

4.9 Conclusions

Examples provided a step-by-step description of the application of the proposed approach. The RBF expansion of the target field was exactly obtainable at a specified time instance due to a nice property of the Gaussian distribution function. For longer time intervals, the mean and variances of each RBF could be matched exactly. In all three examples, the 2D concentration field at $z = 1$ obtained by the control input field was very close to the RBF expansion of the target field.

CHAPTER 5

BASIS FUNCTION BASED 3D SPATIAL FIELD CONTROL

Optimal control problems are formulated and solved in which the manipulation is distributed over a three-dimensional (3D) spatial field with constraints on the spatial variation. These spatial field control problems that arise in applications in acoustics, structures, epidemiology, cancer treatment, and tissue engineering have much higher controllability than boundary control problems, but have vastly higher degrees of freedom. Efficient algorithms are developed for computing optimal manipulated fields by combination of modal analysis and least-squares optimization over a basis function space. Small minimum control error is observed in applications to distributed parameter systems with reaction, diffusion, and convection.

5.1 Introduction

Spatial field control is a class of control problems for distributed parameter systems (DPS) in which manipulation occurs as a spatial field, in contrast to the more commonly studied problem of boundary control (e.g., [191]) in which manipulation only occurs at the boundaries. The interior of a spatial domain provides much more controllability than the boundary, which can be quite limited depending on the shape of the desired spatial field and the spatiodynamics of the DPS. At the same time, spatial field control problems have much more degrees of freedom than the corresponding boundary control problem. The manipulated variable for 3D spatial field control is $u(x, y, z, t)$, compared to boundary control which is only defined on the 2D external surface. While the brute-force application of control vector parameterization [170] may be applied to boundary control and most other optimal control problems, spatial field control problems need to be formulated with care to arrive at a computationally feasible solution. Below is the formal definition of a prototypical problem.

Definition 5.1.1. *The optimal spatial field control problem is the minimization of the quadratic cost*

$$\min_{u(x,y,z,t)\in\mathcal{U}(x,y,z,t)} \int_T \int_V (R(x,y,z,t) - C(x,y,z,t))^2 dV dt, \tag{5.1}$$

where T is the time range of interest, V is the spatial domain of interest, $R(x,y,z,t)$ is the reference (desired) field, $C(x,y,z,t)$ is the controlled field which is related to the manipulated field $u(x,y,z,t)$ by a known partial differential equation (PDE), and $\mathcal{U}(x,y,z,t)$ is the set of allowable manipulated fields, which can be continuous or discrete in space or time.

Spatial field control problems arise in a variety of applications including

1. minimization of vibration throughout a structure by using internally placed piezo-actuators [146],
2. minimization of noise in acoustic enclosures using internally placed loudspeakers and/or microphones [154],
3. control of the spread of disease by placement of insecticide-treated targets or by insecticide spraying to reduce the disease carrier population to zero over large tracts of land [88],
4. control of the differentiation of stem cell populations by internal release of growth factors to produce biological tissues for clinical use [112], and
5. the controlled release of drug cocktails for optimized cancer treatment therapies [192].

The spatial field control literature includes many theoretical results on controllability and the structure of the optimal control for certain classes of PDEs when the spatial field is continuous or consists of a finite number of point sources (e.g., see [15, 124, 125] and citations therein) but has relatively few contributions that compute the optimal control for specific applications. An exception is [146] that computes H_2- and H_∞-optimal vibration controllers for the case in which the manipulation is restricted to discrete positions in the spatial domain. H_2- and H_∞-control for the spatially distributed formulation of the problem results in better performance than the lumped-parameter representation.

This chapter presents a computationally efficient solution to the optimal spatial field control problem for the reaction-diffusion and reaction-diffusion-convection equations in which the manipulation $u(x,y,z,t)$ is continuously distributed throughout the spatial domain with constraints on the spatial variation. These particular control problems are motivated by biomedical control problems [112, 192], in which molecules are released within a biological tissue from fixed embedded polymer nano- and microparticles designed to provide controlled release. The transport of these molecules is described by 3D reaction-diffusion or reaction-diffusion-convection equations, and the control problem is to provide a desired spatial and temporal uptake of these molecules throughout the biological tissue. More details on the biological motivation for the optimal control problem, including numerous references to the biomedical literature, was provided in a paper [112].

The approach taken in this chapter is based on modal analysis and least-squares optimization over a basis function space [134]. This approach does not involve the discretizations of the spatial variables or problem-independent basic function expansions (e.g., proper orthogonal decomposition) that have become popular in the applied PDE control literature (e.g., [117]) but are much more computational expensive when applied to spatial field control problems. Also, this chapter considers 3D optimal nonlinear control problems, in contrast to the literature that primarily considers 1D linear problems, and the chapter also considers coupled systems of PDEs. The algorithmic discussions are followed by a numerical example and the conclusions.

5.2 Reaction-Diffusion-Convection Equation

Consider the reaction-diffusion-convection equation,

$$\frac{\partial C}{\partial t} = D\nabla^2 C - v \cdot \nabla C - g(C) + u(x,y,z,t),$$
$$\forall t > 0, \quad (x,y,z) \in \Omega = (0,1)^3, \tag{5.2}$$

with zero initial condition,

$$C(x,y,z,0) = 0, \tag{5.3}$$

and the Dirichlet boundary condition

$$C(x,y,z,t) = 0, \quad \text{on} \quad \partial\Omega, \tag{5.4}$$

where $C(x,y,z,t)$ is the concentration field, $D > 0$ is an effective diffusion coefficient, v is the vector velocity field assumed to be spatially uniform, $g(C)$ is a sublinear algebraic function that characterizes the net consumption of species by chemical reactions.

The control objective is to determine a continuous minimum-energy manipulated field $u(x,y,z,t)$ of constrained spatial variation that minimizes the control error[1]

$$E = \int_T \int_\Omega (R(x,y,z,t) - C(x,y,z,t))^2 dV dt, \tag{5.5}$$

where T is the time range of interest and $R(x,y,z,t)$ is the reference concentration field.

The spatial variation constraints are specified by the selection of M, N, and L in the Fourier series

$$u(x,y,z,t) = \frac{1}{8} \sum_{m=-M}^{M} \sum_{n=-N}^{N} \sum_{l=-L}^{L} u_{mnl}(t) e^{(m\pi x + n\pi y + l\pi z)j} \tag{5.6}$$

[1] $\int_\Omega dV = \int_0^1 \int_0^1 \int_0^1 dxdydz$

with the optimal control problem involving the determination of $u_{mnl}(t)$ for $-M \leq m \leq M$, $-N \leq n \leq N$, and $-L \leq l \leq L$. For the given boundary conditions, this simplifies to a Fourier sine series[2]

$$u(x,y,z,t) = \sum u_{mnl}(t) \sin m\pi x \sin n\pi y \sin l\pi z \tag{5.7}$$

$$=: u_{MNL}(x,y,z,t). \tag{5.8}$$

Assumptions: The reference field $R(x,y,z,t)$ is

1. continuous on Ω,
2. $R(x,y,z,0) = 0$,
3. $R(x,y,z,t) = 0$ on $\partial\Omega$,
4. square integrable in space, at each time,
5. differentiable in time.

Under these assumptions, the Fourier series of $R(x,y,z,t)$ can be written as a Fourier sine series[3]

$$R(x,y,z,t) := \sum_{}^{\infty} r_{mnl}(t) \sin m\pi x \sin n\pi y \sin l\pi z, \tag{5.9}$$

where

$$r_{mnl}(t) = 8 \int_{\Omega} R(x,y,z,t) \sin m\pi x \sin n\pi y \sin l\pi z \, dV. \tag{5.10}$$

Separate the reference field into its low and high spatial frequencies:

$$R(x,y,z,t) = R_{MNL}(x,y,z,t) + \epsilon_{MNL}(x,y,z,t), \tag{5.11}$$

where[4]

$$R_{MNL}(x,y,z,t) := \sum r_{mnl}(t) \sin m\pi x \sin n\pi y \sin l\pi z, \tag{5.12}$$

and ϵ_{MNL} is a linear combination of the eigenmodes not included in the summation.

Under the assumptions, the following properties hold for all t [11]:

1. by the Dirichlet theorem, the Fourier sine series of $R(x,y,z,t)$ converges pointwise to $R(x,y,z,t)$, i.e.,

$$\lim_{M,N,L\to\infty} |R(x_0,y_0,z_0,t) - R_{MNL}(x_0,y_0,z_0,t)| = 0, \quad \forall (x_0,y_0,z_0) \in \Omega \tag{5.13}$$

[2] $\sum := \sum_{m=1}^{M} \sum_{n=1}^{N} \sum_{l=1}^{L}$
[3] $\sum^{\infty} := \sum_{m=1}^{\infty} \sum_{n=1}^{\infty} \sum_{l=1}^{\infty}$
[4] $\sum := \sum_{m=1}^{M} \sum_{n=1}^{N} \sum_{l=1}^{L}$

2. by the Riesz-Fischer theorem, the Fourier sine series of $R(x,y,z,t)$ converges to $R(x,y,z,t)$ in the space l^2, i.e.,

$$\lim_{M,N,L\to\infty}\int_\Omega (R(x,y,z,t)-R_{MNL}(x,y,z,t))^2 dV = 0. \tag{5.14}$$

To determine a continuous minimum-energy manipulated field $u(x,y,z,t)$, reformulate the problem. By defining

$$\bar{u}(x,y,z,t) := u(x,y,z,t) - v\cdot\nabla C - g(C), \quad \forall t>0, \quad (x,y,z)\in\Omega=(0,1)^3, \tag{5.15}$$

the PDE (5.2) is reduced to

$$\frac{\partial C}{\partial t} = D\nabla^2 C + \bar{u}(x,y,z,t), \tag{5.16}$$

subject to (5.3) and (5.4).

Claim 5.2.1. *For linear $g(C)$, if $\bar{u}(x,y,z,t)$ is in the form of*

$$\bar{u}(x,y,z,t) = \sum \bar{u}_{mnl}(t)\sin m\pi x \sin n\pi y \sin l\pi z \tag{5.17}$$

$$:= \bar{u}_{MNL}(x,y,z,t), \tag{5.18}$$

then $\bar{u}(x,y,z,t)$ and $u(x,y,z,t)$ have the same maximum spatial frequency.

Proof. Let $\omega(u)$ denote the maximum spatial frequency of u. For the PDE (5.16), it can be verified that the manipulated field,

$$\bar{u}_{mnl}(t)\sin m\pi x \sin n\pi y \sin l\pi z, \tag{5.19}$$

excites only the modes $\sin m\pi x$, $\sin n\pi y$, $\sin l\pi z$, that is, the solution to the PDE for that manipulated field (5.19) is of the form

$$C(x,y,z,t) = c_{mnl}(t)\sin m\pi x \sin n\pi y \sin l\pi z, \tag{5.20}$$

which implies that

$$\omega(C) = \omega(\bar{u}). \tag{5.21}$$

Linearity of $g(C)$ implies

$$\omega(g(C)) = \omega(C) = \omega(\bar{u}). \tag{5.22}$$

Since taking the derivative does not change the spatial frequency,

$$\begin{aligned}\omega(u) &= \max\{\omega(\bar{u}), \omega(C), \omega(g(C))\} \\ &= \max\{\omega(\bar{u}), \omega(C)\} \\ &= \omega(\bar{u}). \end{aligned} \tag{5.23}$$

□

The above analysis shows that the spatial frequency constraints on the transformed problem are directly translated to the original problem. A similar analysis can be used to show the converse, so that the satisfaction of spatial frequency constraints on either problem is equivalent to the satisfaction of the same spatial frequency constraints on the other problem.

Claim 5.2.2. *There exists a continuous manipulated field $\bar{u}(x, y, z, t)$ for (5.16) that produces the concentration field*

$$C(x, y, z, t) = R_{MNL}(x, y, z, t). \tag{5.24}$$

Moreover, this continuous manipulated field $\bar{u}(x, y, z, t)$ is given by

$$\bar{u}(x, y, z, t) = \sum \bar{u}_{mnl}(t) \sin m\pi x \sin n\pi y \sin l\pi z \tag{5.25}$$

$$:= \bar{u}^*_{MNL}(x, y, z, t), \tag{5.26}$$

where

$$\bar{u}_{mnl}(t) = \frac{dr_{mnl}}{dt} + D(m^2 + n^2 + l^2)\pi^2 r_{mnl}. \tag{5.27}$$

Proof. The first step is to show that the manipulated field $\bar{u}^*_{MNL}(x, y, z, t)$ results in the concentration field (5.24). Insertion of the manipulated field (5.19) into the PDE (5.16) results in the concentration field (5.20) with $\bar{u}_{mnl}(t)$ and $c_{mnl}(t)$ related by

$$\bar{u}_{mnl}(t) = \frac{dc_{mnl}}{dt} + D(m^2 + n^2 + l^2)\pi^2 c_{mnl}. \tag{5.28}$$

The initial conditions (5.3) and Assumption 2 imply that

$$r_{mnl}(0) = c_{mnl}(0) = 0, \tag{5.29}$$

which implies that, along with (5.27) and (5.28), $c_{mnl}(t) = r_{mnl}(t), \forall t \in T$. This implies that the solution to the PDE for the manipulated field (5.19) is

$$C(x, y, z, t) = r_{mnl}(t) \sin m\pi x \sin n\pi y \sin l\pi z. \tag{5.30}$$

By linearity, the solution to the PDE (5.16) for the manipulated field (5.26) is

$$\begin{aligned} C(x,y,z,t) &= \sum r_{mnl}(t) \sin m\pi x \sin n\pi y \sin l\pi z \\ &= R_{MNL}(x,y,z,t). \end{aligned} \tag{5.31}$$

□

Claim 5.2.3. *$\bar{u}^*_{MNL}(x,y,z,t)$ is the unique minimum-energy manipulated field that produces the concentration field (5.24) for the transformed problem.*

Proof. Apply proof by contradiction. Supposing that there exists an additional minimum-energy manipulated field

$$\begin{aligned} \bar{u}(x,y,z,t) &= \bar{u}^*_{MNL}(x,y,z,t) + \tilde{u}(x,y,z,t) \\ &\neq \bar{u}^*_{MNL}(x,y,z,t) \end{aligned} \tag{5.32}$$

that produces the concentration field (5.24), then[5]

$$R_{MNL}(x,y,z,t) = \int_0^t \int_\Omega \bar{u}(\bar{x},\bar{y},\bar{z},\tau) G(x,y,z,\bar{x},\bar{y},\bar{z},t-\tau) d\bar{V} d\tau, \tag{5.33}$$

for all $t \in T$ where G is the Green's function:

$$G(x,y,z,\bar{x},\bar{y},\bar{z},t) = 8 \sum^{\infty} e^{-D(m^2+n^2+l^2)\pi^2 t} \sin m\pi x \sin n\pi y \sin l\pi z \sin m\pi \bar{x} \sin n\pi \bar{y} \sin l\pi \bar{z}. \tag{5.34}$$

The energy of $\hat{u}(x,y,z,t)$ is[6]

$$\begin{aligned} \int_{T\Omega} \bar{u}^2 dV dt &= \int_{T\Omega} \left(\bar{u}^*_{MNL} + \tilde{u}\right)^2 dV dt \\ &= \int_{T\Omega} \bar{u}^{*2}_{MNL} dV dt + 2 \int_{T\Omega} u^*_{MNL} \tilde{u} dV dt + \int_{T\Omega} \tilde{u}^2 dV dt \\ &= \int_{T\Omega} \bar{u}^{*2}_{MNL} dV dt + \int_{T\Omega} \tilde{u}^2 dV dt \\ &> \int_{T\Omega} \bar{u}^{*2}_{MNL} dV dt. \end{aligned} \tag{5.35}$$

which contradicts the assumption that the additional manipulated field is minimum-energy. The third

[5] $\int_\Omega d\bar{V} = \int_0^1 \int_0^1 \int_0^1 d\bar{x} d\bar{y} d\bar{z}$

[6] $\int_{T\Omega} f dV t := \int_T \int_\Omega f(x,y,z,t) dV dt$

equality follows from

$$
\begin{aligned}
0 &= \int_0^t \int_\Omega \tilde{u}(\bar{x},\bar{y},\bar{z},\tau) G(x,y,z,\bar{x},\bar{y},\bar{z},t-\tau) d\bar{V} d\tau, \quad \forall (x,y,z) \in \Omega, \forall t \in T \\
\Rightarrow 0 &= \int_\Omega \tilde{u}(\bar{x},\bar{y},\bar{z},\tau) G(x,y,z,\bar{x},\bar{y},\bar{z},t-\tau) d\bar{V}, \quad \forall (x,y,z) \in \Omega, \forall t,\tau \in T \\
\Rightarrow 0 &= \int_\Omega \tilde{u}(\bar{x},\bar{y},\bar{z},\tau) \left(8 \sum^{\infty} e^{-D(m^2+n^2+l^2)\pi^2(t-\tau)} \sin m\pi x \sin n\pi y \sin l\pi z \sin m\pi \bar{x} \sin n\pi \bar{y} \sin l\pi \bar{z} \right) d\bar{V}, \\
& \qquad \forall (x,y,z) \in \Omega, \forall t,\tau \in T \\
\Rightarrow 0 &= \sum^{\infty} \int_\Omega \tilde{u}(\bar{x},\bar{y},\bar{z},\tau) \sin m\pi \bar{x} \sin n\pi \bar{y} \sin l\pi \bar{z} d\bar{V} e^{-D(m^2+n^2+l^2)\pi^2(t-\tau)} \sin m\pi x \sin n\pi y \sin l\pi z, \\
& \qquad \forall (x,y,z) \in \Omega, \forall t,\tau \in T \\
\Rightarrow 0 &= \int_\Omega \tilde{u}(x,y,z,t) \sin m\pi x \sin n\pi y \sin l\pi z dV, \quad \forall (m,n,l) \\
\Rightarrow 0 &= \sum \bar{u}_{mnl}(t) \int_\Omega \tilde{u}(x,y,z,t) \sin m\pi x \sin n\pi y \sin l\pi z dV, \\
\Rightarrow 0 &= \int_\Omega \tilde{u}(x,y,z,t) \sum \bar{u}_{mnl}(t) \sin m\pi x \sin n\pi y \sin l\pi z dV, \\
\Rightarrow 0 &= \int_\Omega \tilde{u}(x,y,z,t) \bar{u}_{MNL}(x,y,z,t) dV. \qquad (5.36)
\end{aligned}
$$

The last inequality results from that (5.32) implies

$$\exists (x,y,z,t) \quad \text{s.t.} \quad \tilde{u}(x,y,z,t) \neq 0, \qquad (5.37)$$

since $\hat{u}$ is continuous

$$\int_{T\Omega} \tilde{u}^2 dV t > 0. \qquad (5.38)$$

□

Remarks:

- The optimization for determining $\bar{u}_{mnl}$ for each (m,n,l) is independent. This solution of the optimal control problem is very closely related to *spectral methods* [74] for the numerical simulation of PDEs.
- If the reference field is such that the integral (5.10) can be solved analytically, then (5.26) can be determined analytically from (5.27) and the computational cost of computing the optimal manipulated field is negligible.
- If the integral (5.10) cannot be solved analytically, then the $r_{mnl}(t)$ can be computed efficiently by sampling with a uniform mesh and applying available numerical software for computing multidimensional fast Fourier transforms [84].

Claim 5.2.4. *Consider the optimal control problem with the assumptions*

1. $v = 0$,
2. $g(C)$ *is linear, i.e.,* $g(C) = kC$.

For the minimum-energy manipulated field $\bar{u}^*_{MNL}(x, y, z, t)$ *that achieves* $R_{MNL}(x, y, z, t)$ *for the transformed system, its corresponding manipulated field*

$$u^*_{MNL}(x, y, z, t) = \bar{u}^*_{MNL}(x, y, z, t) + kC \tag{5.39}$$

achieves $R_{MNL}(x, y, z, t)$ *for the original system while having minimum energy.*

Proof. For the manipulated field $u_{MNL}(x, y, z, t)$ that produces the concentration field $R_{MNL}(x, y, z, t)$ in the original problem, the manipulated field

$$\begin{aligned} \bar{u}_{MNL}(x, y, z, t) &= u_{MNL}(x, y, z, t) - kC & (5.40)\\ &= u_{MNL}(x, y, z, t) - kR_{MNL} & (5.41) \end{aligned}$$

produces the concentration field $R_{MNL}(x, y, z, t)$ in the transformed system. Consider a proof by contradiction. Suppose that

$$\bar{u}_{MNL}(x, y, z, t) \neq \bar{u}^*_{MNL}(x, y, z, t), \tag{5.42}$$

then define the difference by

$$\bar{u}_{MNL}(x, y, z, t) = \bar{u}^*_{MNL}(x, y, z, t) + \tilde{u}(x, y, z, t), \tag{5.43}$$

where

$$\int_\Omega \tilde{u}(x, y, z, t) \sin m\pi x \sin n\pi y \sin l\pi z dV = 0, \tag{5.44}$$

from (5.36). The energy of the manipulated field for the original problem is

$$\begin{aligned} &\int_{T\Omega} u^2_{MNL} dV dt \\ &= \int_{T\Omega} \left(\bar{u}^*_{MNL}(x, y, z, t) + \tilde{u}(x, y, z, t) + kR_{MNL}\right)^2 dV dt \\ &= \int_{T\Omega} \left(\bar{u}^*_{MNL}(x, y, z, t) + kR_{MNL}\right)^2 dV dt + \int_{T\Omega} \tilde{u}(x, y, z, t)^2 dV dt \\ &> \int_{T\Omega} \left(\bar{u}^*_{MNL}(x, y, z, t) + kR_{MNL}\right)^2 dV dt. \end{aligned} \tag{5.45}$$

The second equality follows from the orthogonality, and the third inequality follows from (5.38). □

The above result implies that, under the given assumptions, the minimum-energy manipulated field for the original system can be written by the Fourier sine series.

With given M, N, and L for the manipulated field, the minimum control error E in (5.5) is bounded by the output field produced by the manipulated field $\bar{u}^*_{MNL}$:

$$E \leq \int_{T\Omega} \left(R(x,y,z,t) - R_{MNL}(x,y,z,t)\right)^2 dVt \tag{5.46}$$

$$= \int_{T\Omega} \epsilon^2_{MNL}(x,y,z,t) dVt. \tag{5.47}$$

This upper bound is independent of the diffusion coefficient and reaction rate, and is only a function of the portion of the reference field not described by the selected eigenfunctions. Relaxing the spatial variation constraint increases the number of terms in the series and decreases the minimum control error.

Claim 5.2.5. *Under the assumptions*

1. $u(x,y,z,t) = 0$ *on* $\partial\Omega$,
2. $v = 0$,
3. $g(C)$ *is linear,*

the inequality (5.46) is satisfied as an equality.

Proof. Under the assumptions, $\bar{u}(x,y,z,t)$ can be parameterized by using the Fourier sine series,

$$\bar{u}(x,y,z,t) := \sum^{\infty} \bar{u}_{mnl}(t) \sin m\pi x \sin n\pi y \sin l\pi z, \tag{5.48}$$

where

$$\bar{u}_{mnl}(t) = 8 \int_{\Omega} \bar{u}(x,y,z,t) \sin m\pi x \sin n\pi y \sin l\pi z \, dV. \tag{5.49}$$

The manipulated field that satisfies the spatial constraints is of the form

$$\bar{u}(x,y,z,t) = \sum \bar{u}_{mnl}(t) \sin m\pi x \sin n\pi y \sin l\pi z, \tag{5.50}$$

where $\bar{u}_{mnl}(t)$ are to be determined, and its output concentration field is of the form

$$C(x,y,z,t) = \sum c_{mnl}(t) \sin m\pi x \sin n\pi y \sin l\pi z, \tag{5.51}$$

where

$$\bar{u}_{mnl}(t) = \frac{dc_{mnl}(t)}{dt} + D(m^2+n^2+l^2)\pi^2 c_{mnl}(t). \tag{5.52}$$

The control error is

$$E = \int_{T\Omega} \left[\left(\sum (r_{mnl}(t) - c_{mnl}(t)) \sin m\pi x \sin n\pi y \sin l\pi z \right)^2 + \epsilon^2_{MNL}(x, y, z, t) \right] dVt, \tag{5.53}$$

which follows from orthogonality of the eigenfunctions. By setting $c_{mnl} = r_{mnl}$ to determine $\bar{u}_{mnl}$, the equality is achieved. □

The statements in (5.13) and (5.14) become

$$\lim_{M,N,L\to\infty} |R(x_0, y_0, z_0, t) - C(x_0, y_0, z_0, t)| = 0, \quad \forall (x_0, y_0, z_0) \in \Omega, \tag{5.54}$$

and

$$\lim_{M,N,L\to\infty} \int_{\Omega} (R(x, y, z, t) - C(x, y, z, t))^2 \, dV = 0, \tag{5.55}$$

respectively. These imply that the minimum control error satisfies

$$\lim_{M,N,L\to\infty} \int_{T} \int_{\Omega} (R(x, y, z, t) - C(x, y, z, t))^2 \, dV dt = 0. \tag{5.56}$$

Once $\bar{u}(x, y, z, t) = \sum \bar{u}_{mnl}(t) \sin m\pi x \sin n\pi y \sin l\pi z$ is determined, the manipulated field for the original PDE can be determined from (5.15):

$$u(x, y, z, t) = \bar{u}(x, y, z, t) + v \cdot \nabla C + g(C), \tag{5.57}$$

where C is inserted from (5.31). The optimal solution is

$$\begin{aligned} u(x, y, z, t) = g(R) &+ \sum u_{1,mnl}(t) \sin m\pi x \sin n\pi y \sin l\pi z + \sum u_{2,mnl}(t) \cos m\pi x \sin n\pi y \sin l\pi z \\ &+ \sum u_{3,mnl}(t) \sin m\pi x \cos n\pi y \sin l\pi z + \sum u_{4,mnl}(t) \sin m\pi x \sin n\pi y \cos l\pi z, \end{aligned} \tag{5.58}$$

where

$$u_{1,mnl}(t) = \frac{dr_{mnl}}{dt} + D(m^2 + n^2 + l^2)\pi^2 r_{mnl}, \tag{5.59}$$

$$u_{2,mnl}(t) = m\pi v_x r_{mnl}(t), \tag{5.60}$$

$$u_{3,mnl}(t) = n\pi v_y r_{mnl}(t), \tag{5.61}$$

$$u_{4,mnl}(t) = l\pi v_z r_{mnl}(t). \tag{5.62}$$

5.3 Coupled Reaction-Diffusion-Convection Equations

Consider the optimal spatial field control of coupled reaction-diffusion-convection equations:

$$\min_{\substack{u_i(x,y,z,t) \\ \in \mathcal{U}_i(x,y,z,t)}} \sum_i \int_0^{t_f} \int_V (R_i(x,y,z,t) - C_i(x,y,z,t))^2 dV dt, \tag{5.63}$$

where

$$\frac{\partial C_i}{\partial t} = D_i \nabla^2 C_i - v \cdot \nabla C_i - g_i(C_1, \ldots, C_N) + u_i(x,y,z,t), \tag{5.64}$$

$$C_i(x,y,z,t) = 0, \quad \text{on} \quad \partial\Omega, \tag{5.65}$$

and

$$C_i(x,y,z,0) = 0. \tag{5.66}$$

With the definitions

$$\bar{u}_i = u_i(x,y,z,t) - g_i(C_1, \ldots, C_N), \quad i = 1, \ldots, N, \tag{5.67}$$

or

$$\bar{u}_i = u_i(x,y,z,t) - v \cdot \nabla C_i - g_i(C_1, \ldots, C_N), i = 1, \ldots, N, \tag{5.68}$$

the determination of the optimal $\bar{u}_i$ are decoupled. Once the optimal $\bar{u}_i$ have been determined, the species concentration fields C_i and untransformed optimal manipulated fields u_i are determined in the same way as in the previous section.

5.4 Numerical Examples

Consider the spatial field control problem with diffusion, linear chemical reaction kinetics $g(C) = kC$, convection in the x-direction, and reference field[7]

$$R(x, y, z, t) = (e^{-x} - e^{-3x})(e^{-y} - e^{-4y})(e^{-2z} - e^{-4z})(e^{-t} - e^{-2t}). \tag{5.69}$$

In a stem tissue engineering application, this reference field corresponds to a 3D spatial region and time in which a cellular uptake of growth factor is desired to cause the stem cells in that region to differentiate to form a specific type of cell (such as an islet cell in the generation of a pancreas for treatment of a diabetic patient). The reader is referred to a paper for a more detailed discussion of these applications [112].

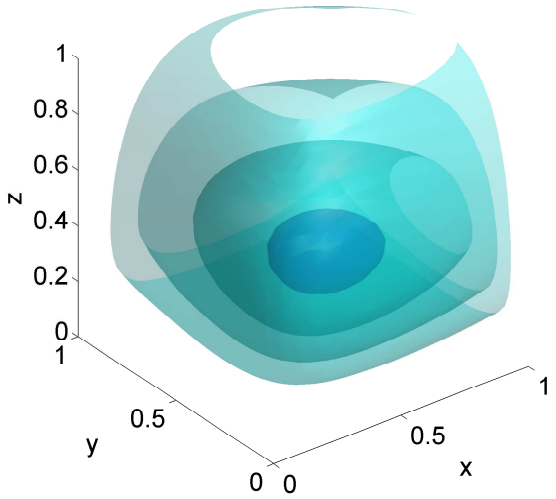

Figure 5.1: Reference concentration fields showing isosurfaces of 0.01, 0.008, 0.006, and 0.004 from inside to outside at $t = 1$.

The isosurfaces for the reference and controlled concentration fields show good correspondence as the number of terms in each of the three spatial directions increases (see Figures 5.1 and 5.2). The mononotic decrease in the control error with the inclusion of increased number of spatial frequencies is shown in Figure 5.3. The control error drops by approximately 50% when going from $N = M = L = 1$ to $N = M = L = 3$ terms. The isosurfaces for the input field is skewed downstream when the process includes convection in the positive x-direction (see Figures 5.4 and 5.5). This skewness agrees with physical intuition, in that an increased control input is needed downstream to compensate for the molecules that leave the domain at $x = 1$ due to convection.

[7] All variables have been rescaled to be in dimensionless form.

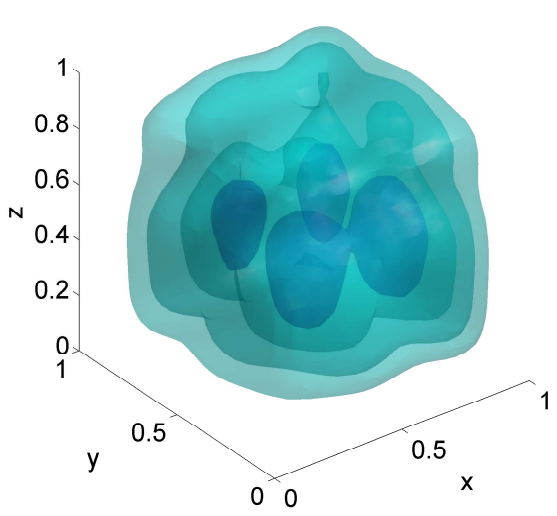

(a) $N = M = L = 5$

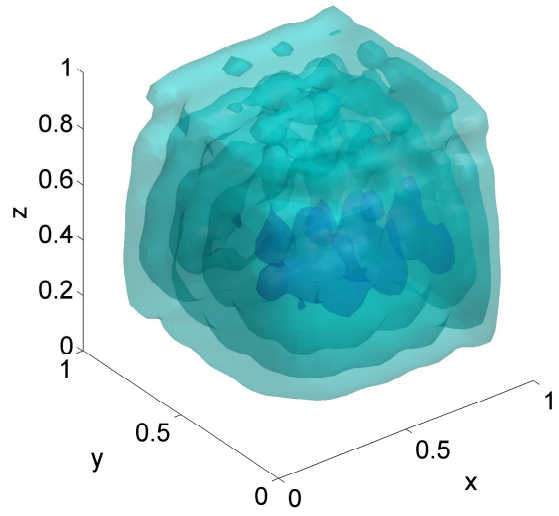

(b) $N = M = L = 10$

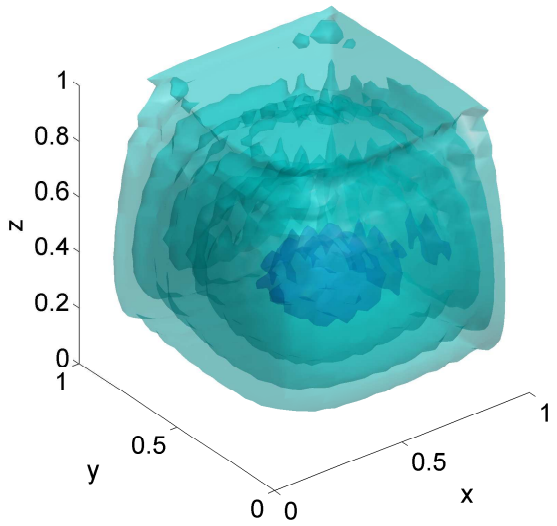

(c) $N = M = L = 20$

Figure 5.2: Optimal concentration fields showing isosurfaces of 0.01, 0.008, 0.006, and 0.004 from inside to outside at $t = 1$.

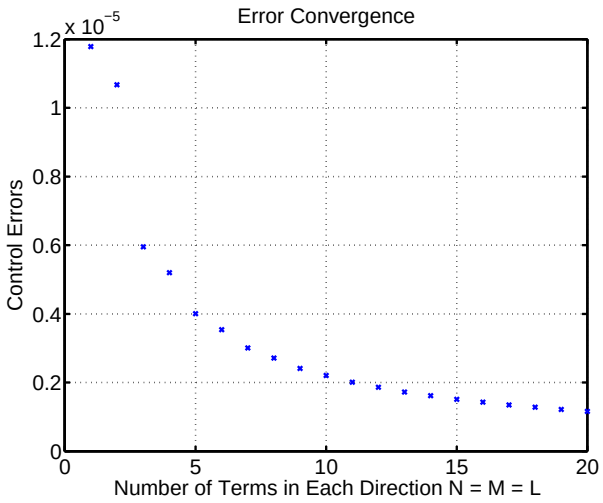

Figure 5.3: The minimum control error, for varying number of basis functions. The minimum control error, the control error is 5.4×10^{-5} if no growth factor is released. These plots are independent of D, $g(C)$ and v.

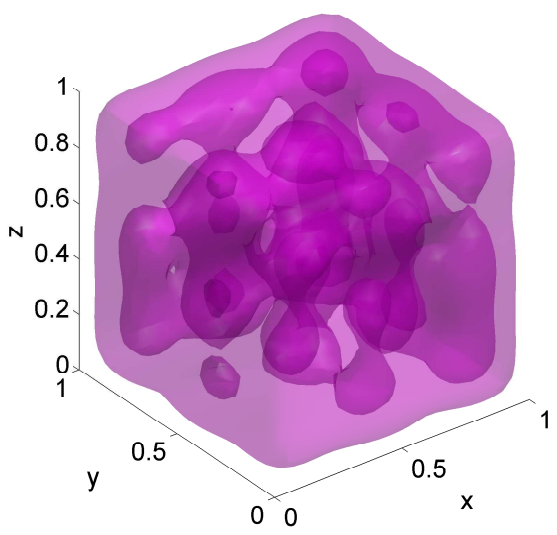

(a) $N = M = L = 5$

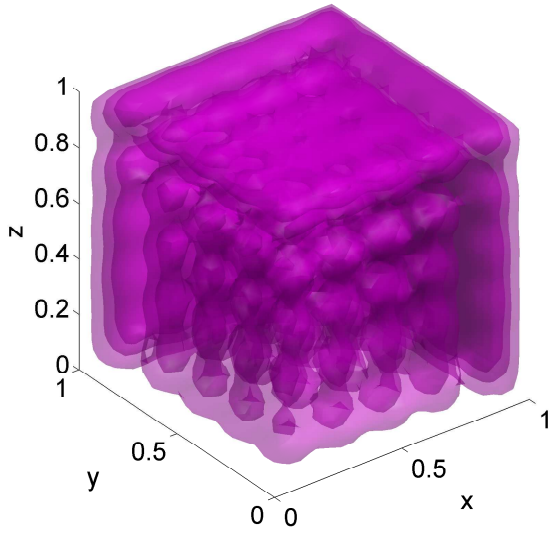

(b) $N = M = L = 10$

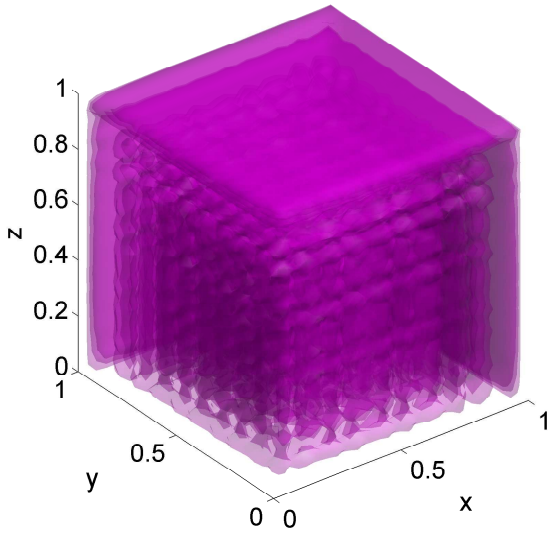

(c) $N = M = L = 20$

Figure 5.4: Optimal input fields showing isosurfaces of 1, 0.5, and 0.1 from inside to outside at $t = 1$ for various number of basis functions with $D = 1$ and $k = 7.6$.

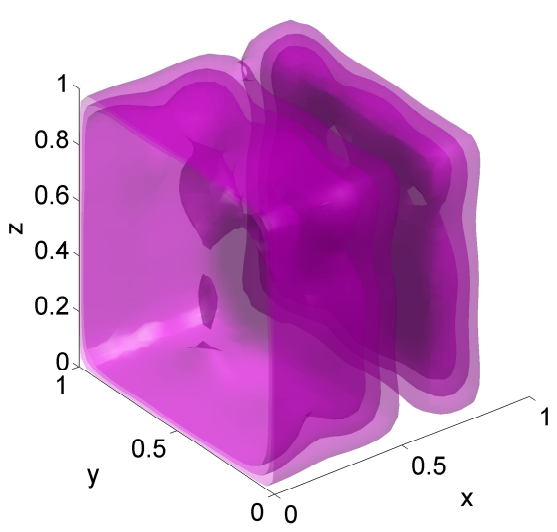

(a) N =M=L= 5

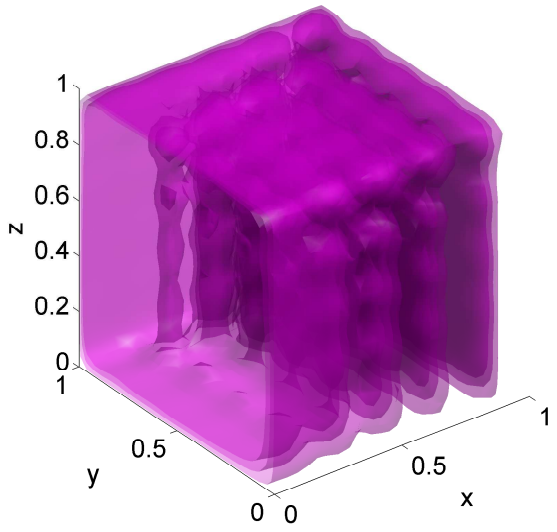

(b) N =M=L= 10

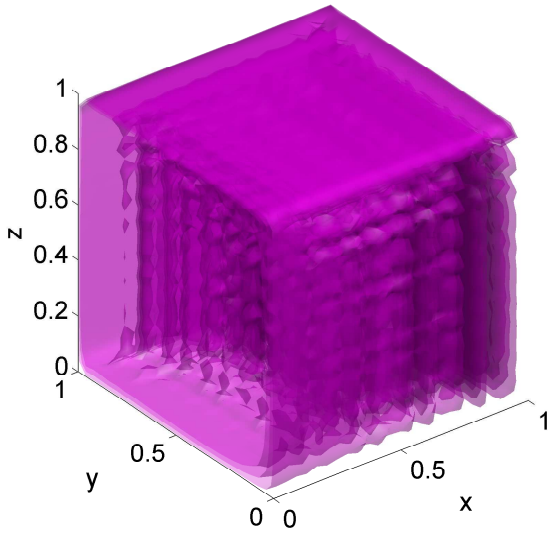

(c) N =M=L= 10

Figure 5.5: Optimal input fields showing isosurfaces of 1, 0.5, and 0.1 from inside to outside at $t = 1$ for various number of basis functions with $D = 1$, $k = 7.6$, and $v_x = 100$.

5.5 Conclusions

A modal control approach is investigated for optimal control problems in which the manipulation is distributed over a 3D spatial field with constraints on its spatial variation. It is shown that the optimal control error is independent of the values of the model parameters and can be obtained by utilizing the fact that all eigenmodes are decoupled. The construction of the unique minimum-energy manipulated field is provided for a transformed problem, which is intimately connected to the minimum-energy manipulated field for the original problem. A simulation demonstrates small optimal control error for a 3D time-varying reference field with modest spatial variation. The extension of the proposed approach to coupled PDEs was also briefly described.

CHAPTER 6

APPLICATION TO TISSUE ENGINEERING

Distributed parameter control problems involving manipulation within the spatial domain arise in a variety of applications including vibration control, active noise reduction, epidemiology, tissue engineering, and cancer treatment. A state-constrained spatial field control problem motivated by a biomedical application is solved in which the manipulation occurs over a spatial field and the state field is constrained both in spatial frequency and by a partial differential equation (PDE) that effects the manipulation. An optimization algorithm combines three-dimensional Fourier series, which are truncated to satisfy the spatial frequency constraints, with exploitation of structural characteristics of the PDEs. The computational efficiency and performance of the optimization algorithm are demonstrated in a numerical example, for which the spatial tracking error is almost entirely due to the limitation on the spatial frequency of the manipulated field. The numerical results suggest that optimal control approaches have promise for controlling the release of macromolecules in tissue engineering applications.

6.1 Introduction

In *spatial field control*, manipulation within a distributed parameter system (DPS) occurs as a spatial field. Spatial field control problems arise in a variety of applications including vibration control using internally placed piezo-actuators [146], active noise reduction in acoustic enclosures [154], active control of communicable disease carriers [88], the engineering of biological tissues and organs [112], and cancer treatment [192]. The ability to manipulate within the spatial domain provides much more controllability than the heavily studied boundary control problems (e.g., [191]), but the enhanced manipulation requires the determination of many more degrees of freedom. For example, for spatial field control problems with three spatial dimensions, the manipulated variable is $u(x, y, z, t), \forall x, y, z, t$, compared to boundary control in which manipulation is defined only on the external surface.

While many theoretical results have been derived for many classes of spatial field control problems [15, 124, 125], few contributions have proposed numerical algorithms that address all of the challenges that arise in real applications. While nonlinear programming methods for solving optimal control problems such as control vector parameterization [151, 170] and direct transcription [21, 102] are directly applicable to boundary control and most other optimal control problems, spatial field control for real applications problems must be carefully formulated to arrive at a computationally feasible solution. This is true whether the algorithms are implemented off-line or on-line with repeated solution at each time instance in a receding-horizon manner (so-called *model predictive control* [143]).

For example, consider an attempt to solve a simple open-loop spatial field control problem using control vector parameterization with a standard finite-difference discretization of a single partial differential equation (PDE) over time and the three spatial dimensions with 100 grid points in each dimension. The resulting nonlinear program with $100^4 = 10^8$ optimization variables is too computationally complex to be solved with existing computer hardware and software. The spatial control problems that arise in most real applications are even more complicated, involving multiple PDEs and typically requiring the satisfaction of spatial constraints on the state or manipulated fields.

This chapter addresses a state-constrained spatial field control problem for a system described by tightly coupled PDEs. As is common in the optimal control of PDEs, basis function expansions are used to reduce the number of degrees of freedom to a manageable size [69, 109, 134]. Unlike the problem-independent basis functions such as Legendre polynomials, radial basis functions, and proper orthogonal decomposition that have been very popular in the last decade [23, 110, 117, 118, 136], the structural characteristics of the PDEs will be exploited to reduce computational complexity. The methodology is presented in the context of a spatial field control problem motivated by tissue engineering [112, 45, 139, 140, 173, 179], in which molecules are released within a biological tissue from fixed embedded polymer microparticles designed to provide controlled release [19, 198]. The transport of these molecules is described by reaction-diffusion-convection equations in three spatial dimensions, and the control problem is to provide a desired spatial and temporal uptake of these molecules throughout the biological tissue. The reader is directed to a paper [112] for more details on the biological motivation for the optimal control problem, including additional references to relevant tissue engineering literature.

6.2 Spatial Field Control Problem

The system has a chemical species initially located in small biostable biocompatible polymer microparticles that are embedded, along with cells, in a tissue scaffold [173, 179]. Over time the chemical species is released from the microparticles and taken up by the surrounding cells, which cause the cells to change their behavior. The control objective is to provide for a desired spatial and temporal cellular uptake rate, which

is related to the local chemical species concentration by

$$R_{uptake}(x,y,z,t) = f(C(x,y,z,t)), \tag{6.1}$$

where f is an invertible algebraic function that can be identified from *in vitro* cell culture experiments [40, 194]. To simplify the mathematical formulation, (6.1) is inverted to derive an expression for a reference concentration field

$$R(x,y,z,t) = f^{-1}(R_{uptake,desired}(x,y,z,t)), \tag{6.2}$$

so that the mathematical control objective is to determine properties of the polymer microparticles that minimize the error between the reference and model species concentration fields.

The concentration field $C(x,y,z,t)$ in the engineered tissue construct is modeled by the reaction-diffusion-convection equation

$$\frac{\partial C}{\partial t} = D\nabla^2 C - v\cdot\nabla C - g(C) + u(x,y,z,t), \quad \forall t>0, \quad (x,y,z)\in\Omega := (0,1)^3, \tag{6.3}$$

which is a parabolic PDE with manipulated field $u(x,y,z,t)$, effective diffusion coefficient $D>0$, spatially uniform velocity vector field v, and net chemical species consumption $g(C)$ by cellular uptake and species degradation. The effects of chemical species reversibly binding with the extracellular matrix can be included with minor modifications of the model. The system is treated as a continuum, which is most accurate for length scales larger than the diameter of a cell (about 10 microns). To simplify the presentation, suppose the zero initial condition

$$C(x,y,z,0) = 0, \tag{6.4}$$

and the Dirichlet boundary condition

$$C(x,y,z,t) = 0, \quad \text{on} \quad \partial\Omega. \tag{6.5}$$

Each polymer microparticle is assumed to consist of a polymer core that initially contains a uniform concentration of chemical species to be released and a polymer shell that initially does not contain the chemical species (see Figure 6.1). Technology is available for manufacturing these core-shell microparticles to have precisely specified physical properties [19]. The manipulated field $u(x,y,z,t)$ associated with the release of a chemical species from core-shell microparticles embedded in the biological tissue is related to the core-shell microparticles by

$$u(x,y,z,t) = 4\pi\rho R_p^2 J\Big|_{r=R_p}, \tag{6.6}$$

where R_p is the outer radius, $4\pi R_p^2$ is the external surface area, ρ is the number density of the core-shell

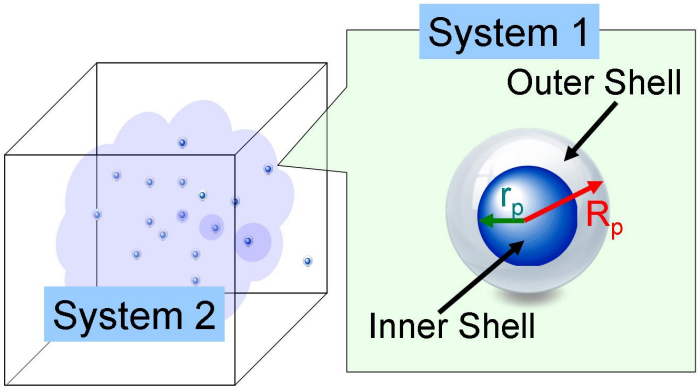

Figure 6.1: Overview of the system.

microparticles, and the flux at the surface of a single core-shell microparticle is

$$J\Big|_{r=R_p} = -\kappa \frac{\partial C_r}{\partial r}\Big|_{r=R_p}, \tag{6.7}$$

where $C_r(r,x,y,z,t)$ is the concentration field and $\kappa > 0$ is the effective diffusion coefficient within the core-shell microparticle. To simplify manufacturing of the tissue construct, the core-shell microparticles are assumed to be identical except for having different initial loading C_{r0}. Technology exists for embedding a specified spatial distribution of these microparticles within a tissue matrix [47, 141]. Changing the number density has exactly the same effect on the spatiotemporal release as changing the initial loading, so the number density ρ is assumed to be spatially uniform in (x,y,z) without changing the achievable value for the control objective. The effective diffusion coefficient κ can be modified by changing the polymer chemistry, molecular weight distribution, porosity, or tortuosity [50].

The transport of species through a biostable biocompatible polymeric core-shell microparticle is described by

$$\frac{\partial C_r}{\partial t} = \kappa \left(\frac{\partial^2 C_r}{\partial r^2} + \frac{2}{r}\frac{\partial C_r}{\partial r} \right), \quad t > t_p, \quad 0 \le r < R_p, \tag{6.8}$$

with initial condition

$$C_r(r,x,y,z,t_p) = \begin{cases} C_{r0}(x,y,z), & 0 \le r < r_p, \\ 0, & r_p \le r < R_p, \end{cases} \tag{6.9}$$

and boundary conditions

$$\frac{\partial C_r}{\partial r}\Big|_{r=0} = 0, \tag{6.10}$$

$$C_r(R_p,x,y,z,t) = k_p C(x,y,z,t), \tag{6.11}$$

where r_p is the radius of the polymer core, k_p is the partition coefficient (which can be modified by changing the polymer chemistry), and t_p is the time for which the core-shell microparticles are activated by a spatially

uniform environmental trigger. Many environmental triggers have been demonstrated in tissue engineering applications including pH, temperature, pressure, light, glucose, electric current, ultrasound, magnetic field, enzymes and other proteins, and ionic strength [34, 114, 163, 166, 177]. Many of these environmental triggers can be activated with spatial uniformity across the biological tissue.

To simplify the analysis, both tissue and microparticle models assume that the effective transport due to Brownian motion is spatially uniform and that the effective diffusion coefficient $\kappa > 0$ is the same in the polymer core and polymer shell. The inclusion of a polymer shell provides a much greater variety of release rates than microspheres, including the creation of a delay in the release profile [19]. The above system consists of two types of systems in feedback. Each microparticle, referred to as *System 1* in Figure 6.1, locally provides the manipulation, which is described by (6.8)-(6.11). These microparticles are embedded in the tissue construct described by (6.3)-(6.5), referred to as *System 2*, whose concentration field is to be controlled. The two types of systems are interconnected through (6.6)-(6.7). Recall that C_r is the concentration of the chemical species in the microparticles and C is the concentration of the same chemical species in the tissue construct.

The spatial field control problem is to determine the optimal properties of the polymer microparticles

$$\{\rho, R_p, r_p, k_p, \kappa, t_p, C_{r0}(x, y, z)\} \tag{6.12}$$

that specify a manipulated field $u(x, y, z, t)$ of constrained spatial variation that minimizes the error between the reference and model species concentration fields[1]

$$E = \int_T \int_\Omega (R(x, y, z, t) - C(x, y, z, t))^2 dV\, dt, \tag{6.13}$$

where T is the time range of interest, $R(x, y, z, t)$ is the reference concentration field which is C^1 in time and C^2 in the spatial directions and satisfies the zero initial condition

$$R(x, y, z, 0) = 0, \tag{6.14}$$

and the Dirichlet boundary condition

$$R(x, y, z, t) = 0, \quad \text{on} \quad \partial\Omega. \tag{6.15}$$

The spatial variation constraints are due to manufacturing constraints, and the initial loading is restricted

[1] $\int_\Omega dV = \int_0^1 \int_0^1 \int_0^1 dx dy dz$

to lower spatial frequencies, given in terms of M, N and L of

$$C_{r0}(x,y,z) = \sum_{m=-M}^{M} \sum_{n=-N}^{N} \sum_{l=-L}^{L} C_{r0,mnl} e^{(m\pi x + n\pi y + l\pi z)j} \tag{6.16}$$

for some complex numbers $C_{r0,mnl}$ for $-M \leq m \leq M$, $-N \leq n \leq N$ and $-L \leq l \leq L$.

6.2.1 Case I: $v = 0$, $g(C) = kC$, $k_p = 0$

For a system with zero partition coefficient, the set of optimization variables is

$$\{\rho, R_p, r_p, \kappa, t_p, C_{r0}(x,y,z)\}. \tag{6.17}$$

The analytical solution to the microparticle equations (6.8)-(6.11) is

$$C_r(r,x,y,z,t) = \frac{2C_{r0}(x,y,z)}{r} \sum_{i=1}^{\infty} \frac{r_p}{i\pi} \sin\frac{i\pi r}{R_p} \underbrace{e^{-\frac{\kappa j^2 \pi^2}{R_p^2} t} \left(\frac{R_p}{i\pi r_p} \sin\frac{i\pi r_p}{R_p} - \cos\frac{i\pi r_p}{R_p} \right)}_{:=u_i(t)} \tag{6.18}$$

and the flux at the microparticle surface from (6.7) is

$$J\Big|_{r=R_p} = \frac{2\kappa r_p C_{r0}(x,y,z)}{R_p^2} \underbrace{\sum_{i=1}^{\infty} (-1)^{i+1} u_i(t)}_{:=u(t)}, \tag{6.19}$$

and insertion into (6.6) gives the manipulated field:

$$u(x,y,z,t) = 8\pi\rho\kappa r_p C_{r0}(x,y,z) u(t). \tag{6.20}$$

To remove redundancy in the optimization variables, define

$$\alpha(x,y,z) := 8\pi\rho\kappa r_p C_{r0}(x,y,z), \tag{6.21}$$

$$\beta := r_p / R_p, \tag{6.22}$$

$$\gamma := \kappa / R_p^2, \tag{6.23}$$

then

$$u_i(t) = e^{-\gamma i^2 \pi^2 t} \left(\frac{\sin i\pi\beta}{i\pi\beta} - \cos i\pi\beta \right), \tag{6.24}$$

and

$$u(x,y,z,t) = \alpha(x,y,z) u(t). \tag{6.25}$$

From this, it can be seen that the optimization in the spatial component depends only on α and temporal component on β and γ.

In the previous chapter, it was shown that for $v = 0$ and $g(C) = kC$ the manipulated field $u(x, y, z, t)$ is a Fourier sine series. With the spatial frequency constraints on the manipulated field, α can be written as a truncated Fourier sine series [2]

$$\alpha(x, y, z) = \sum \alpha_{mnl} \sin m\pi x \sin n\pi y \sin l\pi z \tag{6.26}$$

$$:= \alpha_{MNL}(x, y, z), \tag{6.27}$$

where the real 3D Fourier sine series coefficients α_{mnl} are to be determined. Insertion into (6.25) results in the manipulated field

$$u(x, y, z, t) = \alpha_{MNL}(x, y, z)u(t), \tag{6.28}$$

which produces the output field:[3]

$$C(x, y, z, t) = \int_0^t \int_\Omega u(\bar{x}, \bar{y}, \bar{z}, \tau) G(x, y, z, \bar{x}, \bar{y}, \bar{z}, t - \tau) d\bar{V} d\tau \tag{6.29}$$

$$= \sum \alpha_{mnl} c_{mnl}(t) \sin m\pi x \sin n\pi y \sin l\pi z \tag{6.30}$$

where[4]

$$G(x, y, z, \bar{x}, \bar{y}, \bar{z}, t) = 8 \sum_{}^{\infty} e^{-(D(m^2+n^2+l^2)\pi^2+k)t} \sin m\pi x \sin n\pi y \sin l\pi z \sin m\pi \bar{x} \sin n\pi \bar{y} \sin l\pi \bar{z} \tag{6.31}$$

and

$$c_{mnl}(t) = \sum_{i=1}^{\infty} \frac{1 - e^{-((D(m^2+n^2+l^2)-\gamma i^2)\pi^2+k)t}}{(D(m^2 + n^2 + l^2) - \gamma i^2)\pi^2 + k} (-1)^{i+1} u_i(t). \tag{6.32}$$

The reference field $R(x, y, z, t)$ written in terms of the 3D Fourier series (also known as its spectral decomposition [74]) is a Fourier sine series with the given boundary condition (6.15),

$$R(x, y, z, t) = \sum_{}^{\infty} r_{mnl}(t) \sin m\pi x \sin n\pi y \sin l\pi z, \tag{6.33}$$

where

$$r_{mnl}(t) = 8 \int_\Omega R(x, y, z, t) \sin m\pi x \sin n\pi y \sin l\pi z dV. \tag{6.34}$$

By taking into account a potentially nonzero trigger time t_p, the optimization (6.13) can be written equiva-

[2] $\sum := \sum_{m=1}^{M} \sum_{n=1}^{N} \sum_{l=1}^{L}$
[3] $\int_\Omega d\bar{V} := \int_0^1 \int_0^1 \int_0^1 d\bar{x} d\bar{y} d\bar{z}$
[4] $\sum^{\infty} = \sum_{m=1}^{\infty} \sum_{n=1}^{\infty} \sum_{l=1}^{\infty}$

lently as[5]

$$\min_{\alpha_{mnl},\beta,\gamma,t_p} E = \frac{1}{8} \min_{\alpha_{mnl},\beta,\gamma,t_p} \sum \int_{t_0}^{t_f} \left(r_{mnl}(t) - \alpha_{mnl} c_{mnl}(t-t_p)\right)^2 dt + \frac{1}{8} \sum_{+1}^{\infty} \int_{t_0}^{t_f} r_{mnl}^2(t) dt, \tag{6.35}$$

where $r_{mnl}(t) = 0$, $\forall t < 0$, t_f is the final time of interest and $t_0 = \min\{0, t_p\}$ by application of orthogonality.

The above manipulations reduced the set of optimization variables to

$$\{\alpha_{mnl}, \beta, \gamma, t_p\}. \tag{6.36}$$

The optimization (6.35) is largely decoupled and is solved by a combination of gridding and analytical methods:

1. grid β, γ, and t_p over ranges that are guaranteed to encompass the global solution,
2. for each combination of these parameter values, determine the optimal α_{mnl} for each m, n, and l (this can be done analytically, as discussed below),
3. calculate and store the value of the optimization objective E,
4. repeat Steps 2-3 for each grid point,
5. select the minimum E for all grid points, and
6. refine the grid until the optimal objective no longer reduces significantly.

An initial estimate for the trigger time t_p can be obtained as the time that maximizes r_{mnl} and c_{mnl} for some m, n, and l. The optimization over α_{mnl} in Step 2 is convex and so can be determined by basic calculus as

$$\alpha_{mnl} = \frac{\int_{t_0}^{t_f} r_{mnl}(t) c_{mnl}(t-t_p) dt}{\int_{t_0}^{t_f} c_{mnl}(t-t_p)^2 dt}. \tag{6.37}$$

For initial ranges for β, γ, and t_p that encompass the global minimum, the convexity of the optimization over α_{mnl} and the continuity of the solution of the PDEs as a function of the optimization parameters imply that the optimization algorithm will converge within any specific tolerance of the global optimum.

6.2.2 Case II: $v = 0$, $g(C) = kC$, $k_p \neq 0$

For this case, the set of optimization variables is

$$\{\rho, R_p, r_p, \kappa, t_p, C_{r0}(x,y,z)\}. \tag{6.38}$$

[5] $\sum_{+1}^{\infty} := \sum^{\infty} - \sum$

The analytical solution to the microparticle equations (6.8)-(6.11) is

$$C_r(r,x,y,z,t) = \frac{2C_{r0}(x,y,z)}{r}\sum_{i=1}^{\infty}\frac{r_p}{i\pi}\sin\frac{i\pi r}{R_p}u_i(t) + \frac{2\kappa k_p}{rR_p}\sum_{i=1}^{\infty}\sin\frac{i\pi r}{R_p}(-1)^{i+1}i\pi\int_0^t C(x,y,z,\tau)e^{-\gamma i^2\pi^2(t-\tau)}d\tau \tag{6.39}$$

and the flux at the microparticle surface from (6.7) is

$$J\Big|_{r=R_p} = \frac{2\kappa r_p C_{r0}(x,y,z)}{R_p^2}u(t) + \frac{2\kappa^2 k_p}{R_p^3}\sum_{i=1}^{\infty}(i\pi)^2\int_0^t C(x,y,z,\tau)e^{-\gamma i^2\pi^2(t-\tau)}d\tau. \tag{6.40}$$

Insertion into (6.6) gives the manipulated field:

$$u(x,y,z,t) = 8\pi\kappa\rho r_p C_{r0}(x,y,z)u(t) + \frac{8\pi\kappa^2\rho k_p}{R_p}\sum_{i=1}^{\infty}(i\pi)^2\int_0^t C(x,y,z,\tau)e^{-\gamma i^2\pi^2(t-\tau)}d\tau \tag{6.41}$$

$$= \alpha(x,y,z)u(t) + \delta\sum_{i=1}^{\infty}(i\pi)^2\int_0^t C(x,y,z,\tau)e^{-\gamma i^2\pi^2(t-\tau)}d\tau. \tag{6.42}$$

where

$$\delta := \frac{8\pi\kappa^2\rho k_p}{R_p}. \tag{6.43}$$

By choosing the initial loading in terms of a truncated Fourier sine series (6.28), the output field is also expressed by a truncated Fourier sine series, i.e.,

$$C(x,y,z,t) = \sum\bar{c}_{mnl}(t)\sin m\pi x\sin n\pi y\sin l\pi z \tag{6.44}$$

for some $\bar{c}_{mnl}$. Since most of the error in (6.35) is due to the spatial constraint (we will see this in a later example),

$$\bar{c}_{mnl}(t) \approx r_{mnl}(t). \tag{6.45}$$

By using this approximation,

$$u(x,y,z,t) = \sum u_{mnl}(t)\sin m\pi x\sin n\pi y\sin l\pi z, \tag{6.46}$$

where

$$u_{mnl}(t) \approx \alpha_{mnl}u(t) + \delta\sum_{i=1}^{\infty}(i\pi)^2\int_0^t r_{mnl}(\tau)e^{-\gamma i^2\pi^2(t-\tau)}d\tau, \tag{6.47}$$

and the output field is

$$C(x,y,z,t) = \int_0^t \int_\Omega u(\bar{x},\bar{y},\bar{z},\tau) G(x,y,z,\bar{x},\bar{y},\bar{z},t-\tau) d\bar{V} d\tau \tag{6.48}$$

$$= \sum \tilde{c}_{mnl}(t) \sin m\pi x \sin n\pi y \sin l\pi z. \tag{6.49}$$

where

$$\tilde{c}_{mnl}(t) = \alpha_{mnl} \underbrace{\int_0^t u(\tau) e^{-(D(m^2+n^2+l^2)\pi^2+k)(t-\tau)} d\tau}_{=c_{mnl}(t) \text{ as in (6.32)}} + \tilde{r}_{mnl}(t), \tag{6.50}$$

and

$$\tilde{r}_{mnl}(t) := \delta \sum_{i=1}^{\infty} (i\pi)^2 \int_0^t \int_0^\tau r_{mnl}(\bar{\tau}) e^{-\gamma i^2 \pi^2 (\tau-\bar{\tau})} d\bar{\tau} e^{-(D(m^2+n^2+l^2)\pi^2+k)(t-\tau)} d\tau. \tag{6.51}$$

The optimization strategy is similar to the previous case. By taking into account a potentially nonzero trigger time t_p, the optimization (6.13) becomes

$$\min_{\alpha_{mnl},\beta,\gamma,\delta,t_p} E \iff \min_{\alpha_{mnl},\beta,\gamma,\delta,t_p} \sum \int_{t_0}^{t_f} (r_{mnl}(t) - \alpha_{mnl} c_{mnl}(t-t_p) - \tilde{r}_{mnl}(t))^2 dt. \tag{6.52}$$

The above manipulations reduce the set of optimization variables to

$$\{\alpha_{mnl}, \beta, \gamma, \delta, t_p\}. \tag{6.53}$$

The optimization (6.35) is largely decoupled and is solved by a combination of gridding and analytical methods:

1. grid β, γ, δ, and t_p over ranges that are guaranteed to encompass the global solution,
2. for each combination of these parameter values, determine the optimal α_{mnl} for each m, n, and l (this can be done analytically, as discussed below),
3. calculate and store the value of the optimization objective E,
4. repeat Steps 2-3 for each grid point,
5. select the minimum E for all grid points, and
6. refine the grid until the optimal objective no longer reduces significantly.

The optimization over α_{mnl} in Step 2 is again convex and so can be determined by basic calculus as

$$\alpha_{mnl} = \frac{\int_{t_0}^{t_f} \left(r_{mnl}(t) - \tilde{r}_{mnl}(t)\right) c_{mnl}(t - t_p) dt}{\int_{t_0}^{t_f} c_{mnl}(t - t_p)^2 dt}. \tag{6.54}$$

As before, for initial ranges for β, γ, δ, and t_p that encompass the global minimum, the optimization algorithm will converge within any specific tolerance of the global optimum.

6.3 Optimization in the Manipulated Field

This section considers a different approach to the solution of the optimal control problem, which first determines an optimal manipulated field while ignoring the PDEs for the microparticles and ignoring spatial frequency constraints, and then determines optimization variables that best match this manipulated field while taking constraints into account. This approach may be useful when direct minimization of the error in the concentration field is too computationally expensive. Such cases include when the chemical kinetic rate $g(C)$ is nonlinear, in which case an analytical solution to (6.3) does not exist, or when there is a convection term (i.e., $v \neq 0$) in which case the solution to the PDE (6.3) is no longer a Fourier sine series and orthogonality cannot be used in (6.35).

6.3.1 Justification

To simplify the presentation, consider the 1D case with $D \neq 0$, $v = 0$, $g(C) = kC$, and $t_p = 0$. The control field

$$u^*(x,t) := \frac{\partial R}{\partial t} - D\frac{\partial^2 R}{\partial x^2} - kR \tag{6.55}$$

achieves a perfect matching of the concentration field with the reference field when constraints are ignored. With $u(x,t)$ being the actual input, which must satisfy the control constraints, and the difference defined by

$$\varepsilon(x,t) := u^*(x,t) - u(x,t), \tag{6.56}$$

then

$$\int_T \int_0^1 \left(R(x,t) - C(x,t)\right)^2 dxdt \tag{6.57}$$

$$= \int_T \int_0^1 \left(\int_0^t \int_0^1 \delta(\bar{x},\tau) \sum_{n=1}^{\infty} 2e^{-(D(n\pi)^2+k)(t-\tau)} \sin n\pi x \sin n\pi\bar{x} d\bar{x} d\tau \right)^2 dxdt \tag{6.58}$$

$$= \sum_{n=1}^{\infty} \int_T \left(\int_0^t \int_0^1 \delta(\bar{x},\tau) e^{-(D(n\pi)^2+k)(t-\tau)} \sin n\pi\bar{x} d\bar{x} d\tau \right)^2 dt \tag{6.59}$$

$$= \sum_{n=1}^{\infty} \int_T \left(\int_0^t g_n(\tau) e^{-(D(n\pi)^2+k)(t-\tau)} d\tau \right)^2 dt \tag{6.60}$$

$$\leq \sum_{n=1}^{\infty} \int_T g_n(\tau)^2 dt \int_T e^{-(D(n\pi)^2+k)t} dt \tag{6.61}$$

$$= \sum_{n=1}^{\infty} \int_T \left(\int_0^1 \varepsilon(x,\tau) \sin n\pi x dx \right)^2 dt \left(\int_T e^{-(D(n\pi)^2+k)t} dt \right)^2 \tag{6.62}$$

$$\leq \sum_{n=1}^{\infty} \int_T \left(\int_0^1 \varepsilon(x,\tau) dx \right)^2 dt \left(\int_T e^{-(D(n\pi)^2+k)t} dt \right)^2 \tag{6.63}$$

$$\leq \int_T \int_0^1 \varepsilon^2(x,\tau) dxdt \underbrace{\sum_{n=1}^{\infty} \left(\int_T e^{-(D(n\pi)^2+k)t} dt \right)^2}_{\text{independent of } u(x,t)} \tag{6.64}$$

$$\tag{6.65}$$

where

$$g_n(t) := \int_0^1 \varepsilon(\bar{x},t) \sin n\pi\bar{x} d\bar{x}. \tag{6.66}$$

This above analysis motivates the minimization of

$$\int_T \int_0^1 \varepsilon^2(x,\tau) dxdt \tag{6.67}$$

as an approach for minimizing an upper bound on the control error. If a control input $u(x,t)$ exists that results in a small value for (6.67), this control error will result in a concentration field that is close to the reference field.

6.3.2 Case I: $k_p = 0$

It can be shown that

$$u^*(x,y,z,t) = \frac{\partial R}{\partial t} - D\nabla^2 R + v \cdot \nabla R - g(R) \tag{6.68}$$

$$= \sum_{m=-\infty}^{\infty} \sum_{n=-\infty}^{\infty} \sum_{l=-\infty}^{\infty} \breve{u}^*_{mnl}(t) e^{(m\pi x + n\pi y + l\pi z)j} \tag{6.69}$$

where

$$\breve{u}^*_{mnl}(t) = \int_\Omega \breve{u}^*(x,y,z,t) e^{-(m\pi x + n\pi y + l\pi z)j} dV \tag{6.70}$$

results in exact matching of the concentration field to the reference field. Under the spatial frequency constraint, $u^*(x,y,z,t)$ is truncated to

$$\breve{u}^*_{MNL}(x,y,z,t) = \sum_{m=-M}^{M} \sum_{n=-N}^{N} \sum_{l=-L}^{L} u^*_{mnl}(t) e^{(m\pi x + n\pi y + l\pi z)j}. \tag{6.71}$$

On the other hand, any allowable manipulated field is in the form of

$$\breve{u}_{MNL}(x,y,z,t) = \breve{\alpha}_{MNL} u(t). \tag{6.72}$$

The optimization of the right-hand side of the inequality

$$\int_{t_0}^{t_f} \int_\Omega \left(\sum_{m=-M}^{M} \sum_{n=-N}^{N} \sum_{l=-L}^{L} \left(\breve{u}^*_{mnl}(t) - \breve{\alpha}_{mnl} u(t-t_p) \right) e^{-(m\pi x + n\pi y + l\pi z)j} \right)^2 dV dt$$

$$\leq \sum_{m=-M}^{M} \sum_{n=-N}^{N} \sum_{l=-L}^{L} \int_{t0}^{t_f} \left| \breve{u}^*_{mnl}(t) - \breve{\alpha}_{mnl} u(t-t_p) \right|^2 dt, \tag{6.73}$$

over $\breve{\alpha}_{mnl}$ is decoupled, which can be optimized using similar steps as in the previous section. The inequality becomes an equality if $\breve{u}^*_{MNL}$ is a Fourier sine series or a Fourier cosine series. Finally, $\alpha(x,y,z)$ is constructed as

$$\breve{\alpha}_{MNL}(x,y,z) = \sum_{m=-M}^{M} \sum_{n=-N}^{N} \sum_{l=-L}^{L} \breve{\alpha}_{mnl} e^{(m\pi x + n\pi y + l\pi z)j}. \tag{6.74}$$

6.3.3 Case II: $k_p \neq 0$

As for Case I, determine the control input obtained by replacing $C(x,y,z,t)$ by $R(x,y,z,t)$:

$$\check{u}_{MNL}(x,y,z,t) = \check{\alpha}_{MNL}(x,y,z)u(t) + \delta \sum_{i=1}^{\infty} (i\pi)^2 \int_0^t \check{R}_{MNL}(x,y,z,\tau) e^{-\gamma i^2 \pi^2 (t-\tau)} d\tau, \tag{6.75}$$

where

$$\check{R}_{MNL}(x,y,z,t) := \sum_{m=-M}^{M} \sum_{n=-N}^{N} \sum_{l=-L}^{L} \check{r}_{mnl} e^{(m\pi x + n\pi y + l\pi z)j}, \tag{6.76}$$

$$\check{r}_{mnl} := \int_\Omega R(x,y,z,t) e^{-(m\pi x + n\pi y + l\pi z)j} dV. \tag{6.77}$$

With time shift, the optimization of $\check{\alpha}_{mnl}$ in the right-hand side of the inequality

$$\int_{t0}^{t_f} \int_\Omega \left(\sum_{m=-M}^{M} \sum_{n=-N}^{N} \sum_{l=-L}^{L} (\check{u}^*_{mnl}(t) - \check{\alpha}_{mnl} u(t-t_p) - \delta \sum_{i=1}^{\infty} (i\pi)^2 \int_0^t \check{r}_{mnl}(\tau) e^{-\gamma i^2 \pi^2 (t-\tau)} d\tau \right) \tag{6.78}$$

$$e^{-(m\pi x + n\pi y + l\pi z)j} \Big)^2 dV dt$$

$$\leq \sum_{m=-M}^{M} \sum_{n=-N}^{N} \sum_{l=-L}^{L} \int_{t0}^{t_f} \left(\check{u}^*_{mnl}(t) - \check{\alpha}_{mnl} u(t-t_p) - \delta \sum_{i=1}^{\infty} (i\pi)^2 \int_0^t \check{r}_{mnl}(\tau) e^{-\gamma i^2 \pi^2 (t-\tau)} d\tau \right)^2 dt. \tag{6.79}$$

is decoupled, and can be optimized similarly as in the previous section.

6.4 Numerical Example

Consider the spatial field control problem (6.13) with the dimensionless constants $D = 1$, $k = 0.1$, and $v = 0$ and reference field

$$R(x,y,z,t) = (e^{-x} - e^{-3x})(e^{-y} - e^{-4y})(e^{-2z} - e^{-4z})(e^{-t} - e^{-2t}). \tag{6.80}$$

The manufacturing process that places microparticles within the 3D tissue scaffold is the most efficient when the spatial variation in the initial loading in the microparticles is constrained to low frequencies. First consider the objective of determining the optimal microparticle properties (6.17) when the maximum spatial frequency in any spatial direction is 10π ($M = N = L = 10$).

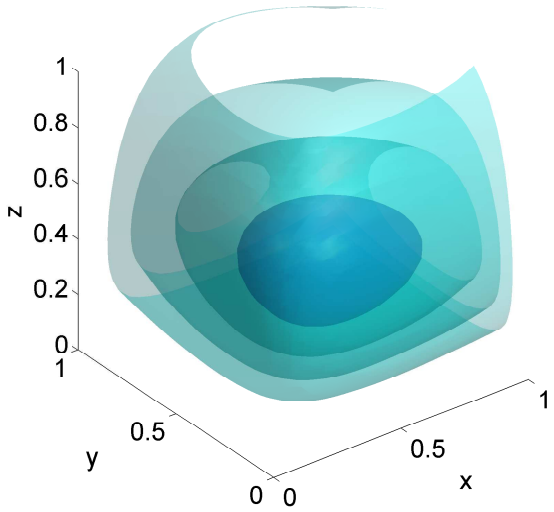

Figure 6.2: Reference field showing isosurfaces of 0.01, 0.008, 0.006, and 0.004 from inside to outside at $t = 0.7$.

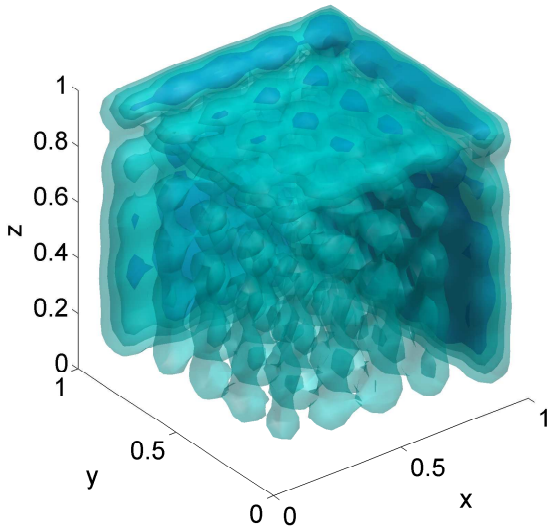

Figure 6.3: Optimal $\alpha(x, y, z)$ for the microparticles showing isosurfaces of 16, 12, 8, and 4 from inside to outside for $M = N = L = 10$.

Figure 6.2 shows the reference field (6.80) at a representative time. The optimal properties of the microparticles are

$$\{r_p/R_p, \kappa/R_p^2, t_p\} = \{0.48, 0.08, -0.20\} \tag{6.81}$$

with $\alpha(x, y, x)$, which is proportional to the optimal initial loading, shown in Figure 6.3. The number density ρ and initial loading $C_{r0}(x, y, z)$ of the core-shell microparticles appear as a product in $\alpha(x, y, x)$, so that the extra degree of freedom can be used to simplify manufacturing. For example, for a fixed optimal $\alpha(x, y, x)$ the number density ρ could be reduced so that fewer microparticles would need to be positioned

in a 3D tissue scaffold, by increasing the initial loading. Similarly, the effective diffusion coefficient κ and radius R_p of the microparticles affect the chemical species release through the inverse time scale κ/R_p^2, so this extra degree of freedom can also be used to simplify manufacturing. By manufacturing to specify the pore size, the porous polymer microparticles can be made with κ having any specified value from arbitrarily small to nearly the value of the effective diffusion coefficient D. This flexibility can be used to select the microparticle radius R_p small enough that the initial loading $C_{r0}(x, y, z)$ and concentration in the model (6.3) behave like a continuum ($R_p \ll 1/\max\{N, M, L\}$). For example, $\kappa/R_p^2 = 0.08$ could be obtained by selecting $R_p = 0.01 \ll 1/10$, which is small enough to spatially resolve the initial loading, and selecting $\kappa = 0.08(0.01)^2 = 8 \times 10^{-6}$, which can be implemented by using very small pore diameters in the polymeric microparticles.

The spatial complexity of the optimal initial loading in Figure 6.3 indicates that it is unlikely that a person would be able to design the optimal initial loading by intuition,[6] which motivates the application of numerical optimization. The concentration field obtained with optimal polymer microparticles is nearly indistinguishable by eye from the approximated reference field (truncated sum of (6.33)), indicating that the microparticles provide a very high degree of controllability within the constraint on the spatial resolution (see Figures 6.4, also compare Figures 6.5 and 6.6).

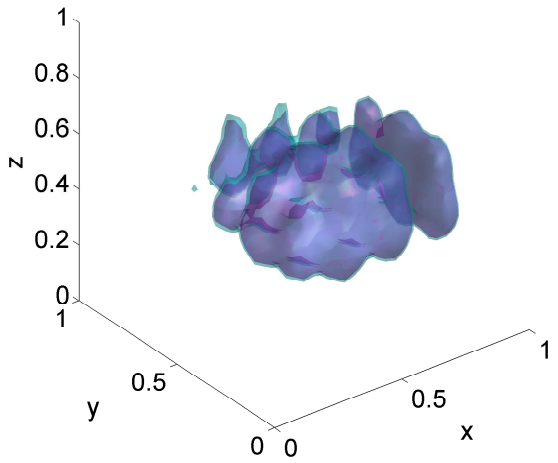

Figure 6.4: Approximated reference (magenta) and optimal concentration (cyan) fields for $M = N = L = 10$ showing the isosurface of 0.01 at $t = 0.7$.

[6]The optimal initial loading is much smaller in the center of the spatial domain than in the surrounding region.

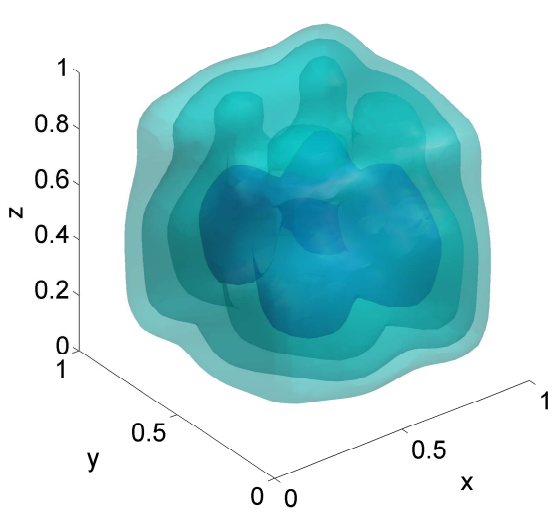

(a) N = 5

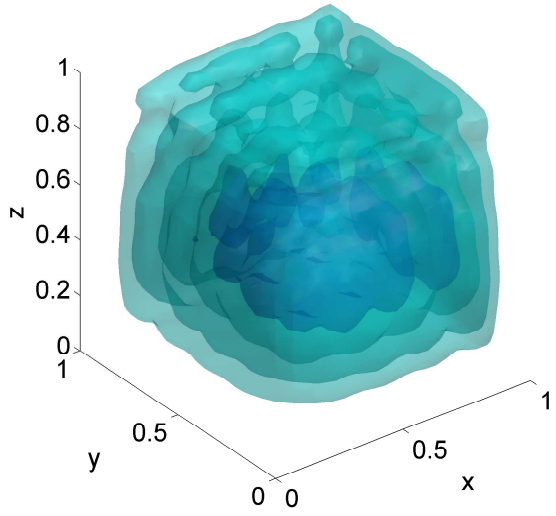

(b) N = 10

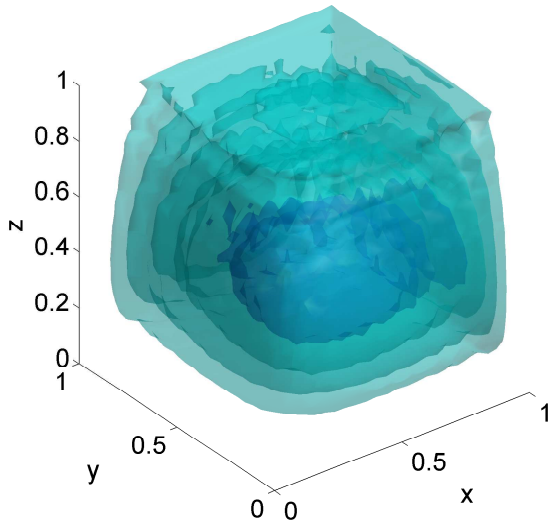

(c) N = 20

Figure 6.5: Optimal concentration fields showing isosurfaces of 0.01, 0.008, 0.006, and 0.004 from inside to outside at $t = 0.7$.

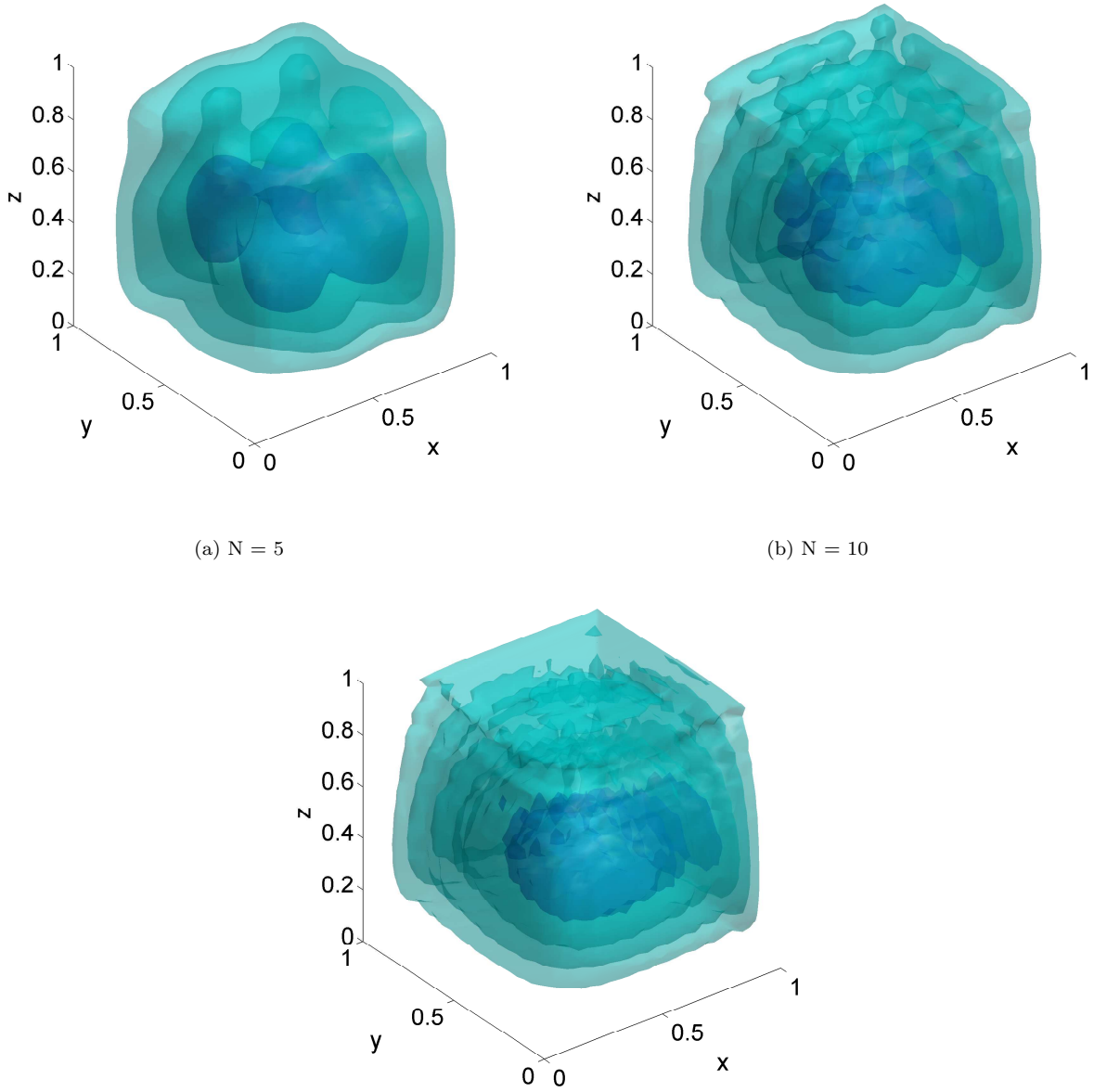

(a) N = 5

(b) N = 10

(c) N = 20

Figure 6.6: Approximated reference concentration fields showing isosurfaces of 0.01, 0.008, 0.006, and 0.004 from inside to outside at $t = 0.7$.

If the microparticles can be spaced more closely together, then M, N, and L increase and the differences between the optimal and reference fields become smaller (compare Figure 6.5 with Figure 6.2). These differences vary with position. For example, the optimal concentration is mostly higher than the reference for the center of the spatial domain but mostly lower than the reference for the off-center position $x = y = z = 1/4$ (see Figure 6.7).

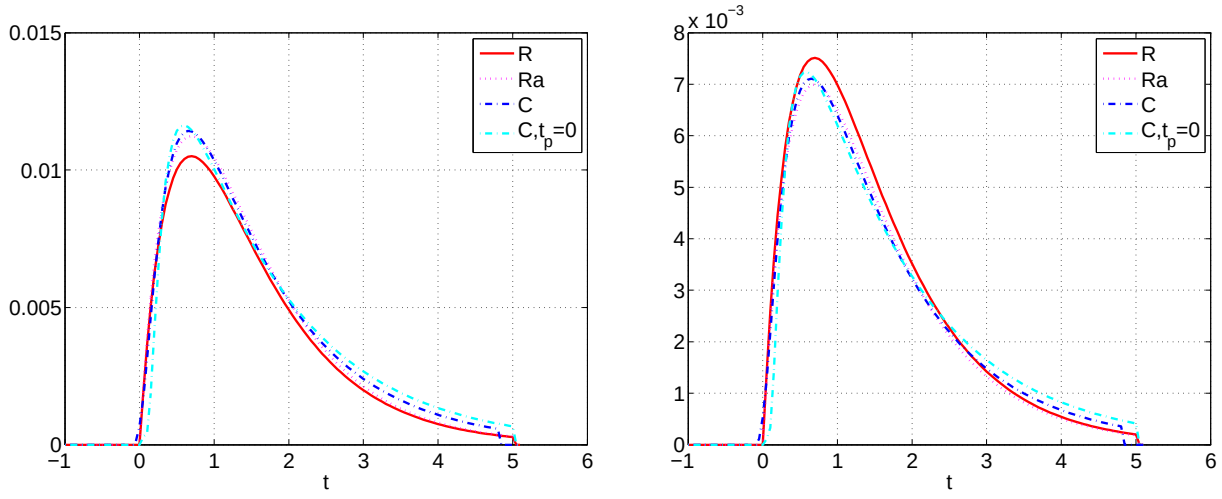

(a) at the center position ($x = y = z = 1/2$)

(b) at an off-center position ($x = y = z = 1/4$)

Figure 6.7: Reference, approximate reference, and optimal concentration profiles for $M = N = L = 10$.

Zeroing the trigger time increases the minimum control error (6.13) by a factor of 7, indicating that this is a useful optimization variable. Although the respective optimal concentration fields look similar at first glance (see Figure 6.7), the zero trigger time is associated with an initial concentration increase at $t = 0$ that is less sharp, which is the primary contribution to the control error. A tissue engineer would have to assess whether the improvement in tracking the 3D concentration field is worth the extra experimental effort of implementing an environmental trigger.

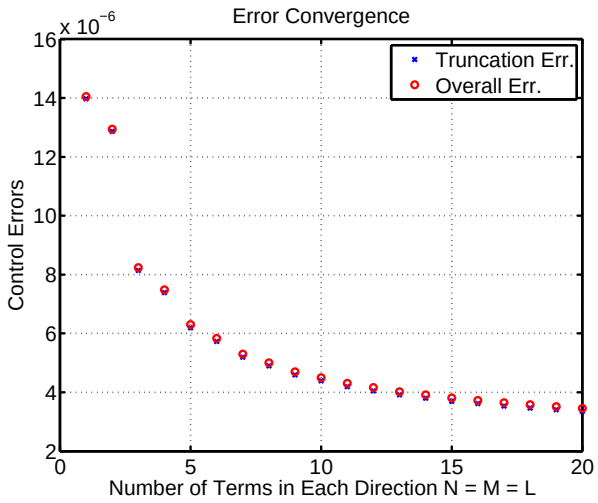

Figure 6.8: The minimum control error (6.35) is the red circles, the second term in (6.35) is the blue crosses, and the control error is 5.45×10^{-5} if no chemical is released.

6.5 Conclusions

This chapter explicitly accounted for the dynamics within polymer microparticles while optimizing their spatial and temporal release of macromolecules within an engineered tissue construct. With its incorporation of state constraints in the form of partial differential equations for the microparticles and limitations on spatial frequencies, the mathematical formulation for the spatial field control problem is significantly more sophisticated than spatial field control problems described in the literature. Spectral decomposition was a useful approach for direct satisfaction of the spatial frequency constraints and reduction of the large number of degrees of freedom in the optimization problem. In the simulation results, the control error was mostly due to the limitation on the spatial resolution, which can be overcome by using smaller microparticles spaced more closely together.

Several directions are promising for future work. Microparticles of different design such as microcapsules or particles constructed with biodegradable polymers could be investigated. Nonlinear cellular uptake kinetics, chemical degradation kinetics, and chemical interactions with the extracellular matrix are also of practical importance. The ultimate objective of this research is to develop a suite of mathematical tools for controlling the spatial and temporal development of an engineered tissue construct that can be used to guide experimental designs and reduce trial-and-error experimentation.

CHAPTER 7

INTERNAL MODEL CONTROL

An internal model control (IMC) design method is proposed that is applicable to linear infinite-dimensional systems. An infinite-dimensional filter is coupled with the inverse of the irrational transfer function between the process input and output, to produce a physically realizable controller with a tuning parameter to trade off nominal performance with robustness. The proposed IMC design technique is applied to two boundary control problems for mass transport described by partial differential equations (PDEs), in which the proposed method provides much better robust performance compared to IMC applied to the finite-dimensional approximation of the transfer function.

7.1 Introduction

The most commonly applied approach for the design of control systems for distributed parameter systems (DPS) is to approximate the PDEs by ordinary differential equations (ODEs) and apply finite-dimensional control design methods. The advantage of this approach is that a finite set of state-space equations or a finite-dimensional transfer function is produced for which many control design methods (e.g., linear quadratic gaussian control, H_∞-optimal control, model predictive control, differential geometric methods, robust optimal control) are directly applicable. A drawback of this approach is that, depending on the spatial dynamics of the particular process, the dimension of the ODEs can be high resulting in high computational cost or the ODEs may not represent the DPS as accurately as desired so that important model behaviors are missed. Also, such an approach can hide the underlying structure and dynamics of the optimal controller for the DPS, with a loss in understanding, elegance, and efficiency that would be obtained by direct solution of the DPS optimal control problem (e.g., see discussion by [9] and citations therein).

Many papers have considered the analysis and control of DPS without approximation by ODEs, such as robust stability analysis for additive plant perturbations [44], the existence of a controller that robustly

stabilizes plants with multiplicative perturbations [105], and H_∞-optimal control for systems with time delay [209]. The internal model principle has been applied to design finite-dimensional low-gain robust controllers for stable DPS that asymptotically track setpoint trajectories and suppress disturbances that are superpositions of polynomials and sinusoids of known frequencies [87, 172, 103]. Controllers designed using the internal model principle embed a model of the dynamical structure of the setpoint and disturbance signals to obtain zero asymptotic steady-state error in the process output [76, 99, 97]. More recent results have applied the internal model principle to design feedforward and feedback controllers for more general inputs, which are only restricted to be bounded and uniformly continuous [99]. Upper bounds on the effects of bounded additive linear perturbations on the output error have been derived [98]. Many of these latter results apply to controllers that are infinite-dimensional [99, 97, 98].

Internal model control (IMC) is a control design method that matured in the 1980s to 1990s in which an analytical solution for an optimal controller for a nominal process model is combined with a low-order filter with an adjustable tuning parameter for trading off control quality with robustness to model uncertainties [148]. This method can be interpreted as augmenting the inverse or an approximate inverse of the transfer function of the nominal process model with a low-order low-pass filter to make the IMC controller proper and provide the tuning parameter. IMC controllers explicitly incorporate the internal model principle, can be easily modified to provide antiwindup compensation during saturation of the manipulated variable [207], and can be applied to the independent design of reference prefilters, cascade controllers, and other multiple degree-of-freedom controllers [148]. Certainly it would be beneficial to have design methods for DPS that share these features.

The above considerations motivate this chapter's development of an IMC design method that is directly applicable to linear infinite-dimensional systems without approximation of the PDEs, in which the IMC controller is designed by analytical solution of an optimal control problem or by inverting the irrational transfer function for the process. Two approaches are developed for designing a physically realizable IMC controller for infinite-dimensional systems: (1) augmenting the IMC controller with an infinite-dimensional filter, or (2) designing the IMC controller for the process model that has been augmented to be semiproper. Section 7.2 provides the definitions and robust analysis results used in Section 7.3 which describes the IMC design method. This is followed by illustrative examples, conclusions, and directions for future investigation.

7.2 Preliminaries

The definitions and structure for infinite-dimensional systems described in this section mirror those for finite-dimensional systems [148].

Definition 7.2.1 (Nominal Performance)**.** *The closed-loop system in Figure 7.1b attains* nominal perfor-

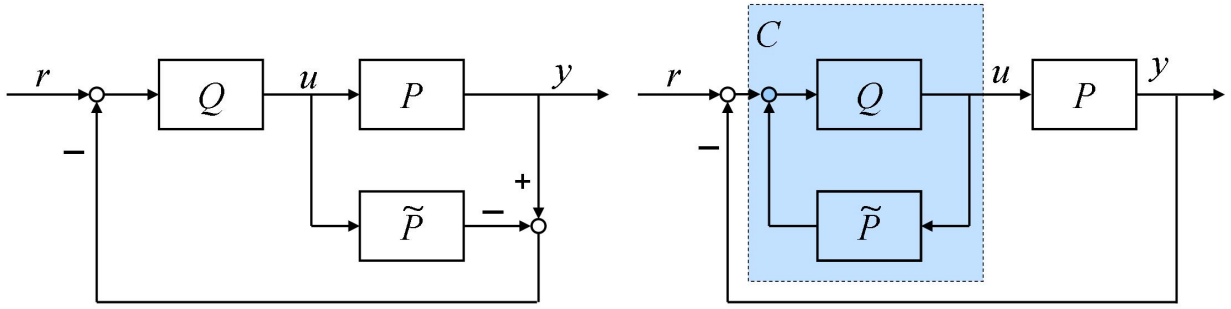

(a) IMC (b) Classical

Figure 7.1: Control structures.

mance *if it is stable*[1] *and*

$$\|W_1 S\|_\infty = \sup_{\omega \in \mathbb{R}} |W_1(j\omega)S(j\omega)| < 1, \tag{7.1}$$

where W_1 *is a weighting function,* $S = 1 - \tilde{P}Q = 1/(1 + \tilde{P}C)$ *is the sensitivity function, and* $\tilde{P}$*,* Q*, and* C *are the nominal process model, IMC, and classical feedback controller transfer functions, respectively.*

The weighting function W_1 is typically selected to be large at low frequencies and small at high frequencies, so as to emphasize performance at low frequencies. A pole at $s = 0$ forces the controller to have integral action. The H_∞-norm is the induced system norm for input and output signals quantified in terms of the L_2-norm, regardless of whether the weight and sensitivity are finite or infinite dimensional [9].

Infinite-dimensional systems are considered that belong to the Callier-Desoer algebra [36]. Some more definitions and a more formal definition of stability for infinite-dimensional systems are needed in the subsequent statement of the generalized Nyquist stability criterion. For $\sigma \in \mathbb{R}$, define

$$L_{1,\sigma} \equiv \left\{ f(\cdot) \,\middle|\, f(\cdot) : \mathbb{R}_+ \to \mathbb{C}, \int_0^\infty |f(t)e^{-\sigma t}| dt < \infty \right\}, \tag{7.2}$$

where $\mathbb{R}_+$ is the nonnegative real line and $\mathbb{C}$ is the field of complex numbers. The convolution algebra $\mathfrak{A}(\sigma)$ consists of the elements of the form

$$f(t) = \begin{cases} 0, & t < 0, \\ f_a(t) + \sum_{i=0}^{\infty} f_i \delta(t - t_i), & t \geq 0, \end{cases} \tag{7.3}$$

where

- $f_a(\cdot) \in L_{1,\sigma}$,
- $t_0 = 0$ and $t_i > 0,\ \forall i = 1, 2, \ldots,$

[1] The precise notion of stability considered in this chapter is discussed later.

- $f_i \in \mathbb{C}$ and $\delta(t - t_i)$ is the Dirac delta distribution applied at t_i, and
- $\sum_{i=0}^{\infty} |f_i| e^{-\sigma t_i} < \infty$.

Definition 7.2.2 ($\mathfrak{A}(\sigma)$-stability)**.** *$f(\cdot)$ is said to belong to $\mathfrak{A}_-(\sigma)$ iff there exists $\sigma_1 \in \mathbb{R}$ with $\sigma_1 < \sigma$ such that $f(\cdot) \in \mathfrak{A}(\sigma_1)$. Further, define $\hat{\mathfrak{A}}(\sigma) = \{\hat{f} | f \in \mathfrak{A}(\sigma)\}$, where $\hat{f}$ is the Laplace transform of f. A system is said to be $\mathfrak{A}(\sigma)$-stable if its transfer function belongs to $\hat{\mathfrak{A}}(\sigma)$.*

A closed-loop system that is $\mathfrak{A}(\sigma)$-stable with $\sigma < 0$ is exponentially stable. The generalized Nyquist stability criterion provides an analytical condition for $\mathfrak{A}(\sigma)$-stability of a closed-loop infinite-dimensional system in terms of a path in the complex s-plane.[2]

Theorem 7.2.3 (Generalized Nyquist Stability Criterion [57])**.** *Let $\mathbb{C}_{\sigma+}$ denote the closed right-half complex plane $\{s \in \mathbb{C} | \ Re\ s \geq \sigma\}$, and $\bar{N}_\infty$ denote a Nyquist path as shown in Figure 7.2. Suppose the following conditions are satisfied:*

1. *$\hat{G}(s) = \hat{n}(s)/\hat{d}(s)$, where $\hat{n}(s) \in \hat{\mathfrak{A}}_-(\sigma_0)$ and $\hat{d}(s) \in \hat{\mathfrak{A}}_-(\sigma_0)$,*
2. *There exist $\hat{u}(s) \in \hat{\mathfrak{A}}_-(\sigma_0)$ and $\hat{v}(s) \in \hat{\mathfrak{A}}_-(\sigma_0)$ such that $\hat{u}(s)\hat{n}(s) + \hat{v}(s)\hat{d}(s) = 1$,*
3. *$\hat{d}(s)$ is analytic and bounded away from zero at ∞ in $\mathbb{C}_{\sigma_0+}$,*
4. *$\hat{G}(s)$ approaches zero as $|s| \to \infty$ in $\mathbb{C}_{\sigma_0+}$.*

Then, the closed-loop system with open-loop transfer function $\hat{G}(s)$ in negative unity feedback is $\mathfrak{A}(\sigma)$-stable iff, for some $\sigma < 0$ and $\forall s \in \bar{N}_\infty$,

- *$1 + \hat{G}(s) \neq 0$,*
- *$1 + \hat{G}(s)$ encircles the origin k times in the counterclockwise sense, where k is the number of open right-half plane zeros of $\hat{d}(s)$, counting multiplicities,*

where $\bar{N}_\infty$ is the Nyquist path, which follows the imaginary axis including the points $+j\infty$ and $-j\infty$ except with ϵ-indentations in the left-half plane around any poles of $\hat{G}(s)$ on the imaginary axis.

Model uncertainties in the form of unmodeled dynamics are represented in terms of a family of processes:

$$\Pi = \{P : P = (1 + \Delta W_2)\tilde{P}, \text{ where } \|\Delta\|_\infty \leq 1; P \text{ and } \tilde{P} \text{ have the same number of unstable poles}\}, \quad (7.4)$$

where $\tilde{P}$ is strictly proper and the uncertainty weight W_2 and perturbation Δ are stable proper (possibly irrational) transfer functions. Below are robustness analysis conditions for infinite-dimensional systems controlled by proper controllers Q and C. The following is the definition of robust stability.

[2]The result is the same as that of Ref. [57] except for the strengthening of Condition 4 as done in Ref. [49].

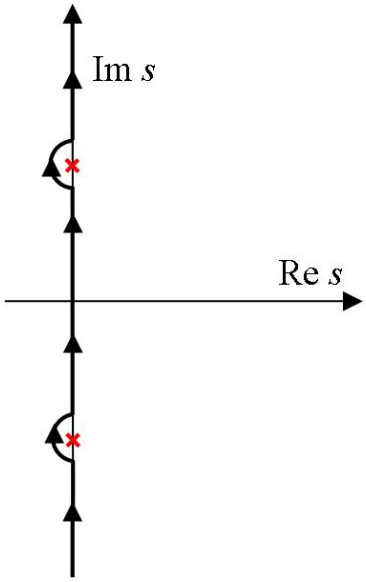

Figure 7.2: Nyquist path $\bar{N}_\infty$: "x" denotes the $j\omega$-axis poles of $G(s)$

Definition 7.2.4 (Robust Stability)**.** *The closed-loop system in Figure 7.1b is* robust stable *if it is* $\mathfrak{A}(\sigma)$*-stable for all* $P \in \Pi$*.*

The next result applies the generalized Nyquist stability criterion to derive a necessary and sufficient analytical condition for the robust stability of infinite-dimensional systems. The proof, which is simpler than that in Ref. [49], follows a similar argument as used for finite-dimensional systems [59, 148], but with more care in distinguishing operators from complex numbers.

Theorem 7.2.5 (Robust Stability)**.** *The closed-loop system in Figure 7.1b is robust stable iff the nominal system is* $\mathfrak{A}(\sigma)$*-stable and*

$$\|W_2 T\|_\infty < 1, \tag{7.5}$$

where $T = \tilde{P}C/(1+\tilde{P}C)$ *is the complementary sensitivity function.*

Proof. ($\Leftarrow$) Suppose

$$\|W_2 T\|_\infty = \sup_{\omega \in \mathbb{R}} |W_2(j\omega)T(j\omega)| < 1, \tag{7.6}$$

then

$$\|\Delta W_2 T\|_\infty \leq \|\Delta\|_\infty \|W_2 T\|_\infty < 1. \tag{7.7}$$

Now consider the equality

$$\begin{aligned} 1 + PC &= 1 + (1 + \Delta W_2)\tilde{P}C \\ &= (1 + \tilde{P}C)(1 + \Delta W_2 T). \end{aligned} \tag{7.8}$$

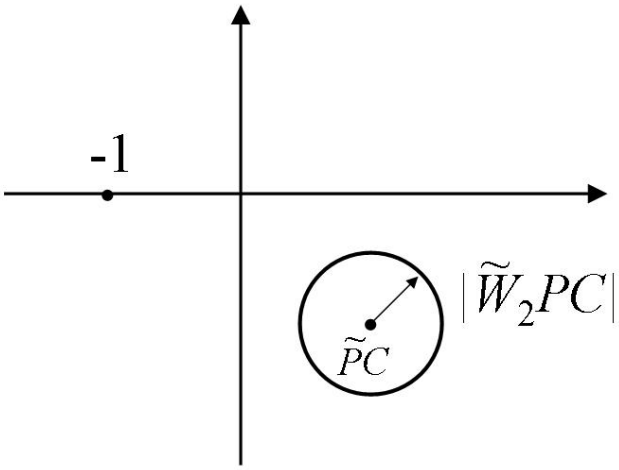

Figure 7.3: Graphical test for robust stability in the complex plane (shown for a single frequency).

Nominal $\mathfrak{A}(\sigma)$-stability and the generalized Nyquist stability criterion imply that $1+\tilde{P}C$ along the Nyquist path is not equal to zero and encircles the origin the k times required for $\mathfrak{A}(\sigma)$-stability. The inequality (7.7) implies that $1+\Delta W_2 T$ is not equal to zero along the Nyquist path and hence does not change the number of encirclements of the origin. That is, $N(1+\tilde{P}C) = N(1+PC)$, where $N(\hat{G}(s))$ is the net number of clockwise encirclements of the origin by the image of the Nyquist path under $\hat{G}(s)$.

($\Rightarrow$) Proof by contrapositive. Suppose

$$\|W_2 T\|_\infty \geq 1, \tag{7.9}$$

then

$$\hat{\Delta} = 1/\|W_2 T\|_\infty \tag{7.10}$$

satisfies

$$\|\hat{\Delta}\|_\infty \leq 1 \tag{7.11}$$

and

$$\|\hat{\Delta} W_2 T\|_\infty = 1. \tag{7.12}$$

Let $\hat{\omega}$ be a frequency in which this equality holds, then $|\hat{\Delta} W_2 T|_{\hat{\omega}}$ is located on a unit circle centered at origin. Select the parameter θ in $\bar{\Delta} = e^{-s\theta}\hat{\Delta}$ so that $|1+\bar{\Delta} W_2 T|_{\hat{\omega}} = 0$. Then $\|\bar{\Delta}\|_\infty \leq 1$ and, by (7.8), $1+PC = 0$ which implies that the system is not robust stable (from the generalized Nyquist stability criterion). □

Definition 7.2.6 (Robust Performance)**.** *The closed-loop system in Figure 7.1b attains robust performance if it is $\mathfrak{A}(\sigma)$-stable and*

$$\left\| \frac{W_1}{1+PC} \right\|_\infty = \sup_{\omega \in \mathbb{R}} \left| \frac{W_1(j\omega)}{1+P(j\omega)C(j\omega)} \right| < 1, \ \forall P \in \Pi. \tag{7.13}$$

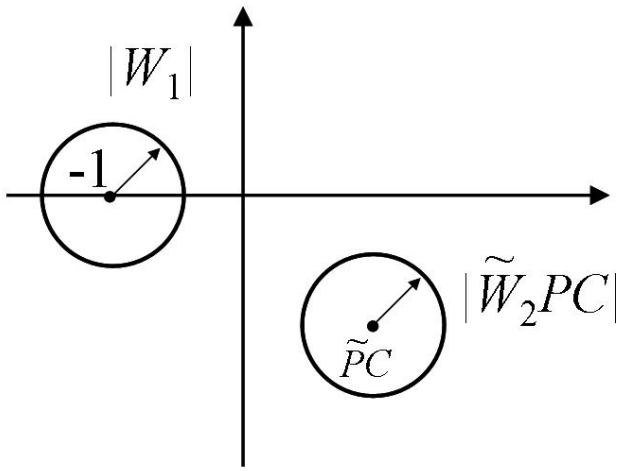

Figure 7.4: Graphical test for robust performance in the complex plane (shown for a single frequency).

Some straightforward algebra implies that robust performance is equivalent to the satisfaction of the inequalities

$$\|W_2T\|_\infty < 1 \quad \text{and} \quad \left\| \frac{W_1S}{1+\Delta W_2T} \right\|_\infty < 1, \quad \forall \|\Delta\|_\infty \leq 1, \tag{7.14}$$

with the first condition being the test for robust stability (Thm. 7.2.5). The next result replaces these two inequalities with a single inequality.

Theorem 7.2.7 (Robust Performance)**.** *The closed-loop system in Figure 7.1b attains robust performance if and only if the nominal system is $\mathfrak{A}(\sigma)$-stable and*

$$\| |W_1S| + |W_2T| \|_\infty < 1. \tag{7.15}$$

Proof. The proof is very similar to that on pages 56-57 of [59] with substitution of Thm. 7.2.5 for the analysis of the robust stability for infinite-dimensional systems. □

7.3 IMC Design for DPS

The analysis conditions for infinite-dimensional systems in the previous section are used to develop an IMC design method for DPS. As in the design method for ODEs, the method can be interpreted as determining an exact or approximate inverse of the nominal process model which is augmented with a filter to derive a proper (physically realizable) controller. Extension of this approach to an infinite-dimensional process model can require the use of an infinite-dimensional filter. The required information for controller design are:

1. nominal process model $\tilde{P}$,

2. performance specification (weighting function W_1), and

3. uncertainty weight W_2.

Two methods are proposed for creation of a physically realizable IMC controller.

7.3.1 Method 1

The IMC controller consists of the optimal controller for the nominal process model followed by filtering to provide robustness.

Nominal performance

Determine the operator $\tilde{Q}$ for the nominal process $\tilde{P}$ that optimizes the nominal performance:

$$\min \|W_1 \tilde{S}\|_\infty, \tag{7.16}$$

where $\tilde{S} = 1 - \tilde{P}\tilde{Q}$ is the nominal sensitivity function. Readers are referred to Ref. [49] for algorithms for solving this minimization for infinite-dimensional processes. If the nominal process is minimum-phase, then the solution is

$$\tilde{Q} = \tilde{P}^{-1}. \tag{7.17}$$

This nominal operator $\tilde{Q}$ is usually improper since the nominal process is usually strictly proper.

Robust stability and performance

Design the IMC controller

$$Q(s) = \tilde{Q}(s)F(s, \lambda) \tag{7.18}$$

which augments $\tilde{Q}$ with a filter F to detune the optimal controller and trade off speed of response with robustness to model uncertainty, insensitivity to measurement noise, and smoothness of the control action. The classical feedback controller C is given by comparison of the IMC and classical control structures in Figure 7.1:

$$C = \frac{Q}{1 - \tilde{P}Q}. \tag{7.19}$$

Usually an infinite-dimensional filter is needed so that the IMC controller Q is proper and the feedback controller C is physically realizable. The filter F should be selected so that the closed-loop system retains desired asymptotic properties as Q is detuned for robustness. In particular, for the error signal resulting

from a step input to approach zero at steady-state, the filter should satisfy

$$\lim_{s\to 0} F(s,\lambda) = 1. \tag{7.20}$$

To provide a one-to-one correspondence to the IMC design method for finite-dimensional systems, the tuning parameter λ in the infinite-dimensional filter F should be defined so that the optimal nominal performance is achieved as $\lambda \to 0$:

$$\lim_{\lambda\to 0} F(s,\lambda) = 1. \tag{7.21}$$

The specific finite value for the tuning parameter λ can be selected in a number of ways, corresponding to the same criteria used to tune IMC controllers for finite-dimensional systems [148]. For example, λ can be selected as small as possible while satisfying the robust stability or robust performance conditions

$$\|W_2 T\|_\infty < 1, \tag{7.22}$$

$$\||W_1 S| + |W_2 T|\|_\infty < 1, \tag{7.23}$$

or to minimize the robust performance condition

$$\min_{\lambda>0} \||W_1 S| + |W_2 T|\|_\infty \tag{7.24}$$

with the design being acceptable if the attained objective is less than one. For stable processes, increasing λ slows the closed-loop dynamics and increases robustness to model uncertainties.

7.3.2 Method 2

This approach first defines a super-set of the nominal process model. For a minimum-phase nominal process model, construct $\tilde{P}_s(s,\lambda) \supset \tilde{P}(s)$ for $\lambda > 0$ such that $\tilde{P}_s(s,\lambda)$ is minimum-phase and semiproper and satisfies

$$\lim_{\lambda\to 0} \tilde{P}_s(s,\lambda) = \tilde{P}(s). \tag{7.25}$$

Then the IMC controller is

$$Q(s,\lambda) = \tilde{P}_s^{-1}(s,\lambda), \tag{7.26}$$

where the IMC tuning parameter λ is selected as described in Method 1. If the nominal process model is non-minimum phase, then $\tilde{P}_s(s,\lambda)$ should be constructed so that the IMC controller Q optimizes the nominal performance (7.16) as $\lambda \to 0$.

7.3.3 Implementation

Method 1 is closest in character to the IMC method for finite-dimensional systems [148] whereas Method 2 is more convenient when inspecting Laplace transform tables to identify suitable forms for the IMC controller. As in the standard IMC method, the form of the filter is up to the designer. The transfer function of the classical controller is determined by (7.19) with the time-domain equations constructed by analytical or numerical solution of the inverse Laplace transform. When the processes in Π (7.4) are stable, then the control system can be implemented using either the IMC or classical feedback structure in Figure 7.1. Of the two control structures, only the classical feedback structure can be implemented when the processes are unstable, and any unstable poles in the nominal process must be canceled by unstable zeros in Q, similarly as in the finite-dimensional case [148].

The allowable error in any finite-dimensional approximation of the infinite-dimensional controller can be quantified by using similar analysis methods as developed in Section 7.2.

Usually the infinite-dimensional controller $\tilde{C}$ is not easy to implement directly, in which case a finite-dimensional approximation C that accurately matches its frequency response over the closed-loop bandwidth can be implemented [202] (the examples in the next section use finite-difference methods). Representing the error in the finite-dimensional approximation of the controller by

$$\Pi_c = \{C : C = (1 + \Delta_c W_c)\tilde{C},\ \|\Delta_c\|_\infty \leq 1,\ C \text{ and } \tilde{C} \text{ have the same number of unstable poles}\}, \tag{7.27}$$

specifies an upper bound on the relative error in the controller implementation

$$\left|\frac{\tilde{C}(j\omega) - C(j\omega)}{\tilde{C}(j\omega)}\right| \leq |W_c(j\omega)|, \quad \forall C(s) \in \Pi_c,\ \forall\omega. \tag{7.28}$$

Considering both this uncertainty and the multiplicative plant uncertainty, application of algebra similarly as before results in the robust stability condition

$$|W_{2,tot}T| < 1, \quad \forall\omega, \tag{7.29}$$

and robust performance condition

$$|W_{2,tot}T| + |W_1 S| < 1, \quad \forall\omega, \tag{7.30}$$

where $W_{2,tot}$ is any transfer function defined to have magnitude

$$|W_{2,tot}| = |W_c| + |W_2| + |W_c||W_2|, \quad \forall\omega. \tag{7.31}$$

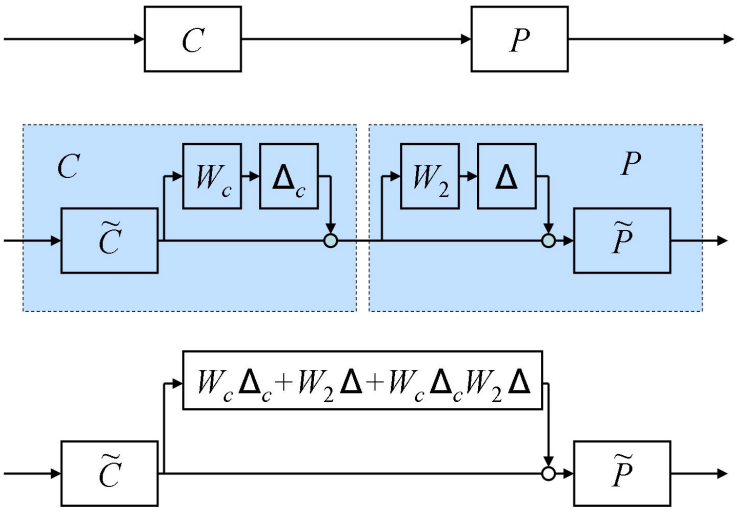

Figure 7.5: Equivalent block diagrams.

Figure 7.5 illustrates the block diagram transformation, where

$$|W_c\Delta_c + W_2\Delta + W_c\Delta_c W_2\Delta| \leq |W_{2,tot}|, \quad \forall\omega, \tag{7.32}$$

is implied by (7.31), by application of the triangle inequality.

7.4 Example 1: A Parabolic Equation

Consider the diffusion equation (as in Figure 7.6)

$$\frac{\partial C}{\partial t} = D\frac{\partial^2 C}{\partial x^2}, \quad \forall x \in (0,a), \quad \forall t > 0, \tag{7.33}$$

with Dirichlet and Neumann boundary conditions

$$C(0,t) = u(t), \tag{7.34}$$

$$\frac{\partial C}{\partial x}\Big|_{x=a} = 0, \tag{7.35}$$

zero initial condition

$$C(x,0) = 0, \tag{7.36}$$

nominal diffusion coefficient $\tilde{D} = 10^{-5}$ m^2/s, and the distance across the domain $a = 10^{-2.5}$ m.

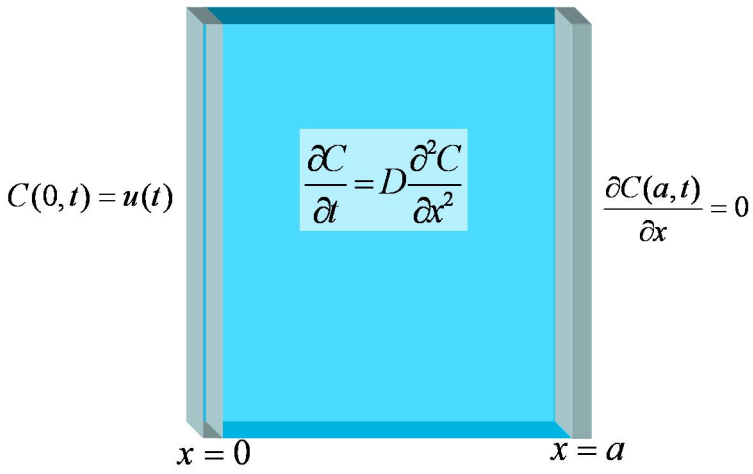

Figure 7.6: Mass transport of molecules by diffusion into a solid film.

The minimum-phase transfer function for the nominal process

$$\tilde{P}(s) = \frac{1}{\cosh\sqrt{s}} \tag{7.37}$$

for the control input $u(t)$ and output $C(a,t)$ is obtained by solving the Laplace transforms of the PDE (7.33) and boundary conditions (7.34) and (7.35).

This application of the IMC design method selected the performance weight

$$W_1 = 0.5\frac{0.06s+1}{0.06s} \tag{7.38}$$

to specify zero steady-state error for a step input (that is, integral action), a peak sensitivity less than 2, and a closed-loop time constant of 0.06.

The model uncertainty is described by the frequency-dependent bound

$$\left|\frac{P(j\omega)-\tilde{P}(j\omega)}{\tilde{P}(j\omega)}\right| \leq |W_2(j\omega)|, \ \forall\omega\in\mathbb{R}, \tag{7.39}$$

with

$$W_2 = \frac{\cosh\sqrt{s}}{\cosh\sqrt{s/1.2}} - 0.8, \tag{7.40}$$

which requires that the closed-loop system is robust to variations in the diffusion coefficient, $0.72\times10^{-5} \leq D \leq 1.2\times10^{-5}$ or up to 20% uncertainty in the steady-state gain.

An invertible semiproper super-set of the nominal process model

$$\tilde{P}_s(s,\lambda) = \frac{\cosh \lambda\sqrt{s}}{\cosh \sqrt{s}}, \tag{7.41}$$

follows naturally from (7.37). The DPS IMC controller

$$Q(s,\lambda) = \frac{\cosh \sqrt{s}}{\cosh \lambda\sqrt{s}} \tag{7.42}$$

is the optimal solution of (7.16) for any fixed $\lambda \geq 0$ with $\tilde{P}_s(s,\lambda)$ in place of the nominal process model. The nominal sensitivity function and complementary sensitivity function for the above Q and $\tilde{P}$ (7.37) are

$$S(s) = 1 - \tilde{P}Q = 1 - \frac{1}{\cosh \lambda\sqrt{s}}, \tag{7.43}$$

$$T(s) = \tilde{P}Q = \frac{1}{\cosh \lambda\sqrt{s}}. \tag{7.44}$$

Figure 7.7 shows that $\lambda = 0.3$ satisfies the robust stability (7.22) and robust performance conditions (7.23), and nearly minimizes (7.24).

Let's verify that $G = \tilde{P}C$ satisfies the conditions of the generalized Nyquist criterion in Thm. 7.2.3. The function G for the nominal process is

$$\begin{aligned} G(s) &= \tilde{P}C \\ &= \frac{\tilde{P}Q}{1 - \tilde{P}Q} \\ &= \frac{\frac{1}{\cosh \lambda\sqrt{s}}}{1 - \frac{1}{\cosh \lambda\sqrt{s}}} \\ &= \frac{1}{\cosh \lambda\sqrt{s} - 1}. \end{aligned}$$

1. Let $\hat{n}(s) = \dfrac{1}{\cosh \lambda\sqrt{s}}$ and $\hat{d}(s) = 1 - \dfrac{1}{\cosh \lambda\sqrt{s}}$, then $\hat{n}(s) \in \hat{\mathfrak{A}}_-(0)$ follows from

$$n(t) = \frac{\pi}{\lambda^2} \sum_{n=1}^{\infty} (-1)^{n-1} (2n-1) e^{-(2n-1)^2 \pi^2 t/4\lambda^2}$$

and $\hat{d}(s) \in \hat{\mathfrak{A}}_-(\sigma_0)$ follows from

$$d(t) = \delta(t) - \frac{\pi}{\lambda^2} \sum_{n=1}^{\infty} (-1)^{n-1} (2n-1) e^{-(2n-1)^2 \pi^2 t/4\lambda^2}.$$

The above set memberships hold for any IMC tuning parameter λ, as each term in the summations is

an exponential whose integral over time rapidly converges to zero as $n \to \infty$.

2. There exist $\hat{u}(s) = 1 \in \hat{\mathfrak{A}}_-(\sigma_0)$ and $\hat{v}(s) = 1 \in \hat{\mathfrak{A}}_-(\sigma_0)$ such that

$$\hat{u}(s)\hat{n}(s) + \hat{v}(s)\hat{d}(s) = \frac{1}{\cosh \lambda\sqrt{s}} + \left(1 - \frac{1}{\cosh \lambda\sqrt{s}}\right) = 1.$$

3. $\hat{d}(s) = 1 - \dfrac{1}{\cosh \lambda\sqrt{s}}$ is analytic in $\mathbb{C}_{0+}$, as $\lambda\sqrt{s}$ is analytic in s for $\mathbb{C}_{0+}$, $\cosh z$ is analytic for any $z \in \mathbb{C}$, and the composition of analytic functions are analytic. Straightforward algebra indicates that $\hat{d}(s)$ is bounded away from zero at ∞ in $\mathbb{C}_{0+}$.

4. $\lim\limits_{|s|\to\infty} \dfrac{1}{\cosh \lambda\sqrt{s} - 1} = 0$ for $\mathrm{Re}\{s\} > 0$ follows from $|\cosh \lambda\sqrt{s}| \to \infty$ as $|s| \to \infty$ for $\mathrm{Re}\{s\} > 0$.

It can also be verified that:

- $1 + \tilde{P}C = 1 + \dfrac{\tilde{P}Q}{1 - \tilde{P}Q} \neq 0$, $\forall s \in \bar{N}_\infty$, since $1 + \dfrac{\tilde{P}Q}{1 - \tilde{P}Q} = 0$ would imply a contradiction:[3]

$$1 + \frac{\tilde{P}Q}{1 - \tilde{P}Q} = 0 \iff 1 = 0.$$

- $\hat{d}(s)$ has no open right-half plane zeros and $1 + \dfrac{1}{\cosh \lambda\sqrt{s} - 1}$ encircles the origin zero times in the counterclockwise sense $\forall s \in \bar{N}_\infty$ (the Nyquist curve does not cross with the imaginary axis).

The DPS IMC controller (7.42) was compared to the finite-dimensional IMC controller [148] designed from the second-order and tenth-order transfer functions obtained by applying a second-order finite-difference spatial discretization to the PDE (7.33) with grid size of 0.5 and 0.1, respectively (denoted by FD IMC controller). The FD IMC controllers used the filter [148]

$$F(s, \lambda) = \frac{1}{(\lambda s + 1)^n} \tag{7.45}$$

with $n = 2$ or 10 to produce a proper Q with physically realizable controller C. In both cases, *no* IMC tuning parameter λ achieved robust performance (see Figures 7.8 and 7.9). The values $\lambda = 0.08$ and $\lambda = 0.01$ were selected for the second- and tenth-order transfer functions, respectively, to minimize the violation of the robust performance condition (7.23), that is, to minimize (7.24). FD IMC controllers were used for comparison because finite-difference spatial discretization (FD) provided a much more accurate fit to the frequency response of the nominal infinite-dimensional process than using modal decomposition (MOD), for the same order (see Figure 7.10). Also, the modal decomposition for the same order introduces minimum-phase zeros that do not appear in the nominal process.

[3]The use of the IMC filter F implies that $1 - \tilde{P}Q \neq 0$; $1 - \tilde{P}Q = 0$ would imply "perfect control," which is not obtainable in practice [148].

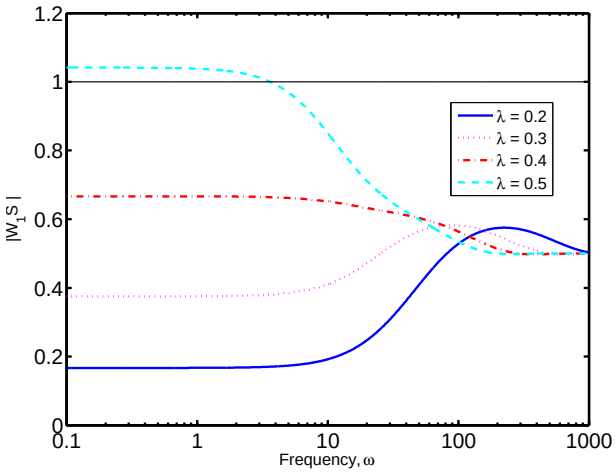

(a) Nominal performance

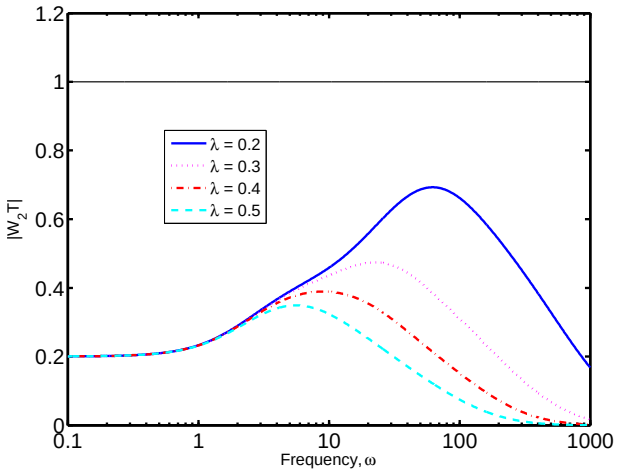

(b) Robust stability

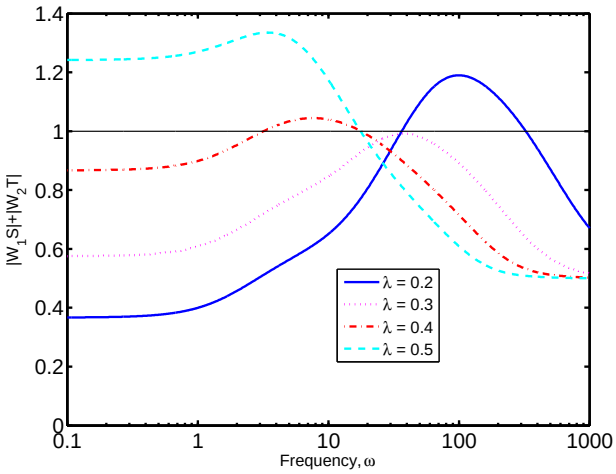

(c) Robust performance

Figure 7.7: Bode plots for the DPS IMC controller (Example 1).

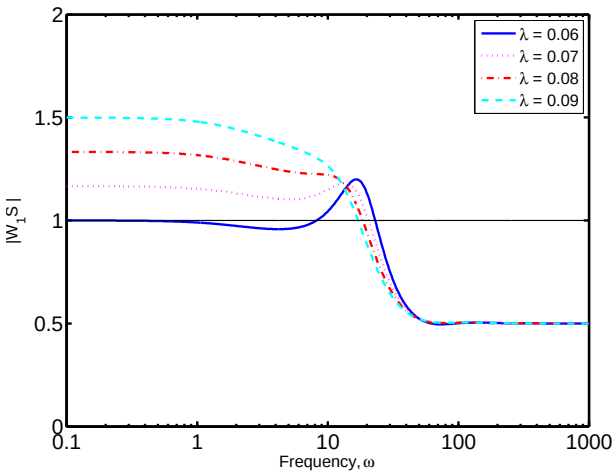

(a) Nominal performance

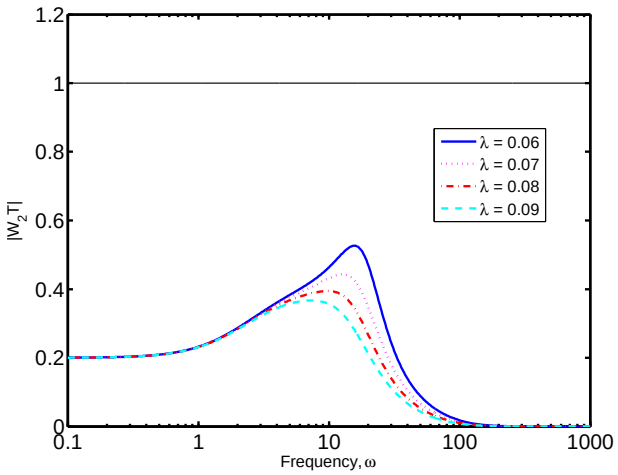

(b) Robust stability

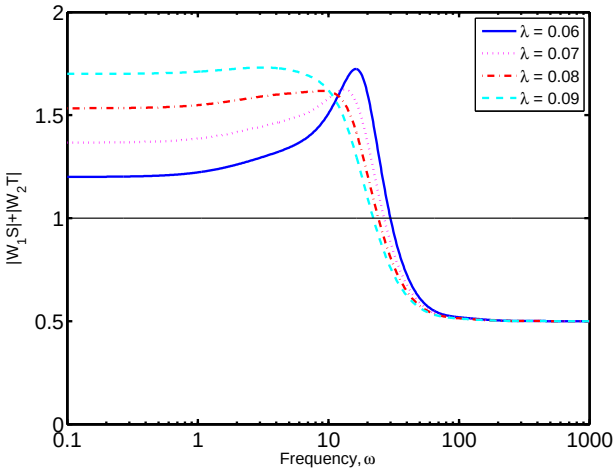

(c) Robust performance

Figure 7.8: Bode plots for the FD IMC controller for a second-order model, $n = 2$ (Example 1).

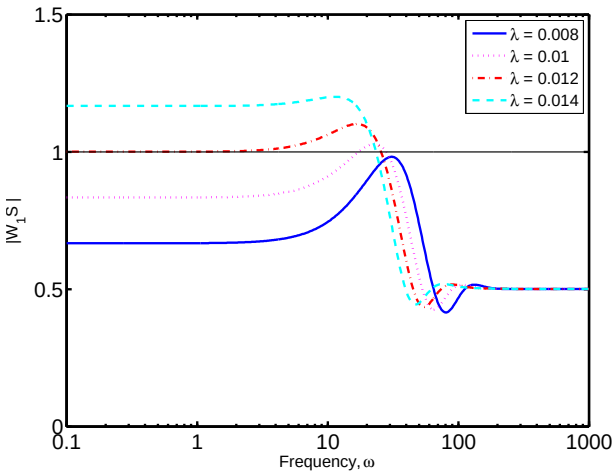

(a) Nominal performance

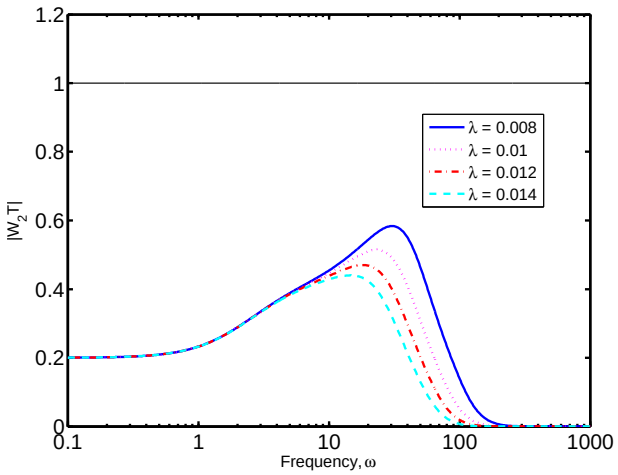

(b) Robust stability

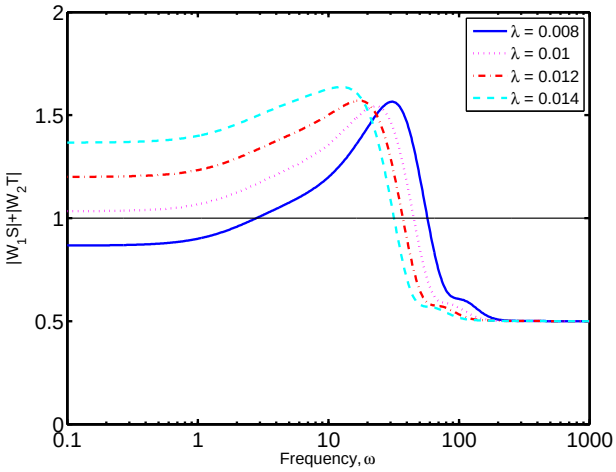

(c) Robust performance

Figure 7.9: Bode plots for the FD IMC controller for a tenth-order model, $n = 10$ (Example 1).

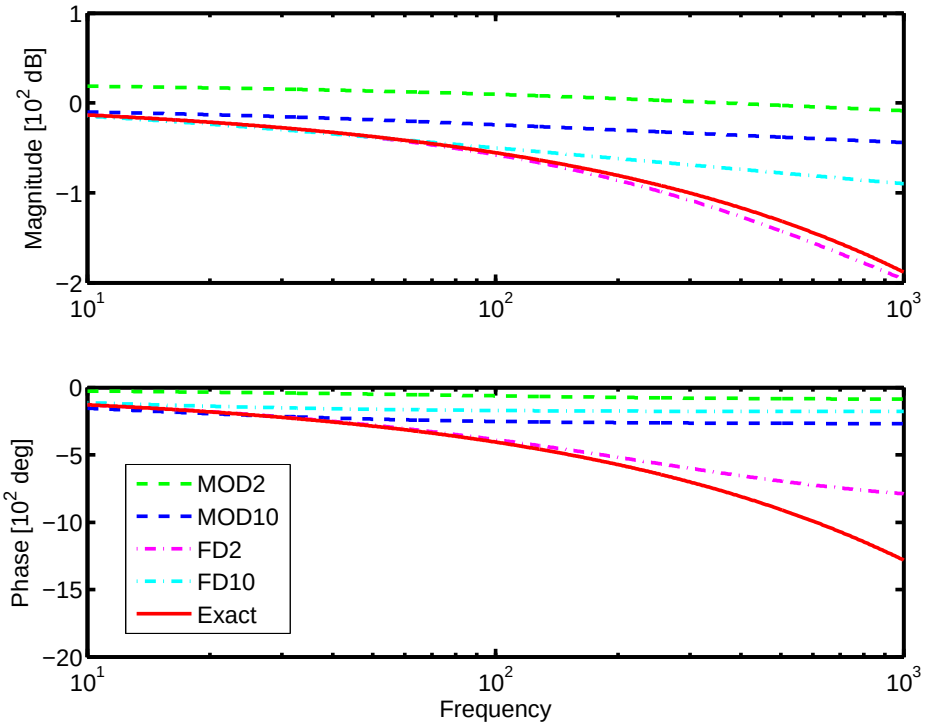

Figure 7.10: Bode magnitude and phase plots of the process and models obtained by different methods.

To investigate the effects of model uncertainty, setpoint tracking responses were simulated assuming that the real process was (7.33) with the diffusion coefficient $D = 1.2 \times 10^{-5}$ which is covered by the model uncertainty description. The DPS IMC controller (7.42) provided much better closed-loop performance than the FD IMC controllers for both sinusoidal and step setpoints (see Figure 7.11 and Table 7.1). Further analysis (not shown here for brevity) indicated that the FD IMC controllers do not provide acceptable robust performance for *any* order for the finite-difference discretization of the PDE (7.33), no matter how high. As the order increases, the frequency response of the finite-difference process model approaches the frequency response of the PDE (7.33), however, the finite-order IMC filter (7.45) is poorly matched to the dynamics of the PDE and this mismatch becomes worse as the order is increased. While IMC filters other than (7.45) could be proposed to attempt to better match the infinite-dimensional dynamics of the process, such guesswork is not required during the DPS IMC design where an appropriate form for the infinite-dimensional filter (7.42) follows naturally from the transfer function of the nominal process model (7.37).

The IMC controllers designed for robust performance applied to finite-dimensional models of increasing order do not converge to the controller designed by the DPS IMC method (see Figure 7.12), regardless of how accurate the finite-dimensional model approximates the infinite-dimensional model. Even if the ultimate goal is to design a finite-dimensional controller, this example indicates that it can be much more efficient and effective to design the infinite-dimensional controller based on the infinite-dimensional process model and then determine a finite-dimensional approximation of the controller. It is straightforward to show, from

Table 7.1: Errors in time-domain signal norms on the controlled variable (Example 1).

Setpoint	FD2 IMC	FD10 IMC	DPS IMC
Sinusoidal $\|\cdot\|_\infty$	0.6879	0.4766	0.2199
Sinusoidal $\|\cdot\|_2$	0.0338	0.0235	0.0108
Step $\|\cdot\|_2$	0.0100	0.0085	0.0043

the continuity of the performance objective with respect to the controller transfer function evaluated at each frequency, that a sufficiently high order finite-dimensional approximation of the DPS IMC controller will satisfy the robust performance criterion (7.23) provided that the criterion is strictly satisfied for the DPS IMC controller and that the frequency response of the finite-dimensional controller converges to the frequency response of the DPS IMC controller as the order is increased.

7.5 Robust Stability and Nominal Performance Conditions

For completeness, this section provides the expressions used to generate Figures 7.8 and 7.9.

Let $\tilde{P}_\infty$ denote the infinite-dimensional plant transfer function with nominal parameter values, Q_∞ denote the infinite-dimensional controller designed by using $\tilde{P}_\infty$, and $\tilde{P}_{FD}$ denote the finite-dimensional plant transfer function with nominal parameter values.

For the infinite-dimensional controller, the necessary and sufficient condition for robust stability is

$$\left\| W_2 \tilde{P}_\infty Q_\infty \right\|_\infty < 1. \tag{7.46}$$

For the finite-dimensional controller, the robust stability condition is

$$\left\| W_2 \frac{\tilde{P}_\infty Q_{FD}}{1 + (\tilde{P}_\infty - \tilde{P}_{FD}) Q_{FD}} \right\|_\infty < 1. \tag{7.47}$$

For the infinite-dimensional controller, the nominal performance condition is

$$\left\| W_1 \left(1 - \tilde{P}_\infty Q_\infty \right) \right\|_\infty < 1. \tag{7.48}$$

For the finite-dimensional controller, the corresponding condition is

$$\left\| W_1 \frac{1 - \tilde{P}_{FD} Q_{FD}}{1 + (\tilde{P}_\infty - \tilde{P}_{FD}) Q_{FD}} \right\|_\infty < 1. \tag{7.49}$$

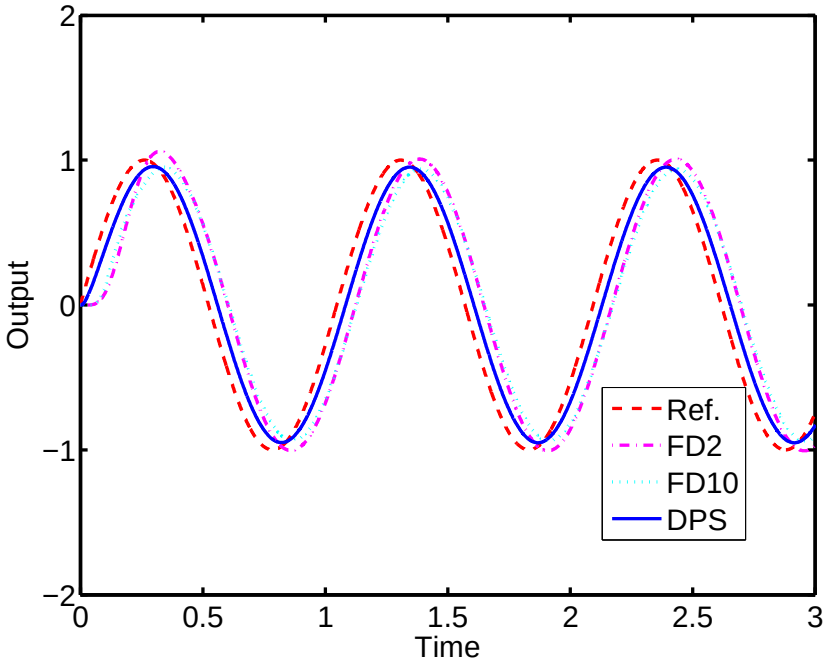

(a) Sinusoidal

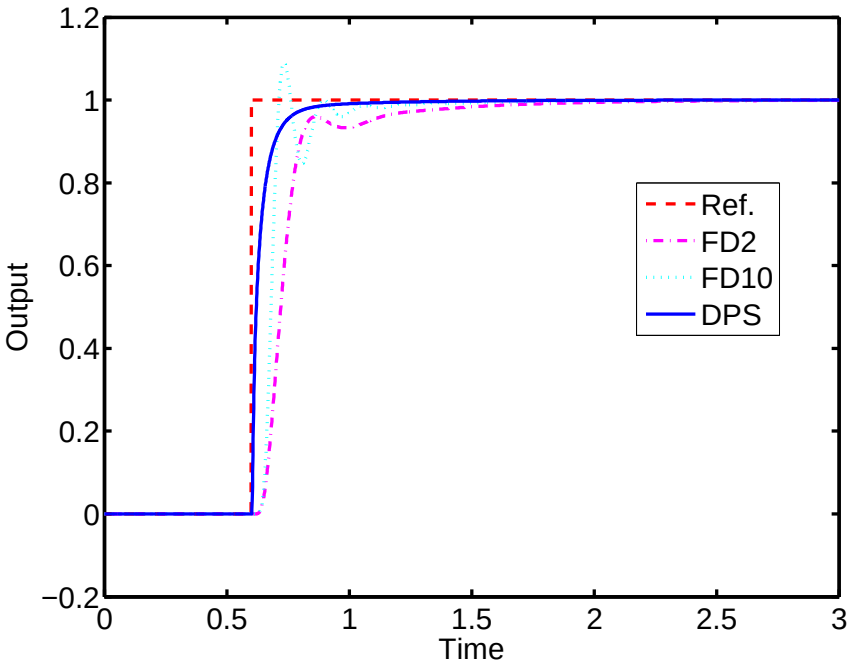

(b) Step

Figure 7.11: Closed-loop responses for setpoint tracking for Example 1. The "exact" process was modeled by the finite-difference method with $n = 50$ and $D = 1.2 \times 10^{-5}$. FD2 and FD10 are the second- and tenth-order IMC controllers designed based on a finite-dimensional process model. The output is written in terms of deviation variables.

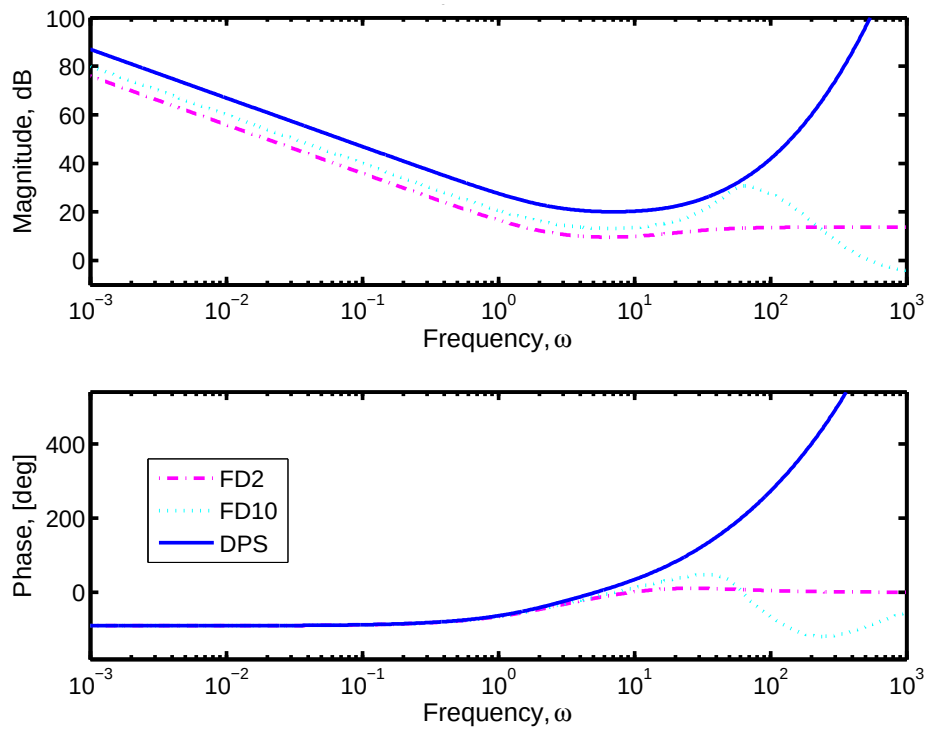

Figure 7.12: Bode plots for the controllers $C(s) = \frac{Q}{1-Q\tilde{P}}$ designed by three ways for Example 1.

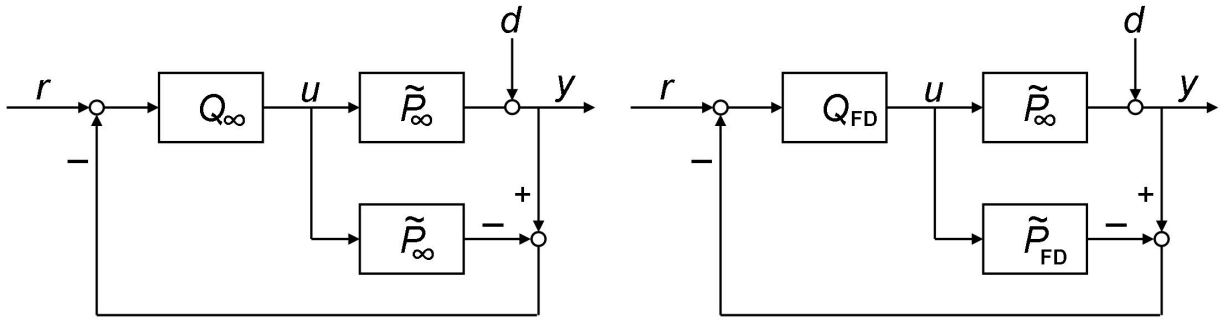

(a) DPS IMC (b) FD IMC

Figure 7.13: IMC control structures based on infinite- and finite-dimensional models.

For the infinite-dimensional controller, the robust performance condition is

$$\left\| W_1 \left(1 - \tilde{P}_\infty Q_\infty\right) \right\|_\infty + \left\| W_2 \tilde{P}_\infty Q_\infty \right\|_\infty < 1. \tag{7.50}$$

For the finite-dimensional controller, the corresponding condition is

$$\left\| W_1 \frac{1 - \tilde{P}_{FD} Q_{FD}}{1 + (\tilde{P}_\infty - \tilde{P}_{FD}) Q_{FD}} \right\|_\infty + \left\| W_2 \frac{\tilde{P}_\infty Q_{FD}}{1 + (\tilde{P}_\infty - \tilde{P}_{FD}) Q_{FD}} \right\|_\infty < 1. \tag{7.51}$$

7.6 Example 2: A Hyperbolic and Parabolic System in Series

This example illustrates the application of the DPS IMC method to an unstable nonminimum-phase process (Figure 7.14). Consider a series connection of two processes (A) and (B), where process (A) is governed by the convection equation:

$$\frac{\partial C_A}{\partial t} + v \frac{\partial C_A}{\partial x} = 0, \quad \forall x \in (0, a), \quad \forall t > 0, \tag{7.52}$$

and process (B) is governed by the diffusion equation:

$$\frac{\partial C_B}{\partial t} = D \frac{\partial^2 C_B}{\partial x^2}, \quad \forall x \in (a, b), \quad \forall t > 0, \tag{7.53}$$

with initial conditions

$$C_A(x, 0) = 0, \tag{7.54}$$

$$C_B(x, 0) = 0, \tag{7.55}$$

and boundary conditions

$$C_A(0, t) = u(t), \tag{7.56}$$

$$\frac{\partial C_B}{\partial x}\Big|_{x=b} = 0, \tag{7.57}$$

$$v C_A(a, t) = -D \frac{\partial C_B}{\partial x}\Big|_{x=a}. \tag{7.58}$$

For the control input $u(t)$ and output $C_B(b, t)$, the nominal process transfer function is

$$\tilde{P}(s) = \frac{\tilde{v} e^{-as/\tilde{v}}}{\sqrt{\tilde{D}s} \sinh \sqrt{\frac{s}{\tilde{D}}}(b - a)} = \tilde{P}_a(s) \tilde{P}_m(s), \tag{7.59}$$

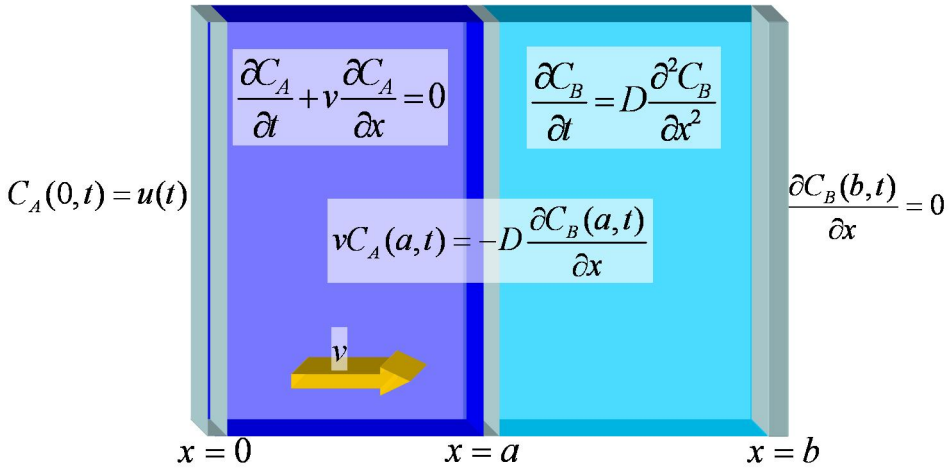

Figure 7.14: A distributed parameter system involving the transport of molecules through a gas and an adjacent solid film.

where

$$\tilde{P}_a(s) = e^{-as/\tilde{v}}, \tag{7.60}$$

$$\tilde{P}_m(s) = \frac{\tilde{v}}{\sqrt{\tilde{D}s}\sinh\sqrt{\frac{s}{\tilde{D}}}(b-a)}. \tag{7.61}$$

This is a nonminimum-phase process involving a hyperbolic PDE coupled with a parabolic PDE, which describes the transport of molecules through adjacent gas and solid films. For $a = 10^{-2.5}$ m, $b = 2 \times 10^{-2.5}$ m, and nominal parameters $\tilde{D} = 10^{-5}$ m/s and $\tilde{v} = 2 \times 10^{-1.5}$ m/s, these nominal transfer functions are

$$\tilde{P}(s) = \frac{20e^{-s/20}}{\sqrt{s}\sinh\sqrt{s}}, \tag{7.62}$$

$$\tilde{P}_a(s) = e^{-s/20}, \tag{7.63}$$

$$\tilde{P}_m(s) = \frac{20}{\sqrt{s}\sinh\sqrt{s}}. \tag{7.64}$$

The performance weight

$$W_1 = 0.3\frac{0.093s + 1}{0.093s} \tag{7.65}$$

specifies zero steady-state gain error for a step input, a closed-loop time constant of 0.093, and a maximum disturbance amplification of 10/3. The parameter combinations shown in Figure 7.15 are within the multiplicative uncertainty description with the weight

$$W_2 = 1.1\frac{\sinh\sqrt{s}}{\sqrt{1.2}\sinh\sqrt{\frac{s}{1.2}}} - 1. \tag{7.66}$$

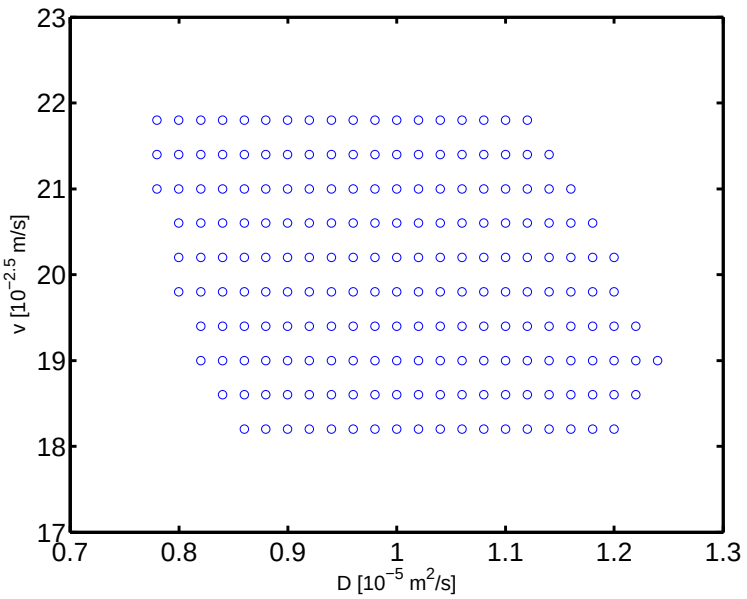

Figure 7.15: Sets of parameters for the velocity v and diffusion coefficient D covered by the multiplicative uncertainty description with W_2 for Example 2.

The invertible semiproper superset of $\tilde{P}_m(s)$

$$\tilde{P}_{ms}(s,\lambda) = \frac{20\cosh\lambda\sqrt{s}}{\sqrt{s}\sinh\sqrt{s}} \tag{7.67}$$

follows naturally from (7.64), which results in the DPS IMC controller

$$Q(s,\lambda) = \frac{\sqrt{s}\sinh\sqrt{s}}{20\cosh\lambda\sqrt{s}}. \tag{7.68}$$

which is the optimal solution of (7.16) for any fixed $\lambda \geq 0$ with $\tilde{P}_{ms}(s,\lambda)$ in place of the nominal process model.

The nominal sensitivity function and complementary sensitivity function for the above Q and $\tilde{P}$ (7.62) are

$$S(s) = 1 - \tilde{P}Q = 1 - \frac{e^{-s/20}}{\cosh\lambda\sqrt{s}}, \tag{7.69}$$

$$T(s) = \tilde{P}Q = \frac{e^{-s/20}}{\cosh\lambda\sqrt{s}}. \tag{7.70}$$

As discussed in Section 7.3.3, the control system is implemented using the classical feedback control structure. The zero at $s = 0$ in the IMC controller Q cancels the pole at $s = 0$ in the nominal process when determining the classical controller from (7.19), and S has a zero at $s = 0$, which is required for nominal stability.[4]

It can be verified that $\lambda = 0.25$ satisfies the robust stability (7.22) and robust performance conditions

[4]Cancellation of the pole at $s = 0$ does not pose any internal stability issues; there is no pole-zero cancellation at $s = 0$ between the nominal process and the classical feedback controller.

(7.23), and nearly minimizes (7.24). By following the same procedure as the Example 1, the values $\lambda = 0.08$ and $\lambda = 0.01$ were selected for the second- and tenth-order transfer functions, respectively. The DPS IMC controller (7.68) provides better setpoint tracking than the FD IMC controllers (see Figure 7.16 and Table 7.2).

Let's verify that $G = \tilde{P}C$ satisfies the conditions of the generalized Nyquist criterion in Thm. 7.2.3. The function G for the nominal process is

$$G(s) = \tilde{P}C = \frac{\tilde{P}Q}{1 - \tilde{P}Q} = \frac{e^{-s/20}}{\cosh \lambda\sqrt{s} - e^{-s/20}}.$$

1. Let $\hat{n}(s) = \dfrac{e^{-s/20}}{\cosh \lambda\sqrt{s}}$ and $\hat{d}(s) = 1 - \dfrac{e^{-s/20}}{\cosh \lambda\sqrt{s}}$, then $\hat{n}(s) \in \hat{\mathfrak{A}}_-(\sigma_0)$ follows from the fact that the inverse Laplace transform of $\dfrac{1}{\cosh \lambda\sqrt{s}}$ is

$$\frac{\pi}{\lambda^2} \sum_{n=1}^{\infty} (-1)^{n-1}(2n-1)e^{-(2n-1)^2\pi^2 t/4\lambda^2},$$

   $e^{-s/20} \in \hat{\mathfrak{A}}_-(\sigma_0)$, and $\hat{n}(s)$ is composition of elements of $\hat{\mathfrak{A}}_-(\sigma_0)$. That $\hat{d}(s) \in \hat{\mathfrak{A}}_-(\sigma_0)$ follows from the inverse Laplace transform of 1 being $\delta(t)$ and $\hat{d}(s)$ is a linear combination of 1 and $\hat{n}(s)$.

2. There exist $\hat{u}(s) = 1 \in \hat{\mathfrak{A}}_-(\sigma_0)$ and $\hat{v}(s) = 1 \in \hat{\mathfrak{A}}_-(\sigma_0)$ such that

$$\hat{u}(s)\hat{n}(s) + \hat{v}(s)\hat{d}(s) = \frac{e^{-s/20}}{\cosh \lambda\sqrt{s}} + \left(1 - \frac{e^{-s/20}}{\cosh \lambda\sqrt{s}}\right) = 1.$$

3. $\hat{d}(s) = 1 - \dfrac{e^{-s/20}}{\cosh \lambda\sqrt{s}}$ is analytic in $\mathbb{C}_{0+}$. Straightforward algebra indicates that $\hat{d}(s)$ is bounded away from zero at ∞ in $\mathbb{C}_{0+}$.

4. $\lim\limits_{|s|\to\infty} \dfrac{e^{-s/20}}{\cosh \lambda\sqrt{s} - e^{-s/20}} = 0$ for $\mathrm{Re}\{s\} > 0$ follows from $\left|\dfrac{e^{-s/20}}{\cosh \lambda\sqrt{s}}\right| \to 0$ as $|s| \to \infty$ for $\mathrm{Re}\{s\} > 0$.

It can also be verified that:

- $1 + \dfrac{\tilde{P}Q}{1 - \tilde{P}Q} \neq 0$, $\forall s \in \bar{N}_\infty$.
- $\hat{d}(s)$ has no open right-half plane zeros and $1 + \dfrac{e^{-s/20}}{\cosh \lambda\sqrt{s} - e^{-s/20}}$ encircles the origin zero times in the counterclockwise sense $\forall s \in \bar{N}_\infty$.

7.7 Conclusions

The IMC method was generalized to the design of controllers for linear DPS. The proposed controller provided improved setpoint tracking and robust performance compared to the IMC method designed from

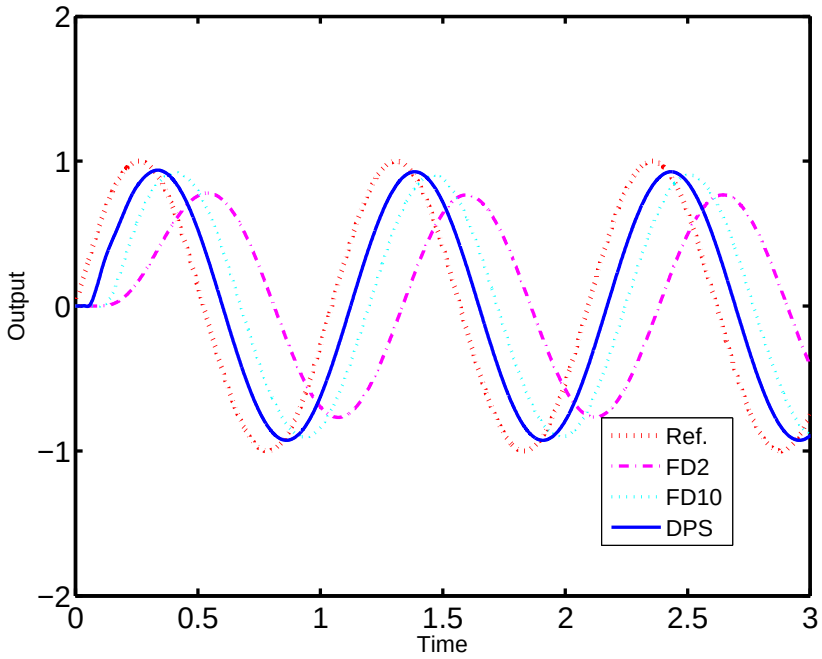

(a) Sinusoidal

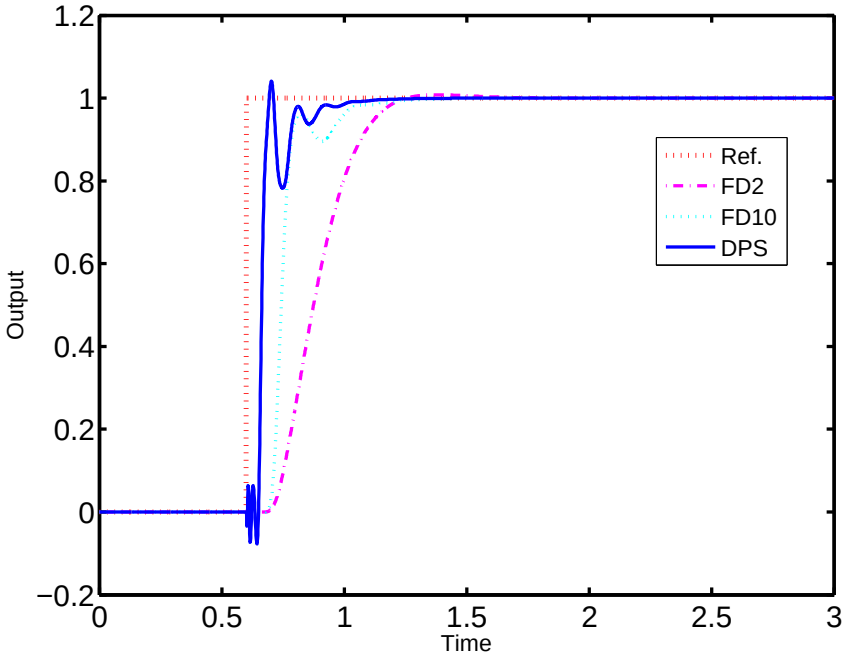

(b) Step

Figure 7.16: Closed-loop responses for setpoint tracking of sinusoidal and step signals (Example 2). The "exact" process was modeled by the finite-difference method with grid size $\Delta x = (b-a)/50$, $D = 1.24 \times 10^{-5}$ m^2/s, and $v = 1.9 \times 10^{-1.5}$ m/s. FD2 and FD10 are the second- and tenth-order IMC controllers designed based on a finite-dimensional process model. The output is written in terms of deviation variables.

Table 7.2: Errors in time-domain signal norms on the controlled variable (Example 2).

Setpoint	FD2 IMC	FD10 IMC	DPS IMC
Sinusoidal $\|\cdot\|_\infty$	1.3563	0.8449	0.4497
Sinusoidal $\|\cdot\|_2$	0.0667	0.0418	0.0223
Step $\|\cdot\|_2$	0.0151	0.0115	0.0080

an approximate finite-dimensional transfer function for two DPS. It can be shown that this new IMC design method can be used to extend all of the features of IMC for finite-dimensional systems listed in the Introduction to infinite-dimensional systems, which means that antiwindup compensation, reference prefilter design, cascade control design, and feedforward-feedback control design which are very well-developed for finite-dimensional systems can be applied to distributed parameter systems in a very similar manner. More theoretical work is needed to extend the DPS IMC approach to nonlinear systems, to mirror the developments for finite-dimensional systems [64]. To do this, systematic techniques to invert nonlinear infinite-dimensional operators need to be developed.

CHAPTER 8

STRUCTURED SPATIAL CONTROL

Feedback control problems for distributed parameter systems arise in a variety of physical, chemical, biological, and mechanical systems. This chapter exploits the algebraic structure of the system of ordinary differential equations that arise from spatial discretization of the partial differential equation (PDE) to analyze and design feedback controllers that are robust to bounded perturbations in the parameters of the original PDE. As a prototypical problem, this chapter investigates the spatial field control of a reaction-diffusion system whose spatial discretization has a state matrix that is circulant symmetric. Structured robust controllers are designed based on internal model control, mixed sensitivity optimization, and Lyapunov-based design. The controllers are shown to be robust to inaccuracies in the spatial manipulation, even for arbitrarily fine spatial discretizations. A comparison with infinite-dimensional analysis is also included.

8.1 Introduction

Spatially distributed interconnected systems arise in the control of vehicle formations [101, 142], paper manufacturing [61, 126, 3], and highway traffic [92], as well as in heat transfer [53], fluid dynamics [91], and other physicochemical phenomena when partial differential equations (PDEs) are approximated by a set of ordinary differential equations (ODEs) by discretizing the spatial domain. Such approximations enable the application of control design methods that are well established for finite-dimensional systems including linear quadratic, H_∞, and robust optimal control. These spatially distributed systems are described by highly structured matrices.

Many papers have exploited algebraic structure during the design of optimal controllers for structured finite-dimensional systems. Design procedures have been developed for the quadratic optimal control of block circulant systems [30], H_2- and H_∞-control of symmetric circulant systems [94], robust control of symmetric circulant, Toeplitz, and related systems [126], and H_2-, H_∞-, and μ-optimal control of systems

in which the singular value decomposition of the transfer function matrices is independent of the Laplace transform variable [93, 195]. Design procedures have also been developed for systems with parallel and block symmetric circulant [94], dyadic [1], and rectangular circulant transfer function matrices [67]. Nearly all papers in this area published before 2005 have been reviewed [196].

Very few papers on the optimal feedback controller design for systems with structured transfer function matrices have actually applied these methods to the spatial discretization of a PDE (a notable exception is the early paper by Brockett and Willems [30]). Here we consider such an application, and further consider the robustness of the structured controller to variations in the parameters in the original PDE. In particular, this chapter considers a spatial field control problem for a reaction-diffusion process whose spatial discretization is symmetric circulant. Internal model control (IMC) and Lyapunov-based control design are applied to the lumped approximation and the original PDE.

IMC has been applied to wide variety of processes including chemical reactors [46, 78], robot manipulators [130], and AC machines [89]. In IMC, an analytical solution for an optimal controller for the nominal process model is combined with a low-pass filter with an adjustable tuning parameter for trading off performance with robustness to model uncertainties [78, 148]. We will see in this chapter that IMC control for the reaction-diffusion process is especially simple to implement, analyze, and tune.

Lyapunov-based design [104] produces a controller which dissipates the total energy of the system. In addition to being the foundation for linear matrix inequality-based and many model predictive control methods [26, 143], Lyapunov-based design has been widely used in the nonlinear control of mechanical systems [55] and has been applied to systems on lattices [100].

The main novelty of this chapter is the analysis of the effects of uncertainties in the physicochemical parameters in the reaction-diffusion system and in the finite-dimensional approximation as the spatial resolution is increased. The minimum singular value of the transfer function matrix approaches zero and its condition number approaches infinity as the discretization grid size becomes smaller. Since such processes can be extremely sensitive to actuator uncertainty [189], the chapter analyzes these effects on robustness to inaccuracies in the manipulated field.

This chapter is organized as follows. Section 8.2 describes the distributed parameter control problem and its finite-dimensional approximation, which generalizes a control problem introduced by Brockett and Willems [30] to include reaction. Section 8.3 describes and discusses the parametric uncertainties. Section 8.4 describes the IMC design with analysis of robust stability and performance, and Section 8.6 concludes the chapter.

8.2 System Description

Consider the control of the distributed parameter system with reaction and diffusion:

$$\frac{\partial C(\theta,t)}{\partial t} = D\frac{\partial^2 C(\theta,t)}{\partial \theta^2} - kC(\theta,t) + u(\theta,t), \tag{8.1}$$

where $C(\theta,t)$ is the spatially distributed state, $u(\theta,t)$ is a spatially distributed manipulated variable, $D > 0$ is a diffusion coefficient, $k > 0$ is a reaction rate constant, and $\theta \in [0, 2\pi)$ is an angular coordinate (see Figure 8.1). This control problem is motivated by processes with circular symmetry, such as in silicon wafer processing [205] and blown film extrusion [69], and by spatial field control problems for reaction-diffusion processes that arise in drug delivery [186], tissue engineering [113], epidemiology [88], and cancer treatment [192]. For a chemical process, $u(\theta,t)$ would be the injection of molecules along the circumference, whereas $u(\theta,t)$ for a biological process would be the injection of nutrients (e.g., glucose).

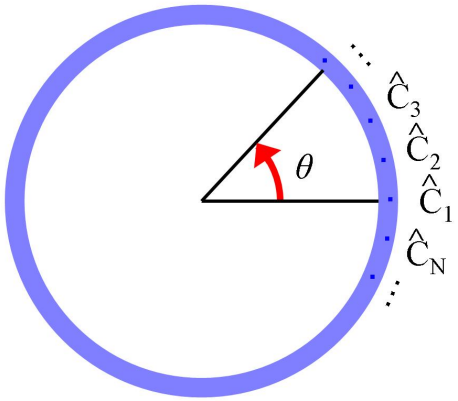

Figure 8.1: The spatial domain showing the distributed state C at uniformly spaced positions along the circumference.

Define $P_\infty : u \mapsto C$ as the mapping from $u(\theta,t)$ to $C(\theta,t)$ satisfying the PDE (8.1).

Finite-difference approximation of the second-order spatial derivative (8.1) results in a system of ODEs

$$\frac{d\hat{C}_i}{dt} = D\frac{\hat{C}_{i+1} - 2\hat{C}_i + \hat{C}_{i-1}}{\Delta^2} - k\hat{C}_i + u_i(t), \;\; i = 1, \cdots, N, \tag{8.2}$$

that is a representation of the PDE and spatially accurate to second order, where

$$\hat{C}_i(t) := \hat{C}(\theta_i, t), \tag{8.3}$$

$$\Delta := 2\pi/N, \tag{8.4}$$

$$\theta_i := \Delta/N, \tag{8.5}$$

and $\lim_{N\to\infty} |\hat{C}(\theta_i,t) - C(\theta_i,t)| = 0$. Equation (8.2) can be written in matrix form as

$$\frac{d}{dt}\begin{bmatrix}\hat{C}_1\\ \vdots \\ \hat{C}_N\end{bmatrix} = \underbrace{\begin{bmatrix} c_1 & c_2 & 0 & \cdots & 0 & c_2 \\ c_2 & c_1 & c_2 & 0 & \cdots & 0 \\ 0 & c_2 & c_1 & \ddots & \ddots & \vdots \\ \vdots & \ddots & \ddots & \ddots & c_2 & 0 \\ 0 & \cdots & 0 & c_2 & c_1 & c_2 \\ c_2 & 0 & \cdots & 0 & c_2 & c_1 \end{bmatrix}}_{:=A}\begin{bmatrix}\hat{C}_1\\ \vdots \\ \hat{C}_N\end{bmatrix} + \begin{bmatrix}u_1\\ \vdots \\ u_N\end{bmatrix}, \tag{8.6}$$

where

$$c_1 = -2\frac{D}{\Delta^2} - k, \quad c_2 = \frac{D}{\Delta^2}. \tag{8.7}$$

The output for this finite-dimensional system is equal to its state vector, and its transfer function

$$P(s) = B(sI_N - A)^{-1}C = (sI_N - A)^{-1} \tag{8.8}$$

follows from its state matrices A, $B = C = I_N$, and $D = 0$, where I_N is the $N \times N$ identity matrix. The matrix A defined in (8.6) is symmetric circulant and can be diagonalized by using the real Fourier matrix R [94]:

$$A = R^T \Lambda_A R, \tag{8.9}$$

where

$$\Lambda_A = \text{diag}\{\lambda_1, \cdots, \lambda_N\}, \tag{8.10}$$

and

$$\lambda_i = c_1 + 2c_2 \cos\frac{2\pi(i-1)}{N} < 0, \quad i = 1, \cdots, N \tag{8.11}$$

are the eigenvalues of A that are linear in c_1 and c_2. By using this eigenvalue decomposition, the transfer function for the finite-dimensional system can be written as

$$\begin{aligned} P(s) &= (sI_N - A)^{-1} \\ &= (sI_N - R^T\Lambda_A R)^{-1} \\ &= \left(R^T\left(sI_N - \Lambda_A\right)R\right)^{-1} \\ &= R^T\left(sI_N - \Lambda_A\right)^{-1}R \\ &= R^T\Lambda(s)R, \end{aligned} \tag{8.12}$$

where

$$\Lambda(s) = \operatorname{diag}\left\{\frac{1}{s-\lambda_1}, \cdots, \frac{1}{s-\lambda_N}\right\}$$
$$:= \operatorname{diag}\left\{P_1(s), \cdots, P_N(s)\right\}. \tag{8.13}$$

To simplify the presentation, the following assumptions are made throughout the manuscript.

Assumption 8.2.1. *The initial conditions are zero for the spatially distributed state $C(\theta,t)$ and reference trajectory $r(\theta,t)$, i.e., $C(\theta,0) = r(\theta,0) = 0$, $\forall\theta \in [0,2\pi)$.*

Assumption 8.2.2. *The reference trajectory r is C^1 in time and C^2 in space.*

These assumptions are very mild. Regarding Assumption 8.2.1, it is well-known that introducing an input with the Dirac delta function in time $\delta(t-\epsilon)$ into a linear system causes the state to jump at $t = \epsilon$ to a different value. This result can be applied to a system that initially has zero initial state to jump to a nonzero initial state at some time arbitrarily close to $t = 0$.

The symbol P will be used to represent the operator between the manipulated input and process output within the same domain, regardless of whether the domain is time or Laplace, as the domain will be clear from context. Similar notation is commonly used in the time domain in some fields of physics (e.g., [156]).

8.3 Uncertainty Description

The true diffusion coefficient D and reaction rate constant k are expressed as:

$$D = \tilde{D} + \Delta_D, \quad k = \tilde{k} + \Delta_k, \tag{8.14}$$

respectively, where $\tilde{D}$ and $\tilde{k}$ are nominal values and the real scalar perturbations Δ_D and Δ_k satisfy

$$|\Delta_D| \le M_D < \tilde{D}, \quad |\Delta_k| \le M_k < \tilde{k}. \tag{8.15}$$

The uncertainty set for the PDE (8.1) is given by

$$\Pi_\infty = \{P_\infty : u \mapsto C \text{ satisfying (8.1) with (8.14) \& (8.15)}\}. \tag{8.16}$$

To quantify the effects of this uncertainty on the finite-dimensional transfer function, insertion of the nominal and true parameter values in (8.11) results in the eigenvalues for the nominal and "true" processes:

$$\tilde{\lambda}_i = -2\frac{\tilde{D}}{\Delta^2}\left(1-\cos\frac{2\pi(i-1)}{N}\right)-\tilde{k}, \quad i=1,\cdots,N, \tag{8.17}$$

$$\begin{aligned}\lambda_i &= -2\frac{D}{\Delta^2}\left(1-\cos\frac{2\pi(i-1)}{N}\right)-k \\ &= -2\frac{\tilde{D}+\Delta_D}{\Delta^2}\left(1-\cos\frac{2\pi(i-1)}{N}\right)-(\tilde{k}+\Delta_k) \\ &= \tilde{\lambda}_i+\delta_i, \quad i=1,\cdots,N,\end{aligned} \tag{8.18}$$

where

$$\delta_i = -2\frac{\Delta_D}{\Delta^2}\left(1-\cos\frac{2\pi(i-1)}{N}\right)-\Delta_k, \quad i=1,\cdots,N, \tag{8.19}$$

is the uncertainty in the ith eigenvalue. This real parametric uncertainty has a *nonconservative* bound:

$$-M_{\delta_i} \le \delta_i \le M_{\delta_i}, \tag{8.20}$$

where

$$M_{\delta_i} = 2\frac{M_D}{\Delta^2}\left(1-\cos\frac{2\pi(i-1)}{N}\right)+M_k \tag{8.21}$$

and (8.15) implies

$$\tilde{\lambda}_i + M_{\delta_i} < 0. \tag{8.22}$$

Usually bounding a single parameter based on bounds on two uncertain parameters leads to conservatism. No such conservatism occurs in the set description (8.21), due to the linear dependency of the eigenvalues on the uncertain parameters and that the coefficients associated with each perturbation in (8.19) cannot be opposite in sign. This clean result is also enabled by the fact that the real Fourier matrix R that diagonalized the state matrix does not depend on the specific values of the perturbation; that is, R is the correct eigenvector matrix for the entire set of uncertain parameters.

The above expressions motivate the definition of an uncertainty set for the ith subprocess

$$\Pi_i = \left\{ P_i(s) = \frac{1}{s-\tilde{\lambda}_i-\delta_i} : \delta_i \in [-M_{\delta_i}, M_{\delta_i}] \right\}. \tag{8.23}$$

By applying the same steps used to derive (8.13), the nominal finite-dimensional process transfer function $\tilde{P}(s)$ can be written as

$$\tilde{P}(s) = R^T\tilde{\Lambda}(s)R, \tag{8.24}$$

with

$$\tilde{\Lambda}(s) = \text{diag}\left\{\frac{1}{s-\tilde{\lambda}_1}, \cdots, \frac{1}{s-\tilde{\lambda}_N}\right\}, \tag{8.25}$$

and the "true" finite-dimensional process transfer function $P(s)$ as

$$P(s) = R^T \Lambda(s) R, \tag{8.26}$$

with

$$\Lambda(s) = \text{diag}\left\{\frac{1}{s-\tilde{\lambda}_1-\delta_1}, \cdots, \frac{1}{s-\tilde{\lambda}_N-\delta_N}\right\}. \tag{8.27}$$

At first glance, a control engineer may expect some conservatism to occur if the correlations between the perturbations δ_i are not taken into account. Such correlations do not introduce conservatism in this application, as will be seen later in this manuscript.

In the subprocesses where $\cos(2\pi(i-1)/N) \approx 1$ (i.e., i near 1 or near N), the uncertainty in the diffusion coefficient D has almost no effect on its eigenvalue, and the subprocess transfer function $P_i(s)$ is almost independent of the discretization N (see Figure 8.2), and for $i = 1$, the subprocess is totally independent of the diffusion coefficient D:

$$P_1(s) = \frac{1}{s+k}. \tag{8.28}$$

At the other extreme, subprocesses with $\cos(2\pi(i-1)/N) \approx -1$ (i.e., $i \approx N/2$) are largely affected by N and uncertainty in the diffusion coefficient D (e.g., compare the spread of the Bode plots for $N = 10$ and $N = 100$ in Figure 8.2). The subprocess for $i = [N/2] + 1$,[1]

$$P_{[N/2]+1}(s) = \frac{1}{s + 4D/\Delta^2 + k}. \tag{8.29}$$

Therefore, the associated condition number is

$$\begin{aligned}\lim_{|s|\to 0} \kappa(P(s)) &= \lim_{|s|\to 0} \left|\frac{s + 4D/\Delta^2 + k}{s+k}\right| \\ &= \frac{DN^2}{k\pi^2} + 1 \\ &\approx \frac{DN^2}{k\pi^2}, \qquad \text{for large } N,\end{aligned} \tag{8.30}$$

that approaches infinity as $N \to \infty$. Unlike most processes [70], this large condition number does not induce any uncertainties in the decoupling matrix R or the subprocess transfer functions in (8.26)-(8.27), as these operators were derived analytically as a result of process symmetry rather than identified from experimental data. We will see later that, for the feedback controller design in this chapter, these properties of $P(s)$ do *not* result in sensitivity to manipulation inaccuracies, which is very different for other symmetric circulant

[1] $[\cdot]$ is the nearest integer function [79]

processes such as blown film extrusion [69] or for most other processes such as distillation columns [189].

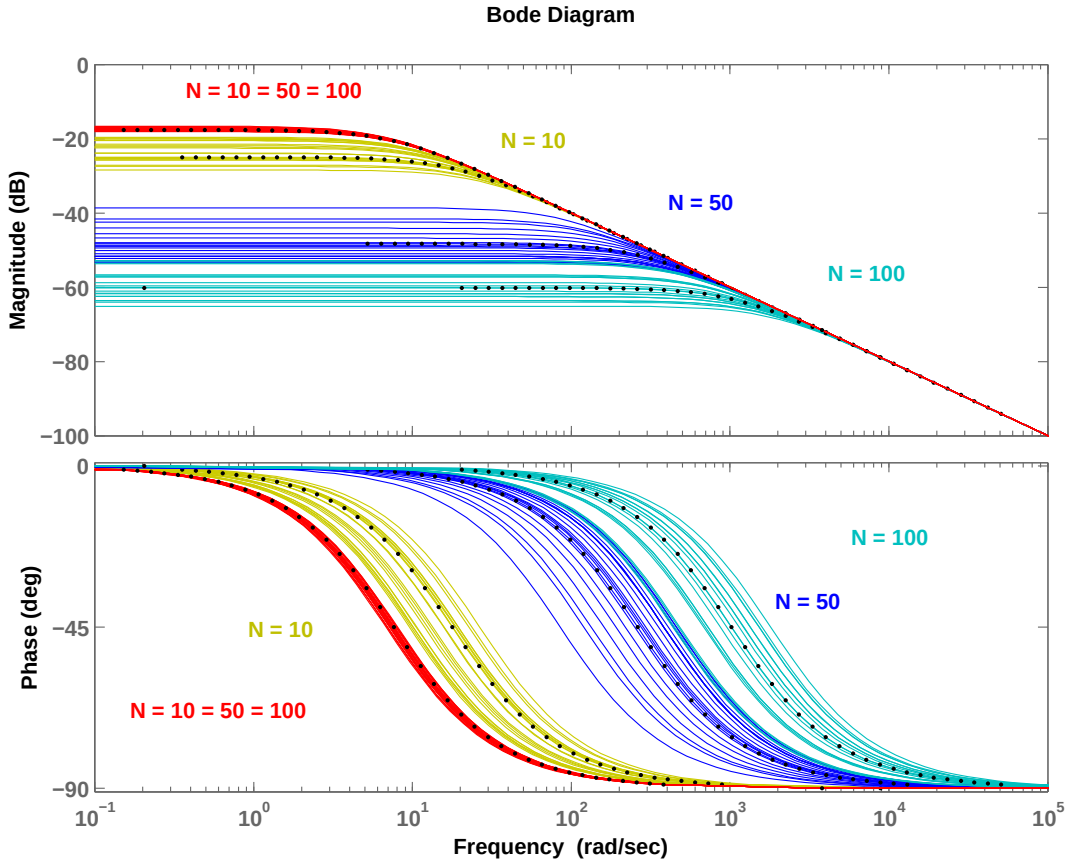

Figure 8.2: Bode magnitude and phase plots for the subprocess $P_1(s)$ (red lines marked with "N = 10 = 50 = 100") are independent of N. Bode magnitude and phase plots for the subprocess $P_{[N/2]+1}(s)$ are strongly dependent on N (mustard, dark blue, and cyan lines). Dots are for the nominal model parameters $\tilde{D} = 1$ and $\tilde{k} = 7.6$, and lines are for the model parameters spanning the full range of allowable perturbations with $M_D = 0.8$ and $M_k = 1$.

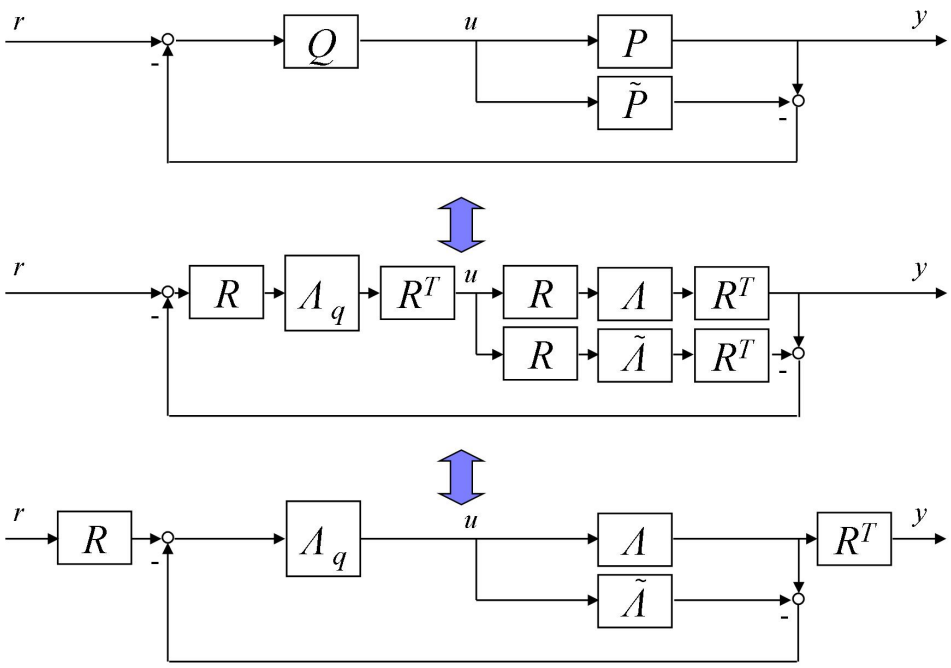

Figure 8.3: Original and diagonalized IMC structures.

8.4 Internal Model Controller Design

8.4.1 Finite-Dimensional Controller Design

When applying the internal model control (IMC) design method to the finite-dimensional process, a single-input single-output IMC controller can be designed independently for each nominal subprocess $\tilde{P}_i(s)$, as only the diagonal matrices will remain inside the IMC structure after rearrangement of the block diagram (see Figure 8.3). Each $\tilde{P}_i(s)$ is a strictly proper first-order stable real-rational transfer function, and the associated controller $Q_i(s)$ is the inverse of $\tilde{P}_i(s)$ augmented with a first-order filter with tuning parameter τ_i:

$$Q_i(s) = \frac{s - \tilde{\lambda}_i}{\tau_i s + 1}, \tag{8.31}$$

where $\tau_i > 0$. Each Q_i is equivalent to a PI controller that has a left-half-plane zero that cancels the left-half-plane pole of $\tilde{P}_i$ [148].

Consider the nominal performance achieved by the multivariable controller

$$Q(s) = R^T \mathrm{diag}\{Q_1(s), \cdots, Q_N(s)\} R = R^T \Lambda_q R. \tag{8.32}$$

As the H_2- and H_∞-norms used to characterize the performance of IMC controllers are invariant to the matrices R and R^T on the outside of the IMC structure in Figure 8.3, the closed-loop nominal performance criterion for the multivariable process can be characterized in terms of the closed-loop nominal performance of the individually controlled subprocesses [93]. Consider the commonly used multivariable closed-loop performance criterion of the H_∞-norm of the weighted sensitivity

$$\|w(1-\tilde{P}Q)\|_\infty < 1 \tag{8.33}$$

with performance weight

$$w(s) = b\frac{as+1}{as} \tag{8.34}$$

where parameters $a > 0$ and $0 < b < 1$ [148]. This criterion specifies zero steady-state offset to step changes in the reference or an output disturbance with a closed-loop bandwidth of $1/a$. If the nominal performance requirement holds for each subprocess i:

$$\begin{aligned}\|w(1-\tilde{P}_iQ_i)\|_\infty &= \left\| b\frac{as+1}{as}\frac{\tau_i s}{\tau_i s+1}\right\|_\infty \\ &= \left\| \frac{b\tau_i}{a}\frac{as+1}{\tau_i s+1}\right\|_\infty < 1\end{aligned} \tag{8.35}$$

then the multivariable system will satisfy the nominal performance criterion (8.33) for the same weight. For a controller with this IMC structure, the nominal performance criterion for the multivariable process is satisfied if and only if all of the controller design parameters τ_i are selected to satisfy $\tau_i < a/b$.

More specifically, an analytical expression for (8.33) is

$$\|w(1-\tilde{P}Q)\|_\infty = \max_i\{b, b\tau_i/a\}, \tag{8.36}$$

which indicates that IMC tuning for nominal performance is *independent* of the eigenvalues of nominal process $\tilde{P}$ and *independent of the spatial resolution* N. If the IMC tuning parameters are all selected for the closed-loop dynamics to be sufficiently fast (i.e., $\tau_i < a, \forall i$), then $\|w(1-\tilde{P}Q)\|_\infty = b$ and the H_∞-norm is not reduced by further reduction in τ_i. If the IMC tuning parameter satisfies nominal performance but has $\tau_i > a$ for any i, then $\|w(1-\tilde{P}Q)\|_\infty = (b/a)\max_i\{\tau_i\}$, which is a linear function of only the largest IMC tuning parameter. The τ_i can be easily tuned for nominal performance of the finite-dimensional system by setting all of the τ_i equal and sufficiently small.

The uncertainty bounds for the parameters in (8.15) can be analytically translated into a frequency-dependent bound on the relative error in the ith subprocess

$$\left|\frac{P_i-\tilde{P}_i}{\tilde{P}_i}\right| = \left|\frac{\delta_i}{s-\tilde{\lambda}_i-\delta_i}\right| \le \left|\frac{M_{\delta_i}}{s-\tilde{\lambda}_i-M_{\delta_i}}\right|, \quad \forall s = j\omega,\ \forall P_i \in \Pi_i, \tag{8.37}$$

which motivates the multiplicative uncertainty weight

$$l_i(s) = \frac{M_{\delta_i}}{s - \tilde{\lambda}_i - M_{\delta_i}}. \tag{8.38}$$

The ith subprocess P_i is stable for all $P_i \in \Pi_i$ provided that

$$\left\| \tilde{P}_i Q_i l_i \right\|_\infty = \left\| \frac{1}{\tau_i s + 1} l_i \right\|_\infty < 1. \tag{8.39}$$

From (8.12)-(8.13), the multivariable process $P(s)$ is robustly stabilized by $Q(s)$ provided that (8.39) holds for all i:

$$\max_i \left\| \frac{1}{\tau_i s + 1} l_i \right\|_\infty < 1. \tag{8.40}$$

An analytical expression can be derived for this robust stability condition:

$$\max_i \left\| \frac{1}{\tau_i s + 1} l_i \right\|_\infty = \max_i \frac{-M_{\delta_i}}{\tilde{\lambda}_i + M_{\delta_i}} < 1, \tag{8.41}$$

which interestingly does not depend on the IMC tuning parameters τ_i. The above inequality is equivalent to

$$\frac{-M_{\delta_i}}{\tilde{\lambda}_i + M_{\delta_i}} < 1, \ \forall i \iff \tilde{\lambda}_i + M_{\delta_i} < -M_{\delta_i}. \tag{8.42}$$

This inequality is conservative for the analysis of robustness to real perturbations in D and k, as it can be shown the robust stability holds for all τ_i, i.e., the closed-loop transfer function for the ith subprocess

$$\frac{P_i Q_i}{1 + Q_i(P_i - \tilde{P}_i)} = \frac{s - \tilde{\lambda}_i}{\tau_i s^2 + (1 - \tau_i \lambda_i)\, s - \tilde{\lambda}_i} \tag{8.43}$$

is stable since both λ_i and $\tilde{\lambda}_i$ are negative. This conservatism of (8.41) is not due to the lack of consideration of correlations in the uncertainties in the eigenvalues of different processes, but is instead modeling the real uncertainty by the complex uncertainty (8.37).[2] The *robust performance* condition for the ith subprocess is

$$\|w(1 - P_i Q_i)\|_\infty < 1, \quad \forall P_i \in \Pi_i, \tag{8.44}$$

[2]Equation (8.40) is a necessary and sufficient condition for analyzing robust stability to multiplicative uncertainties, $P = \tilde{P}(I + \text{diag}\{l_i\}\Delta)$, $\forall \|\Delta\| \leq 1$, see [93, 195].

which is equivalent to

$$|w(1-\tilde{P}_iQ_i)|+|\tilde{P}_iQ_il_i|<1, \quad \forall s=j\omega, \tag{8.45}$$

$$\iff \left|\frac{b\tau_i}{a}\frac{as+1}{\tau_is+1}\right|+\left|\frac{1}{\tau_is+1}\frac{M_{\delta_i}}{s-\tilde{\lambda}_i-M_{\delta_i}}\right|<1, \quad \forall s=j\omega. \tag{8.46}$$

From (8.12)-(8.13), the multivariable process $P(s)$ achieves robust performance provided that (8.46) holds for all i. An analytical expression can be derived for this robust performance condition when $\tau_i > a, \forall i$:

$$\max_i\left\{\frac{b\tau_i}{a}-\frac{M_{\delta_i}}{\tilde{\lambda}_i+M_{\delta_i}}\right\}<1, \tag{8.47}$$

which holds provided each tuning parameter τ_i satisfies

$$\tau_i<\frac{a}{b}\left(1+\frac{M_{\delta_i}}{\tilde{\lambda}_i+M_{\delta_i}}\right). \tag{8.48}$$

If these inequalities and $\tau_i > a, \forall i$ are infeasible for a given a and b, then the implicit inequality (8.46) can be used to determine the τ_i from the Bode magnitude plots of the left-hand side of (8.46) for a range of τ_i for each i. If no feasible solution exists, then a and/or b can be relaxed.

From the unitary-invariance of the H_∞-norm, the multivariable IMC controller with these τ_i satisfies the robust performance criterion for the overall closed-loop system.

8.4.2 Robustness to Joint Real Parametric Uncertainty and Manipulation Inaccuracies

Inaccuracies in the manipulation are modeled by insertion of $I+\hat{w}\hat{\Delta}$ in front of the true plant P in Figure 8.3, where $\hat{w}$ is a scalar transfer function with $|\hat{w}(0)|<1$ that quantifies the magnitude and frequency characteristics of the manipulation inaccuracies and $\hat{\Delta}$ is an unstructured matrix with H_∞-norm less than one (this uncertainty description is known in the robust control literature as multiplicative input uncertainty [148]). This insertion results in the set of closed-loop transfer functions

$$\begin{aligned}
\frac{y}{r} &= \{P(I+\hat{w}\hat{\Delta})(I+Q(P(I+\hat{w}\hat{\Delta})-\tilde{P}))^{-1}Q\} \\
&= \{R^T\Lambda R(I+\hat{w}\hat{\Delta})(I+R^T\Lambda_qR(R^T\Lambda R(I+\hat{w}\hat{\Delta})-R^T\tilde{\Lambda}R))^{-1}R^T\Lambda_qR\} \\
&= \{R^T\Lambda(I+\hat{w}\hat{\Delta})R(R^T(I+\Lambda_q(\Lambda(I+\hat{w}\hat{\Delta})-\tilde{\Lambda}))R)^{-1}\Lambda_qR\} \\
&= \{R^T\Lambda(I+\hat{w}\hat{\Delta})(I+\Lambda_q(\Lambda(I+\hat{w}\hat{\Delta})-\tilde{\Lambda}))^{-1}\Lambda_qR\} \\
&= \{R^T\Lambda(I+\hat{w}\hat{\Delta})(I+\Lambda_q(\Lambda-\tilde{\Lambda})+\hat{w}\Lambda_q\Lambda\hat{\Delta})^{-1}\Lambda_qR\} \\
&= \{R^T\Lambda(I+\hat{w}\hat{\Delta})(I+(I+\hat{w}\Lambda_q(\Lambda-\tilde{\Lambda}))^{-1}\Lambda_q\Lambda\hat{\Delta})^{-1}(I+\Lambda_q(\Lambda-\tilde{\Lambda}))^{-1}\Lambda_qR\},
\end{aligned} \tag{8.49}$$

where the nomenclature $\{\cdot\}$ represent the set of operators obtained for the uncertainty set. The above equivalences exploited that the set of norm-bounded perturbations Δ is set-invariant to multiplication by orthogonal matrices, which allowed $R(I + \hat{w}\hat{\Delta})$ to be replaced by $(I + \hat{w}\hat{\Delta})R$, and that the inverse of $I + \Lambda_q(\Lambda - \tilde{\Lambda})$ exists and is asymptotically stable using similar manipulations as was used to prove that (8.43) is stable.

From the small gain theorem, the closed-loop system is robustly stable for the set of processes with real parametric variation and unmodeled dynamics if and only if

$$\begin{aligned}
&\|(I + \hat{w}\Lambda_q(\Lambda - \tilde{\Lambda}))^{-1}\Lambda_q\Lambda\hat{\Delta}\|_\infty < 1, \quad \forall P_i \in \Pi_i, \quad \|\hat{\Delta}\|_\infty \leq 1 \\
\Leftrightarrow\ &\|\hat{w}(I + \Lambda_q(\Lambda - \tilde{\Lambda}))^{-1}\Lambda_q\Lambda\|_\infty < 1, \quad \forall P_i \in \Pi_i \\
\Leftrightarrow\ &\left\| \frac{Q_i P_i \hat{w}}{1 + Q_i(P_i - \tilde{P}_i)} \right\|_\infty < 1, \quad \forall P_i \in \Pi_i. \\
\Leftrightarrow\ &\left\| \frac{\hat{w}(s - \tilde{\lambda}_i)}{\tau_i s^2 + (1 - \tau_i\lambda_i)\, s - \tilde{\lambda}_i} \right\|_\infty < 1, \quad \forall P_i \in \Pi_i.
\end{aligned} \tag{8.50}$$

This equation can be used to assess the potential sensitivity to manipulation inaccuracies to fine spatial discretization of the PDE. The inequality is trivially satisfied by very large margins for both large s and small s ($|\hat{w}(0)| < 1/10$ for realistic manipulation inaccuracies), and τ_i can be selected to limit the size of the peak in the Bode magnitude plot. The IMC controller results in a closed-loop system that is insensitive to manipulation inaccuracies, even as $N \to \infty$.

The above analysis appears to be the first to exploit algebraic structure while analyzing robustness to both real parametric uncertiainties and unmodeled dynamics for a system with a structured transfer function. Earlier papers considered robustness to real parametric uncertainties [126] *or* robustness to unmodeled dynamics [93, 195].

8.4.3 Infinite-Dimensional Controller Design

Under Assumption 8.2.2, the optimal control for the nominal process can be obtained by replacing C with the reference r in (8.1) with the nominal parameter values and rearranging:

$$u(\theta, t) = \frac{\partial r}{\partial t} - \tilde{D}\frac{\partial^2 r}{\partial \theta^2} + \tilde{k}r, \quad \theta \in [0, 2\pi). \tag{8.51}$$

For the nominal process this $u(\theta, t)$ results in perfect control $C(\theta, t) = r(\theta, t)$, for all $\theta \in [0, 2\pi)$ and $t > 0$ under Assumption 8.2.1.

If a filter of the same form as for the IMC controllers for the subprocesses is augmented to (8.51), the

controller map $Q_\infty : r - e \mapsto u$ is

$$Q_\infty = \left(\frac{\partial}{\partial t} - \tilde{D} \frac{\partial^2}{\partial \theta^2} + \tilde{k} \right) * \frac{e^{-t/\tau(\theta)}}{\tau(\theta)}, \tag{8.52}$$

where $*$ is the convolution operator and

$$e(\theta, t) := (P_\infty - \tilde{P}_\infty) u(\theta, t) \tag{8.53}$$

is the error, where P_∞ and $\tilde{P}_\infty$ are given by (8.1) with true and nominal parameter values, respectively.

The *nominal performance* is similar to the finite-dimensional case,

$$\begin{aligned} \left\| w(1 - \tilde{P}_\infty Q_\infty) \right\|_\infty &= \left\| b \frac{as+1}{as} \left(1 - \frac{1}{\tau(\theta)s + 1} \right) \right\|_\infty \\ &= \left\| \frac{b\tau(\theta)}{a} \frac{as+1}{\tau(\theta)s+1} \right\|_\infty < 1, \end{aligned} \tag{8.54}$$

which holds for all θ if and only if $\tau(\theta) < a/b, \forall \theta$.

By using the Green's function, the transfer function from θ_{in} to θ_{out} is

$$G(\theta_{in}, \theta_{out}, s) = \frac{1}{2\pi} \left[\frac{1}{s+k} + 2 \sum_{n=1}^{\infty} \frac{1}{s + k + n^2 D} \left(\cos n \left(\theta_{in} - \theta_{out} \right) \right) \right], \tag{8.55}$$

where θ_{in} and θ_{out} are input and output spatial locations, respectively.

$$\begin{aligned} \left| \frac{P_\infty - \tilde{P}_\infty}{\tilde{P}_\infty} \right| &= \left| \frac{\dfrac{\tilde{k} - k}{(s+k)(s+\tilde{k})} + 2 \displaystyle\sum_{n=1}^{\infty} \dfrac{\tilde{k} - k + n^2(\tilde{D} - D)}{(s + k + n^2 D)(s + \tilde{k} + n^2 \tilde{D})} \cos n\theta_{in} - \theta_{out})}{\dfrac{1}{s+\tilde{k}} + 2 \displaystyle\sum_{n=1}^{\infty} \dfrac{1}{s + \tilde{k} + n^2 \tilde{D}} \cos n(\theta_{in} - \theta_{out})} \right| \\ &\leq \left| \frac{\dfrac{M_k}{(s + \tilde{k} - M_k)(s + \tilde{k})} + 2 \displaystyle\sum_{n=1}^{\infty} \dfrac{M_k + n^2 M_D}{(s + \tilde{k} - M_k + n^2(\tilde{D} - M_D))(s + \tilde{k} + n^2 \tilde{D})} \cos n(\theta_{in} - \theta_{out})}{\dfrac{1}{s+\tilde{k}} + 2 \displaystyle\sum_{n=1}^{\infty} \dfrac{1}{s + \tilde{k} + n^2 \tilde{D}} \cos n(\theta_{in} - \theta_{out})} \right|, \end{aligned} \tag{8.56}$$

where the last inequality is obtained by inserting $k = \tilde{k} - M_k$ and $D = \tilde{D} - M_D$. This motivates the

multiplicative uncertainty weight

$$l(\theta_{in},\theta_{out},s)=\frac{\dfrac{M_k}{(s+\tilde{k}-M_k)(s+\tilde{k})}+2\displaystyle\sum_{n=1}^{\infty}\frac{M_k+n^2M_D}{(s+\tilde{k}-M_k+n^2(\tilde{D}-M_D))(s+\tilde{k}+n^2\tilde{D})}\cos n(\theta_{in}-\theta_{out})}{\dfrac{1}{s+\tilde{k}}+2\displaystyle\sum_{n=1}^{\infty}\frac{1}{s+\tilde{k}+n^2\tilde{D}}\cos n(\theta_{in}-\theta_{out})}. \tag{8.57}$$

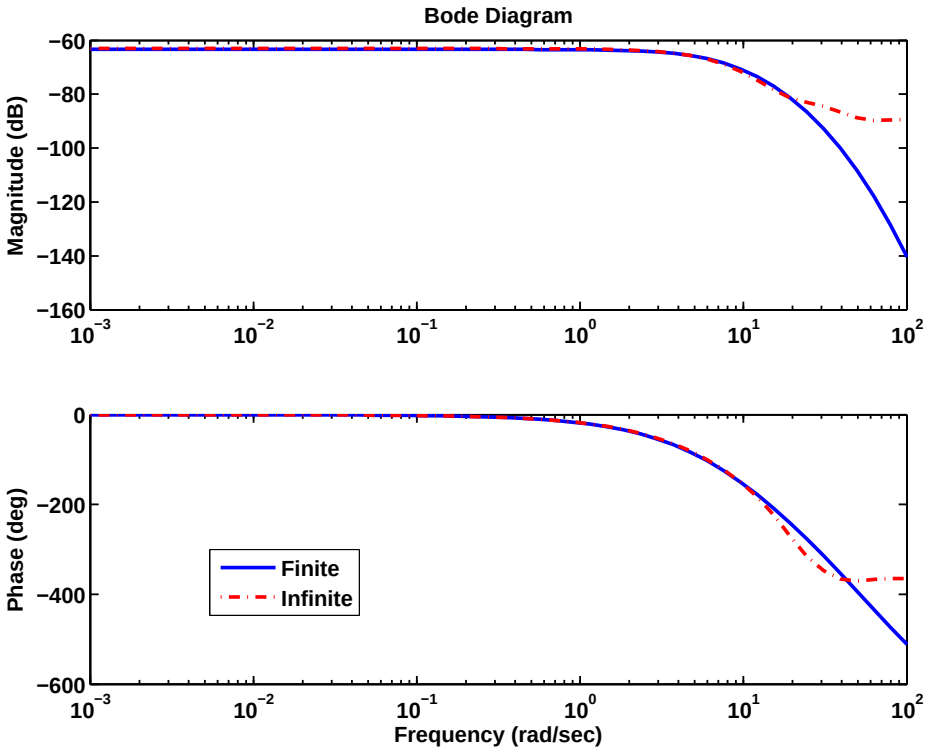

Figure 8.4: Bode plots for the finite- and infinite-dimensional process transfer functions from $2\pi(9/N)$ to $2\pi(2/N)$ of (8.8) and (8.55) with order $N=30$, respectively. Equation (8.55) was multiplied by $2\pi/N$ for normalization.

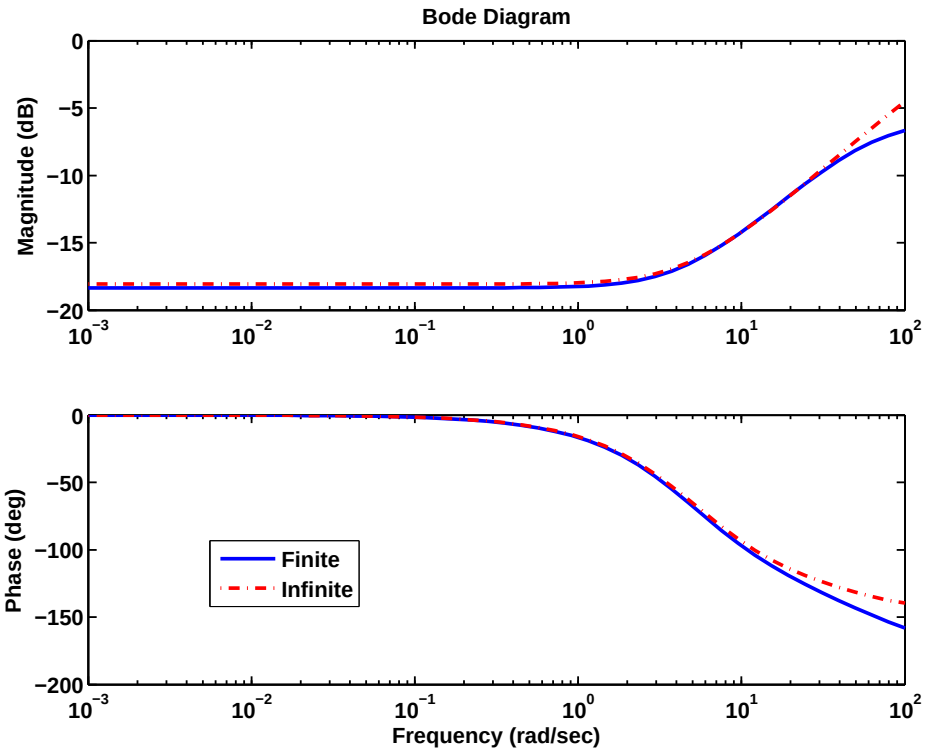

Figure 8.5: Multiplicative uncertainty weight for finite- and infinite- dimensional process transfer functions from $2\pi 9/N$ to $2\pi 2/N$ of (8.38) and (8.57) with order $N = 30$ respectively. (8.38) was pre- and post-multiplied by the Fourier matrix for comparison.

The *robust stability* condition is

$$\left\| \tilde{P}_\infty Q_\infty l(\theta_{in}, \theta_{out}, s) \right\|_\infty < 1, \quad \forall \theta_{in}, \theta_{out}. \tag{8.58}$$

The *robust performance* condition is

$$\left\| w(1 - P_\infty Q_\infty) \right\|_\infty < 1, \quad \forall P_\infty \in \Pi_\infty, \tag{8.59}$$

which is equivalent to

$$\left| w(1 - \tilde{P}_\infty Q_\infty) \right| + \left| \tilde{P}_\infty Q_\infty l(\theta_{in}, \theta_{out}) \right| < 1, \quad \forall \theta_{in}, \theta_{out}, \omega, \theta \in [0, 2\pi), \tag{8.60}$$

$$\iff \left| \frac{b\tau(\theta)}{a} \frac{as+1}{\tau(\theta)+1} \right| + \left| \frac{1}{\tau(\theta)s+1} l(\theta_{in}, \theta_{out}) \right| < 1, \quad \forall \theta_{in}, \theta_{out}, \omega, \theta \in [0, 2\pi). \tag{8.61}$$

8.4.4 Comparison of Early with Late Spatial Discretization for Zero Filtering

From (8.51), the manipulated variables at N spatial locations are

$$u_i(t) = \frac{\partial r_i}{\partial t} - \tilde{D}\frac{\partial^2 r_i}{\partial \theta^2} + \tilde{k} r_i, \quad i = 1, \cdots, N. \tag{8.62}$$

The transfer function for the ODE system obtained by spatial discretization of this equation by second-order central finite differences is

$$\begin{bmatrix} u_1 \\ \vdots \\ u_N \end{bmatrix} = \underbrace{\begin{bmatrix} q_1 & q_2 & 0 & \cdots & 0 & q_2 \\ q_2 & q_1 & q_2 & 0 & \cdots & 0 \\ 0 & q_2 & q_1 & \ddots & \ddots & \vdots \\ \vdots & \ddots & \ddots & \ddots & q_2 & 0 \\ 0 & \cdots & 0 & q_2 & q_1 & q_2 \\ q_2 & 0 & \cdots & 0 & q_2 & q_1 \end{bmatrix}}_{=R\Lambda_q R^T} \begin{bmatrix} r_1 - e_1 \\ \vdots \\ r_N - e_N \end{bmatrix} \tag{8.63}$$

where

$$q_1 = s + 2\tilde{D}\frac{1}{\Delta^2} + \tilde{k}, \quad q_2 = -\tilde{D}\frac{1}{\Delta^2}, \tag{8.64}$$

$$\Lambda_q = \text{diag}\{\lambda_{q1}, \cdots \lambda_{qN}\}, \quad \lambda_{qi} = s - \lambda_i, \tag{8.65}$$

and e_i is (8.53) evaluated at the i spatial position.

With the IMC tuning parameters set to zero, the finite-dimensional approximation of the infinite-dimensional IMC controller Q_∞ produces exactly the same manipulated variable at the N spatial locations as the IMC controller designed from the finite-dimensional approximation of the PDE. These manipulated variable actions converge in the limit $\tau_i, \tau(\theta) \to 0$.

8.4.5 Optimal H_∞-control for the Lumped Approximation

An alternative to the IMC method is to solve the well-known H_∞-mixed sensitivity problem, which is to minimize

$$\|M\|_\infty = \left\| \begin{matrix} w(I - \tilde{P}Q) \\ L\tilde{P}Q \end{matrix} \right\|_\infty, \tag{8.66}$$

over Q, where $L = \text{diag}\{l_1, \cdots, l_N\}$. By inserting $Q = \tilde{P}^{-1}F$, $F = \text{diag}\{F_1, \cdots, F_N\}$, and $F_i = 1/(\tau_i s + 1)$,

$$\min_Q \|M\|_\infty = \min_F \left\| \begin{matrix} w(I-F) \\ LF \end{matrix} \right\|_\infty \tag{8.67}$$

$$= \min_{F_i} \max_i \left\{ \left\| \begin{matrix} w(1-F_i) \\ l_i F_i \end{matrix} \right\|_\infty \right\} \tag{8.68}$$

$$= \min_{\tau_i} \max_i \left\{ \left\| \begin{matrix} b\dfrac{as+1}{as}\left(1 - \dfrac{1}{\tau_i s+1}\right) \\ \dfrac{M_{\delta_i}}{s - \tilde{\lambda}_i - M_{\delta_i}} \dfrac{1}{\tau_i s+1} \end{matrix} \right\|_\infty \right\} \tag{8.69}$$

$$= \min_{\tau_i} \max_i \left\{ \left\| \begin{matrix} \dfrac{b\tau_i}{a}\dfrac{as+1}{\tau_i s+1} \\ \dfrac{M_{\delta_i}}{\left(s - \tilde{\lambda}_i - M_{\delta_i}\right)(\tau_i s+1)} \end{matrix} \right\|_\infty \right\}. \tag{8.70}$$

The IMC filter time constants are particularly simple to optimize if the IMC filter time constants are selected such that $\tau_i \geq a$, $\forall i$, then

$$\|M\|_\infty^2 = \min_{\tau_i \geq a} \max_i \left\{ \sup_\omega \left\{ \left| \frac{b\tau_i}{a} \frac{a\omega j + 1}{\tau_i \omega j + 1} \right|^2 + \left| \frac{M_{\delta_i}}{\left(\omega j - \tilde{\lambda}_i - M_{\delta_i}\right)(\tau_i \omega j + 1)} \right|^2 \right\} \right\} \tag{8.71}$$

$$= \min_{\tau_i \geq a} \max_i \left\{ \sup_\omega \left\{ \left(\frac{b\tau_i}{a}\right)^2 \frac{a^2\omega^2 + 1}{\tau_i^2 \omega^2 + 1} + \frac{M_{\delta_i}^2}{\left(\omega^2 + \left(\tilde{\lambda}_i + M_{\delta_i}\right)^2\right)(\tau_i^2 \omega^2 + 1)} \right\} \right\} \tag{8.72}$$

$$= \min_{\tau_i \geq a} \max_i \left\{ \left(\frac{b}{a}\right)^2 \tau_i^2 + \frac{M_{\delta_i}^2}{\left(\tilde{\lambda}_i + M_{\delta_i}\right)^2} \right\}. \tag{8.73}$$

Regardless of which element achieves the above maximum over i, the minimizing τ_i is achieved by setting its value to the minimum, $\tau_i = a$:

$$\|M\|_\infty^2 = \max_i \left\{ b^2 + \frac{M_{\delta_i}^2}{\left(\tilde{\lambda}_i + M_{\delta_i}\right)^2} \right\} \tag{8.74}$$

$$= b^2 + \max_i \left\{ \frac{M_{\delta_i}^2}{\left(\tilde{\lambda}_i + M_{\delta_i}\right)^2} \right\}. \tag{8.75}$$

If $\tau_i = a$ does not provide adequate closed-loop performance, then some IMC tuning parameters should be selected so that $\tau_i < a$ for some i. An upper bound can be derived:

$$\|M\|_\infty^2 = \min_{\tau_i} \max_i \left\{ \sup_\omega \left\{ \left(\frac{b\tau_i}{a}\right)^2 \frac{a^2\omega^2+1}{\tau_i^2\omega^2+1} + \frac{M_{\delta_i}^2}{\left(\omega^2 + \left(\tilde{\lambda}_i + M_{\delta_i}\right)^2\right)(\tau_i^2\omega^2+1)} \right\} \right\} \tag{8.76}$$

$$\leq \min_{\tau_i} \max_i \left\{ \sup_\omega \left\{ \left(\frac{b\tau_i}{a}\right)^2 \frac{a^2\omega^2+1}{\tau_i^2\omega^2+1} \right\} + \sup_\omega \left\{ \frac{M_{\delta_i}^2}{\left(\omega^2 + \left(\tilde{\lambda}_i + M_{\delta_i}\right)^2\right)(\tau_i^2\omega^2+1)} \right\} \right\} \tag{8.77}$$

$$= \min_{\tau_i} \max_i \left\{ \max\left\{ b^2, \left(\frac{b\tau_i}{a}\right)^2 \right\} + \frac{M_{\delta_i}^2}{\left(\tilde{\lambda}_i + M_{\delta_i}\right)^2} \right\} \tag{8.78}$$

$$= b^2 + \max_i \left\{ \frac{M_{\delta_i}^2}{\left(\tilde{\lambda}_i + M_{\delta_i}\right)^2} \right\}, \tag{8.79}$$

which is the same as the exact solution obtained when the IMC tuning parameters were constrained to satisfy $\tau_i \geq a$, $\forall i$. More generally, the globally optimal $\|M\|_\infty^2$ is usually achieved at an intermediate frequency between $0 < \omega < \infty$. The global optimum can be determined graphically from (8.76). The supremum over ω can be read as the peak of a Bode plot for each i, which can plotted for a range of values for τ_i to determine the optimizing τ_i.

For the second terms of (8.75) and (8.79),

$$\arg\max_i \frac{M_{\delta_i}^2}{\left(\tilde{\lambda}_i + M_{\delta_i}\right)^2} = \arg\max_i \left| \frac{M_{\delta_i}}{\tilde{\lambda}_i + M_{\delta_i}} \right| \tag{8.80}$$

$$= \arg\max_i -\frac{M_{\delta_i}}{\tilde{\lambda}_i + M_{\delta_i}} \tag{8.81}$$

$$= \arg\min_i \frac{M_{\delta_i}}{\tilde{\lambda}_i + M_{\delta_i}}. \tag{8.82}$$

A relatively simple analytical expression for the minimum can be derived for almost all values for the parametric uncertainty:

$$\min_i \frac{M_{\delta_i}}{\tilde{\lambda}_i + M_{\delta_i}} = \min_i \left\{ \frac{2\frac{M_D}{\Delta^2}\left(1 - \cos\frac{2\pi(i-1)}{N}\right) + M_k}{-2\frac{\tilde{D}}{\Delta^2}\left(1 - \cos\frac{2\pi(i-1)}{N}\right) - \tilde{k} + 2\frac{M_D}{\Delta^2}\left(1 - \cos\frac{2\pi(i-1)}{N}\right) + M_k} \right\} \tag{8.83}$$

$$= \begin{cases} \dfrac{M_k}{-\tilde{k} + M_k}, & \text{for } M_k\tilde{D} - M_D\tilde{k} > 0, \quad \text{with } i = 0, \\ \dfrac{4\frac{M_D}{\Delta^2} + M_k}{-4\frac{\tilde{D}}{\Delta^2} - \tilde{k} + 4\frac{M_D}{\Delta^2} + M_k}, & \text{for } M_k\tilde{D} - M_D\tilde{k} < 0, \quad \text{with } i = [N/2] + 1. \end{cases} \tag{8.84}$$

For small Δ, the above expressions simplify to

$$\|M\|_\infty \leq \begin{cases} \sqrt{b^2 + \left(\dfrac{M_k}{\tilde{k} - M_k}\right)^2}, & \text{for } M_k\tilde{D} - M_D\tilde{k} > 0, \quad \text{with } i = 0, \\ \sqrt{b^2 + \left(\dfrac{M_D}{\tilde{D} - M_D}\right)^2}, & \text{for } M_k\tilde{D} - M_D\tilde{k} < 0, \quad \text{with } i = [N/2] + 1, \end{cases} \tag{8.85}$$

with equalities holding for $\tau_i \geq a$, $\forall i$.

8.5 Lyapunov-based Design

8.5.1 Many SISO Controllers

Let the states of the ith subplant P_i be p_i:

$$\frac{dp_i}{dt} = \left(\tilde{\lambda}_i + \delta_i\right) p_i + v_i, \tag{8.86}$$

where v_i is the control trajectory for the ith SISO plant, the reference trajectory for p_i is p_{ri} defined by

$$\frac{dp_{ri}}{dt} = f_i(t) = f_i(t) - \tilde{\lambda}_i p_{ri} + \tilde{\lambda}_i p_{ri}, \tag{8.87}$$

and the error $e_i = p_{ri} - p_i$ is given by

$$\frac{de_i}{dt} = -\tilde{\lambda}_i e_i + f_i(t) - \tilde{\lambda}_i p_{ri} + \delta_i p_i - v_i. \tag{8.88}$$

Select

$$v_i(t) = f_i(t) - \tilde{\lambda}_i p_{ri} + \text{sgn}(e_i)\phi_i(t) + g_i(e_i), \tag{8.89}$$

where $\phi_i(t)$ is chosen so that

$$|\delta_i p_i(t)| \leq M_{\delta_i}|p_i(t)| \leq \phi_i(t), \tag{8.90}$$

and $g_i(e_i)$ is a function satisfying $g_i(e_i)e_i \geq 0$ (can be $g_i(e_i) \equiv 0$) that is specified to achieve a desired speed of convergence. The Lyapunov function

$$V_i = \frac{1}{2}e_i^2, \tag{8.91}$$

$$\begin{aligned}\frac{dV_i}{dt} &= e_i \frac{de_i}{dt} \\ &= e_i \left(-\tilde{\lambda}_i e_i + \delta_i p_i - \text{sgn}(e_i)\phi_i(t) - g_i(e_i)\right) \\ &= -\tilde{\lambda}_i e_i^2 - g_i(e_i)e_i + \underbrace{\left(\delta_i p_i - \text{sgn}(e_i)\phi_i(t)\right) e_i}_{\text{negative}} < 0,\end{aligned} \tag{8.92}$$

implies that the output trajectory is stabilized along the reference trajectory.

8.5.2 Infinite-Dimensional Controller

This section describes the extension of the above Lyapunov-based approach to the original PDE system. Given (8.1) and the reference trajectory $r(\theta, t)$ satisfying

$$\frac{\partial r}{\partial t} = f(\theta, t), \tag{8.93}$$

and the error $e(\theta, t) = r(\theta, t) - C(\theta, t)$, then

$$\begin{aligned}\frac{\partial e}{\partial t} &= f(\theta, t) - D\frac{\partial^2 C}{\partial \theta^2} + kC - u(\theta, t) \\ &= \tilde{D}\frac{\partial^2 e}{\partial \theta^2} - \tilde{k}e + f(\theta, t) - \tilde{D}\frac{\partial^2 r}{\partial \theta^2} + \tilde{k}r - \Delta_D \frac{\partial^2 C}{\partial \theta^2} + \Delta_k C - u(\theta, t).\end{aligned} \tag{8.94}$$

Select the control law as

$$u(\theta, t) = f(\theta, t) - \tilde{D}\frac{\partial^2 r}{\partial \theta^2} + \tilde{k}r + \text{sgn}(e)\phi(\theta, t) + g(e), \tag{8.95}$$

where $\phi(\theta, t)$ is chosen so that

$$\left|\Delta_D \frac{\partial^2 C}{\partial \theta^2} - \Delta_k C\right| \leq M_D \left|\frac{\partial^2 C}{\partial \theta^2}\right| + M_k |C| \leq \phi(\theta, t) \tag{8.96}$$

and $g(e)$ satisfying $g(e)e \geq 0$ (can be $g(e) \equiv 0$) is selected to achieve a desired speed of convergence.

The value for $\phi(\theta, t)$ can be selected by iteration of (8.95) and (8.96), with an initial iteration starting with $e = 0$.

The Lyapunov analysis

$$V(\theta,t) = \frac{1}{2}e^2(\theta,t), \tag{8.97}$$

$$\begin{aligned}\frac{dV}{dt} &= e\left(\tilde{D}\frac{\partial^2 e}{\partial\theta^2} - \tilde{k}e - \Delta_D\frac{\partial^2 C}{\partial\theta^2} + \Delta_k C - \mathrm{sgn}(e)\phi(\theta,t) - g(e)\right)\\ &= e\left(\tilde{D}\frac{\partial^2 e}{\partial\theta^2} - \tilde{k}e\right) - g(e)e + \left(-\Delta_D\frac{\partial^2 C}{\partial\theta^2} + \Delta_k C - \mathrm{sgn}(e)\phi(\theta,t)\right)e < 0.\end{aligned} \tag{8.98}$$

ensures that the output trajectory is stabilized along the reference trajectory.

8.6 Conclusions

IMC was applied to the design of spatial manipulation for a reaction-diffusion process based directly on the PDE and the systems of ODEs obtained by spatial discretization. Analytical expressions were provided for the latter IMC controller, which exploited the algebraic structure of the process and was easy to implement, analyze, and tune. The controllers were simultaneously robust to uncertainties in the model parameters in the PDE and to manipulation inaccuracies, even for arbitrarily fine spatial discretizations. Unlike the vast majority of processes, the large condition number of the transfer function matrix for the finite-dimensional process model did not result in high sensitivities to model uncertainties.

Constraints on the manipulated variable for the designed feedback controllers can be addressed by employing an antiwindup strategy originally developed for web forming processes that prioritizes the control of subprocesses based on their steady-state gain [174]. Sufficient conditions on the PI controller tuning parameters have been derived that ensure the closed-loop system with antiwindup compensation is globally asymptotically stable for the known decoupling matrix R, and the antiwindup compensation has been observed to be nearly globally optimal in simulations [174].

APPENDIX A

MATHEMATICAL BACKGROUND

This appendix provides an overview of mathematical tools repeatedly used in this thesis. This chapter collects material from several books [66, 68, 86, 90, 149, 182, 203].

A.1 Partial Differential Equations

A partial differential equation (PDE) contains one or more partial derivatives of an unknown function of two or more independent variables. The *order* of a PDE is the order of its highest derivative. A PDE is *linear* if

- the dependent variable and each partial derivative appear affinely, and
- the coefficients of the dependent variable and the coefficients of each partial derivative are constants or algebraic functions of the independent variables.

A PDE that is not linear is *nonlinear*. A PDE is *quasi-linear* if it is linear in its highest order derivative terms.

A general second-order linear PDE with two independent variables:

$$a(x,t)\frac{\partial^2 C}{\partial x^2} + b(x,t)\frac{\partial^2 C}{\partial x \partial t} + c(x,t)\frac{\partial^2 C}{\partial t^2} + d(x,t)\frac{\partial C}{\partial x} + e(x,t)\frac{\partial C}{\partial t} + f(x,t)C + g = 0 \tag{A.1}$$

is classified by discriminant, $b^2 - 4ac$, at each point (x,t):

- Elliptic: $b^2 - 4ac < 0$
  describes a dissipative physical process with two spatial dimensions that is at steady-state (in which case the variable t is a spatial variable rather than time)

- Parabolic: $b^2 - 4ac = 0$

  describes the temporal evolution of a dissipative physical process with one spatial dimension

- Hyperbolic: $b^2 - 4ac > 0$

  describes a nondissipative physical process in one spatial dimension

A PDE of one type for the entire domain is said to be of that type; otherwise the PDE is said to be of *mixed type*. Most chapters in this thesis consider linear second-order parabolic PDEs, with the Internal Model Control chapter applying to time-dependent PDEs of any type or order.

If the domain of the PDE is finite, then boundary conditions are required for the solution of the PDE to be well-defined:

- A *Dirichlet condition* has a fixed value on the boundary:

$$C \text{ given}, \quad \text{on } \partial\Omega. \tag{A.2}$$

- A *homogeneous Dirichlet condition* has zero on the boundary:

$$C = 0, \quad \text{on } \partial\Omega. \tag{A.3}$$

- A *Neumann condition* has the first-order spatial derivative specified:

$$\frac{\partial C}{\partial x} \text{ given}, \quad \text{on } \partial\Omega, \tag{A.4}$$

  which specifies the flux on the boundary. The *insulating* boundary condition has zero derivative on the boundary.

- A *Robin condition* is a linear combination of the Dirichlet and Neumann boundary conditions, for example,

$$\frac{\partial C}{\partial x} = hC, \quad \text{on } \partial\Omega \tag{A.5}$$

  appears in many mass and heat transfer applications.

A.2 Transfer functions for PDEs

An expression for the transfer function can be obtained by applying the Laplace transform with respect to time to PDEs.

Definition A.2.1. *For any* $u \in L^1(\mathbb{R}_+)$,[1] *its* Laplace transform $\mathcal{L}u = \hat{u}$ *is*

$$\hat{u}(s) := \int_0^\infty e^{-st} u(t) dt, \quad s \geq 0. \tag{A.6}$$

The space variables are treated as fixed when applying the Laplace transform with respect to time to a PDE with time variable defined on the domain $0 < t < \infty$. Throughout this thesis, it is assumed that the second-order partial derivatives with respect to the spatial variables and the Laplace integral with respect to time are well defined for all values of spatial variables, so that differentiation and integration can be interchanged.

Example

Consider the diffusion equation in one spatial dimension (Figure A.1)

$$\frac{\partial C}{\partial t} = \frac{\partial^2 C}{\partial x^2}, \quad \forall x \in (0,1), \quad \forall t > 0, \tag{A.7}$$

with initial and boundary conditions

$$C(x,0) = 0, \tag{A.8}$$

$$C(0,t) = 0, \tag{A.9}$$

$$C(1,t) = u(t), \tag{A.10}$$

where

- C: dependent variable, depends on x and t
- t: independent temporal variable,
- x: independent spatial variable.

This PDE is *first order* in time since the highest order partial derivative in t is first order, and *second order* in space since the highest order partial derivative in x is second order.

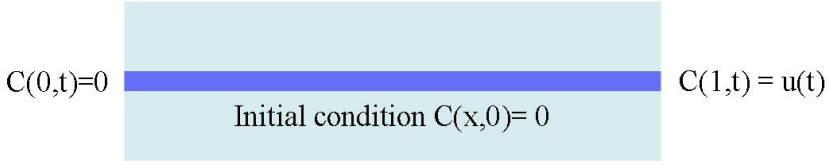

Figure A.1: Diffusion with a homogeneous Dirichlet condition at $x = 0$ and a time-varying Dirichlet condition at $x = 1$.

[1] $\mathbb{R}_+ = (0, \infty)$

With the initial condition (IC) (A.8), the Laplace transform with respect to time of the left-hand side of (A.7) is

$$\begin{aligned}\mathcal{L}\left\{\frac{\partial C}{\partial t}\right\} &= \int_0^\infty e^{-st}\frac{\partial C}{\partial t}(x,t)dt \\ &= s\int_0^\infty e^{-st}C(x,t)dt + e^{-st}C(x,t)\Big|_{t=0}^{t=\infty} \\ &= s\hat{C}(x,s),\end{aligned} \tag{A.11}$$

by application of integration by parts. The Laplace transform of the right-hand side of (A.7) is

$$\begin{aligned}\mathcal{L}\left\{\frac{\partial^2 C}{\partial x^2}\right\} &= \int_0^\infty e^{-st}\frac{\partial^2 C}{\partial x^2}(x,t)dt \\ &= \frac{d^2}{dx^2}\int_0^\infty e^{-st}C(x,t)dt \\ &= \frac{d^2}{dx^2}\hat{C}(x,s).\end{aligned} \tag{A.12}$$

The Laplace transform of the PDE (A.7) is

$$s\hat{C}(x,s) = \frac{d^2}{dx^2}\hat{C}(x,s). \tag{A.13}$$

Similarly, the Laplace transforms

$$\mathcal{L}\{C(0,t)\} = \int_0^\infty e^{-st}C(0,t)dt = \hat{C}(0,s) \tag{A.14}$$

and

$$\mathcal{L}\{0\} = \int_0^\infty e^{-st}0dt = 0 \tag{A.15}$$

imply that the Laplace transform of the boundary condition (BC) (A.9) is

$$\hat{C}(0,s) = 0. \tag{A.16}$$

The Laplace transforms

$$\mathcal{L}\{C(1,t)\} = \int_0^\infty e^{-st}C(1,t)dt = \hat{C}(1,s) \tag{A.17}$$

and

$$\mathcal{L}\{u(t)\} = \int_0^\infty e^{-st}u(t)dt = \hat{u}(s) \tag{A.18}$$

imply that the Laplace transform of the BC (A.10) is

$$\hat{C}(1,s) = \hat{u}(s). \tag{A.19}$$

The input-output relation of this diffusive system can be obtained from analytical solution of the second-order ordinary differential equation (A.13) with the BCs (A.16) and (A.19). From (A.13), the characteristic equation is

$$\lambda^2 - s = 0, \tag{A.20}$$

which has zeros $\lambda = \pm\sqrt{s}$. The solution is of the form of

$$\hat{C}(x,s) = Ae^{\sqrt{s}x} + Be^{-\sqrt{s}x}. \tag{A.21}$$

The BCs (A.16) and (A.19) imply

$$\hat{C}(0,s) = A + B = 0, \tag{A.22}$$

and

$$\hat{C}(1,s) = Ae^{\sqrt{s}} + Be^{-\sqrt{s}} = \hat{u}(s), \tag{A.23}$$

respectively. Solving (A.22) and (A.9) for A and B gives

$$A = \frac{1}{e^{\sqrt{s}} - e^{-\sqrt{s}}}\hat{u}(s), \tag{A.24}$$

$$B = -\frac{1}{e^{\sqrt{s}} - e^{-\sqrt{s}}}\hat{u}(s). \tag{A.25}$$

Hence the solution to the ordinary differential equation (ODE) (A.13) is

$$\begin{aligned}\hat{C}(x,s) &= \frac{e^{\sqrt{s}x} - e^{-\sqrt{s}x}}{e^{\sqrt{s}} - e^{-\sqrt{s}}}\hat{u}(s) \\ &= \frac{\sinh(\sqrt{s}x)}{\sinh(\sqrt{s})}\hat{u}(s).\end{aligned} \tag{A.26}$$

This implies that the transfer function $G(x,s)$ from $u(t)$ to $C(x,t)$ is

$$G(x,s) = \frac{\sinh(\sqrt{s}x)}{\sinh(\sqrt{s})}. \tag{A.27}$$

The Laplace transform with respect to time can be interpreted as "projecting" the xt plane onto the

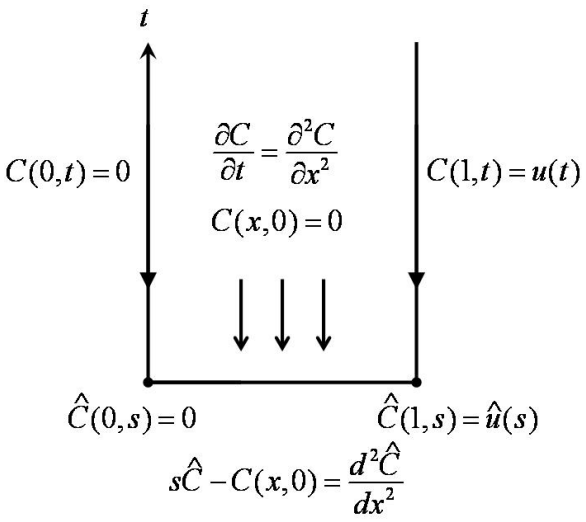

Figure A.2: Laplace transforms for the PDE.

x axis,[2] with coefficients parameterized by s, and the original PDE, IC, and BCs transformed into a new differential equation and BCs (Figure A.2). In this thesis, the " ˆ " denoting the Laplace transform is sometimes dropped when clear from the context.

Another approach is to seek a solution of the form $C(x,t) = e^{st}C_0(x)$ with the input $u(t) = e^{st}$, which leads to the same ODE and the same solution [210]. The transfer function for infinite-dimensional systems is surveyed in [48] and discussed deeply in [210].

A.3 Spatial Discretization and the Method of Lines

The finite-difference method replaces all of the derivatives with algebraic approximations to produce a system of algebraic equations. For simulation and control design purposes, it is more convenient to approximate only the spatial derivatives of a time-dependent PDE, to produce a system of ODEs. This approach is often called the "*method of lines*" (MOL).

Once a process model in the form of a PDE or system of PDEs is approximated by a system of ODEs, many existing control theory and tools can be applied (e.g., linear quadratic gaussian control, H_∞-optimal control, model predictive control, differential geometric methods, μ-optimal control). In most applications, these control systems will provide good performance when applied to the original PDE.[3]

[2]This "projection" should not be confused with projection as defined in matrix theory.

[3]This approach does not work for some applications, which has motivated the development of alternative approaches such as described in the chapter on Internal Model Control.

Example

Consider the same diffusive process equation in the previous section:

$$\frac{\partial C}{\partial t} = \frac{\partial^2 C}{\partial x^2}, \quad \forall x \in (0,1), \quad \forall t > 0, \tag{A.28}$$

with initial and boundary conditions

$$C(x,0) = 0, \tag{A.29}$$

$$C(0,t) = 0, \tag{A.30}$$

$$C(1,t) = u(t). \tag{A.31}$$

Introduce spatial mesh points $x_i = i\Delta x$, $i = 0, \cdots, N$, where $\Delta x = 1/N$, and replace the spatial second-order derivative with the finite-difference approximation

$$\left.\frac{\partial^2 C}{\partial x^2}\right|_{x=x_i} \approx \frac{C_{i+1} - 2C_i + C_{i-1}}{(\Delta x)^2}, \tag{A.32}$$

where

$$C_i(t) \approx C(x_i, t). \tag{A.33}$$

Substituting (A.32) into (A.28) results in the set of ODEs:

$$\frac{dC_i}{dt} = \frac{C_{i+1} - 2C_i + C_{i-1}}{(\Delta x)^2}, \quad i = 1, \cdots, N-1, \tag{A.34}$$

with

$$C_0(t) = 0, \tag{A.35}$$

and

$$C_N(t) = u(t). \tag{A.36}$$

The system of ODEs can be written as a matrix form:

$$\frac{d}{dt}\begin{bmatrix} C_1 \\ C_2 \\ \vdots \\ C_{N-1} \end{bmatrix} = \frac{1}{(\Delta x)^2}\begin{bmatrix} -2 & 1 & 0 & \cdots & 0 \\ 1 & -2 & 1 & \ddots & \vdots \\ 0 & \ddots & \ddots & \ddots & 0 \\ \vdots & \ddots & 1 & -2 & 1 \\ 0 & \cdots & 0 & 1 & -2 \end{bmatrix} + \frac{1}{(\Delta x)^2}\begin{bmatrix} 0 \\ 0 \\ \vdots \\ 0 \\ 1 \end{bmatrix} u(t). \tag{A.37}$$

The transfer function $G(x_i, s)$ from $u(t)$ to $C(x_i, t)$ is

$$G(x_i, s) = C(sI - A)^{-1}B, \tag{A.38}$$

where

$$A = \frac{1}{(\Delta x)^2}\begin{bmatrix} -2 & 1 & 0 & \cdots & 0 \\ 1 & -2 & 1 & \ddots & \vdots \\ 0 & \ddots & \ddots & \ddots & 0 \\ \vdots & \ddots & 1 & -2 & 1 \\ 0 & \cdots & 0 & 1 & -2 \end{bmatrix}, \quad B = \frac{1}{(\Delta x)^2}\begin{bmatrix} 0 \\ 0 \\ \vdots \\ 1 \end{bmatrix}, \tag{A.39}$$

$$C = \begin{bmatrix} 0 & \cdots & 0 & \underbrace{1}_{i\text{th element}} & 0 & \cdots & 0 \end{bmatrix}. \tag{A.40}$$

Alternative methods such as spectral decomposition and finite-element methods convert a PDE into a system of ODEs by using different basis functions.

REFERENCES

[1] J. Anthonis and H. Ramon. Linear mechanical systems and dyadic transfer function matrices. *Automatica*, 39:1353–1363, 2003.

[2] A. C. Antoulas. *Approximation of Large-scale Dynamical Systems.* Cambridge University Press, Cambridge, MA, 2005.

[3] J. G. Van Antwerp and R. D. Braatz. Model predictive control of large scale processes. *J. of Process Control*, 10:1–8, 2000.

[4] R. Aris. On the dispersion of a solute in a fluid flowing through a tube. *Proc. R. Soc. London, Ser. A*, 235:67–77, 1956.

[5] R. Aris. On the dispersion of linear kinematic waves. *Proc. R. Soc. London A*, 245:268–277, 1958.

[6] S. A. Avdonin and I. Avdonin. *Families of Exponentials: The Method of Moments in Controllability Problems for Distributed Parameter Systems.* Cambridge University Press, New York, 1995.

[7] G. Balas, R. Chiang, A. Packard, and M. Safonov. *Robust Control Toolbox User's Guide.* The MathWorks, Inc., Natick, MA, 2008.

[8] G. Balas, R. Chiang, A. Packard, and M. Safonov. *Robust Control Toolbox 3: User's Guide.* The Mathworks, Inc., Natick, MA, 2010. Release 2010a.

[9] B. Bamieh, F. Paganini, and M. A. Dahleh. Distributed control of spatially invariant systems. *IEEE Trans. on Automatic Control*, 47:1091–1107, 2002.

[10] R. A. Bartlett, L. T. Biegler, J. Backstrom, and V. Gopal. Quadratic programming algorithms for large-scale model predictive control. *J. of Process Control*, 12:775–795, 2002.

[11] R. Beals. *Analysis: An Introduction.* Cambridge University Press, New York, 2004.

[12] R. W. Beard, G. N. Saridis, and J. T. Wen. Galerkin approximations of the generalized Hamilton-Jacobi-Bellman equation. *Automatica*, 33:2159–2177, 1997.

[13] C. E. Beaty and W. M. Saltzman. Controlled growth-factor delivery induces differential neurite outgrowth in 3-dimensional cell-cultures. *J. of Controlled Release*, 24:15–23, 1993.

[14] A. Bemporad, M. Morari, and N. L. Ricker. *Model Predictive Control Toolbox for Use with MATLAB: User's Guide.* The Mathworks Inc, Natick, MA, 2004.

[15] A. Bensoussan, G. Da Prato, M. C. Delfour, and S. K. Mitter. *Representation and Control of Infinite Dimensional Systems.* Birkhauser, Boston, 2nd edition, 2007.

[16] C. Berkland, A. Cox, K. Kim, and D. W. Pack. Three-month, zero-order piroxicam release from monodispersed double-walled microspheres of controlled shell thickness. *J. of Biomedical Materials Research Part A*, 70A:576–584, 2004.

[17] C. Berkland, M. King, A. Cox, K. Kim, and D. W. Pack. Precise control of PLG microsphere size provides enhanced control of drug release rate. *J. of Controlled Release*, 82:137–147, 2002.

[18] C. Berkland, M. Kipper, B. Narasimhan, K. Kim, and D. W. Pack. Microsphere size, precipitation kinetics and drug distribution control drug release from biodegradable polyanhydride microspheres. *J. of Controlled Release*, 94:129–141, 2004.

[19] C. Berkland, E. Pollauf, D. W. Pack, and K. Kim. Uniform double-walled polymer microspheres of controllable shell thickness. *J. of Controlled Release*, 96:101–111, 2004.

[20] D. P. Bertsekas. *Dynamic Programming and Optimal Control*, volume I. Athena Scientific, Belmont, MA, second edition, 2001.

[21] J. T. Betts, S. L. Campbell, and A. Engelsone. Direct transcription of optimal control problems with high order state constraints: Theory vs. practice. *Optim. Eng.*, 8:1–19, 2007.

[22] P. Bianco and P. G. Robey. Stem cells in tissue engineering. *Nature*, 414(6859):118–121, 2001.

[23] M. Blatt and K. Schittkowski. Optimal control of one-dimensional partial differential algebraic equations with applications. *Annals of Operations Research*, 98:45–64, 2000.

[24] L. G. Bleris and M. V. Kothare. Reduced order distributed boundary control of thermal transients in microsystems. *IEEE Trans. on Control Systems Technology*, 13:853–867, 2005.

[25] D. M. Boskovic, M. Krstic, and W. J. Liu. Boundary control of an unstable heat equation via measurement of domain-averaged temperature. *IEEE Trans. on Auto. Control*, 46:2022–2028, 2001.

[26] S. Boyd, L. El Ghaoul, E. Feron, and V. Balakrishnan. *Linear Matrix Inequalities in System and Control Theory*. SIAM Press, Philadelphia, PA, 1997.

[27] R. D. Braatz. Advanced control of crystallization processes. *Annual Reviews in Control*, 26:87–99, 2002.

[28] R. D. Braatz and E. L. Russell. Robustness margin computation for large scale systems. *Comp. & Chem. Eng.*, 23:1021–1030, 1999.

[29] R. D. Braatz, P. M. Young, J. C. Doyle, and M. Morari. Computational complexity of μ calculation. *IEEE Transactions on Automatic Control*, 39:1000–1002, 1994.

[30] R. W. Brockett and J. L. Willems. Discretized partial differential equations: Examples of control systems defined on modules. *Automatica*, 10:507–515, 1974.

[31] J. A. Burns and B. B. King. Optimal sensor location for robust control of distributed parametersystems. In *Proc. of IEEE Conference on Decision and Control*, pages 3967–3972, Lake Buena Vista, FL, 1994.

[32] A. G. Butkovsky and A. J. Lerner. Optimal control systems with distributed parameters. *Autom. Remote Control*, 21:472–477, 1960.

[33] A.G. Butkovsky. *Distributed Control System*. Elsevier, Amsterdam, 1969.

[34] M. E. Byrne and V. Salian. Molecular imprinting within hydrogels II: Progress and analysis of the field. *Int. J. of Pharmaceutics*, 364:188–212, 2008.

[35] G. C. Calafiore, F. Dabbene, and R. Tempo. Randomized algorithms for probabilistic robustness with real and complex structured uncertainty. *IEEE Trans. Automat. Contr.*, 45:2218–2235, 2000.

[36] F. M. Callier and C. A. Desoer. Stabilization, tracking and disturbance rejection in multivariable convolution systems. *Memorandum*, UCB/ERL:1–55, 1978.

[37] M. Cannon, W. Liao, and B. Kouvaritakis. Efficient MPC optimization using Pontryagin's minimum principle. *Int. J. of Robust & Nonlinear Control*, 18:831–844, 2008.

[38] L. Cao and D. J. Mooney. Spatiotemporal control over growth factor signaling for therapeutic neovascularization. *Advanced Drug Delivery Reviews*, 59:1340–1350, 2007.

[39] E. Casas and J. P. Raymond. Error estimates for the numerical approximation of Dirichlet boundary control for semilinear elliptic equations. *SIAM J. on Control & Optimization*, 45:1586–1611, 2006.

[40] M. Cereijido and C. A. Rotunno. *Introduction to the Study of Biological Membranes*. Gordon and Breach Science Publishers, New York, 1970.

[41] G. Chan and D. J. Mooney. New materials for tissue engineering: Towards greater control over the biological response. *Trends in Biotechnology*, 28:382–392, 2008.

[42] S. P. Chaudhuri. Optimal control computational techniques for a class of nonlinear distributed parameter systems. In *Proc. of the IEEE Conf. on Decision and Control*, pages 617–621, 1971. vol.10.

[43] J. Chen, M. K. H. Fan, and C. N. Nett. Structured singular values and stability analysis of uncertain polynomials. Part 1: The generalized mu. *Systems & Control Letters*, 23:53–65, 1994.

[44] M. J. Chen and C. A. Desoer. Necessary and sufficient conditions for robust stability of linear distributed feedback systems. *Int. J. Control*, 35:255–267, 1982.

[45] R. R. Chen and D. J. Mooney. Polymeric growth factor delivery strategies for tissue engineering. *Pharmaceutical Research*, 20:1103–1112, 2003.

[46] M. S. Chiu, S. Cui, and Q. G. Wang. Internal model control design for transition control. *AIChE J.*, 46:309–320, 2000.

[47] L. G. Cima and M. J. Cima. Tissue regeneration matrices by solid free form fabrication techniques, 1996. U.S. Patent #5,518,680.

[48] R. Curtain and K. Morris. Transfer functions of distributed parameter systems: A tutorial. *Automatica*, 45:1101–1116, 2009.

[49] R. F. Curtain and H. Zwart. *An Introduction to Infinite-dimensional Linear Systems Theory*. Springer, New York, 1995.

[50] E. L. Cussler. *Diffusion*. Cambridge University Press, U.K., second edition, 1997.

[51] G. V. Cybenko. Approximation by superpositions of a sigmoidal function. *Mathematics of Control, Signals & Systems*, 2(4):303–314, 1989.

[52] M. Dadvara and M. Sahimi. Pore network model of deactivation of immobilized glucose isomerase in packed-bed reactors. Part III: Multiscale modelling. *Chem. Eng. Sci.*, 58:4935–4951, 2003.

[53] R. D'Andrea and G. E. Dullerud. Distributed control design for spatially interconnected systems. *IEEE Trans. on Automatic Control*, 48:1478–1495, 2003.

[54] Abraham de Moivre. *The Doctrine of Chances*. H. Woodfall, London, 2nd edition, 1738.

[55] M. S. de Queiroz, D. M. Dawson, S. P. Nagarkatti, and F. Zhang. *Lyapunov-based control of mechanical systems*. Birkhauser, Cambridge, MA, first edition, 2000.

[56] W. M. Deen. *Analysis of Transport Phenomena*. Oxford University Press, Oxford, UK, 1998.

[57] C. A. Desoer and Y. T. Wang. On the generalized nyquist stability criterion. *IEEE Trans. on Automatic Control*, 25:187–196, 1980.

[58] D. E. Discher, D. J. Mooney, and P. W. Zandstra. Growth factors, matrices, and forces combine and control stem cells. *Science*, 324(5935):1673–1678, 2009.

[59] J. C. Doyle, B. A. Francis, and A. R. Tannenbaum. *Feedback Control Theory*. MacMillan, New York, 1992.

[60] G. E. Dullerud and F. Paganini. *A Course in Robust Control Theory*. Springer, New York, 2000.

[61] S. R. Duncan and G. F. Bryant. The spatial bandwidth of cross-directional control systems for web processes. *Automatica*, 33:139–153, 1997.

[62] S. R. Duncan, W. P. Heath, A. Halouskova, and M. Karny. Application of basis functions to the cross-directional control of web processes. In *Proc. of the UKACC Int. Conf. on Control '96*, pages 1278–1283, Stevenage, England, 1996. IEE.

[63] J. W. Eaton and J. B. Rawlings. Feedback-control of chemical processes using online optimization techniques. *Comp. & Chem. Eng.*, 14:469–479, 1990.

[64] C. G. Economou, M. Morari, and B. O. Palsson. Internal model control. 5. Extension to nonlinear systems. *Ind. Eng. Chem. Process Des. Dev.*, 25:403–411, 1986.

[65] G. Elnagar, M. A. Kazemi, and M. Razzaghi. The pseudospectral Legendre method for discretizing optimal-control problems. *IEEE Trans. on Automatic Control*, 40:1793–1796, 1995.

[66] L. C. Evans. *Partial Differential Equations*. American Mathematical Society, Providence, RI, 2010.

[67] J. Fan, G. E. Stewart, and G. A. Dumont. Two-dimensional frequency analysis for unconstrained model predictive control of cross-directional processes. *Automatica*, 40:1891–1903, 2004.

[68] S. J. Farlow. *Partial Differential Equations for Scientists and Engineers*. Dover Publications Inc., Mineola, NY, 1993.

[69] A. P. Featherstone and R. D. Braatz. Control-oriented modeling of sheet and film processes. *AIChE J.*, 43:1989–2001, 1997.

[70] A. P. Featherstone and R. D. Braatz. Integrated robust identification and control of large-scale processes. *Ind. Eng. Chem. Res.*, 37:97–106, 1998.

[71] A. P. Featherstone, J. G. VanAntwerp, and R. D. Braatz. *Identification and Control of Sheet and Film Processes*. Springer Verlag, London, 2000.

[72] G. Ferreres and V. Fromion. Computation of the robustness margin with the skewed μ tool. *Systems & Control Letters*, 32(4):193–202, 1997.

[73] C. Fischbach and D. J. Mooney. Polymers for pro- and anti-angiogenic therapy. *Biomaterials*, 28:2069–2076, 2007.

[74] N. Flyer and P. N. Swarztrauber. The convergence of spectral and finite difference methods for initial-boundary value problems. *SIAM J. on Scientific Computing*, 23:1731–1751, 2002.

[75] Joseph Fourier. *Théorie Analytique de la Chaleur*. Académie des Sciences, Paris, France, 1822.

[76] B. A. Francis and W. M. Wonham. The internal model principle for linear multivariable regulators. *Applied Mathematics & Optimization*, 2:170–194, 1975.

[77] A. V. Fursikov. Stabilization for the 3D Navier-Stokes system by feedback boundary control. *Discrete and Continuous Dynamical Systems*, 10:289–314, 2004.

[78] C. E. Garcia and M. Morari. Internal model control. 1. A unifying review and some new results. *Ind. Eng. Chem. Process Des. Dev.*, 21:308–323, 1982.

[79] L. J. Gerstein. *Introduction to mathematical structures and proofs*. Springer, New York, 1996.

[80] J. W. Gibbs. Fourier's series. *Nature*, 59:200, 1898.

[81] W. L. Goffe. SIMANN. http://www.netlib.org/opt/simann.f.

[82] C. J. Goh and K. L. Teo. Control parametrization - A unified approach to optimal-control problems with general constraints. *Automatica*, 24:3–18, 1988.

[83] Q. Gong, W. Kang, and I. M. Ross. A pseudospectral method for the optimal control of constrained feedback linearizable systems. *IEEE Trans. on Automatic Control*, 51:1115–1129, 2006.

[84] A. Guessoum and R. M. Mersereau. Fast algorithms for the multidimensional discrete Fourier-transform. *IEEE Trans. on Acoustics Speech and Signal Processing*, 34:937–943, 1986.

[85] R. Gunawan, D. L. Ma, M. Fujiwara, and R. D. Braatz. Identification of kinetic parameters in a multidimensional crystallization process. *Int. J. of Modern Physics B*, 16:367–374, 2002.

[86] R. Haberman. *Applied Partial Differential Equations*. Prentice Hall, Upper Saddle River, NJ, 2003.

[87] T. Hämäläinen and S. Pohjolainen. A finite-dimensional robust controller for systems in the CD-algebra. *IEEE Trans. on Automatic Control*, 45:421–431, 2000.

[88] J. W. Hargrove. Optimized simulation of the control of tsetse flies Glossina pallidipes and G-m. morsitans (Diptera: Glossinidae) using odour-baited targets in Zimbabwe. *Bulletin of Entomological Research*, 93:19–29, 2003.

[89] L. Harnefors and H. P. Nee. Model-based current control of AC machines using the internal model control method. *IEEE Trans. on Industry Applications*, 34:133–141, 1998.

[90] M. T. Heath. *Scientific Computing*. McGraw-Hill, New York, 2002.

[91] C. M. Ho and Y.C. Tai. Review: MEMS and its applications for flow control. *ASME J. of Fluid Engineering*, 118:437–447, 1996.

[92] R. Horowitz and P. Varaiya. Control design of an automated highway system. *Proc. of the IEEE*, 88:913–925, 2000.

[93] M. Hovd, R. D. Braatz, and S. Skogestad. SVD controllers for H_2-, H_∞- and μ-optimal control. *Automatica*, 33:433–439, 1997.

[94] M. Hovd and S. Skogestad. Control of symmetrically interconnected plants. *Automatica*, 30:957–973, 1994.

[95] H. P. Hua. Numerical solution of optimal control problems. *Optimal Control Applications & Methods*, 21:233–241, 2000.

[96] H. M. Hulburt and S. Katz. Some problems in particle technology. *Chem. Eng. Sci.*, 19:555–574, 1964.

[97] E. Immonen. On the internal model structure for infinite-dimensional systems: Two common controller types and repetitive control. *SIAM J. on Control and Optmization*, 45:2065–2093, 2007.

[98] E. Immonen. Practical output regulation for bounded linear infinite-dimensional state space systems. *Automatica*, 43:786–794, 2007.

[99] E. Immonen and S. Pohjolainen. Feedback and feedforward output regulation of bounded unifomly continuous signals for infinite-dimensional systems. *SIAM J. on Control and Optimization*, 45:1714–1735, 2006.

[100] M. R. Jovanovic and B. Bamieh. Lyapunov-based distributed control of systems on lattices. *IEEE Trans. on Automatic Control*, 50:422–433, 2005.

[101] M. R. Jovanovic, J. M. Fowler, B. Bamieh, and R. D'Andrea. On the peaking phenomenon in the control of vehicular platoons. *Systems & Control Letters*, 57:528–537, 2008.

[102] S. Kameswaran and L. T. Biegler. Advantages of nonlinear-programming-based methodologies for inequality path-constrained optimal control problems - A numerical study. *SIAM J. on Scentific Comp.*, 30:957–981, 2007.

[103] Z. Ke, H. Logemann, and R. Rebarber. Approximate tracking and disturbance rejection for stable infinite-dimensional systems using sampled-data low-gain control. *SIAM J. on Control and Optimization*, 48:641–671, 2009.

[104] H. K. Khalil. *Nonlinear Systems*. Prentice Hall, Englewood, NJ, third edition, 2001.

[105] P. P. Khargonekar and K. Poola. Robust stabilization of distributed systems. *Automatica*, 22:77–84, 1986.

[106] J. Kim, M. J. Yaszemski, and L. Lu. Three-dimensional porous biodegradable polymeric scaffolds fabricated with biodegradable hydrogel porogens. *Tissue Engineering C*, 15:583–594, 2009.

[107] M. Kishida and R. D. Braatz. Internal model control of distributed parameter systems. In *Proc. of IEEE Conference on Decision and Control*, pages 1434–1441, 2008.

[108] M. Kishida and R. D. Braatz. Robustness analysis of distributed parameter systems with application to the 2D reaction-diffusion equation. In *Proc. of Mathematical Theory of Networks and Systems*, page SSRussell1.4, Blacksburg, VA, 2008.

[109] M. Kishida and R. D. Braatz. Optimal field control of spatially distributed systems. In *Proc. of the American Control Conference*, pages 32–37, Piscataway, NJ, 2009. IEEE Press.

[110] M. Kishida and R. D. Braatz. RBF-based 2D optimal spatial control of the 3D reaction-convection-diffusion equation. In *Proc. of the European Control Conference*, pages 1949–1954, 2009.

[111] M. Kishida and R. D. Braatz. Structured spatial control of the reaction-diffusion equation with parametric uncertainties. In *Proc. of IEEE Multi-Conference on Systems and Control*, 2010. in press.

[112] M. Kishida, A. N. Ford, D. W. Pack, and R. D. Braatz. Optimal control of cellular uptake in tissue engineering. In *Proc. of the American Control Conference*, pages 2118–2123, Piscataway, NJ, 2008. IEEE Press.

[113] M. Kishida, D. W. Pack, and R. D. Braatz. State-constrained optimal spatial field control for controlled release in tissue engineering. In *Proc. of the American Control Conf.*, pages 4361–4366, 2010.

[114] J. Kost, K. Leong, and R. Langer. Ultrasound-enhanced polymer degradation and release of incorporated substances. *Proceedings of the National Academy of Sciences U.S.A.*, 86:7663–7666, 1989.

[115] M. Krstic and A. Smyshlyaev. *Boundary Control of PDEs. A Course on Backstepping Designs*. SIAM, Philadelphia, PA, 2008.

[116] I. Kucuk and I. Sadek. An efficient computational method for the optimal control problem for the Burgers equation. *Mathematical & Computer Modelling*, 44:973–982, 2006.

[117] K. Kunisch and S. Volkwein. Control of the Burgers equation by a reduced-order approach using proper orthogonal decomposition. *J. of Optimization Theory & Applications*, 102:345–371, 1999.

[118] S. Lall, J. E. Marsden, and S. Glavaski. A subspace approach to balanced truncation for model reduction of nonlinear control systems. *Int. J. of Robust and Nonlinear Cont.*, 12:519–535, 2002.

[119] J. Lang. Adaptive computation for boundary control of radiative heat transfer in glass. *J. of Computational and Applied Mathematics*, 183:312–326, 2005.

[120] R. Langer. Drug delivery and targeting. *Nature*, 392(6679):5–10 Suppl. S, 1998.

[121] R. Langer. Perspectives: Drug delivery - Drugs on target. *Science*, 293(5527):58–59, 2001.

[122] R. Langer and J. P. Vacanti. Tissue engineering. *Science*, 260(5110):920 – 926, 1993.

[123] I. Lasiecka. Control of systems governed by partial differential equations: A historical perspective. In *Proc. of the IEEE Conf. on Decision and Control*, pages 2792–2796, New Orleans, Louisiana, USA, 1995.

[124] I. Lasiecka and R. Triggiani. *Control Theory for Partial Differential Equations: Continuous and Approximation Theories I - Abstract Parabolic Systems*. Cambridge University Press, Cambridge, U.K., 2000.

[125] I. Lasiecka and R. Triggiani. *Control Theory for Partial Differential Equations: Continuous and Approximation Theories II - Abstract Hyperbolic-like Systems over a Finite Time Horizon*. Cambridge University Press, Cambridge, U.K., 2000.

[126] D. L. Laughlin, M. Morari, and R. D. Braatz. Robust performance of cross-directional basis-weight control in paper machines. *Automatica*, 29:1395–1410, 1993.

[127] J. Lee, M. J. Cuddihy, and N. A. Kotov. Three-dimensional cell culture matrices: State of the art. *Tissue Engineering B*, 14:61–86, 2008.

[128] J. H. Lee, M. Morari, and C. E. Garcia. State-space interpretation of model predictive control. *Automatica*, 30:707–717, 1994.

[129] Y. I. Lee, B. Kouvaritakis, and M. Cannon. Constrained receding horizon predictive control for nonlinear systems. *Automatica*, 38:2093–2102, 2002.

[130] Q. Li, A. N. Poo, and C. M. Lim. Internal model structure in the control of robot manipulators. *Mechatronics*, 6:571–590, 1996.

[131] J. L. Lions. *Optimal Control of Systems Governed by Partial Differential Equations*. Springer-verlag, New York, 1971.

[132] J. S. Liu. *Monte Carlo Strategies in Scientific Computing*. Springer-Verlag, New York, 2001.

[133] W. J. Liu. Boundary feedback stabilization of an unstable heat equation. *SIAM J. on Control and Optimization*, 42:1033–1043, 2003.

[134] D. G. Luenberger. *Optimization by Vector Space Methods*. Wiley Interscience, New York, 1997.

[135] D. L. Lukes and D. L. Russell. The quadratic criterion for distributed systems. *SIAM J. Control*, 7:101–121, 1969.

[136] H. V. Ly and H. T. Tran. Modeling and control of physical processes using proper orthogonal decomposition. *Mathematical & Computer Modelling*, 33:223–236, 2001.

[137] D. L. Ma and R. D. Braatz. Worst-case analysis of finite-time control policies. *IEEE Trans. on Control Systems Technology*, 9(5):766–774, SEP 2001.

[138] D. L. Ma, D. K. Tafti, and R. D. Braatz. High resolution simulation of multidimensional crystal growth. *Ind. Eng. Chem. Res.*, 41:6217–6223, 2002.

[139] M. J. Mahoney and W. M. Saltzman. Controlled release of proteins to tissue transplants for the treatment of neurodegenerative disorders. *J. Pharm. Sci.*, 85:1276–1281, 1996.

[140] M. J. Mahoney and W. M. Saltzman. Transplantation of brain cells assembled around a programmable synthetic microenvironment. *Nature Biotech.*, 19:934–939, 2001.

[141] G. Mapili, Y. Lu, S. C. Chen, and K. Roy. Laser-layered microfabrication of spatially patterned functionalized tissue-engineering scaffolds. *J. of Biomedical Materials Research Part B-Applied Biomaterials*, 75B:414–424, 2005.

[142] J. A. Marshall, M. E. Broucke, and B. A. Francis. Formations of vehicles in cyclic pursuit. *IEEE Trans. on Automatic Control*, 49:1963–1974, 2004.

[143] D. Q. Mayne, J. B. Rawlings, and C. V. Rao. Constrained model predictive control: Stability and optimality. *Automatica*, 36:789–814, 2000.

[144] C. Meyer and A. Rosch. L-infinity-estimates for approximated optimal control problems. *SIAM J. on Control & Optimization*, 44:1636–1649, 2005.

[145] A. G. Mikos, S. W. Herring, P. Ochareon, J. Elesseeff, H. H. Lu, R. Kandel, F. J. Schoen, M. Toner, D. Mooney, A. Atala, M. E. Van Dyke, D. Kaplan, and G. Vunjak-Novakovic. Engineering complex tissues. *Tissue Engineering*, 12:3307–3339, 2006.

[146] S. O. R. Moheimani, D. Halim, and A. J. Fleming. *Spatial Control of Vibration: Theory and Experiments*. World Scientific, Hackensack, NJ, 2004.

[147] C. B. Moler. *Numerical Computing with Matlab*. SIAM, Philadelphia, PA, 2004.

[148] M. Morari and E. Zafiriou. *Robust Process Control*. Prentice Hall, Upper Saddle River, NJ, 1989.

[149] K. W. Morton and D. F. Mayers. *Numerical Solution of Partial Differential Equations*. Cambridge University Press, Cambridge, MA, 1995.

[150] Z. K. Nagy and R. D. Braatz. Robust nonlinear model predictive control of batch processes. *AIChE Journal*, 49(7):1776–1786, 2003.

[151] Z. K. Nagy and R. D. Braatz. Open-loop and closed-loop robust optimal control of batch processes using distributional and worst-case analysis. *J. of Process Control*, 14:411–422, 2004.

[152] Z. K. Nagy and R. D. Braatz. Distributional uncertainty analysis using power series and polynomial chaos expansions. *J. of Process Control*, 17:229–240, 2007.

[153] A. H. Nayfeh, J. F. Nayfeh, and D. T. Mook. On methods for continuous systems with quadratic and cubic nonlinearities. *Nonlinear Dynamics*, 3:145–162, 1992.

[154] P. A. Nelson and S. J. Elliot. *Active Control of Sound*. Academic Press, San Diego, CA, 1992.

[155] M. P. Newlin, , and R. Smith. A generalization of the structure singular value and its application to model validation. *IEEE Transactions on Automatic Control*, 43(7):901–907, 1998.

[156] K. Nowozynski. Estimation of magnetotelluric transfer functions in the time domain over a wide frequency band. *Geophys. J. Int.*, 158:32–41, 2004.

[157] A. C. Or and J. L. Speyer. Robust control for convection suppression in a fluid layer: The effects of boundary properties, actuator lag, and major parameter uncertainties. *Phys. Rev. E*, 73:046307, 2006.

[158] M. J. L. Orr. Recent advances in radial basis function networks. Technical report, Institute for Adaptive and Neural Computation, Division of Informatics, Edinburgh University, Edinburgh, Scotland, UK, 1999. http://anc.ed.ac.uk/rbf/rbf.html.

[159] W. Pan, M. A. Tatang, G. J. McRae, and R. G. Prinn. Uncertainty analysis of indirect radiative forcing by anthropogenic sulfate aerosols. *J. Geophys. Res.*, 103:3815–3823, 1998.

[160] J. Park and I. W. Sandberg. Universal approximation using radial basis function networks. *Neural Computation*, 3:246–257, 1991.

[161] J. Park and I. W. Sandberg. Approximation and radial basis function networks. *Neural Computation*, 5:305–316, 1993.

[162] A. A. Patwardhana, G. T. Wright, and T. F. Edgar. Nonlinear model-predictive control of distributed-parameter systems. *Chem. Eng. Sci.*, 47:721–735, 1992.

[163] N. A. Peppas, P. Buresa, W. Leobandunga, and H. Ichikawab. Hydrogels in pharmaceutical formulations. *European J. of Pharmaceutics and Biopharmaceutics*, 50:27–46, 2000.

[164] A. S. Poznyak and A. R. Palacios. Robust boundary control for linear time-varying infinite dimensional systems. *Int. J. of Control*, 72:392–403, 1999.

[165] D. M. Prett, B. L. Ramakar, and C. R. Cutler. Dynamic matrix control process, 1982. U.S. Patent #80,966 filed in 1979.

[166] Y. Qiu and K. Park. Environment-sensitive hydrogels for drug delivery. *Adv. Drug Delivery Reviews*, 53:321–339, 2001.

[167] C. V. Rao, S. J. Wright, and J. B. Rawlings. Application of interior-point methods to model predictive control. *JOTA*, 99:723–757, 1998.

[168] J. B. Rawlings, S. M. Miller, and W. R. Witkowski. Model identification and control of solution crystallization processes: A review. *Ind. Eng. Chem. Res.*, 32:1275–1296, 1993.

[169] W. H. Ray. Some recent applications of distributed parameter systems theory - A survey. *Automatica*, 14:281–287, 1978.

[170] W. H. Ray. *Advanced Process Control*. McGraw-Hill, New York, 1980.

[171] M. Razzaghi, A. Tahai, and A. Arabshahi. Solution of linear 2-point boundary-value problems via Fourier-series and application to optimal-control of linear systems. *J. of the Franklin Institute*, 326:523–533, 1989.

[172] R. Rebarber and G. Weiss. Internal model based trackingand disturbance rejection for stable well-posed systems. *Automatica*, 39:1555–1569, 2003.

[173] T. P. Richardson, M. C. Peters, A. B. Ennett, and D. J. Mooney. Polymeric system for dual growth factor delivery. *Nature Biotechnology*, 19:1029–1034, 2001.

[174] O. J. Rojas, G. C. Goodwin, and G. V. Johnston. Spatial frequency antiwindup strategy for cross-directional control problems. *IEE Proc.-Control Theory & Applications*, 149:414–422, 2002.

[175] D. L. Russell. Nonharmonic fourier series in the control theory of distributed parameter systems. *J. Math Anal. Appl.*, 18:542–560, 1967.

[176] E. L. Russell, C. P. H. Power, and R. D. Braatz. Multidimensional realization of large scale uncertain systems for multivariable stability margin computation. *Int. J. of Robust and Nonlinear Control*, 7:113–125, 1997.

[177] S. E. Sakiyama-Elbert and J. A. Hubbell. Development of fibrin derivatives for controlled release of heparin-binding growth factors. *J. of Controlled Release*, 65:389–402, 2000.

[178] W. M. Saltzman. *Drug Delivery - Engineering Principles for Drug Therapy*. Oxford University Press, Oxford, UK, 2001.

[179] W. M. Saltzman and W. L. Olbricht. Building drug delivery into tissue engineering. *Nature Reviews Drug Discovery*, 1:177–186, 2002.

[180] R. M. Sanner and J. J. E. Slotine. Gaussian networks for direct adaptive-control. *IEEE Trans. on Neural Networks*, 3:837–863, 1992.

[181] A. Satoh. *Introduction to Molecular-Microsimulation of Colloidal Dispersions*. Elsevier, Amsterdam, Netherlands, 2003.

[182] W. E. Schiesser and G. W. Griffiths. *A Compendium of Partial Differential Equation Models Method of Lines Analysis with Matlab*. Cambridge University Press, New York, 2009.

[183] N. M. Shah and D. J. Anderson. Integration of multiple instructive cues by neural crest stem cells reveals cell-intrinsic biases in relative growth factor responsiveness. *PNAS*, 94:11369–11374, 1997.

[184] H. Shang, J. F. Forbes, and M. Guay. Model predictive control for quasilinear hyperbolic distributed parameter systems. *Ind. Eng. Chem. Res.*, 43:2140–2149, 2004.

[185] H. Shanga, J. F. Forbes, and M. Guay. Computationally efficient model predictive control for convection dominated parabolic systems. *J. of Process Control*, 17:379–386, 2007.

[186] J. Siepmann and A. Gopferich. Mathematical modeling of bioerodible, polymeric drug delivery systems. *Advanced Drug Delivery Reviews*, 48:229–247, 2001.

[187] E. A. Silva and D. J. Mooney. Spatiotemporal control of vascular endothelial growth factor delivery from injectable hydrogels enhances angiogenesis. *J. Thromb. Haemost.*, 5:590–598, 2007.

[188] J. Sjoberg, Q. H. Zhang, L. Ljung, A. Benveniste, B. Delyon, P. Y. Glorennec, H. Hjalmarsson, and A. Juditsky. Nonlinear black-box modeling in system identification: A unified overview. *Automatica*, 31:1691–1724, 1995.

[189] S. Skogestad, M. Morari, and J. C. Doyle. Robust control of ill-conditioned plants: High-purity distillation. *IEEE Trans. on Automatic Control*, 33:1092–1105, 1988.

[190] S. Skogestad and I. Postlethwaite. *Multivariable Feedback Control Analysis and Design*. John Wiley & Sons, Hoboken, NJ, 2nd edition, 2005.

[191] A. Smyshlyaev and M. Krstic. On control design for PDEs with space-dependent diffusivity or time-dependent reactivity. *Automatica*, 41:1601–1608, 2005.

[192] A. Stephanou, S. R. McDougall, A. R. A. Anderson, and M. A. J. Chaplain. Mathematical modelling of flow in 2D and 3D vascular networks: Applications to anti-angiogenic and chemotherapeutic drug strategies. *Mathematical & Computer Modelling*, 41(10):1137–1156, 2005.

[193] P. Tayalia and D. J. Mooney. Controlled growth factor delivery for tissue engineering. *Advanced Materials*, 21:3269–3285, 2009.

[194] G. A. Truskey, F. Yuan, and D. F. Katz. *Transport Phenomena in Biological Systems*. Prentice Hall, Upper Saddle River, NJ, 2004.

[195] J. G. VanAntwerp, A. P. Featherstone, and R. D. Braatz. Robust cross-directional control of large scale sheet and film processes. *J. of Process Control*, 11:149–177, 2001.

[196] J. G. VanAntwerp, A. P. Featherstone, B. A. Ogunnaike, and R. D. Braatz. Cross-directional control of sheet and film processes. *Automatica*, 43:191–211, 2007.

[197] L. Vandenberghe, S. Boyd, and M. Nouralishahi. Robust linear programming and optimal control. In *Proc. of the 15th IFAC World Congress on Automatic Control*, volume 15, pages 271–276, 2002.

[198] N. K. Varde and D. W. Pack. Microspheres for controlled release drug delivery. *Expert Opinion on Biological Therapy*, 4:35–51, 2004.

[199] M. Vidyasagar and V. Blondel. Probabilistic solutions to some NP-hard matrix problems. *Automatica*, 37:1397–1405, 2001.

[200] J. Vlassenbroeck. A Chebyscheff polynomial method for optimal-control with state constraints. *Automatica*, 24:499–506, 1988.

[201] J. Vlassenbroeck and V. D. Rene. A Chebyshev technique for solving nonlinear optimal control problems. *IEEE Trans. on Automatic Control*, 33:333–340, 1988.

[202] B. Wahlberg. System identification using laguerre models. *IEEE Trans. on Automatic Control*, 36:551–562, 1991.

[203] A. Wazwaz. *Partial Differential Equations: Methods and Applications*. Taylor & Francis, Florence, KY, 2002.

[204] H. Wilbraham. On a certain periodic function. *Cambridge & Dublin Math. J.*, 3:198–201, 1848.

[205] S. Wolf and R. N. Tauber. *Silicon Processing for the VLSI Era - Vol. 1*. Lattice Press, Sunset Beach, CA, 2nd edition, 2000.

[206] P. M. Young and J. C. Doyle. A lower bound for the mixed μ problem. *IEEE Trans. on Automatic Control*, 42:123–128, 1997.

[207] A. Zheng, M. V. Kothare, and M. Morari. Anti-windup design for internal model control. *Int. J. of Control*, 60:1015–1024, 1994.

[208] K. Zhou, J. C. Doyle, and K. Glover. *Robust and Optimal Control*. Prentice Hall, Upper Saddle River, NJ, 1995.

[209] K. Zhou and P. P. Khargonekar. On the weighted sensitivity minimization problem for delay systems. *Systems & Control Letters*, 8:307–312, 1987.

[210] H. Zwart. Transfer functions for in nite-dimensional systems. *Systems & Control Letters*, 52:247–255, 2004.

AUTHOR'S BIOGRAPHY

Masako Kishida was born in Osaka, Japan in 1981. She received the B.S.E. in Aerospace Engineering with minor in Mathematics in 2004, the M.S.E. in Aerospace Engineering and the M.S. in Applied and Interdisciplinary Mathematics both in 2006, all from the University of Michigan, Ann Arbor. In 2010, she received the Ph.D. degree in Mechanical Engineering from the University of Illinois at Urbana-Champaign.